The roles of glutathione in the control of plant growth, development and signalling in *Arabidopsis thaliana*

Daniel Schnaubelt

Submitted in accordance with the requirements for the degree of Doctor of Philosophy

The University of Leeds

Faculty of Biological Sciences

December 2013

The candidate confirms that the work submitted is his own, except where work which has formed part of jointly-authored publications has been included. The contribution of the candidate and other authors to this work has been explicitly indicated below. The candidate confirms that appropriate credit has been given within the thesis where reference has been made to the work of others.

GARCÍA-GIMÉNEZ J.L., MARKOVIC J., DASÍ F., QUEVAL G., SCHNAUBELT D., FOYER C.H. & PALLARDÓ F.V. (2013) Nuclear glutathione. *Biochimica Biophysica Acta* 1830, 3304-3316.:

Figure 1 (D-F)

Figure 3 (B)

SCHNAUBELT D., SCHULZ P., HANNAH M.A., YOCGO R.E., & FOYER C.H. (2013) Perturbations in cellular GSH homeostasis influence shoot and root development but have no negative effects on abiotic stress tolerance in *Arabidopsis thaliana*. *Frontiers in Plant Physiology*. doi:10.3389/fpls.2013.00416.

Figures 1-7

SCHNAUBELT D., QUEVAL G., DONG Y., DIAZ-VIVANCOS P., MAKGOPA M.E., HOWELL G., DE SIMONE A., BAI J., HANNAH M.A. AND FOYER C.H. (2013) Low glutathione regulates gene expression and the redox potentials of

the nucleus and cytosol in *Arabidopsis thaliana. Plant Cell and Environment.* doi: 10.1111/pce.12252.:

Figure 1 (B, C)

Figure 2

Figure 5

Figure 6

Figure 7

Figure 8

Acknowledgements

I would like to deeply thank my supervisor Professor Christine Foyer for giving me the opportunity to undertake this PhD research in her lab and to work together with her on this appealing project. I am very thankful to both my supervisors Prof. Christine Foyer and Dr. Christopher West for the support and guidance during the last years.

Furthermore I would like to extend my gratitude to the European Union for funding my PhD studentship (EU-ITN PITN-GA-2008-215174) in the framework of Chloroplast Signals (COSI) and to the Leeds Food Security Hub for covering my financial sustenance during the last 8 months of my PhD research.

My special thanks go to our project partner Bayer BioSciences N.V. in Ghent, Belgium and in particular to Matthew Hannah who was a great supervisor and colleague during my exchange to Ghent. Without their contribution the microarray analysis would not have been possible.

I would also like to thank to Dr. Guillaume Queval for the constructive talks and suggestions regarding the analysis of microarray results, and Ying Ping Dong for providing data from her experiments on the intracellular partitioning of glutathione between cytosol and nucleus during the cell cycle.

Many thanks also to Professor Karl Kunert, not only for discussions of ideas and future perspectives, but also for the many conversations outside work.

Abstract

Reduced glutathione (GSH) is an abundant low molecular weight thiol that fulfils multiple functions in plants, many of which remain poorly characterised. The following studies were undertaken in order to characterise the roles of GSH in growth, development and signalling in *Arabidopsis thaliana.* In the first experiments, a phenomics approach was used to investigate the effects of GSH deficiency on growth and stress tolerance using mutants that are either defective either in GSH synthesis (*cad2-1*, *pad2-1* and *rax1-1*) or the export of γ-glutamylcysteine and GSH from the chloroplast (*clt1clt2clt3*). Whereas the *clt1clt2clt3* mutant had a greater rosette area than the wild-type under low light growth conditions, the GSH deficient mutants were significantly smaller. Moreover, lateral root densities were significantly decreased in GSH deficient and *clt1clt2clt3* mutants. The redox potentials of the nucleus and cytosol in the root cells of the wild-type seedlings measured using roGFP were over -300mV. However, in roots grown in the presence of the GSH synthesis inhibitor buthionine sulfoximine (BSO), the redox potentials of the nucleus and cytosol increased to approximately -260mV. Low GSH-responsive genes were identified by transcript profiling analysis of the GSH-deficient *root meristemless 1-1* (*rml1-1*) mutant. These included a large number of transcription factors, proteins involved in cell division, redox regulation and auxin signalling. Many transcripts modified by low GSH influence plant growth and development, and explain the altered root development observed the low GSH mutants. These results demonstrate that low GSH leads to significant increases in the redox states of the nucleus and cytosol and results in specific responses in gene expression that are distinct from those observed under

oxidative stress. Moreover, the findings suggest that the cytosolic/nuclear GSH pool is important in the control of root development and that low GSH *per se* does not enhance overall sensitivity to abiotic stresses.

Table of Contents

Abbreviations

CLSM	confocal laser scanning microscope / microscopy
CLT	chloroquine-resistance-transporter (CRT)-like transporter
CLT	cloroquine-resistance transporter (CRT)-like transporter (plant homologs of *Plasmodium falciparum* CRT)
CMFDA	5-Chloromethylfluorescein diacetate
CRT	chloroquine-resistance transporter
DTNB	5,5'-dithiobis-2-nitrobenzoic acid; Ellman's agent
DTT	dithiothreitol
EDTA	ethylenediaminetetraacetic acid
γ-EC	γ-glutamylcysteine
γ-ECS	γ-glutamylcysteine synthetase
GCL	glutamate-cysteine ligase
GPX	glutathione peroxidases
GR	glutathione reductase
GRX	glutaredoxin
GSH	reduced glutathione, γ-L-glutamyl-L-cysteinylglycine
GSH-S	glutathione synthetase
GSNOR	nitrosoglutathione reductase
GSSG	oxidised glutathione, glutathione disulphide
GST	glutathione S-transferase
HMGSH	S-(hydroxymethyl)glutathione
mNPB	modified nuclear purification buffer (NPB plus 0.3 M Mannitol)
MS	Murashige & Skoog
NPB	nuclear purification buffer

NTR	NADPH-dependent thioredoxin reductase
NTRA	NADPH-dependent thioredoxin reductase A
NTRB	NADPH-dependent thioredoxin reductase B
PARP	poly (ADP-ribose) polymerase
PCS	phytochelatin synthase
QC	quiescent centre
qRT-PCR	quantative real-time PCR
roGFP	reduction-oxidation sensitive GFP
ROS	reactive oxygen species
SEM	scanning electron microscope / microscopy
VPD	2-vinylpyridine

Table of Figures

Table of Tables

1 Introduction

Plant performance and the predictability of crop yield are severely hampered by environmental factors. Collectively, these "abiotic stresses" restrict plant vigour and create a "yield gap". This is the difference between the theoretical maximum or "yield potential" of the crop, and the actual yield achieved by the farmer. Over the last 50 years, plant breeders have improved the yield potential, but the yield gap remains. Why does the yield gap occur? Plants grow best in certain ranges of environmental conditions, and stop growing, for example at low or high temperatures, and so yield is reduced. If we can widen the range in which plants grow, then crops would perform closer to their theoretical maximum. Unlike animals, plants grow continuously and growth requires new cells to provide the building blocks.

When plants perceive stress, specific signals block cell division. Under extreme conditions, this is beneficial, but evidence suggests that plants shut down cell division early as a precaution in response to stress. Therefore they stop growing, even though conditions are not really bad enough to require this. How does abiotic stress stop cell division? An important factor is the cell's ability to regulate its capacity for reduction and oxidation (redox), and to protect itself from uncontrolled oxidation. The cells reducing power is stored as pools of reductant and antioxidant compounds. One of the most important cellular antioxidants is glutathione. When cells are depleted of glutathione pool, cell division is blocked at a point in the cell cycle called G1. Due to this arrest at G1 in response to glutathione depletion, plant development comes to a halt. In the following, GSH

refers only to the reduced glutathione, whereas the term glutathione refers both to the total pool (GSH plus glutathione disulphide; GSSG).

1.1 Glutathione synthesis, regulation of synthesis and degradation

Glutathione synthesis

The thiol tripeptide, glutathione (GSH; γ-L-glutamyl-L-cysteinylglycine), is found in almost all organisms. The pathway of GSH synthesis (Figure 1-1) is well established in plants and animals (Foyer and Noctor, 2011; Noctor et al., 2011; Noctor et al., 2012). It involves two ATP-dependent steps. Firstly, γ-glutamylcysteine (γ-EC) is produced from glutamate and cysteine in a reaction catalysed enzyme γ-glutamylcysteine synthetase (γ-ECS). This enzyme is also called glutamate-cysteine ligase (GCL). Glycine is then added in a reaction catalysed by glutathione synthetase (GSH-S, Figure 1-1; Foyer and Noctor, 2011; Noctor et al., 2011; Noctor et al., 2012). While the first step solely occurrs in the chloroplast, the second step of glutathione synthesis can occur in both chloroplast and cytosol. The genes encoding γ-EC and γ-ECS are GSH1 and GSH2, respectively. Each gene specifically encodes one enzyme of the glutathione synthetic pathway. While GSH1 encodes the solely chloroplastic γ-EC, at least for γ-ECS, which is encoded by GSH2, alternate splicing results in variants of the enzyme that are targeted to either the chloroplast or cytosol (Foyer and Noctor, 2011; Noctor et al., 2011; Noctor et al., 2012)).

Regulation of glutathione synthesis

While glutathione biosynthesis is affected by many factors, the most important are considered to be cysteine availability and γ-ECS activity (Noctor et al., 2012). Earlier studies were able to demonstrated that overexpression of the first enzyme of the glutathione synthesis pathway (γ-ECS) or of enzymes involved in the synthesis of cysteine resulted in constitutive increases in glutathione (Strohm et al., 1995; Harms et al., 2000). However, particularly transient overexpression of γ-ECS resulted in light intensity-dependent chlorosis or necrosis in these plants reflecting more oxidized conditions (Creissen et al., 1999). This oxidative damage seems to be the result of an impaired redox sensing process in these plants (Creissen et al., 1999). And although transcriptional- or post-transcriptional changes may result in increases in γ-ECS activity relatively through increases in *GSH1* and *GSH2* transcripts only few conditions could cause changes in the expression of these two genes (May et al., 1998; Noctor et al., 2012). Studies, in which *Arabidopsis* plants were grown in the presence of cadmium or copper, revealed that plants respond with increased transcription of *GSH1* and *GSH2* to heavy metals, particularly those that are thought to be scavenged by phytochelatins (Xiang & Oliver, 1998). Subsequent experiments further demonstrated that neither oxidative stress, nor oxidized or reduced glutathione levels were responsible for the activation of transcription in those two genes (Xiang & Oliver, 1998). However, neither externally applied or internally generated H_2O_2 were able to cause increases in *GSH1* or *GSH2* transcripts (Smith et al., 1984; May & Leaver, 1993; Willekens et al., 1997; Xiang & Oliver, 1998). Also jasmonic acid was demonstrated to induce mRNA levels of *GSH1* and *GSH2* while parallel

increasing the capacity for glutathione synthesis, but without altering the overall glutathione content (Xiang & Oliver, 1998).

Despite some evidence that production of γ-ECS is regulated at the transcriptional level more attention has been given to post-translational redox-control, as initial studies were able to show that purified tobacco γ-ECS can be inhibited by dithiols and that similar effects could also be observed in other species (Hell & Bergmann, 1990; Jez et al., 2004; Noctor et al., 2012).

Earlier studies demonstrated structural differences between mammalian and *Arabidopsis thaliana* γ-ECS (AtECS), where the mammalian γ-ECS consists of a catalytic- and a regulatory-subunit, while the AtECS is regulated and functions as a monomeric protein (Jez et al., 2004). These differences also allow for conformational changes of the AtECS in response to oxidative stress (Jez et al., 2004). Moreover, the *Brassica juncea* γ-ECS forms a homodimer that is linked by two intramolecular redox-sensitive disulphide bonds (Hothorn et al., 2006; also described later in Figure 1-4A, left, CC1 & CC2;). Upon reduction of one of these disulphide bonds the structure of the γ-ECS is modified, resulting in a β-hairpin motif preventing the access of substrates to the active site (Hothorn et al., 2006). Reduction of the second disulphide bond is implicated in the activation of the γ-ECS by reversibly affecting the transition from dimer to monomer (Jez et al., 2004; Hothorn et al., 2006; Hicks et al., 2007; Gromes et al., 2008). These mechanisms are very likely important factors in the reversible posttranslational modulation of γ-ECS activity (Jez et al., 2004; Hothorn et al., 2006; Hicks et al., 2007; Noctor et al., 2012).

A further important mechanism to regulate glutathione homeostasis is feedback inhibition of γ-ECS by reduced glutathione (GSH). While alleviation of feedback inhibition, caused by conditions in which glutathione is consumed (e.g. in the synthesis of phytochelatins), is very likely an important mechanism leading to increased glutathione synthesis rates, the mechanistic links between feedback inhibition and thiol/disulphide redox regulation of γ-ECS remain to be clarified (May et al., 1998; Noctor et al., 2012).

Glutathione degradation

Breakdown of glutathione can be initiated by four different types of enzymes, some of which can directly use GSH, while others show higher affinities for GSSG or GS-conjugates (Noctor et al., 2012). These four types of enzymes are carboxypeptidase, phytochelatin synthase (PCS), γ-glutamyl transpeptidase (GGT) and γ-glutamyl cyclotransferase (GGC) (Orlowski & Meister, 1973; Steinkamp & Rennenberg, 1984; Steinkamp et al., 1987; Meister, 1988; Blum et al., 2007 & 2010).

For example, carboxypeptidase activity, which was detected in barley vacuoles, could lead to degradation of glutathione or GS-conjugates (Steinkamp & Rennenberg, 1985; Wolf et al., 1996). The cytosolic enzyme phytochelatin sythase has also been implicated in the breakdown of GS-conjugates (Blum et al., 2007 & 2010). For example, studies in Arabidopsis using the xenobiotic bimane to track GS-conjugates, revealed that PCS1 provides the major activity for the conversion of bimane-GS conjugates and that it fulfils a double role: mediation of heavy metal tolerance and degradation of GS-conjugates (Blum et al., 2007 & 2010). However, it remains unclear to

which extent GS-conjugates can accumulate in the cytosol as they are usually rapidly transported to the vacuole, outcompeting carboxypeptidation of the γ-EC-bimane intermediate via cytosolic PCS (Grzam et al., 2006). Nevertheless, PCS may play some role in certain cell types or when the enzyme is activated by heavy metals (Grzam et al., 2006; Noctor et al., 2012).

Furthermore, γ-glutamyl transpeptidase (GGT) has been demonstrated to act in the mammalian γ-glutamyl cycle and to catalyse the hydrolysis or transpeptidation of GSH at the plasma membrane (Meister et al., 1988; Martin & Slovin, 2000; Storozhenko et al., 2002). The resulting γ-glutamyl amino acid derivates are then further processed by γ-glutamyl cyclotransferase (GGC) and 5-oxoprolinase (5-OPase) to produce free glutamate (Martin & Slovin, 2000; Storozhenko et al., 2002). In Arabidopsis, GGTs are encoded by at least three functional genes, two of which (*GGT1* and *GGT2*) encode apoplastic enzymes (Martin & Slovin, 2000; Storozhenko et al., 2002) that are probably involved in countering oxidative stress or salvaging excreted GSSG (Ohkama-Ohsu et al., 2007; Ferretti et al., 2009; Destro et al., 2011). Studies employing *ggt1* and *ggt2* mutant plants were able to demonstrate that cotyledons and older leaves of *ggt1* plants turned yellow very early during development, while *ggt2* plants did not exhibit any discernable phenotype (Ohkama-Ohsu et al., 2007). These observations suggested that particularly GGT1 is involved in the prevention of oxidative stress through metabolizing of GSSG, while GGT2 might facilitate glutathione import into the developing seed (Ohkama-Ohsu et al., 2007). Furthermore, the GGTs encoded by *GGT1* and *GGT2* show activity against GSH, GSSG as well as GS-conjugates (Martin & Slovin, 2000; Storozhenko et al., 2002; Ohkama-Ohsu et al., 2007). In animals, γ-glutamyl peptides

produced by GGT are further metabolized by GGC to 5-oxoproline. Until now only one gene (*OXP1*) could be identified in *Arabidopsis* to likely encode the enzyme 5-OPase, which catalyses the hydrolysis of 5-oxoproline. (Ohkama-Ohtsu et al., 2008 & 2011). However, studies based on *oxp1* single mutants and *oxp1 ggt1 ggt4* triple mutants allowed to propose that the predominant GSH-degradation pathway is initiated by GGC and occurs in the cytosol, rather than being initiated by vacuolar or extracellular GGT activity (Ohkama-Ohtsu et al., 2007 & 2008). Hence, GGC is considered another type of enzymes potentially involved in the initiation of GSH-degradation, despite the fact that both rat and tobacco GGC have been demonstrated to be unable to use GSH (Orlowski & Meister, 1973; Steinkamp et al., 1987).

Due to the high complexity and the many possible routes for the glutathione degradation, many questions remain on glutathione degradation in plants, such as cellular/tissue specificities, activities against different forms of glutathione, as well as the extent to which glutathione turnover and re-synthesis occur (Noctor et al., 2012).

1.2 Mutants with defects in the glutathione synthetic pathway

In *Arabidopsis thaliana,* γ-ECS is encoded by the *GSH1* gene (Figure 1-1). Knockout mutations in *GSH1* produce an embryo-lethal phenotype (Cairns et al., 2006).

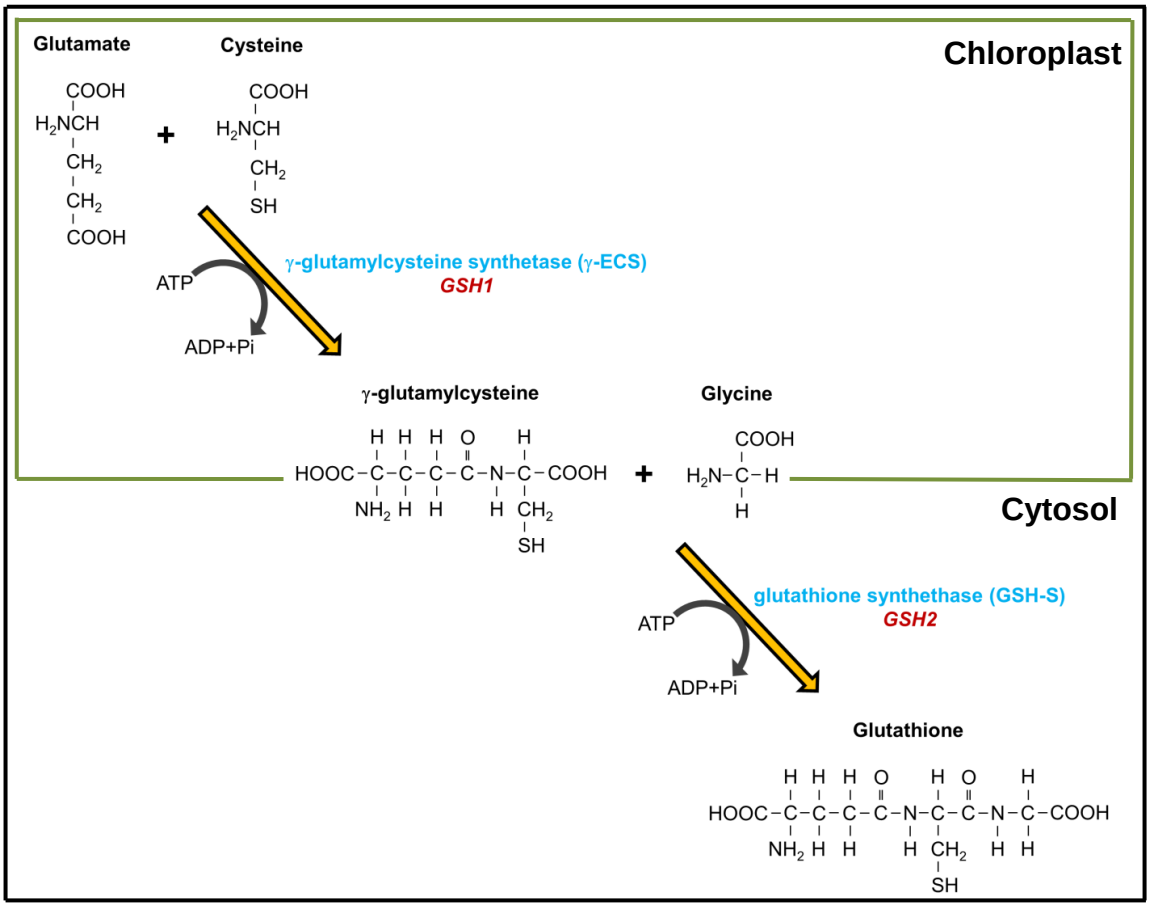

Figure 1-1: A schematic overview of the glutathione synthesis pathway. Enzymes are shown in blue; Genes encoding these enzymes are shown in red.

Less severe alleles of this gene, which produce partial decreases in glutathione contents, produce viable plants, which have been extremely useful in elucidating the functions of glutathione (Howden et al., 1995; Cobbett et al., 1998; Vernoux et al., 2000; Ball et al., 2004; Parisy et al., 2007; Schlaeppi et al., 2008). However, the mutants that have low glutathione contents have some marked phenotypic characteristics. For example, the *rootmeristemless1-1* (*rml1-1)* mutant that has less than 5% of wild-type glutathione contents, fails to develop a root apical meristem because the embryonic root cells arrest at the G1 phase of the cell cycle (Vernoux et al., 2000A; Table 1-1).

Table 1-1: Literature information on the *Arabidopsis thaliana* mutants, which are either defective in either glutathione synthesis or intracellular partitioning. Amino acid: AA

Mutant line	AGI code	Glutathione content	Reference	Mutation	Description
cadmium hypersensitive 2-1 (cad2-1)	AT4G23100	20 - 25%	Cobbett et al., 1998	6-bp deletion, at AA position 237 and 238	Mutation in GCL. Required for cell proliferation at the root tip. Mutants sensitive to cadmium.
phytoalexin deficient 2-1 (pad2-1)	AT4G23100	20%	Parisy et al., 2007	point mutation, S to N transition at AA position 298	Mutation in GCL. Required for cell proliferation at the root tip. Mutants deficient in phytoalexin camalexin.
regulator of APX2 1-1 (rax1-1)	AT4G23100	≤50%	Ball et al., 2004	point mutation, R to K transition at AA position 229	Mutation in GCL. Required for cell proliferation at the root tip. Mutants constitutively express APX2.
root meristemless 1-1 (rml1-1)	AT4G23101	<5%	Vernoux et al., 2000A & Cheng et al., 1995	point mutation, D to N transition at AA position 258	Mutation in GCL. Required for cell proliferation at the root tip. Mutants fail to establish active postembryonic root development.
CRT-like transporter 1,2 and 3 triple mutant (clt)	AT5G19380 (CLT1) AT4G24460 (CLT2) AT5G12170 (CLT3)	cytosolic GSH decreased 4-fold; chloroplastic GSH unaltered	Maughan et al., 2010	mutations in transporter genes CLT1, CLT2 and CLT3	Encodes all of the CRT-Like transporters (CLT1, CLT2 & CLT3). Required for glutathione homeostasis and stress responses. Glutathione restricted to chloroplast

The shoot phenotype in this mutant is much less affected than the root. By combining the *rml1-1* mutation with mutations in the two genes encoding NADPH-thioredoxin (TRX) reductases (*NTRA*, *NTRB*), it was shown that there is functional redundancy between glutathione and TRX systems in the control of shoot apical meristem functions (Reichheld et al., 2007).

Several other mutations in *GSH1* decrease glutathione to a residual but still significant level (about 25 to 50% of wild-type). These mutants have not been reported to have a markedly different shoot phenotype to the wild-type or to show altered development, but were selected on the basis of altered responses to biotic and abiotic environmental stress (Parisy et al., 2007; Schlaeppi et al., 2008; Table 1-1). For example, the *pad2-1* mutant, which is phytoalexin-deficient and has decreased camalexin contents, shows enhanced susceptibility to pathogens such as the oomycete *Phytophthora brassicae* (Figure 1-2; Table 1-1). These findings demonstrate that glutathione deficiency has a negative effect on disease resistance (Parisy et al., 2007).

Furthermore, the *cad2–1* mutant was identified by its enhanced sensitivity to cadmium (Howden et al., 1995). This mutant has decreased GCS activity (Cobbett et al., 1998). Moreover, root growth and GCS activity in the *cad2-1* mutant were less sensitive to inhibition by buthionine sulfoximine (BSO) than in the wild-type, indicating that the mutation alters the affinity of the inhibitor binding site (Cobbett et al., 1998; Table 1-1).

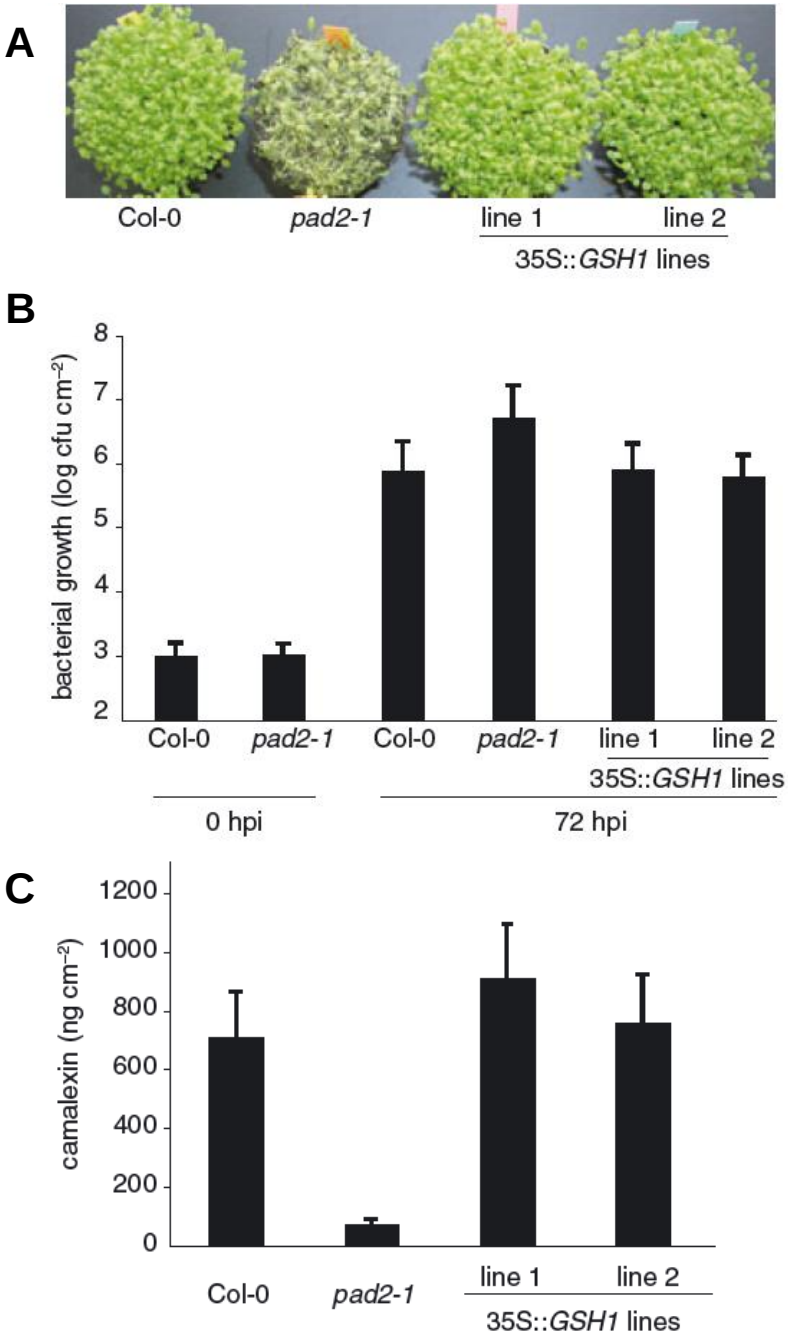

Figure 1-2: Complementation of camalexin deficiency and disease resistance phenotypes of the *pad2-1*. A: Disease resistance phenotype of four-week-old Col-0, *pad2-1* and complemented lines of *pad2-1* (35S::*GSH1*) after inoculation with *P. brassicae*. B: Bacterial titer determined on leaves of 4.5-week-old plants of Col-0, *pad2-1* and complemented lines of *pad2-1* (35S::*GSH1*) at 0 and 72h after infection. At 72 hours post infection, the bacterial titer in the pad2-1 was significantly higher than in the other three genotypes ($p<0.01$). C: Camalexin content of Col-0, *pad2-1* and complemented lines of *pad2-1* (35S::*GSH1*). The figure was taken from Parisy et al. 2007.

The mutant regulator of APX2 1-1 (*rax1-1*) was identified by altered expression of the *ASCORBATE PEROXIDASE2* (*APX2*) gene, which is induced by photo-oxidative stress (Ball et al., 2004, Figure 1-3; Table 1-1). The *rax1-1* and *cad2–1* mutants showed altered expression of stress-responsive genes, particularly under photo-oxidative stress conditions.

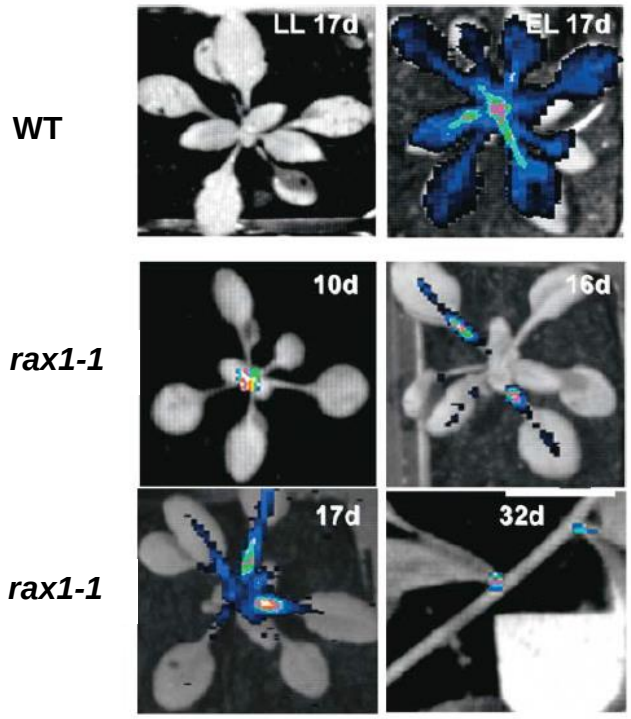

Figure 1-3: Comparison of false colour images of transgenic *Arabidopsis thaliana* wild-type and *rax1-1* plants constitutively expressing APX2LUC. Shown are typical false colour images of luciferase activity in a long day/low light–grown, 17-day-old wild-type APX2LUC Arabidopsis rosette before and after exposure to a 10-fold excess light stress for 45 min (LL 17d and EL 17d, respectively) and in long day–grown APX2LUC/rax1-1 plants at 10, 16, 17, and 32 days after germination. The image was taken from Ball et al., 2004.

The wild-type phenotype can be restored in *gsh2* mutants by complementing with targeted expression of the enzyme to the cytosol alone (Pasternak et al., 2008). Interestingly, *GSH2* knockout mutants lack the typical polygonal

endoplasmic reticulum (ER) network and accumulate swollen ER-derived bodies (Au et al., 2012). These studies showed that the *gsh2* mutants did not lack an unfolded protein response or suffer from constitutive oxidative ER stress, but the accumulation of γ-EC perturbed ER morphology rather than a deficiency in GSH (Au et al., 2012).

The structure of the γ-ECS protein (Figure 1-4A) is crucially affected by mutations in the *GSH1* gene (Figure 1-4B), resulting in altered substrate binding affinities and catalysis rates (Hothorn et al., 2006). While little information is available regarding the effects of the *GSH1* allele found in the *pad2-1* mutant on the structure of the GCL, the alleles found in *rax1-1*, *cad2-1* and *rml1-1* mutants have been described in more detail. For example, the point mutation found in the *GSH1* gene the *rax1-1* mutant causes a substitution of Arginine (R) with Lysine (K) at position 229 of the protein (Table 1-1; Figure 1-4B; Ball et al., 2004; Hothorn et al., 2006). The Arginine was identified to be at the proximal side of the cysteine binding pocket of the protein, and substitution was shown to alter binding affinity of the γ-ECS, increasing the cysteine affinity approximately 5-fold while the affinity for glutamate and ATP remained unaffected (Figure 1-4B; Hothorn et al., 2006). This shift can account for the significantly reduced glutathione levels found in the *rax1-1* mutant (Ball et al., 2004; Hothorn et al., 2006).

On the other hand, the 6-bp deletion in the *GSH1* allele of the *cad2-1* mutant result in the loss of the amino acids at position 237 and 238 of the γ-ECS protein (Table 1-1; Figure 1-4B; Cobbett et al., 1998; Hothorn et al., 2006).

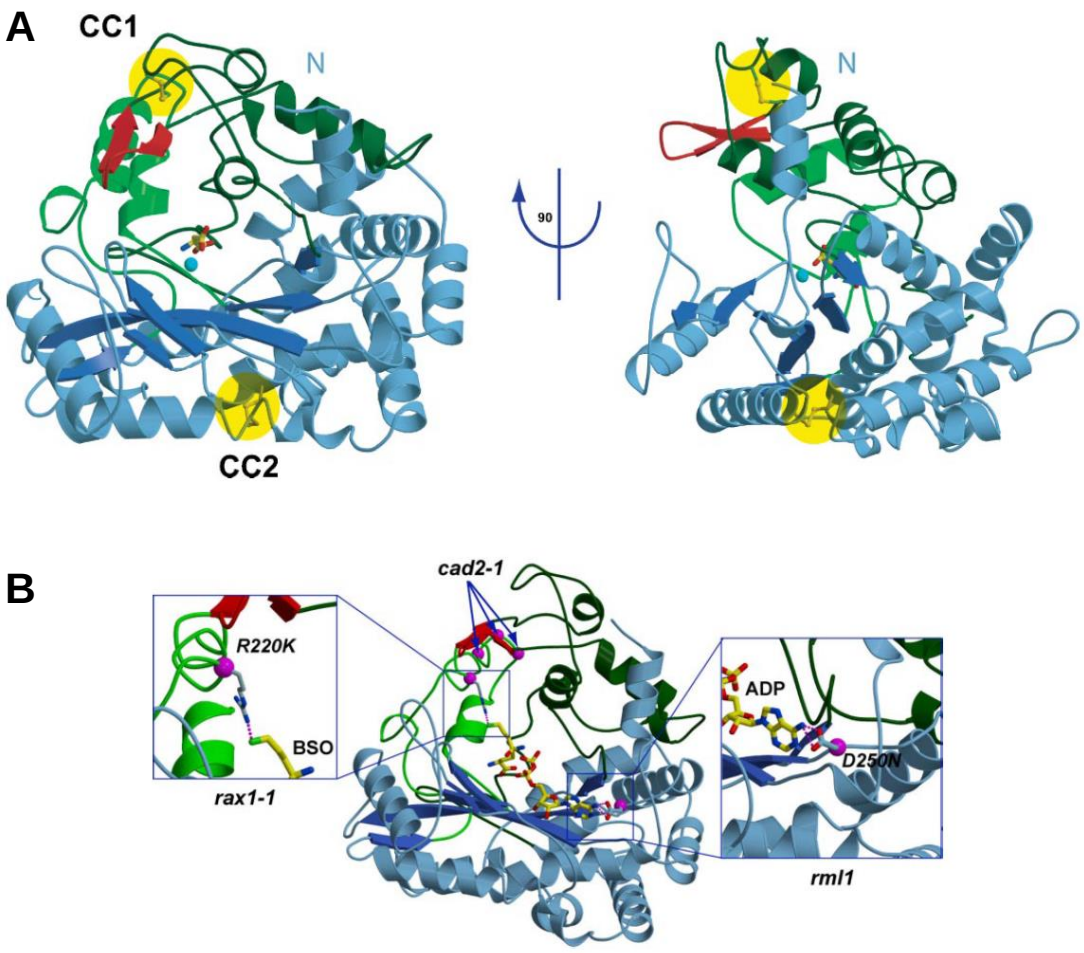

Figure 1-4: Plant GCL structural features and known mutations in the *Arabidopsis* GCL gene. A, Front (left) and side (right) views of *Brassica juncea* γ-ECS shown in ribbon representation. The central β-sheet is depicted in *dark blue*, the N- and C-terminal helical regions in *light blue*, and the plant unique arms in *dark* and *light green*, respectively. The L-glutamate bound in the active site is represented in bond representation along with the Mg^{2+} ion (in *cyan*). The two disulfide bridges CC1 and CC2 are highlighted in *yellow*; the β-hairpin module is shown in *red*. B, known mutations in the *Arabidopsis* GSH1 gene are in proximity of the substrate binding sites in plant γ-ECS. γ-ECS in ribbon representation is shown with BSO and ADP (modeled) in bonds representation (in *yellow*). *Small spheres* indicate the positions of residues affected in *Arabidopsis thaliana* γ-ECS mutant plants (in *magenta*). Enlarged versions provide models on how the affected residues in *rax1-1* and *rml1-1* mutants may interact with γ-ECS substrates. The *rax1-1* arginine residue (Arg^{220}) is shown in a modeled rotamer configuration bringing its guanidinium group in close proximity to the terminal methyl of BSO that corresponds to the sulfhydryl group of cysteine (in *green*). Interactions are highlighted by *dotted lines* (in *magenta*). Images taken from Hothorn et al., 2006.

The loss of these residues, which are described to be located in a loop region, very likely result in altered position of residues involved in substrate binding and thereby the lower γ-ECS activity and resulting lower amounts of glutathione, found in the *cad2-1* mutant, can be explained (Cobbett et al., 1998; Hothorn et al., 2006).

The most severe glutathione depletion was found in the *rml1-1* mutant (Cheng et al., 1995; Vernoux et al., 2000A). A single point mutation in the *GSH1* gene results in a substitution of aspartic acid (D) with asparagine (N) at position 258 of the GCL protein in the *rml1-1* mutant (Table 1-1; Figure 1-4B; Cheng et al., 1995; Vernoux et al., 2000A; Hothorn et al., 2006). This substitution results in a complete loss of GCL activity in the rml1-1 mutant, reflecting the importantce of the importance of the aspartic acid residue for the binding of the adenine nucleotide (Howthorn et al., 2006).

1.3 Buthionine sulfoximine and identification of the chloroquinone-like transporter

As well as mutants that are defective in GSH synthesis capacity, pharmacological tools have proved very useful in the analysis of glutathione functions in plants. In particular, buthionine sulfoximine (BSO), which is a specific inhibitor of γ-ECS that binds to the active site of the enzyme, has been widely used to inhibit GSH synthesis. BSO is structurally homologous to methionine sulfoximine (MSO), which inhibits both γ-ECS and glutamine synthetase (Griffith and Meister, 1979). Unlike MSO, however, BSO does not inhibit glutamine synthetase (Griffith and Meister, 1979) and so can be used in

studies specifically focused on the role of glutathione synthesis and concentration in plants. A screen for BSO-insensitive Arabidopsis mutants revealed the identity of the chloroplast γ-EC and GSH transporter, called chloroquine-resistance-transporter (CRT)-like transporter (CLT; Maughan et al., 2010). Three CLTs (CLT1, CLT2 and CLT3) have to date been identified in screens using knock out plants in these transporters (Maughan et al., 2010). While the growth of wild-type seedlings in the presence of BSO causes severely restricted root development (Figure 1-5), mutants lacking a functional CLT (CLT1) produced roots comparable to the wild-type, as knock-out of CLT transporters renders plants unable to facilitate BSO import into the chloroplasts, which in turn makes BSO inhibition of GSH1 impossible (Figure 1-5; Maughan et al., 2010). Additionally, all three CLTs have been confirmed to be plastid-localize in screens using transgenic plants that expressed CLT1:GFP, CLT2::GFP or CLT3:GFP respectively (Maughan et al., 2010). However, CLT1 and CLT3 in particular seem to transport BSO into the plastid (Maughan et al., 2010). And although high resistance to BSO could only be demonstrated for *clt1* mutants, *clt1clt3* double mutants exhibit even higher resistance to BSO treatment compared to *clt1* mutant plants, suggesting some functional redundancy between CLT1 and CLT3 in the maintenance of the GSH pool (Maughan et al., 2010). On the other hand, CLT2 seems to contribute much less to the mutant phenotype observed in triple *clt1clt2clt3* mutants (Maughan et al., 2010). And although complementary experiments monitoring the uptake of GSH in Xenopus oocytes, expressing either CLT1, CLT2 or CLT3, showed that all three transporters are capable of GSH transport, it seems that only CLT1 and CLT3 transport BSO into the plastid *in planta*.

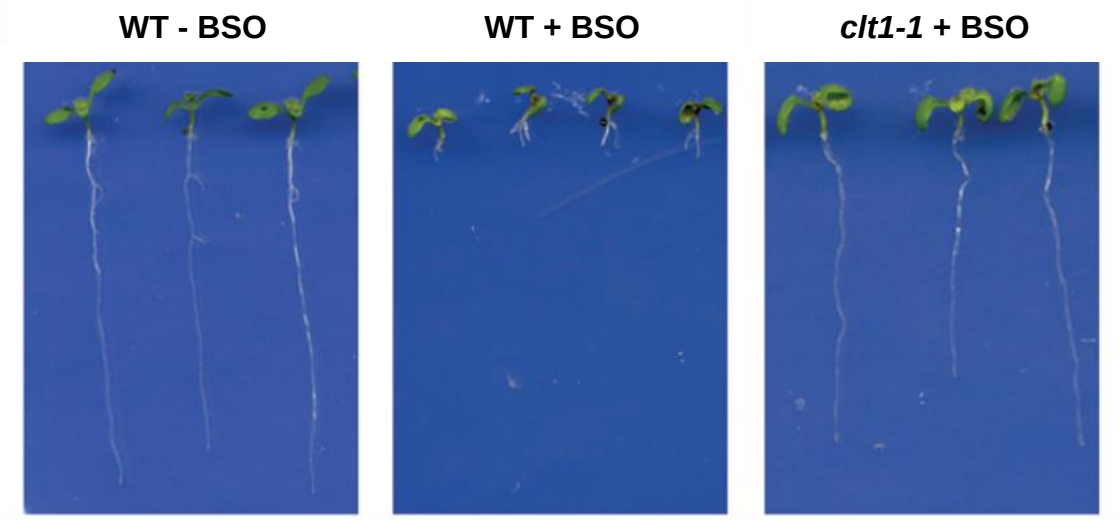

Figure 1-5: A comparison of wild-type and clt mutants grown in the presence of BSO (+ BSO) with wild-type plants grown in the absence of BSO (- BSO). WT and *clt1-1* mutant seedlings were grown for 7 days in the absence and presence of 0.8-mM BSO on vertical plates. BSO arrests WT primary root growth, whereas *clt1-1* mutations confer resistance to BSO. The image was taken from Maughan et al., 2010.

Figure 1-6: A comparison of the sensitivity to infection with *Phytophthora brassicae* for the *clt1clt2clt3* triple mutant, the *cad2-1* mutant and the wild-type. A: WT, *cad2-1*, and *clt1clt2clt3* plants were infected with *Phytophthora brassicae* and leaves were observed for spread of the infection. Even though WT plants were resistant, neither *cad2-1* nor *clt1clt2clt3* could halt the spread of infection (n = 5). B: PR1 expression was measured in leaves by qRT-PCR 3 day post infection and expressed relative to levels in the WT (mean, n = 3). The image was taken from Maughan et al., 2010.

This would also explains why a loss of function of the CLT2, which is expressed in the same tissues as CLT1 and CLT3, has little impact on the phenotypes observed in *clt1*, *clt3*, *clt1clt3* and *clt1clt2clt3* mutants (Maughan et al., 2010).

Further analysis revealed that the shoots and roots of the triple *clt* mutants (*clt1clt2clt3*) had similar amounts of glutathione compared to the wild-type, but the intracellular partitioning of glutathione between the plastids and cytosol was changed (Maughan et al., 2010). The triple *clt1clt2clt3* knockout mutant is depleted in cytosolic GSH and enriched chloroplastic GSH (Maughan et al., 2010).

Additionally, the CLT family of transporter proteins were shown transport both γ-EC and glutathione, and that depletion of the cytosolic GSH pool, as observed in *clt1clt2clt3* mutants, resulted in a more oxidized glutathione redox potential in the cytosol, as well as enhanced sensitivity to pathogens, similar to that observed in the glutathione-deficient *cad2-1* mutant (Figure 1-6). The higher sensitivity to pathogens was linked to decreased expression of pathogenesis related (PR) proteins (Maughan et al., 2010).

1.4 The functions of glutathione

Glutathione has multiple functions in plants. For example, it is involved in the detoxification of xenobiotics particularly heavy metals and in plant responses to pathogens (Parisy et al., 2007; Schlaeppi et al., 2008). GSH is the precursor for the synthesis of phytochelatins, which are oligomers of GSH that chelate heavy

metals for detoxification. The enzyme phytochelatin synthase (PCS), which is responsible for the production, also functions in xenobiotic metabolism by processing GSH S-conjugates. However, overexpression of an *Arabidopsis* PC synthase (*AtPCS1*) in transgenic plants led to an unexpected enhanced sensitivity to cadmium (Lee et al., 2003). This result is very interesting, as higher capacities to produce phytochelatins had been expected to lead to enhanced tolerance to cadmium (Lee et al., 2003). However, it was also suggested that hypersensitivity to cadmium may result from a toxicity of overly abundant phytochelatins (Lee et al., 2003).

Many of the functions of GSH in xenobiotic metabolism require enzymes called glutathione S-transferases (GST), which catalyse the S-conjugation of electrophilic xenobiotics with GSH (Edwards and Dixon, 2000). Plants contain many types of GST, for example, the Arabidopsis genome contains 55 genes encoding GST isoforms, which are often divided into 8 groups (Dixon et al., 2010). Glutathione can form an array of conjugates with endogenous and xenobiotic electrophilic compounds thanks to GST activities. Moreover, GSH interacts with nitric oxide (NO) to form S-nitrosoglutathione (GSNO; Figure 1-7), a metabolite that is important in the S-nitrosylation of protein cysteine (Cys) residues, a dominant mechanism for the regulation of many plant proteins. Enzymes called nitrosoglutathione reductases (GSNOR) or S-(hydroxymethyl)glutathione (HMGSH) dehydrogenases catalyses the NADH-dependent reduction of GSNO. GSNO may serve as a reservoir of NO in cells and may possibly also act as a transport form and NO donor in distant cells and tissues (Foyer and Noctor, 2011; Noctor et al., 2011; Noctor et al., 2012).

Many of the functions of glutathione are linked to reversible redox reactions involving the cysteine sulphur group. Like other thiols, glutathione can undergo numerous redox reactions (Figure 1-7). Oxidized forms include disulphides, either with another glutathione cysteine residue to produce glutathione disulphide (GSSG) or with a different thiol to form 'mixed disulphides', as well as more oxidized forms in which the thiol group is converted to sulfenic, sulfinic or sulfonic acids (Foyer and Noctor, 2011; Noctor et al., 2011; Noctor et al., 2012).

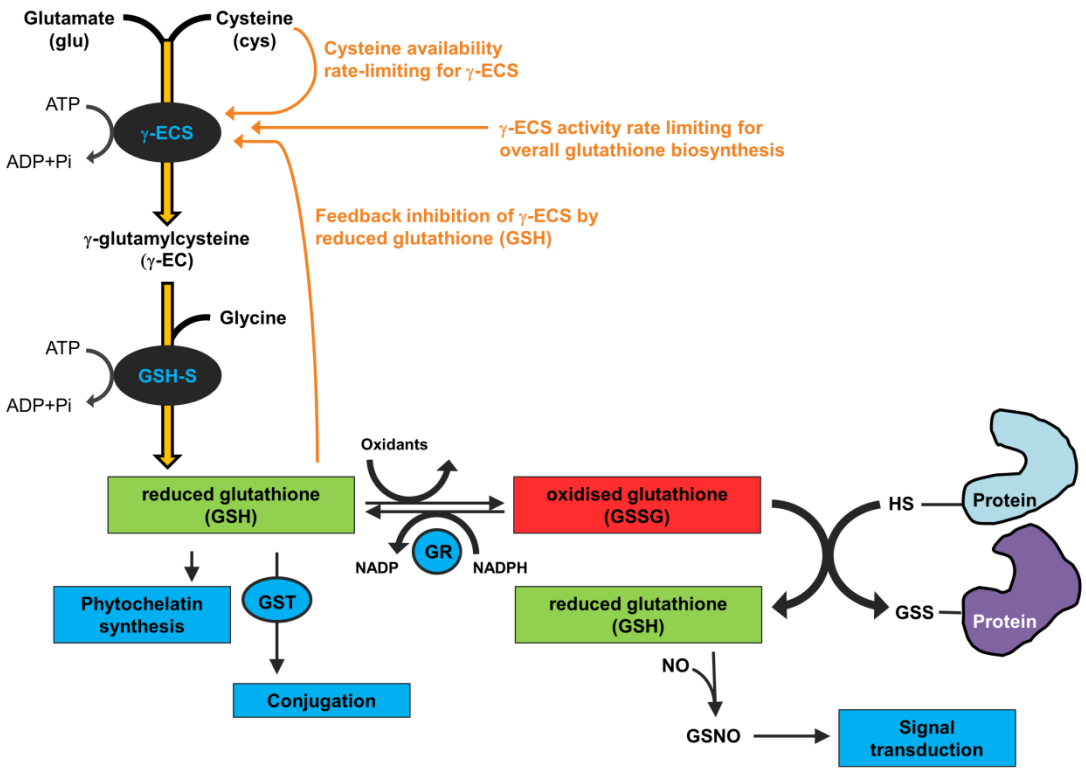

Figure 1-7: A simple model of glutathione homeostasis and functions.

Glutathione is a major low molecular weight antioxidant functioning alongside ascorbate and catalases in plant defence systems against oxidative stress. Through its interactions with ascorbate and peroxiredoxins, GSH participates

in high capacity H_2O_2-processing pathways that regulate cellular redox homeostasis and signalling (Foyer & Noctor, 2005A&B; Foyer & Noctor, 2011; Noctor et al., 2011; Noctor et al., 2012). For example, in the ascorbate-glutathione pathway GSH regenerates ascorbate by reducing DHA, either chemically or via DHARs (Dixon et al., 2002; Dixon et al., 2010). DHARs are enzymes that constitute a class of glutathione S-transferases (Dixon et al., 2010). Despite the importance of glutathione in maintaining the ascorbate pool in a mainly reduced state, the regeneration of ascorbate may be independent of GSH, as DHAR represents only one of several routes for GSH oxidation and some GSTs have previously been shown to be H_2O_2-inducible (Levine et al., 1994; Willekens et al., 1997; Vanderauwera et al., 2005; Dixon et al., 2009; Dixon et al., 2010; Foyer & Noctor, 2011).

While plant GPXs use TRXs more efficiently than GSH (Iqbal et al., 2006), some glutathione S-transferases show GSH-dependent peroxidase activity against H_2O_2 directly as well as organic peroxides (Dixon et al., 2009). Furthermore, some GST-encoding genes were shown to be strongly induced by oxidative stress (Vanderauwera et al., 2005). GSH oxidation that is independent of DHA or of chemical reactions with ROS could also occur through GRX-dependent peroxiredoxin (Rouhier et al., 2002; Tarrago et al., 2009; Foyer & Noctor, 2011).

Additionally, reactive oxygen species (ROS) such as superoxide and the hydroxyl radical were shown to be able to directly oxidize GSH at high rates. However, the relatively high cellular concentration of glutathione make it an effective antioxidant and allow it to form a highly reducing chemical barrier that

prevents excessive or uncontrolled oxidation of sensitive cellular components (Foyer & Noctor, 2011; Noctor et al., 2011; Noctor et al., 2012). The cellular glutathione pool is maintained in a predominantly reduced state by the enzyme GR which is found in the cytosol, plastids, mitochondria, and peroxisomes of plants cells and has a high affinity for GSSG and NADPH (Creissen et al., 1995; Chew et al., 2003; Kataya & Reumann, 2010; Foyer & Noctor, 2011; Noctor et al., 2011; Noctor et al., 2012). Hence, GR plays a crucial role in maintaining cellular glutathione homeostasis (Creissen et al., 1995; Chew et al., 2003; Kataya & Reumann, 2010; Foyer & Noctor, 2011; Noctor et al., 2011; Noctor et al., 2012). In Arabidopsis two GRs can be found: GR1 (cytosolic/peroxisomal localized) and GR2 (plastid-localized; Creissen et al., 1995; Chew et al., 2003; Kataya & Reumann, 2010; Yu et al., 2013).

Maintenance of a reducing environment is crucial to prevent uncontrolled oxidation of proteins and thereby maintaining their functions. And although oxidation of proteins might directly lower of overall plant vigour, it is becoming more and more evident that oxidation of target or signal molecules represents an important mechanism in plants in the perception and response to environmental and developmental triggers and that glutathione might be directly involved in determining the longevity of these signals (Foyer & Noctor, 2011; Noctor et al., 2011; Noctor et al., 2012).

1.5 Glutathione and the control of growth

While a complete description of the control of plant growth and its primary machinery controlling cell division, the cell cycle, would be too complex and

extensive for this thesis, a short induction will be presented in the following. More detailed information can be found in the following publications: Dewitte & Murray, 2003; Inze & De Veylder, 2006; Francis, 2007; Gutierrez, 2009; Komaki & Sugimoto, 2012.

To understand the control of growth in plants knowledge of the basic machinery that controls growth, the cell cycle, is required. The cell cycle is comprised of four sequential ordered stages, which can be divided into two gap phases (G1, postmitotic interphase and G2, premitotic interphase) that separate the replication of DNA (S phase, DNA synthesis) and the segregation of chromosomes (M phase, mitosis). A fifth phase would be resting stage (G0), in which cells have left the cell cycle and do not actively divide anymore (Dewitte & Murray, 2003; Inze & De Veylder, 2006; Francis, 2007; Gutierrez, 2009; Komaki & Sugimoto, 2012). G1 and G2 phase can easily be distinguished from each other by the set of chromosomes: G1 exhibits one set of chromosomes, while G2 has duplicated set of chromosomes in the nucleus (Dewitte & Murray, 2003; Inze & De Veylder, 2006; Francis, 2007; Gutierrez, 2009). Regulatory proteins, such as cyclins (CYC) and cyclin-dependent kinases (CDK) govern progression through the cell cycle (Dewitte & Murray, 2003; Inze & De Veylder, 2006; Francis, 2007; Gutierrez, 2009). Different CDK-cyclin complexes can phosphorylate a large number of substrates at two key transition points within the cell cycle to trigger the onset of DNA replication and mitosis, respectively (Dewitte & Murray, 2003; Inze & De Veylder, 2006; Francis, 2007; Gutierrez, 2009; Komaki & Sugimoto, 2012). As G1 and G2 gap phases are considered control points within the cell cycle that allow the operation of control mechanisms, which ensure that the respective previous

stage has been fully completed, the above mentioned key transition points are G1 to S (G1/S) and G2 to M (G2/M), each allowing for a possible arrest of the cell cycle (Dewitte & Murray, 2003; Inze & De Veylder, 2006; Francis, 2007; Gutierrez, 2009; Komaki & Sugimoto, 2012).

While research over the past 50 years provided detailled insights into the impact of plant hormones on cell proliferation, showing the crucial importance of cytokinins and auxins, as well as their direct influence on cell proliferation (Dewitte & Murray, 2003), a further focus was given to the cellular redox status as a further regulator of cell cycle progression (May et al., 1998). Cytokinins that act in concert with auxin, were shown to directly induce the cyclin CYCD3;1 (Dewitte & Murray, 2003). But further evidence strengthens the view that the cellular redox status regulates the progression of the cell cycle, particularly leading to an arrest of the cell cycle upon exposure to stress in plant cells (May et al., 1998), and that the cellular redox status also acts as a crucial regulator of the cell cycle in embryonic stem cells (Menon et al., 2003; Menon and Goswami, 2007). As unravelling the interplay of hormones and cellular redox state in the control of the cell cycle is very complex, further research needs to evaluate the individual contribution of hormones and cellular redox state in the control of cell proliferation. Glutathione as one of the major antioxidants in plants was therefore the main focus of this thesis. The aim was to determine its impact on plant growth and to evaluate the extent to which it participates in the control of the cell cycle. For example, it has been proposed that there is a change in the intracellular compartmentation of GSH between the nucleus and cytosol at G1, as illustrated in Figure 1-8 (Diaz-Vivancos et al., 2010B).

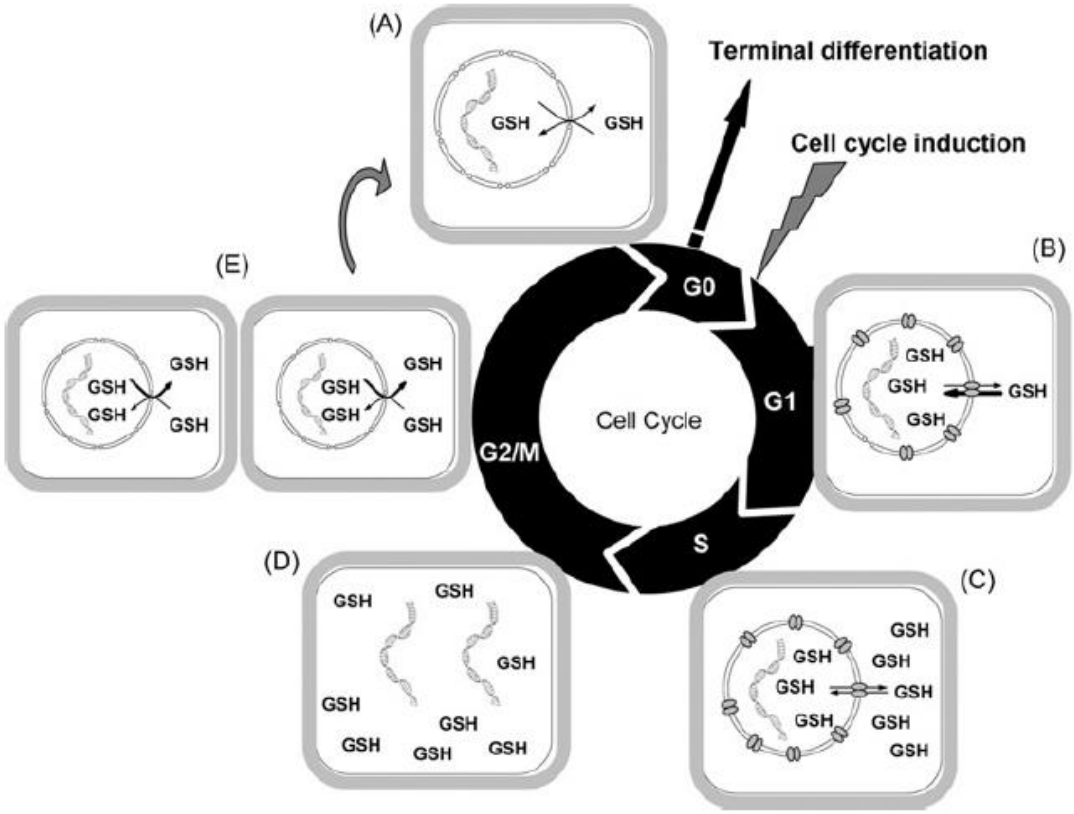

Figure 1-8: The glutathione cycle within the eukaryotic cell cycle. Shown here is a model for intracellular GSH partitioning between nucleus and the cytoplasm and its effects on whole cell glutathione homeostasis during the cell cycle derived from studies on mammalian and plant cells (Markovic et al., 2007; Pallardó et al., 2009; Diaz-Vivancos et al., 2010A, B; Pellny et al., 2009). Prior to initiation of the cell cycle (A) GSH is equally distributed between cytoplasm and nucleus. An appropriate cell cycle trigger (cell cycle induction) causes changes in nuclear envelope transport properties (B) that include orchestration of GSH-transporting proteins that are either rapidly synthesised *de novo* or activated in order to recruit and sequester GSH in the nucleus. GSH sequestration into the nucleus has immediate repercussions for the cytoplasm that is starved of GSH. This causes rapid *de novo* GSH synthesis and accumulation. GSH synthesis is stimulated until the GSH pools in the nucleus and cytoplasm reach similar levels (C). The cellular GSH pool is divided between the newly formed daughter cells (re-distribution; D). Some GSH degradation may occur, so that the cellular GSH pools fall to a low level. Presumably, the GSH-transporting proteins in the nuclear envelope are either inactivated or degraded so that the GSH pools reach in the nucleus and cytoplasms are again in equilibrium (A). Image was taken from Diaz-Vivancos et al., 2010A.

GSH co-localises with nuclear DNA at the early stages of cell proliferation in plant and animal cells (Markovic et al., 2007; Pallardó et al., 2009; Diaz-Vivancos et al., 2010A, B; Pellny et al, 2009). In particular cytosolic GSH is essential in preventing uncontrolled oxidation of proteins and can therefore be considered to form a barrier protecting (Diaz-Vivancos et al., 2010A & B). However, GSH recruitment and sequestration in the nucleus during the G1 and S phases of the cell cycle was shown to have a profound impact on gene expression.

In particular, the cellular oxidative protection is lowered when GSH is localized in the nucleus, possibly leading to more oxidized conditions in the cytosol (Diaz-Vivancos et al., 2010A & B).

Furthermore, the root phenotype of the *rml1-1* mutants and wild-type plants treated with BSO, as illustrated in Figure 1-9, is also linked to effects on the cell cycle (Cheng et al., 1995; Vernoux et al, 2000). As discussed above the *Arabidopsis rml1-1* mutant, which has only about 3 % of the wild-type GSH levels, is characterised by a drastically reduced root system, all illustrated in Figure 1-9 (Cheng et al., 1995; Vernoux et al, 2000). The growth of the primary root of the *rml1-1* mutants stops at the stage of 17 cells in length because of cell cycle arrest (Cheng et al., 1995). Nevertheless, the embryonic root undergoes some differentiation with the formation of vascular tissue etc. Such observations demonstrate the requirement for GSH in the maintenance of cell proliferation at the root tip, after the stage where the root primordium has fully formed.

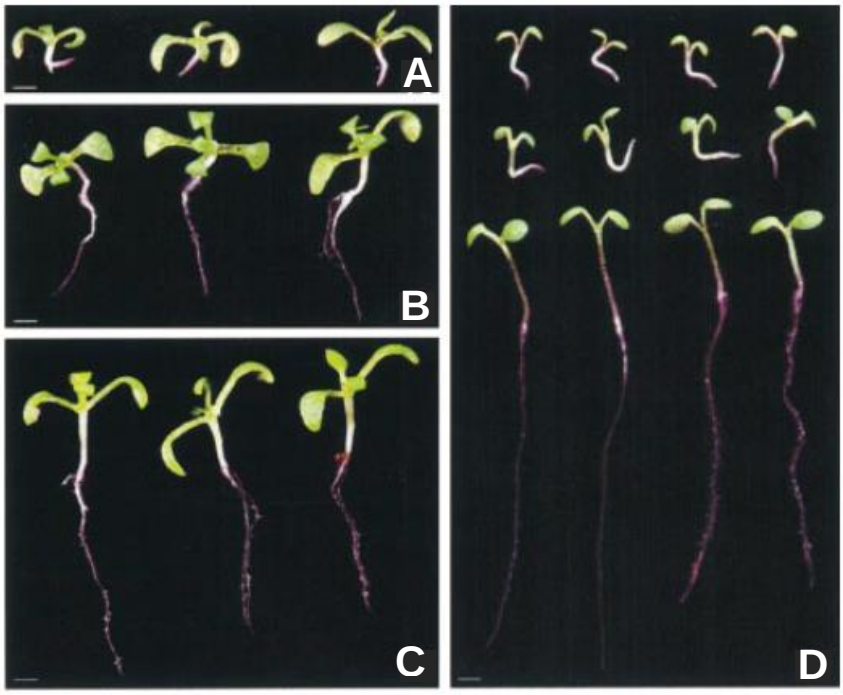

Figure 1-9: A comparison of *rml1-1* with wild-type plants grown in the absence and presence of BSO. A: *rml1-1* seedlings at 14 days after germination (DAG) grown on two fifths MS medium. Note the short (~1 mm) roots. B: *rml1-1* seedlings at 14 DAG grown on two-fifths MS medium supplemented with 250 mM γ-EC. C: *rml1-1* seedlings at 14 DAG grown on two-fifths MS medium supplemented with 250 mM GSH. D: Top, *rml1-1* seedlings at 7 DAG grown on two-fifths MS medium; middle, wild-type seedlings at 7 DAG grown on two-fifths MS medium supplemented with 2.5 mM BSO; bottom, wild-type seedlings at 7 DAG grown on two-fifths MS medium. The image was taken from Vernoux et al., 2000A.

1.6 Interactions between glutathione and auxin in the regulation of root development

Auxin is an important plant hormone controlling plant growth and development. It is involved in the development of many organs, gametogenesis, embryogenesis, seedling growth, vascular patterning and the initiation of floral and root meristems including lateral roots, as well as in other processes such as gravitropism, (Mattsson et al., 2003; Zhao, Y., 2010; Marchent et al., 1999; De Smet et al., 2010).

Recent studies have revealed a link between glutathione and auxin in control of root growth in Arabidopsis (Bashandy et al., 2010; Koprivova et al., 2010). The inhibition of GSH biosynthesis by BSO provided evidence of mis-regulation in auxin transport (Koprivova et al., 2010). Some auxin signalling mutants such as *axr1-12* and *axr3-1* were shown to be less sensitive to BSO-mediated inhibition of root growth than the wild-type (Koprivova et al., 2010). Moreover, the addition of BSO led to a disappearance of the auxin maximum in the root tips and the loss of expression of the auxin efflux carrier PIN1 and of the quiescent centre (QC) marker $AGL42_{Pro}$::GFP at higher BSO concentrations, as illustrated in Figure 1-10 (Koprivova et al., 2010).

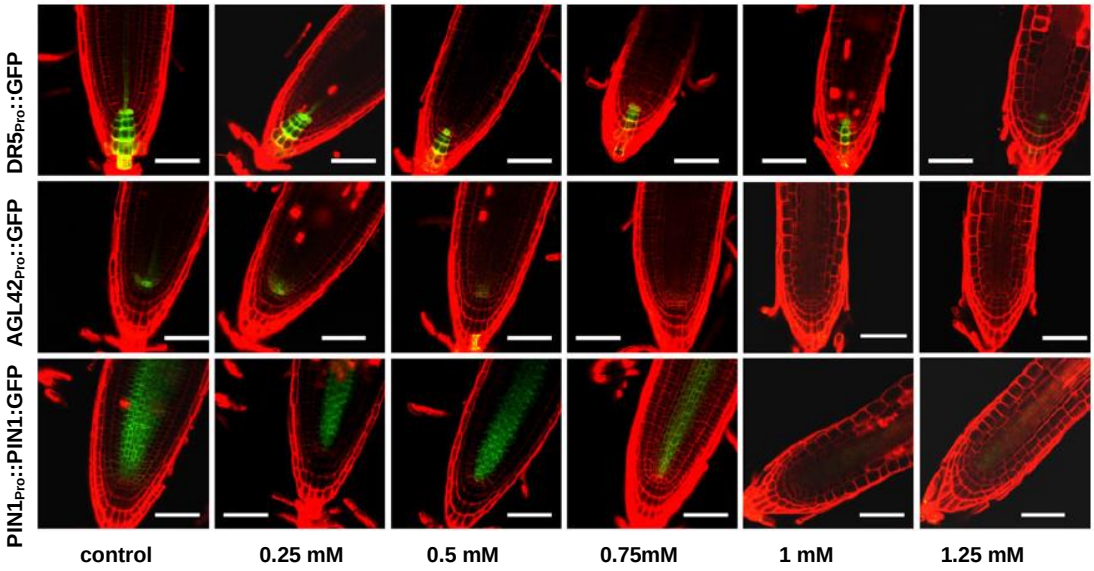

Figure 1-10: BSO inhibits the expression of the auxin efflux transporter PIN1. Arabidopsis $DR5_{Pro}$::GFP, $AGL42_{Pro}$::GFP and $PIN1_{Pro}$::PIN1:GFP lines were grown for 6 days on vertical MS-phytagel plates supplemented with increasing concentrations of BSO. Roots were stained with propidium iodide and GFP fluorescence was recorded by confocal microscopy. Bar 50 µm. Image was taken from Koprivova et al., 2010.

However, a microarray analysis of BSO-treated wild-type roots relative to wild-type roots in the absence of the inhibitor showed that the expression of less than 100 genes was significantly changed and no specific pathways or processes that were regulated by BSO could be identified (Koprivova et al., 2010). Nevertheless, there was some similarity between some of the genes up-regulated by BSO and those affected by inhibitors of auxin synthesis and transport. In the analysis reported by Koprivova et al. (2010), the effects of BSO were complemented by dithiothreitol (DTT) leading to the conclusion that a post-transcriptional redox mechanism was involved in the regulation of PIN proteins, and hence auxin transport to the root tip.

Studies performed crossing of the *ntra ntrb* mutants that lack the cytosolic and mitochondrial thioredoxin reductases (NTR) NTRA and NTRB, with *rml1-1* led to the failure of meristematic activity in shoots as well as roots, demonstrating overlapping functions of the glutathione and thioredoxin systems in shoot meristem activity (Reichheld et al., 2007). In contrast, the *ntra ntrb cad2* triple mutants that retain a greater capacity for glutathione biosynthesis than *rml1-1* mutations provided evidence that thiol reduction pathways are required for developmental processes associated with auxin signalling (Bashandy et al., 2010). The *ntra ntrb cad2* mutant has an interesting phenotype with the loss of apical dominance, vasculature defects, and reduced secondary root production that suggest impaired auxin signalling (Bashandy et al., 2010). Crucially, the *ntra ntrb cad2* mutants develop in a similar manner to the wild-type during vegetative development, but following the floral transition, the *ntra ntrb cad2* mutants produced naked stems, as illustrated in Figure 1-11. The flowerless phenotype of the *ntra ntrb cad2* mutant is similar to the phenotypes of mutants

affected in polar auxin transport or biosynthesis (*pin1*; Vernoux et al., 2000B; Bashandy et al., 2010; 2011).

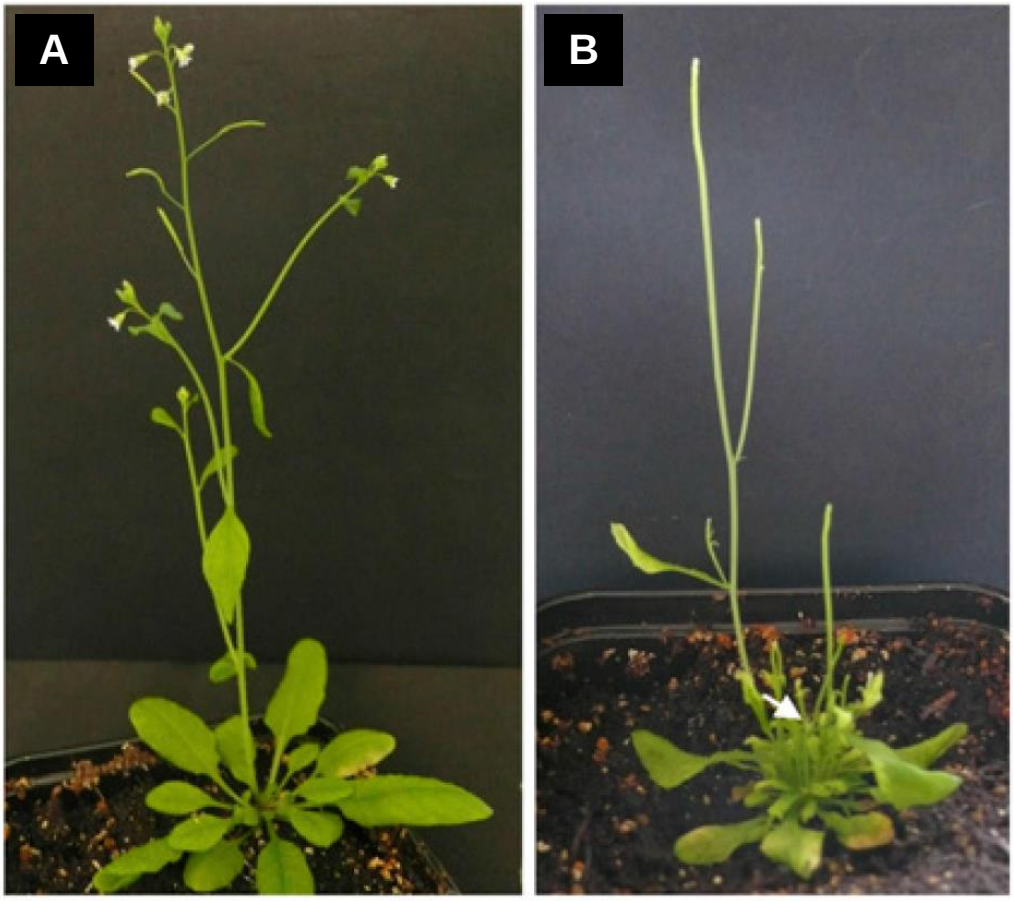

Figure 1-11: A comparison of the phenotype of the *ntra ntrb cad2* mutant the wild-type. A comparison of the phenotypes was performed in five-week-old wild-type (Col-0) (A) and *ntra ntrb cad2* (B) plants. Arrows indicate emergence of secondary rosette stems in *ntra ntrb cad2*, which were not observed in the wild-type at this stage. The image was taken from Bashandy et al., 2010.

An analysis of the different phenotypes listed in Figure 1-12, led to the conclusion that the pin-like phenotype of *ntra ntrb cad2* shoots illustrated in Figure 1-11 is the result of a combination of effects related to perturbed auxin synthesis and auxin transport while the root phenotype is may be more related to the perturbation of polar auxin transport. These observations led to the model shown in Figure 1-13 as a way to explain the links between GSH and

TRX pathways in the control of inflorescence development in Arabidopsis (Bashandy et al., 2011).

	Wt	*cad2*	*ntra ntrb*	*ntra ntrb cad2*	*pin1*
P.A.T.	++	+/-	+	-	-
auxin level	+	+	+	+/-	+
pin-like phenotype	-	-	-	+	+
root growth	-	+/-	+/-	+	+/-

Gray cells represent parameters that are affected in the mutants. ++, +, +/-, - represent different levels of perturbations.

Figure 1-12: Summary of auxin-related phenotypes observed in the mutants in the study by Bashandy et al. (2011). The image was taken from Bashandy et al., 2011. P.A.T. = polar auxin transport.

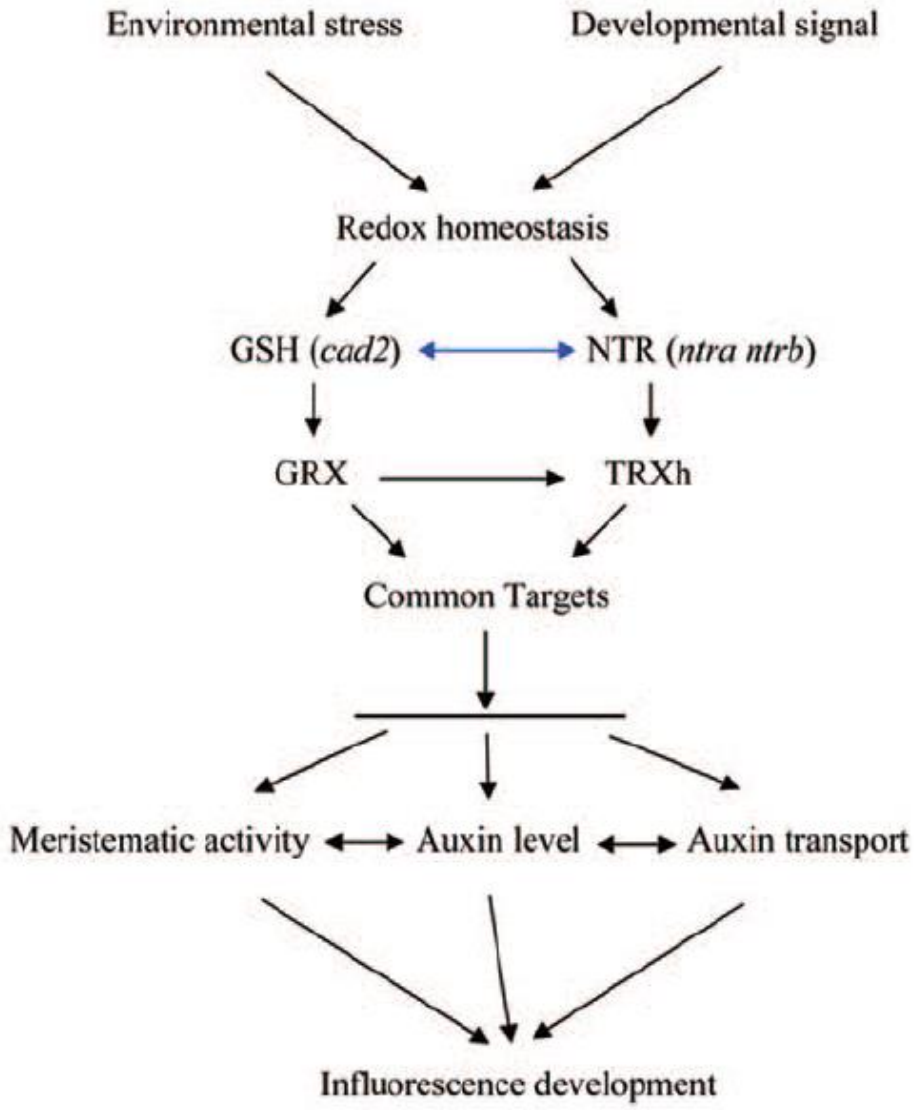

Figure 1-13: Hypothetical model explaining the link between cellular redox status and auxin signaling in controlling inflorescence development in Arabidopsis. The image was taken from Bashandy et al., 2011. Modification of redox homeostasis triggered by environmental stress or by developmental signals is relayed by glutathione and NTR .The triple *ntra ntrb cad2* mutant generated by crossing *ntra ntrb* and *cad2* mutants (blue doubleheaded arrow) is mimicking the redox perturbation. Inactivation of NTR and decreased GSH availability is relayed by mis-reduction of GRX and TR Xh and subsequently of TR Xh/GRX target protein(s). These redox regulated target protein(s) are involved in meristem activity or/and auxin metabolism and their mis-reduction in the *ntra ntrb cad2* leads to perturbation of inflorescence development and auxin metabolism. Black arrows refer to the direction of reduction, crossing is marked by a blue double-headed arrow and inefficient reduction by a horizontal line. The *ntra ntrb cad2* developmental defect is caused by meristematic activity, auxin level, auxin transport or a combination of the three (Bashandy et al., 2011).

1.7 Hypothesis

Although GSH is clearly required for the operation of the cell cycle, with other roles apparent in plant growth and development, the mechanisms by which it exerts these effects remain poorly characterised. An in-depth characterisation of the growth and defence responses of mutants that are defective in glutathione synthesis will provide new insights into the mechanisms that underpin the multiple functions of GSH in plants. Moreover, transcript profiling of the *rml1-1* mutant will increase our understanding of GSH-dependent regulation of gene expression that underpins effects on plant growth and development.

2 Project aims

The overall aim of this project was to provide new mechanistic information concerning the GSH functions in plants, with a particular focus on growth and abiotic stress tolerance in *Arabidopsis thaliana*. A multidisciplinary approach was employed in these studies incorporating phenomic and transcriptomic techniques, as well as *in vivo* measurements of the glutathione redox potentials of the nucleus and cytosol using a roGFP probe.

A range of *Arabidopsis thaliana* mutants with defects in either the synthesis or transport of GSH was used in this study. Together with a pharmacological approach using BSO, these mutant lines were used to characterise the glutathione redox potentials of the nucleus and cytosol and to define GSH-responsive genes. The ultimate aim was to link the information obtained from these different approaches with effects of low GSH, or of altered intracellular partitioning of GSH, on growth and abiotic stress tolerance in order to identify the mechanisms of GSH action in plants.

3 Chapter 3: Materials and Methods

3.1 Plant materials and growth conditions

Seeds for wild-type *Arabidopsis thaliana* accession Columbia 0 (Col0), *cad2-1* (Cobbett et al, 1998), *pad2-1* (Parisy et al., 2007), *rax1-1* (Ball et al., 2004), *rml1-1* (Vernoux et al., 2000A & Cheng et al., 1995) and *clt* triple mutants (Maughan et al., 2010), were used in these studies. Seeds of the *rml1-1* and *rax1-1* mutants were obtained from Jean-Philippe Reichheld (Universitè de Perpignan, France) and Phil Mullineaux (University of Essex, United Kingdom) respectively. Seeds of the triple *clt* and the *cad2-1* mutants were obtained from Christopher Cobbett (University of Melbourne, Australia). All mutant lines have the Col0 background. The transgenic lines GL2 (Deal and Henikoff, 2010b) and roGFP2 (Meyer et al., 2007) were obtained from Roger B. Deal and Steven Henikoff (Fred Hutchinson Cancer Research Centre, Seattle, USA) and from Andreas Meyer (Heidelberg Institute of Plant Sciences, Heidelberg, Germany) respectively. Seeds were surface sterilized either in 70% Ethanol or with a mixture of bleach and hydrogen chloride (HCl) prior to sowing.

All plants were grown on agar media on plates in controlled environmental cabinets under an irradiance of 150 µmol m^{-2} s^{-1} with a photoperiod of 16 hours, a constant temperature of 22 °C ± 2 °C, and a relative humidity of 60 %, for up 21 days. The following types of plates were used in these experiments: 90 mm round plates (Thermo Fisher Scientific, Sterilin, Cat. No.: BS EN 24998:2008, Waltham, MA, USA), 150 mm round Falcon dishes (BD Falcon, Cat. No.: 353025, Franklin Lakes, NJ, USA) or 120 x 120 mm square plates (Gosselin, Cat. No.: BP124-05, Hazebrouck, France). Plates were sealed

either with Parafilm (Parafilm, Chicago, IL, USA), Urgopore (Urgo GmbH, Sulzbach, Germany) or Micropore (3M Company, Maplewood, MN, USA) tape.

3.2 Growth media

Several types of media (designated I, II, III and IV) were used in these experiments (see Appendix I to IV for media compositions). Media were sterilized in an autoclave at 121 °C for 20 minutes at a pressure of 1 bar, and then allowed to cool to 55 °C before plates were poured under sterile conditions in a laminar flow hood. For the stress experiments, described in sections 3.4.2.1 (Induced stress treatments) and 3.4.2.2 (Continuous stress treatments) various reagents were added to the media after sterilization. Plates were poured immediately prior to each experiment.

3.3 Determinations of root growth

Root growth was measured on 90 mm round petri dishes or 120 x 120 mm square plates containing solid growth medium III or medium IV (Appendix III; Appendix IV). For the experiments on round petri dishes, the upper third of the medium was removed. In all cases, except for the *rml1-1*, where root growth was determined for roots grown inside the medium, surface sterilized seeds were placed along the cut edge of the medium as illustrated in Figure 3-1A, leaving a distance of 5 to 7 mm between seeds, so that the roots grew vertically into the media, leaving sufficient space for root growth, ensuring that the roots from each seedling did not grow into each other. In the case of the *rml1-1* seeds were placed directly on top of the media. For the experiments on

square plates, seeds were placed in two rows onto the media as illustrated in Figure 3-1B such that roots grew along the surface of the media.

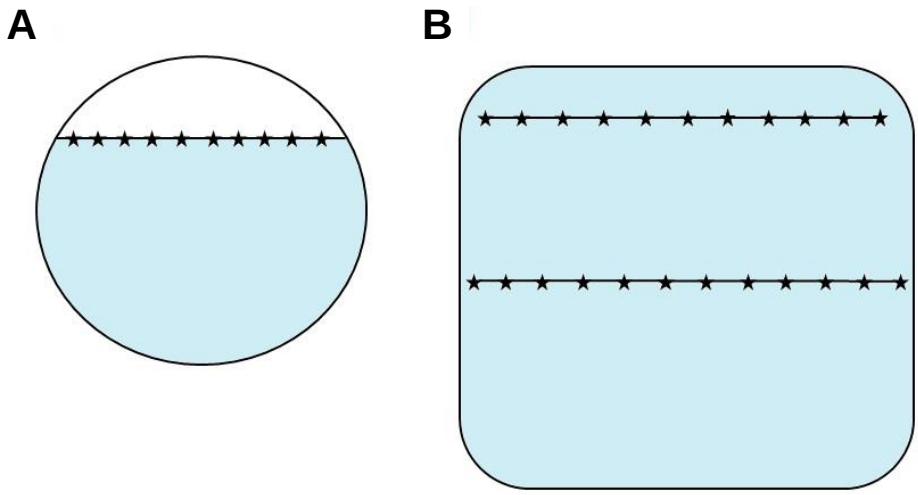

Figure 3-1: Schematic representation of seed placement for the root architecture experiments. A: 9 cm round petri dishes with upper third of the medium removed. B: 120x120mm square plates; blue represents the media; the black stars represent the individual seeds.

Each experiment consisted of 5 plates per genotype containing either 10 (round petri dishes) or 23 (square plates) seeds per plate. In all cases, plates were sealed using Parafilm and placed in a vertical orientation, in the growth chambers, as shown in Figure 3-2.

Plants were allowed to grow for either 7 (square plates) or 10 days (round petri dishes) after which photographs of the roots were taken against a black background at a distance of 35 cm using either a Panasonic Lumix DMC-TC9 camera (Panasonic Corporation, Osaka, Japan) or a Nikon D5100 with an 18-55 mm f/3.5-5.6G VR objective (Nikon Corporation, Tokyo, Japan).

Measurements of primary root length, lateral root length and the number of lateral roots were made from the photographs using Image J version 1.41a software (http://rsbweb.nih.gov/ij/; Rasband et al., 1997-2012; Abramoff et al., 2004).

Figure 3-2: Representative picture of plates in vertical orientation in growth chambers. A: 90 mm round plates and B: 120 x 120 mm square plates.

Data obtained was further processed in Microsoft Excel 2010 (Microsoft Corporation, Redmond, WA, USA) and statistical analysis was performed using SPSS 20 (IBM Corporation, Armonk, NY, USA).

3.4 Determinations of shoot growth and stress tolerance

This part of the work was undertaken in collaboration with Bayer BioScience N.V., who was a partner on the EU ITN Network that supported my PhD research project. Bayer BioScience N.V., is located in Gent, Belgium (Figure 3-3) and is the largest innovation centre of Bayer CropScience world-wide engaging in research, development and marketing of seeds and solutions derived from breeding and biotechnology.

The Gent site houses an extensive phenomics facility, where plants are routinely screened for growth and stress tolerance. The experiments described in the following were performed according to parameters (, such as e.g. light intensities, length of stress exposure and evaluation of experiments) of these routine screenings within Bayer BioScience N.V.

Figure 3-3: Building of Bayer BioScience N.V., Gent, Belgium (http://www.mybayerjob.be/export/sites/erecruiting_be/images/Image_gallery/ Ghent .jpg)

3.4.1 Determinations of shoot growth under standard conditions

Seeds of the wild-type (Col-0) and *cad2-1*, *pad2-1*, *rax1-1* and *clt* mutants were sown on a sterile 1 µm filter mesh, which was placed on the growth medium II (Appendix II) prior to sowing. Shoot growth was determined over a period of 17 days under standard conditions or 17 days in short-term stress treatments, and 14 days for plants subjected to long- term stress conditions. Stress treatments were performed as described below.

For standard growth conditions, photographs were taken with a Canon EOS 450 D (Canon Inc., Tokyo, Japan) at 66 cm distance with automatic zoom and

a shutter speed of 1/250 and an aperture of 1/11, on days 7, 10, 11, 12, 14 and 17 after sowing. Leaf area was measured using ImageJ 1.41a and values processed using Microsoft Excel 2010.

3.4.2 Determinations of shoot growth under stress conditions

For induced stress treatments, photographs were taken on days 10, 11, 12, 14 and 17, and for continuous stress treatments, photographs were taken only on days 11 and 14. Images were analysed using Fiji ImageJ (http://fiji.sc/, Schindelin et al., 2012) with an in-house macro from Bayer BioSciences N.V. and statistical analysis of the data was performed with R (www.r-project.org, Hornik, 2013) using in-house macros from Bayer BioScience N.V.

3.4.2.1 Induced stress treatments

For these experiments, seeds were sown on a sterile 1 µm filter mesh, which was placed on the growth medium II (Appendix II: Composition of growth medium II:) prior to sowing. Seedlings were grown for 10 days under standard conditions and then transferred with the mesh to plates containing growth medium II with no further additions (control), or growth media II containing either paraquat (1 µM), hydrogen peroxide (4 mM), sorbitol (100 mM), or sodium chloride (75 mM). Seedlings were then grown for a further 8 days under these conditions and growth analysis performed as described below.

A further set of experiments was performed to study the effects of high light stress. For this treatment, seedlings were grown for 10 days under standard light levels and then transferred to high irradiance (400 µmol m^{-2} s^{-1}) for

4 days, after which they were transferred back to standard light conditions for a further 4 days. Although 400 µmol m^{-2} s^{-1} used in the high light experiments cannot be considered photoinhibitory conditions, this was the maximum possible light intensity that could be obtained. However, relative to the standard conditions (150 µmol m^{-2} s^{-1}) 400 µmol m^{-2} s^{-1} can be considered as relative high light. Each experiment consisted of four plates (32 seeds per plate) per genotype and stress treatment. Each experiment was repeated 3 times.

3.4.2.2 Continuous stress treatments

For these experiments, seeds were sown on plates containing growth medium II with no further additions (control), or containing paraquat (0.1 µM), 3-methoxybenzamide (0.2 mM), paraquat (0.1 µM) plus 3-methoxybenzamide (0.2 mM), sorbitol (100 mM) and sodium chloride (75 mM). Seedlings were grown for 14 days under stress conditions. Each experiment consisted of four plates (32 seeds per plate) per genotype and stress treatment. Each experiment was repeated 3 times.

3.5 Transcriptome analysis

For these experiments, seeds of the wild-type (Col0) and a heterozygous population of *rml1-1* seeds were placed on growth medium III (Appendix III:) and grown on vertical plates for 7 days. In total, this experiment comprised 100 plates for the wild-type and 3000 plates for the *rml1-1*. After 7 days the homozygous *rml1-1* plantlets were identified by their characteristic root

phenotype (an arrest of root growth) compared to heterozygous *rml1-1* and wild-type plants, as illustrated in Figure 3-4.

The shoots of the wild-type and *rml1-1* seedlings were removed from the roots with sharp fine scissors by cutting across the transition zone between stem and root. Samples with a minimum of 100 roots or shoots per sample were prepared. Pooled material was placed in labelled 1.5 mL Eppendorf tubes on ice during harvest. Samples were immediately frozen in liquid N_2 and stored at -80°C until RNA extraction. A total of three biological replicates were prepared for the wild-type shoot and root tissues. In the case of the *rml1-1* mutant three biological replicates could be prepared for the shoot. However, only one biological replication could be obtained for *rml1-1* root tissue.

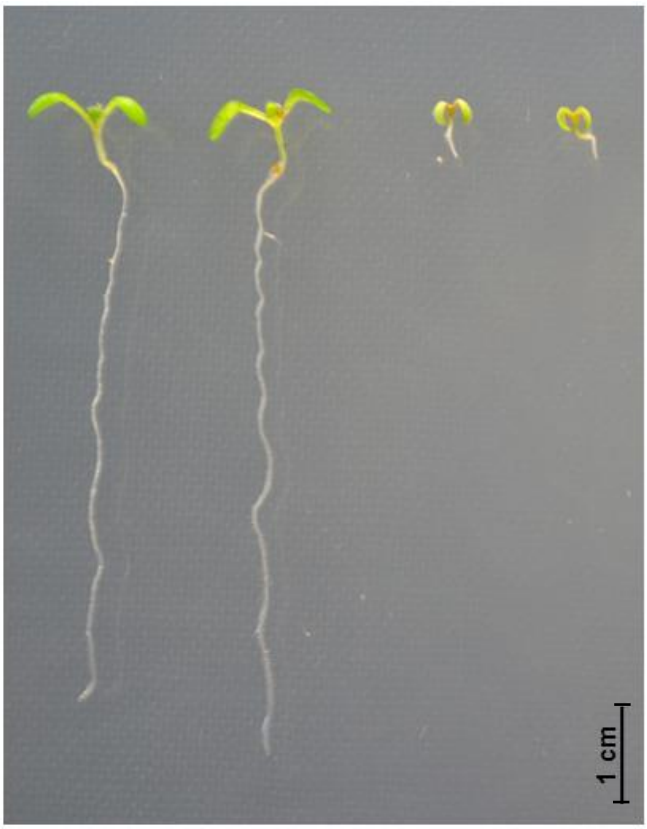

Figure 3-4: Comparison of wild-type plants with the *rml1-1* phenotype on the day of harvest. Shown are 7-day old plants; left: wild-type, Col0; right: *rml1-1.*

3.5.1 RNA extractions

Samples were ground to a fine powder in 1.5 mL Eppendorf tubes and RNA extractions were performed according to the protocol of the RNAeasy Mini Kit (Qiagen, Cat. No.: 74904, Hilden, Germany). The purity of the samples and RNA concentrations were measured using a Nano Drop ND-1000 device (Nano Drop Technologies, Wilmington, DE, USA). The RNA extracts used in these experiments had a ratio of absorbance of 1.8-2.0 (A_{280}/A_{260}) when measured at 280 nm and 260 nm respectively and >1.8 (A_{260}/A_{230}) when measured at 260 nm and 230 nm respectively, in order to assure sufficient purity.

3.5.2 Agronomics1 tiling arrays

RNA samples were sent to the microarray facility of the Vlanders Institute of Biotechnology in Leuven, Belgium (MAF VIB, Leuven, Belgium; http://www.nucleomics.be/) for microarray analysis on Agronomics1 tiling arrays (http://www.agron-omics.eu/index.php/resource_center/tiling-array). Microarray target preparation and array hybridization were performed at the VIB according to the Agronomics1 Standard Operating Procedures (Agronomics1 SOP, 2011; www.agron-omics.eu; Rehrauer et al., 2010), as described below. Data and gene ontology analyses were performed at the University of Leeds as described further below. And the full microarray data can be found at NCBI GEO as Series GSE36893 (http://www.ncbi.nlm.nih.gov/geo/query/acc.cgi?acc=GSE36893).

Microarray target preparation

Preparation of the RNA samples for array hybridization was performed using the GeneChip® 3' IVT Express Kit (Affymetrix, Cat. No.: 901229, Santa Clara, CA, USA). This Kit includes the steps of reverse transcription of the first cDNA strand, synthesis of the second cDNA strand, biotin labelling of antisense RNA (aRNA), purification and fragmentation. An overview of the workflow is depicted in Figure 3-5.

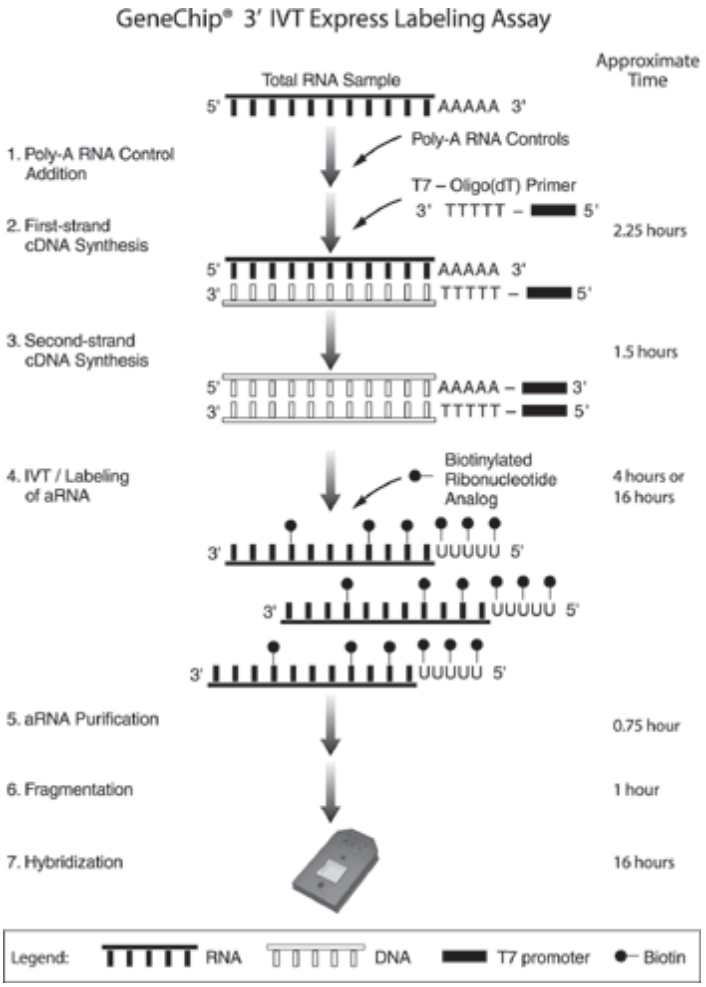

Figure 3-5: Schematic representation of the GeneChip® 3' IVT Express assay. (http://www.affymetrix.com/_media/images/figures/expresskit_labeling _assay_lg.gif, 2011).

A minimum of 50 ng of RNA were required for double-strand cDNA synthesis. After synthesis of double-stranded cDNA the quality and quantity of biotinylated cRNA was tested using a NanoDrop ND 1000 and Bioanalyzer 2100, prior to random fragmentation into 35-200 bp fragments at 94 °C in fragmentation buffer (Affymetrix, Cat. No.: 900371, Santa Clara, CA, USA).

Array hybridization

The fragmented aRNA samples were mixed with Hybridization Mix (Affymetrix, Cat. No.: 900720, Santa Clara, CA, USA), Hybridization Controls and Control Oligonucleotide B2 (Affymetrix, Cat. No.: 900454, Santa Clara, CA, USA) to a final volume of 300 µL according to manufacturer's recommendations.

The samples were then hybridized onto Agronomics1 arrays for 16 hours at 45 °C. After these 16 hours the arrays were washed in an Affymetrix Fluidics Station 450 using the FS450_0004 protocol and the arrays were subsequently scanned on an Affymetrix GeneChip Scanner 3000 (Agronomics1 SOP, 2011; www.agron-omics.eu; Rehrauer et al., 2010).

Data analysis

The data generated from the Agronomics1 tiling arrays was provided MAF VIB as a Microsoft Excel file containing robust microarray averaging (RMA) expression values, false discovery rates (FDR), fold-changes (FC) as well as p-values, Affymetrix IDs and AGI codes. A pre-selection of the transcripts in shoot datasets was performed based on p-values ($p<0.05$) and false discovery rate ($FDR<0.05$), in order to retain only transcripts whose abundance was significantly different in *rml1-1* tissues relative to wild-type. Thereafter,

transcripts with a 2-fold or higher change in abundance relative to wild-type were selected for further analysis. Despite major efforts, extractable RNA from the roots of the *rml1-1* allowed only for the analysis of on biological replication. Hence, for the root datasets, the selection of transcripts was based only on fold-change values.

Gene ontology analysis

Gene ontology analysis was performed using BINGO cytoscape 2.8.1 (Maere et al., 2005) and MapMan 3.5.1 (Thimm et al., 2004). Multi experiment Viewer 4.6.2 (from The Institute for Genomic Research; TIGR-MeV) was used for the generation of heat maps (Saeed et al., 2003).

3.6 Quantitative Real-Time (RT)-PCR (qRT-PCR)

In all cases qRT-PCR was performed on tissues harvested from 7 day-old plants that had been grown on vertical plates containing growth medium III (Appendix III: **Composition of growth medium III**), as described above. Root and shoot samples were harvested and pooled as described above and placed in 2.0 mL Eppendorf tubes containing two 3 mm stainless steel beads (Qiagen, Cat. No.: 69997, Hilden Germany) and extraction performed essentially as described in section 2.6 (Transcriptome analysis) except that frozen samples were ground to a fine powder in a TissueLyser LT (Qiagen, Cat. No.: 85600, Hilden, Germany) with five, 30 s bursts at 40 Hz.

3.6.1 cDNA synthesis

The synthesis of cDNA from RNA samples (1 µg) was performed using the QuantiTect Reverse Transcription Kit (Qiagen, Cat. No.: 205311, Hilden, Germany).

3.6.2 qRT-PCR procedure

The cDNA equivalent of 20 ng of total RNA was used in a 20 µL PCR reaction on a C1000 Thermal Cycler real-time PCR system (BioRad Laboratories, Hercules, CA, USA). The 20 µL reaction volume was comprised of 10 µL 2x QuantiFast SYBR Green PCR Kit (Qiagen, Cat. No.: 204054, Hilden, Germany), 1 µL Primer Mix (0.5 µM final concentration for each primer) and 9 µL template cDNA (20 ng/9 µL). In all experiments three biological replicates of each sample were processed and per sample two to three technical replications were performed. Reactions were set up in skirted, low-profile 96-well PCR plates (StarLab International GmbH, Cat. No.: E1403-5200, Hamburg, Germany). Real-time cycler conditions were as follows: (1) 95 °C for 5 minutes; (2) 40 cycles of amplification consisting of 95 °C for 10 seconds, 55-60 °C (combined annealing and extension; temperature depending on melting temperature of primer pairs); (3) melting curve analysis (to monitor possible mispriming or primer dimer artefacts). In all experiments AT1G13320 (*PDF2 – Protein phosphatase 2A subunit A3)* was used as reference gene for normalization of qRT-PCR data (Czechowski et al., 2005). *PDF2* was chosen as initial experiments confirmed stable expression of this transcript in all experimental conditions and all tissues.

All primer combinations were designed using Primer3 (http://primer3.wi.mit.edu/; Version 3.0.0; Rozen and Skaletsky, 2000; Untergasser et al., 2012) and specificity to the desired target was confirmed using the NCBI BLAST tool for *A. thaliana* (http://blast.ncbi.nlm.nih.gov/Blast.cgi). The primer combinations used, including sequences and target accessions, are displayed in Table 3-1 (Primers for auxin-related transcripts) and Table 3-2 (Primers for cell cycle-related transcripts). To avoid unwanted amplification of genomic DNA, all primer pairs were designed to span introns, or to span exon-exon junctions, respectively. Amplification efficiencies of al primer combinations were calculated using the LinReg software (Ramakers et al., 2003). Relative expressions were calculated using the Livak method ($2^{-\Delta\Delta C}{}_T$; Livak and Schmittgen, 2001).

Table 3-1: Primers used for qRT-PCR of auxin-related transcripts in *A. thaliana.*

Primer	Sequence	Target accession
ACHT 5 FWD	5'-CTGGGGTTTCTCCATTTTCA-3'	AT5G61440
ACHT 5 REV	5'-TTCTCCCACCATCTCATTCC-3'	
GRXS 17 FWD	5'-GTGAAGGAGAATGCGAAAGC-3'	AT4G04950
GRXS 17 REV	5'-TTTCCTGCTAAACCCACACC-3'	
HEC 1 FWD	5'-CAATAATGGCACGAACATGG-3'	AT5G67060
HEC 1 REV	5'-TGCAAAATCCGAATCCTCTC-3'	
HEC 2 FWD	5'-GAATCCGTAAAGCCACCAAA-3'	AT3G50330
HEC 2 REV	5'-GTTAACCACCGCATGTTCCT-3'	
IAA 20 FWD	5'-GGACATCCTCAGGGACTCAA-3'	AT2G46990
IAA 20 REV	5'-ATGGATGCGTTGAACATGAA-3'	
MYB 15 FWD	5'-AGGACCATGGACACCTGAAG-3'	AT3G23250
MYB 15 REV	5'-CTGCAATCGCTGACCATCTA-3'	
MYB 75 FWD	5'-CGACTGCAACCATCTCAATG-3'	AT1G56650
MYB 75 REV	5'-TGTCCCCCTTTTCTGTTGTC-3'	
RSM 1 FWD	5'-GGCATCAGGCTCAATGTCTT-3'	AT2G21650
RSM 1 REV	5'-CCATTCTCGATGCTTTCGAT-3'	
RSM 3 FWD	5'-AGAGGGCCTTGGCAGTTTAC-3'	AT1G75250
RSM 3 REV	5'-CAAAGGGACACGACCAGTCT-3'	
SPT FWD	5'-TTTCTCATCATCCACCGTCA-3'	AT4G36930
SPT REV	5'-CCTTCCTCGCTTTCACAGTC-3'	
TH 7 FWD	5'-TCCATGAAAGGCTCAAACAA-3'	AT1G59730
TH 7 REV	5'-GTTTGGCTCCAACAACCCTA-3'	
TH 8 FWD	5'-CCTTGAACCAAAGCTCGAAG-3'	AT1G69880
TH 8 REV	5'-ACCTTCACACCCACAACCAT-3'	

Table 3-2: Primers used for qRT-PCR for cell cycle-related transcripts in *A. thaliana.*

Primer	Sequence	Target accession
CDKB1;2 FWD	5'-ATACCACCAACGGCTCTCC-3'	AT2G38620
CDKB1;2 REV	5'-ACGCAGAGGAGACGAACG-3'	
CDKB2;1 FWD	5'-ATGTGGCCAGGAGTGAGC-3'	AT1G76540
CDKB2;1 REV	5'-GAGGTTTGGAACAGCAGAGG-3'	
CDKB2;2 FWD	5'-TGTTGGGAACACCAAACG-3'	AT1G20930
CDKB2;2 REV	5'-CTCAACGGTTTCCATTGC-3'	
CYCA1;1 FWD	5'-CGTTAATGCCAGTTTCTCTAGC-3'	AT1G44110
CYCA1;1 REV	5'-TGAGCCATCATCAGATTTGC-3'	
CYCB1;2 FWD	5'-TTCTTGGAAACCTCGAATGG-3'	AT5G06150
CYCB1;2 REV	5'-TCTGGATCAGACATCGAAGC-3'	
CYCB1;3 FWD	5'-TCTGTCCTTCCATGCTTGC-3'	AT3G11520
CYCB1;3 REV	5'-ATTCGGAGTAGCCTGTGTGG-3'	
CYCB1;4 FWD	5'-GCTGTGATCGACATTGATGC-3'	AT2G26760
CYCB1;4 REV	5'-TCCTTCCTCTTCCACAGTCC-3'	
CYCB2;1 FWD	5'-CCTCAGTTCCAAGTGCTAACG-3'	AT2G17620
CYCB2;1 REV	5'-GGTTTCTCAAGCGACATTGG-3'	
CYCB2;2 FWD	5'-GGTATCCACCATCGTTACTCG-3'	AT4G35620
CYCB2;2 REV	5'-GCTGTTCCATTCACTGAAGC-3'	
CYCB2;4 FWD	5'-CCAGCTGGTTCAATTCTTGC-3'	AT1G76310
CYCB2;4 REV	5'-AAGCGCTTCTGGAATGTTCG-3'	
CYCD3;1 FWD	5'-AACAGTCCTTCATCTGGGAG-3'	AT4G34160
CYCD3;1 REV	5'-CTGCTATGTGCATCAGCCAT-3'	

3.7 Glutathione measurements

Determinations of the total glutathione pool, GSH and GSSG in the roots of the different genotypes were performed as described by Queval and Noctor (2007). For this analysis, seedlings were grown for 7 days on vertical plates containing medium IV (Appendix IV: Composition of growth medium IV:). Whole root samples (50-150 mg per sample) were harvested, weighed and immediately frozen in liquid N_2. The samples were stored at -80 °C until analysis.

3.7.1 Extraction Procedures

Frozen root samples were ground to a fine powder in liquid N_2, 1 M $HClO_4$ (1 mL per 150 mg sample) was added and ground with the frozen root material. As the mixture thawed, the samples were mixed again to ensure rapid arrest of metabolism. Upon thawing, insoluble material was removed by centrifugation in a desktop centrifuge (maximum speed) at 4 °C for 5 minutes. Samples (0.5 mL) of the supernatant were decanted into fresh tubes and 0.12 M NaH_2PO_4 (pH=5.6; 0.1 mL) was added to each.

Thereafter, sufficient K_2CO_3 was added to bring the pH of the samples to between pH 5 and pH 6. Per 500 µL 1 M $HClO_4$ used in the extraction approximately 30-40 µL 5 M K_2CO_3 were required for neutralization. The samples were then centrifuged once more to remove insoluble $KClO_4$. The supernatants were decanted into fresh tubes (placed on ice) and glutathione was immediately assayed.

3.7.2 Principle of glutathione measurement using DTNB

Total and oxidized glutathione are measured as the NADPH-driven glutathione-dependent reduction of 5,5'-dithiobis-2-nitrobenzoic acid (DTNB, Ellman`s reagent). DTNB is a reagent containing a disulphide bond which can be reduced by other thiols. The reduced (thiol) form of DTNB has much greater absorbance at 412 nm (A_{412}). In the presence of glutathione and glutathione reductase (GR), the reaction proceeds as follows:

$$2\ GSH + DTNB_{ox} <=> GSSG + DTNB_{red} \qquad \text{(increase in } A_{412}\text{)}$$

$$GSSG + NADPH + H^{+} <=> 2\ GSH + NADP^{+} \qquad \text{(catalysed by GR)}$$

Thus, there is no net consumption of glutathione in the reaction – it cycles between the reduced and oxidised forms, and acts as an intermediate in the electron transfer from NADPH to DTNB.

As can be demonstrated easily with GSH standards, the rate of the reaction is proportional to glutathione concentration over a wide range. Because inclusion of GR in the assay means that glutathione cycles, the assay will measure both GSH and GSSG (as 2 GSH) without distinction.

To distinguish between GSH and GSSG, aliquots of extracts are pre-treated with 2-vinylpyridine (VPD). VPD complexes with GSH (but not GSSG) and so only GSSG can be measured in treated samples.

3.7.3 Assay Procedures

The total glutathione pool (GSH & GSSG) and oxidized glutathione (GSSG) were assayed as described below on a FLUOstar Omega microplate reader (BMG Labtech GmbH, Ortenberg, Germany) using flat-bottom 96-well Costar UV plates (Corning Incorporated, Cat. No.: 3635, Corning, NY, USA). The absorbance changes at 412 nm (A_{412}) were measured for 5 minutes in a procedure that comprised 12 measurement cycles with mixing before each cycle. In all cases, statistical analysis of the data was performed in Microsoft Excel 2010.

3.7.3.1 Reaction Mixture: Total glutathione

The reaction mixture contained 0.12 M NaH_2PO_4 (pH 7.5), 6 mM EDTA, 0.01 mL 50 mM NADPH, 0.1 mL 6 mM DTNB and 0.02-0.05 mL extract in a total volume of 1 mL. Reactions were started by addition of 0.01 mL GR. Each assay included a standard curve incorporating 0, 0.2, 0.4 and 1.0 nM GSH.

3.7.3.2 Reaction mixture: Oxidized glutathione (GSSG)

For this analysis VPD (5 µL per sample) was added to extracts (0.2 mL), mixed well and left to stand at room temperature for 20 min. The samples were then centrifuged at 4 °C at maximum speed for 15 minutes to remove the VPD complexes. Aliquots (0.16 mL) of supernatant were transferred to fresh tubes and centrifuged again. Aliquots (0.1 mL) of supernatant were then measured as for total glutathione. Each assay included a standard curve incorporating 0, 0.02, 0.04 and 0.08 nM GSSG.

3.8 In-vivo measurement of glutathione

For these experiments transgenic *Arabidopsis thaliana* plants, which constitutively express roGFP2, were used. As mentioned above, these roGFP2 plants were obtained from Roger B. Deal and Steven Henikoff (Fred Hutchinson Cancer Research Centre, Seattle, USA) and from Andreas Meyer (Heidelberg Institute of Plant Sciences, Heidelberg, Germany). They transformed *Arabidopsis thaliana* plants using the pBinAR binary vector carrying the 35S::roGFP2 construct, which had then been electroporated into *Agrobacterium tumefaciens* strain C58C1 (Meyer et al., 2007). These bacteria were then ultimately utilized to transform *Arabidopsis thaliana* plants using the floral dip method. A selection of transformants was subsequently performed on medium containing 50 µg/ml kanamycin (Meyer et al., 2007).

To study glutathione partitioning between the nucleus and cytosol, these roGFP2 (35S:roGFP2) seedlings were grown for 7 days on vertical square plates containing growth medium IV (Appendix IV: Composition of growth medium IV:) in the absence (control) or presence of various concentrations of BSO (0.25 mM, 0.5 mM, 0.75 mM and 1 mM BSO). Each experiment involved an analysis of 57 seedlings per plate, with 3 plates per treatment.

3.8.1 Principle of glutathione measurement using confocal microscopy

In-vivo measurements of glutathione are based on the redox properties of the roGFP2 probe, which can be reversibly reduced and oxidized in the presence

of glutathione. The reduced form has an excitation maximum at 488 nm while the oxidized form has an excitation maximum at 405 nm (Figure 3-6).

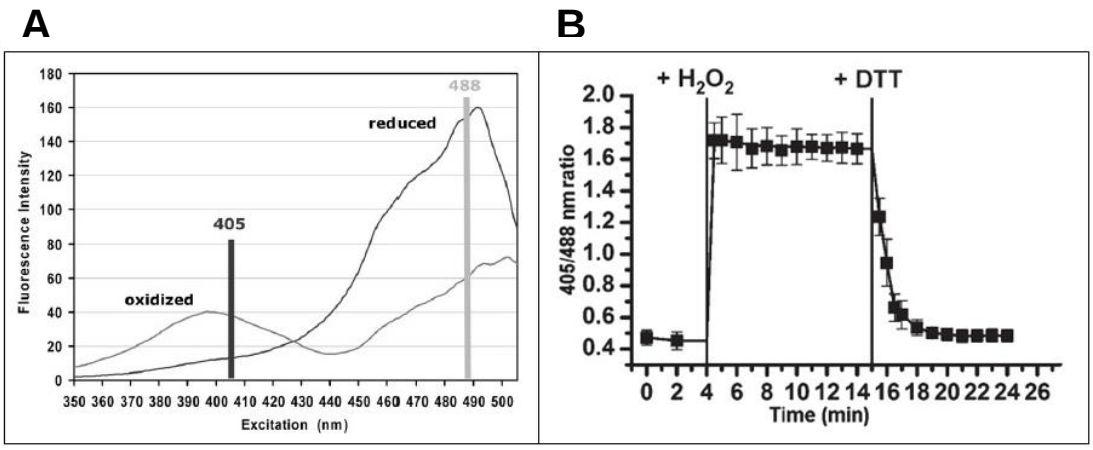

Figure 3-6: Overview of the properties of the roGFP2 biosensor. A: Fluorescent excitation spectra for oxidized and reduced recombinant roGFP2 protein isolated from *Escherichia coli* (*E. coli*) (Meyer, 2008). B: Time course experiment for ratio values calculated from CLSM images during successive oxidation and reduction (Meyer et al., 2007)

The roGFP2 measurements can be used to estimate the redox potential of glutathione via glutaredoxin (GRX) in various cellular compartments. GRX mediates the reaction between roGFP2 and glutathione. An analysis of the relative fluorescence following excitation at these two wavelengths provides data that enables the determination of the degree of oxidation of the glutathione pool, provided that the concentration of glutathione within the sample is known or calculated (Meyer et al., 2007; Schwarzlaender et al., 2008).

3.8.2 Calculation of the redox state of the glutathione pool

Two standards were used in each experiment. The first standard was produced by incubating whole seedlings in 2 mM H_2O_2 in liquid growth medium IV for 5 minutes prior to analysis. The second standard was produced by incubating whole seedlings in 2 mM DTT in liquid growth medium IV for 5 minutes prior to analysis. These standards are considered to represent the maximum oxidized and maximum reduced states of the glutathione pool respectively and were measured with 405 nm and 488 nm excitation immediately after incubation, together with the samples from the different BSO treatments.

The degree of oxidation of the roGFP2 sensor was calculated according to the following formula (Figure 3-7). The redox potential of the glutathione pool can then calculated from the OxD_{roGFP} values, according to the formula shown in Figure 3-8 using the mid-point potential of roGFP2, which had previously been described to be -272 mV (Hanson, et al. 2004).

$$OxD_{roGFP} = \frac{R - R_{\mathrm{red}}}{\frac{I_{488\mathrm{ox}}}{I_{488\mathrm{red}}}(R_{\mathrm{ox}} - R) + (R - R_{\mathrm{red}})}$$

Figure 3-7: Formula for the calculation of the degree of oxidation for the roGFP2 sensor. R = ratio of excitation at 405/488 nm, R_{red} = ratio of fully reduced roGFP2; R_{ox} = ratio of fully oxidized roGFP2; I_{488ox} and I_{488red}: intensities at 488 nm for fully oxidized respectively reduced roGFP (Schwarzlaender et al., 2008).

$$E' = E'^{pH}_{0(roGFP)} - \frac{2.303RT}{zF} \log_{10} \frac{1 - OxD_{roGFP}}{OxD_{roGFP}}$$

Figure 3-8: Formula for the calculation of the redox potential of glutathione. R = gas constant (8.315 J K-1 mol -1); T = absolute temperature (298.15 K); z = number of transferred electrons (2); F = Faraday constant (9.648 * 10^4 C mol-1); $E'^{pH}_{0(roGFP)}$ = mid-point redox potential (Schwarzlaender et al., 2008).

3.8.3 Procedure of glutathione measurement using confocal microscopy

A LSM 510 META confocal microscope (Carl Zeiss, Jena, Germany) with lasers for 405 nm and 488 nm excitation using a 505-530 nm emission band-pass filter was used in all experiments. The power of the lasers was set to 10 % to avoid photo-bleaching during data acquisition. Images were acquired as Z-Stacks of 1-1.5 µm slices depending on the thickness of the sample. Each Z-Stack was adjusted to yield a maximum of 25 slices. Images were collected using a Plan-Neofluar 40x/1.3 Oil DIC objective (Carl Zeiss, Jena, Germany) in multi-track mode with line switching between 405 nm and 488 nm illumination. Slides were prepared using liquid growth medium IV without BSO. Ratiometric analysis was performed using ImageJ 1.41a to measure fluorescence intensities from photographs acquired with the LSM 510 META. The intensity values of 405 and 488 nm pictures were copied into Microsoft Excel 2010 for the calculation of 405/488 nm ratios.

3.9 Extraction of intact nuclei

3.9.1 Principle of nuclei extraction

The method used for nuclei extraction is a modified procedure of the INTACT (isolation of nuclei tagged in specific cell types) method (Deal and Henikoff, 2010A, B). The technique is an affinity-based isolation of nuclei, employing a plant line (GL2) that produces biotin-labelled outer envelopes of nuclei via transgenic co-expression of a nuclear target fusion protein (NTF) under control of a cell-type specific promoter (GLABRA2, GL2) and a constitutively expressed biotin ligase (BL) from *E. coli*. The GL2 promoter targets expression of the NTF to non-root hair specific cell types, while constitutive expression of the biotin ligase assures biotinylation of outer nuclear envelopes. A schematic representation of both NTF and BL constructs for the GL2 transgenic line is displayed in Figure 3-9.

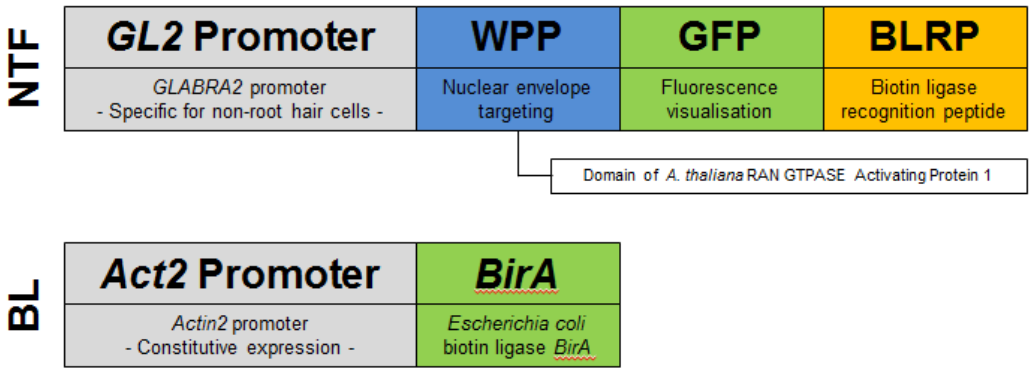

Figure 3-9: Schematic representation of the constructs used to generate the GL2 transgenic line. Shown are nuclear target fusion protein (NTF) and *E. coli* biotin ligase (BL) constucts with their respective promoter combinations (as described by Deal and Henikoff, 2010B).

3.9.2 Procedure of nuclei extraction

All steps of the nuclear extraction and purification process were performed at 4 °C in a cold room on ice. Nuclei were extracted from roots (5 g) of GL2 seedlings that contain a biotin-labelled nuclear envelope tag (GL2; Deal and Henikoff, 2010B) that had been grown for 7 days on vertical 120 x 120 mm square plates containing growth medium IV.

Harvested roots were placed in a glass petri dish containing modified nuclear isolation buffer (mNPB; described in Appendix V:). The roots were first cut into small pieces in 5 mL mNPB with an autoclaved razorblade and the crude extracts were then filtered through a 70 µm nylon cell strainer (BD Falcon, Cat. No.: 352350, Franklin Lakes, NJ, USA) into a 50 mL Falcon tube to reduce cell debris. The roots were placed in 5 mL fresh mNPB, cut again into smaller pieces and then filtered again pooling all extracts in one Falcon tube. Extracts (~10 ml) were incubated for 20 minutes with streptavidin-coated beads (M-280 Dynabeads, Cat.No.112-05D, Invitrogen, Carlsbad, CA, USA) that had previously been washed in NPB (1ml). During the incubation period, the tubes were gently inverted four times to ensure mixing. The procedure used for the purification of nuclei, in which the beads with nuclei are captured on the inside of a 1 mL pipette tip and then re-suspended in fresh mNPB, is illustrated in Figure 3-10.

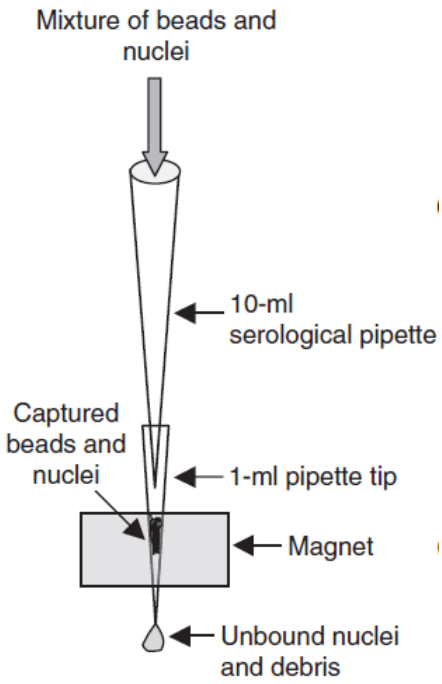

Figure 3-10: Schematic representation of setup for nuclei purification from crude nuclear extract. The image was taken from Deal and Henikoff, 2010B.

In this procedure, the suspension containing beads with bound nuclei is diluted using mNPB to achieve a final volume of 10 mL and then carefully drawn into a 10 mL serological pipette. The serological pipette is then placed into a 1 mL pipette tip that is inserted into the groove of the separation magnet. Nuclei are purified by allowing the suspension to flow past the magnet, at a flow rate of approximately 0.75 mL min^{-1}, into a 15 mL Falcon tube. Nuclei that are bound to beads were captured on the inside of the 1 mL pipette tip, which was then removed from the magnet. The nuclei were immediately re-suspended in 1 mL mNPB and used for analysis. Fluorescence microscopy was used to determine whether intact nuclei were present in these extracts.

3.9.2.1 Fluorescence stereomicroscopy determination of intact nuclei

Fluorescence microscopy was performed using an Olympus BX61 multicolour fluorescence microscope (Olympus, Tokya, Japan) at 40x or 60x magnification on nuclei and bead suspensions and final purified nuclei. Aliquots of samples were incubated for 5-10 minutes with Hoechst 33342 (1:100,000) prior to image acquisition. Images were then taken of aliquots for bright-field, GFP (509 nm emission; nuclear envelope) and Hoechst 33342 (461 nm emission; chromatin) stain.

3.9.2.2 Scanning electron microscopy (SEM) determination of intact nuclei

For determination of intact nuclear envelopes in solutions of purified nuclei bound to beads a FEI Quanta 200 F environmental scanning electron microscope was used (FEI Company, Hillsboro, OR, USA). Pictures were acquired at 5 or 10 kV with magnifications between 500x up to 80,000x. Prior to SEM experiments, purified nuclei were fixed onto 5 mm^2 polysine slide pieces (VWR International, Cat. No.: 631-0107, Radnor, PA, USA) using a method described for yeast nuclei (Kisleva et al., 2007). Nuclei were fixed using 2 fixative solutions. Fixative solution 1 contained 4 % Paraformaldehyde, 20 mM Potassium phosphate (pH=6.5), 0.5 mM Magnesium chloride and 0.2 M Sucrose. Fixative solution 2 comprised 2 % Glutaraldehyde, 0.2 % Tannic acid, 20 mM Potassium phosphate (pH=6.5) and 0.5 mM Magnesium chloride. Both fixative solutions were prepared freshly and filter sterilized using a 0.2 µm Minisart syringe filter (Sartorius AG, Cat. No.: 16532, Göttingen, Germany).

Only fixative solution 2 was pH adjusted to pH 7.4 prior to filter sterilization. All fixation steps were carried out at room temperature. Aliquots (8 µL) of purified nuclei were pipetted onto the polysine slides and nuclei were allowed to adhere to the slides for 5 minutes. Slides were then submerged into fixative solution 1 and incubated for 10 minutes. A further fixation step was then performed by submerging slides into fixative solution 2 for again 10 minutes. After fixation slides were briefly rinsed with H_2Odd, fixed in aqueous 1 % osmium tetroxide for 10 minutes, rinsed again with H_2Odd and stained using 1 % uranyl acetate for 10 minutes. The fixed samples were then dehydrated through submerging the slides for 2 minutes into a series of Ethanol. Dehydration was performed in 30 %, 50 %, 70 %, two times 95 % and three times 100 % Ethanol baths. A final dehydration was performed in liquid CO_2 in a critical point drying apparatus (to less than 5 p.p.m. water) before coating with 1 nm platinum.

4 Chapter 4: Phenomics analyses of the effects of glutathione depletion

4.1 Introduction

The effects of glutathione depletion on plant development have not been fully characterised to date. Earlier studies have shown that knockout mutations in the *GSH1* or *GSH2* genes, which encode for the first and second enzymes of the glutathione synthesis pathway, result in embryo- or seedling-lethal phenotypes respectively (Cairns et al., 2006). The seeds of the *root meristemless 1-1* (*rml1-1*) mutants, which have glutathione levels of less than 5 % of the wild-type, are able to germinate but they are unable to establish a post-embryonic root meristem (Vernoux et al., 2000A). Furthermore, mutants with other defects in the *GSH1* gene, which restrict glutathione production to levels of between 20 to 50 % of the wild-type, exhibit higher sensitivities to certain abiotic and biotic stresses, e.g. exposure to cadmium or to virulent strains of *Pseudomonas syringae* or *Phytophthora brassicae* (Cobbett et al., 1998; Vernoux et al., 2000A; Ball et al., 2004; Cairns et al., 2006; Parisy et al., 2006; Schlaeppi et al., 2008). These studies show that glutathione levels play an important role in the control of plant development. In addition, the intracellular partitioning of glutathione between the different cellular compartments is also crucial to glutathione functions. This is demonstrated by the properties of the *chloroquine-resistance transporter* (CRT)-*like resistance transporter* (*clt)* mutants that exhibit functional knockout mutations in three genes encoding plastid thiol (γ-glutamylcysteine and glutathione) transporters. In the *clt1clt2clt3* mutants, the cytosol is depleted in glutathione and its

precursor γ-glutamylcysteine, which are largely restricted to the chloroplast (Maughan et al., 2010). The cytosolic concentrations of glutathione in the *clt* mutants are 4-fold lower than the wild-type (Maughan et al., 2010). Cytosolic glutathione deficiency induces hypersensitivity to abiotic and biotic stresses in the mutants (Maughan et al., 2010). These findings demonstrate the importance of the cytosolic γ-glutamylcysteine and glutathione pools in the control of plant responses to abiotic and biotic stresses.

The following studies were conducted in order to gain greater insights into the role of glutathione in plant development and in plant responses to abiotic stresses. The relationships between overall tissue glutathione contents and shoot and root growth were determined in *A. thaliana* under standard growth conditions. The responses of shoot growth to a range of different abiotic stresses were then compared in the wild-type and in several mutant lines that are deficient in overall tissue glutathione contents. Thereafter, the effects of cytosolic glutathione depletion in the *clt* triple mutants (*clt1clt2clt3*) on shoot and root growth were determined under standard growth conditions. The responses of shoot growth in the *clt* mutants to a range of different abiotic stresses were compared to those of the wild-type.

4.2 Results – Mutants with low glutathione

4.2.1 Shoot phenotypes

The effects of low tissue glutathione levels on shoot development were determined on seedlings grown for 14 days on horizontal agar plates under

standard growth conditions. Rosette growth rates were determined as leaf areas under low and highlight growth regimes. The mutant (*cad2-1*, *pad2-1* and *rax1-1*) genotypes with lower tissue glutathione levels had significantly lower leaf areas than the wild-type plants under standard growth conditions (Table 4-1; Figure 4-1). The decreases in leaf area varied in the *cad2-1*, *pad2-1* and *rax1-1* mutants, with the *cad2-1* mutant having the greatest leaf area of these mutant genotypes (83.2 % of the wild-type). The *pad2-1* mutant had the lowest leaf area (77.3 % of the wild-type). The *rax1-1* had 79.4 % of the leaf area measured in the wild-type plants (Figure 4-1).

Table 4-1: Comparison of leaf area in a range of GSH deficient mutant genotypes grown under standard growth conditions. A comparison of leaf area was performed in a range of 14-day old mutant seedlings defective in glutathione synthesis compared to wild-type (*wt*) *Arabidopsis*. Data are shown as mean ± standard error and number of plants assessed. Leaf areas are also shown in graphical form in Figure 4-1 with complementary information.

Genotype	Leaf area (mm²)	Number of plants
wt	41.91 ± 0.511	743
cad2-1	34.86 ± 0.460	792
pad2-1	32.41 ± 0.654	285
rax1-1	33.28 ± 0.450	756
Total		**2576**

Despite the differences in leaf area between the wild-type and mutant genotypes, the relative growth rates were similar in all lines under low or high light conditions (Figure 4-2A-D). The relative growth rates of the leaves decreased with increasing age of the plant (Figure 4-2A-D). However, some small variations in relative growth rates between the genotypes were observed. For example, the leaves of the *pad2-1* mutants had higher relative

growth rates than the wild-type and other mutant genotypes on days 11 and 12 but they were similar on days 12 and 14 (Figure 4-2C).

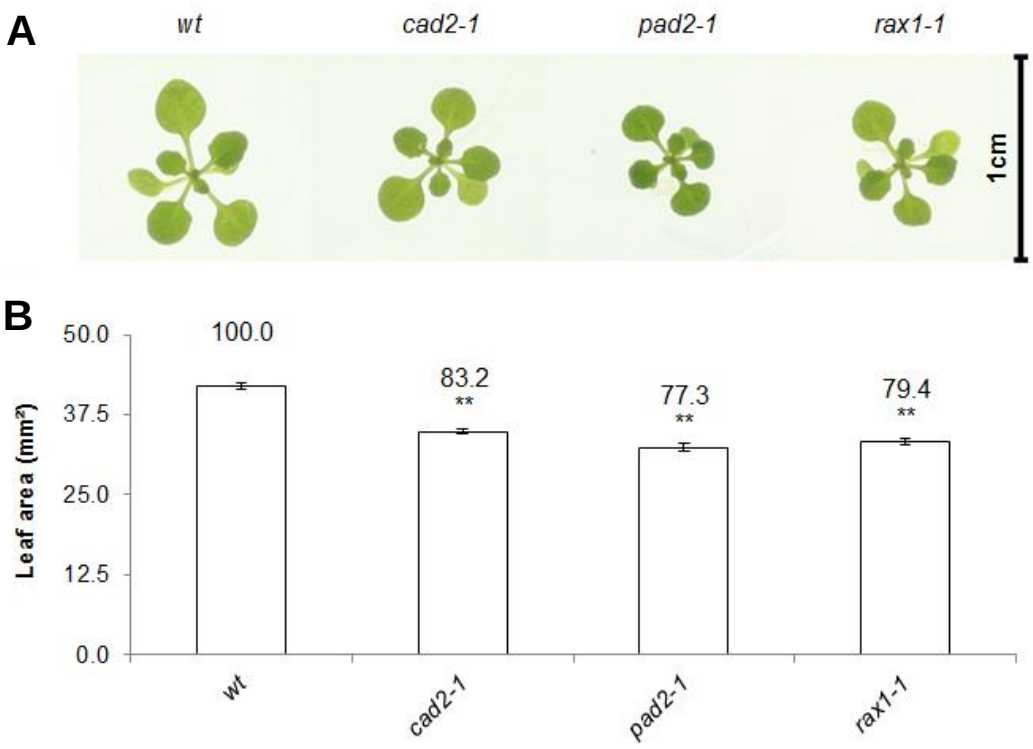

Figure 4-1: Comparison of leaf area in a range of GSH deficient mutant genotypes grown under standard growth conditions. Comparison of leaf area was performed in a range of 14-day old mutant seedlings defective in glutathione synthesis compared to wild-type (*wt*) *Arabidopsis*, grown under standard (low light) conditions. A) Comparison of the leaf area phenotypes. B) Histogram comparison of leaf areas. Asterisks indicate the significant differences compared to *wt* a $p<0.01$. Data are shown as mean ± standard error. The percentages relative to the *wt*, which were calculated on average leaf areas, are displayed above each bar. The bar represents 1 cm.

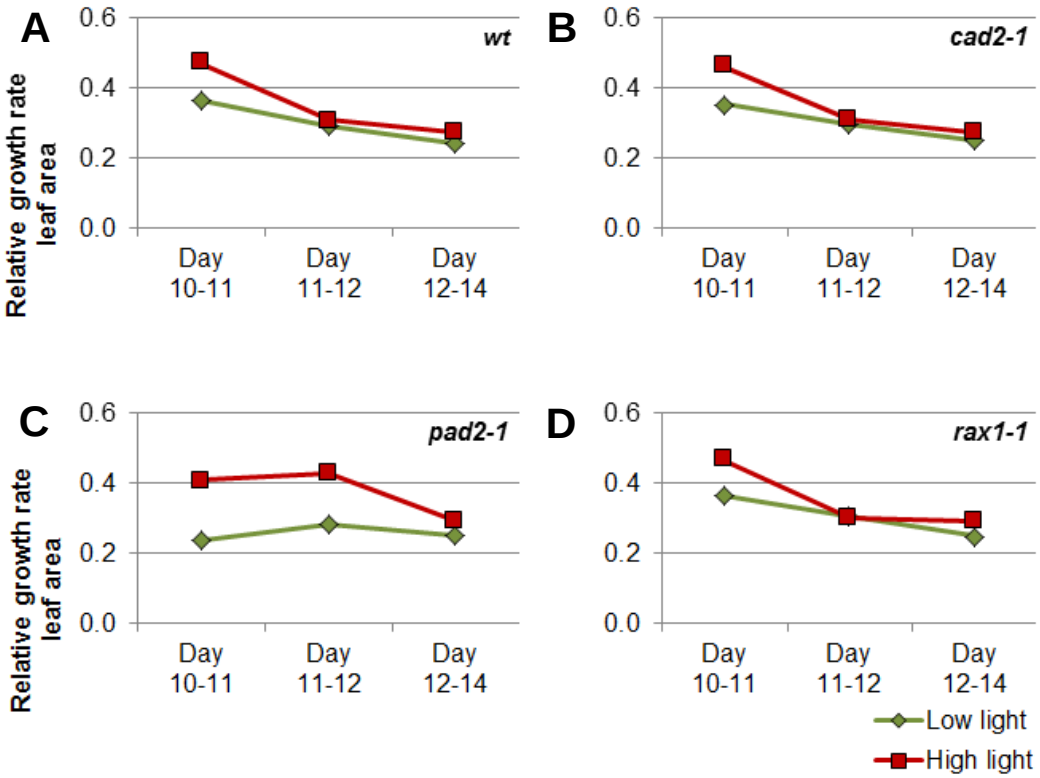

Figure 4-2: Comparison of growth rates in a range of GSH deficient mutant genotypes. A comparison of growth rates was performed for a range of mutant plants deficient in glutathione synthesis (*cad2-1*, *pad2-1*, *rax1-1*) relative to wild-type *Arabidopsis* (*wt*). Plants were grown for 10 days under either standard (low light, 150 µmol*m^{-2}*sec^{-1}) conditions before they were transferred for another 4 days to either standard (low light) or high light (400 µmol*m^{-2}*sec^{-1}) conditions. Data are shown as mean growth rates of the leaf area for A: *wt*, B: *cad2-1*, C: *pad2-1* and D: *rax1-1*. Growth rates were calculated by division of the leaf areas of older plants by leaf area of the younger plant, e.g.: leaf area day 11 / leaf area day 10 (Day10-11).

4.2.2 Root phenotypes

The effects of glutathione deficiency on root development were determined on seedlings grown on vertical plates for either 7 days along the surface of the medium or 10 days inside the medium under standard growth conditions. As root growth determinations are not easy and resistance of the medium might impair root development, these two sets of independent experiments were performed to obtain objective results.

4.2.2.1 Roots grown inside medium

Seeds of the wild-type and glutathione deficient mutant lines were sown along the cut edge of the medium and roots were allowed to grow inside the medium on vertical plates. After 10 days the primary root lengths, the number of lateral roots and lateral root densities were determined. Root architecture was determined in a total of 2083 plants (Table 4-2). The lengths of the primary roots and the number of lateral roots were significantly different in the GSH-deficient mutants than the wild-type (Figure 4-3). The *rml1-1* mutant showed the greatest decrease in primary root length (1.96 mm) relative to the wild-type (Table 4-2; Figure 4-3). Moreover, the *rml1-1* mutant did not produce any visible lateral roots (Figure 4-3A, C and D; Table 4-2). The *pad2-1* mutant showed the smallest decrease in primary root length relative to the wild-type, with an average length of 24.48 mm. The *cad2-1* and *rax1-1* genotypes had similar primary root lengths with values of 21.96 mm and 21.45 mm respectively (Figure 4-3A, B; Table 4-2).

Table 4-2: Comparison of root architecture in a range of GSH deficient mutant genotypes grown inside the medium. A comparison of root architecture was performed in 10-day old plantlets of wild-type (*wt*) and mutant plantlets deficient in glutathione synthesis (*cad2-1*, *pad2-1*, *rax1-1* and *rml1-1*), which were grown on vertical plates inside the medium. Data are displayed as mean± standard error and corresponding number of plantlets assessed. This data is also shown in graphical form in Figure 4-3 with complementary information.

Genotype	Primary root length (mm)	Number of lateral roots	Number of plants
wt	27.74 ± 0.596	1.195 ± 0.065	655
cad2-1	21.96 ± 0.590	0.712 ± 0.061	468
pad2-1	24.48 ± 0.953	0.959 ± 0.118	193
rax1-1	21.45 ± 0.628	0.495 ± 0.052	398
rml1-1	1.69 ± 0.018	0.000	369
Total			**2083**

Similar trends to those observed for the effects of glutathione deficiency on primary root lengths were found for effects on the number of lateral roots and for lateral root densities (Figure 4-3C). The *pad2-1* mutants had the highest number of lateral roots of all the GSH-deficient mutant lines compared to the wild-type, which had lateral root density values of around 1.19 lateral roots per cm primary root length (Figure 4-3C). In comparison, the *pad2-1* had lateral root density values of 0.95. The lateral root density values in the *cad2-1* mutant was 0.71 and in the *rax1-1* mutant this value was 0.49 (Figure 4-3C, D).

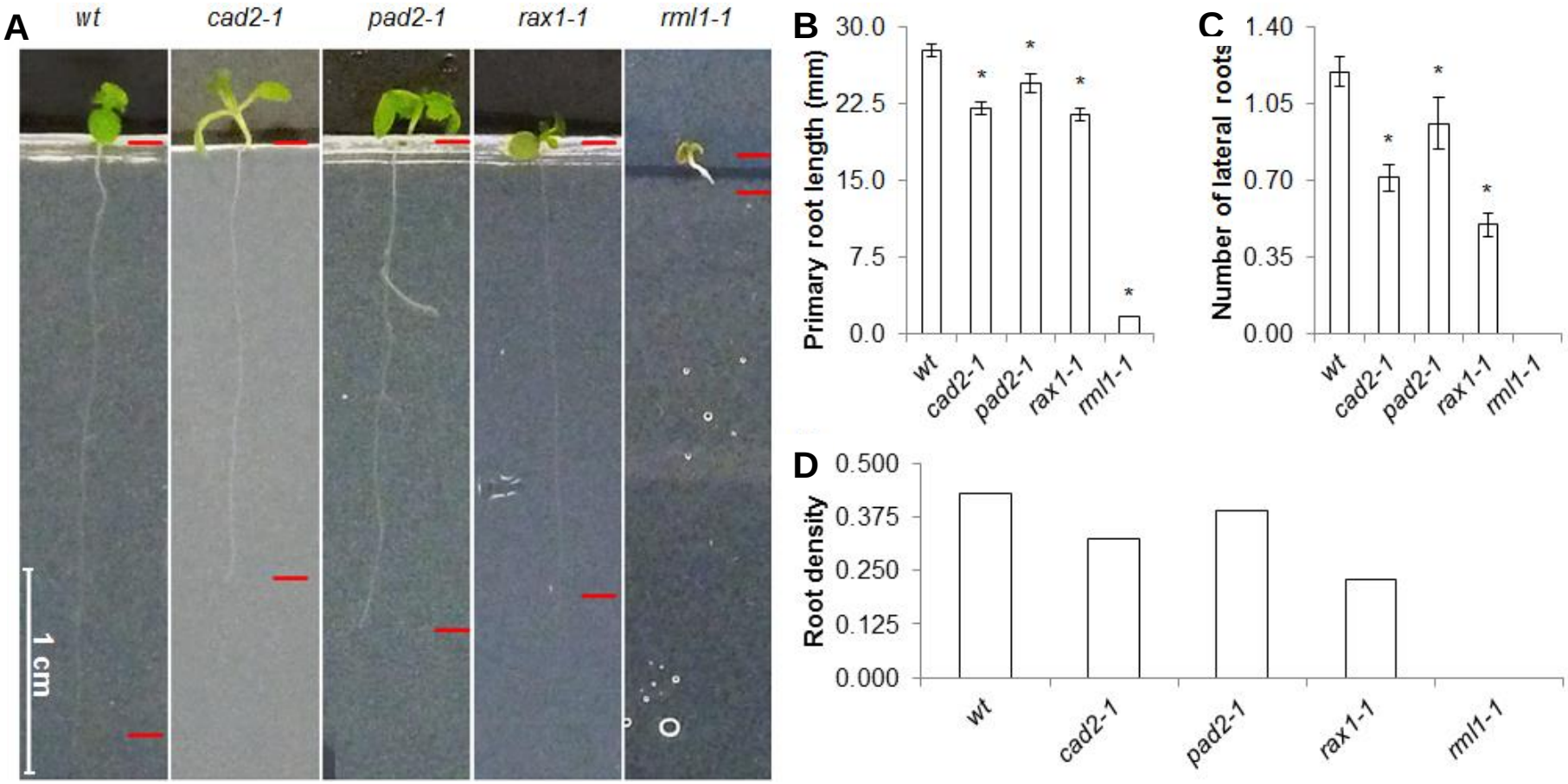

Figure 4-3: Comparison of root architecture in a range of GSH deficient mutant genotypes grown inside the medium. A comparison of root architecture was performed in 10-day old wild-type (*wt*) with a range of mutant plantlets deficient in glutathione synthesis (*cad2-1*, *pad2-1*, *rax1-1* and *rml1-1*). A: Comparison of phenotypes of *wt* and mutant plantlets. The white bar represents 1 cm and the red lines show start and end of the root; B: shows the average length of the primary root; C: the average number of lateral roots and D: the root density as number of lateral roots per cm primary root. Data are shown as mean ± standard error. Asterisks represent significant differences $p<0.01$.

4.2.2.2 A comparison of the architecture of roots grown on top of the medium

Seeds of the wild-type and glutathione deficient mutant lines were sown on the top of the media and roots were allowed to grow along the surface of the media. After 7 days the primary root lengths, the number of lateral roots and lateral root densities were determined. Root architecture was determined in a total of 391 plants (Table 4-3).

Under these growth conditions, the seedlings had longer primary roots and more lateral roots than those of the plants described above, where roots were allowed to grow inside the media of vertical plates for 10 days (Figure 4-4). Comparisons of the architecture of roots grown along the surface of the media revealed that the *cad2-1* mutant genotype had similar values for the primary root length to the wild-type. In contrast, under these conditions the *pad2-1* mutants had significantly longer primary roots than the wild-type seedlings. However, the *rax1-1* and *rml1-1* mutants had significantly shorter roots than the wild-type under these conditions (Figure 4-4; Table 4-3; Figure 4-5A). The growth conditions had no effect on the architecture of the *rml1-1* roots. This mutant was only able to develop short primary roots (1.48 mm).

Lateral root densities in the *pad2-1*, *cad2-1* and *rax1-1* mutant genotypes were decreased relative to the wild-type. The trend to lower lateral root densities in the mutants relative to the wild-type was observed when roots were grown along the surface of the media, and followed a similar pattern to that reported above for roots growing inside the media.

Table 4-3: Comparison of root architecture in a range of GSH deficient mutant genotypes grown along the surface of the medium. A comparison of root architecture was performed in 7-day old plantlets of wild-type (wt), wild-type grown in the presence of 1mM BSO (*wt*+BSO) and mutant plantlets deficient in glutathione synthesis (*cad2-1*, *pad2-1*, *rax1-1* and *rml1-1*), which were grown on vertical plates along the surface of the medium. Data are displayed as mean ± standard error with corresponding number of plantlets assessed. This data is also shown in graphical form in Figure 4-4 with complementary information.

Genotype	Primary root length (mm)	Number of lateral roots	Number of plants
wt	36.34 ± 0.672	3.275 ± 0.186	91
cad2-1	36.47 ± 0.618	2.526 ± 0.176	61
pad2-1	39.06 ± 0.954	3.220 ± 0.209	65
rax1-1	33.21 ± 0.558	1.237 ± 0.104	64
rml1-1	1.48 ± 0.054	0.000	40
wt+BSO	2.27 ± 0.059	0.000	70
Total			**391**

The wild-type plants had the highest lateral root densities, followed by *pad2-1*, *cad2-1* and *rax1-1* mutants (Figure 4-5C).

The architecture of wild-type roots treated with BSO

When wild-type plants were grown in the presence of BSO, which is an inhibitor of the first enzyme of glutathione synthesis, primary root length was decreased relative to the wild-type in the absence of this inhibitor. The average lengths of the roots of the wild-type seedlings grown in the presence of BSO were almost the same as those of the *rml1-1* mutants and no lateral roots developed (Figure 4-4; Figure 4-5C). Lateral root densities were therefore not calculated in the *rml1-1* mutant or the wild-type plants grown in the presence of 1 mM BSO in these studies (Figure 4-5C).

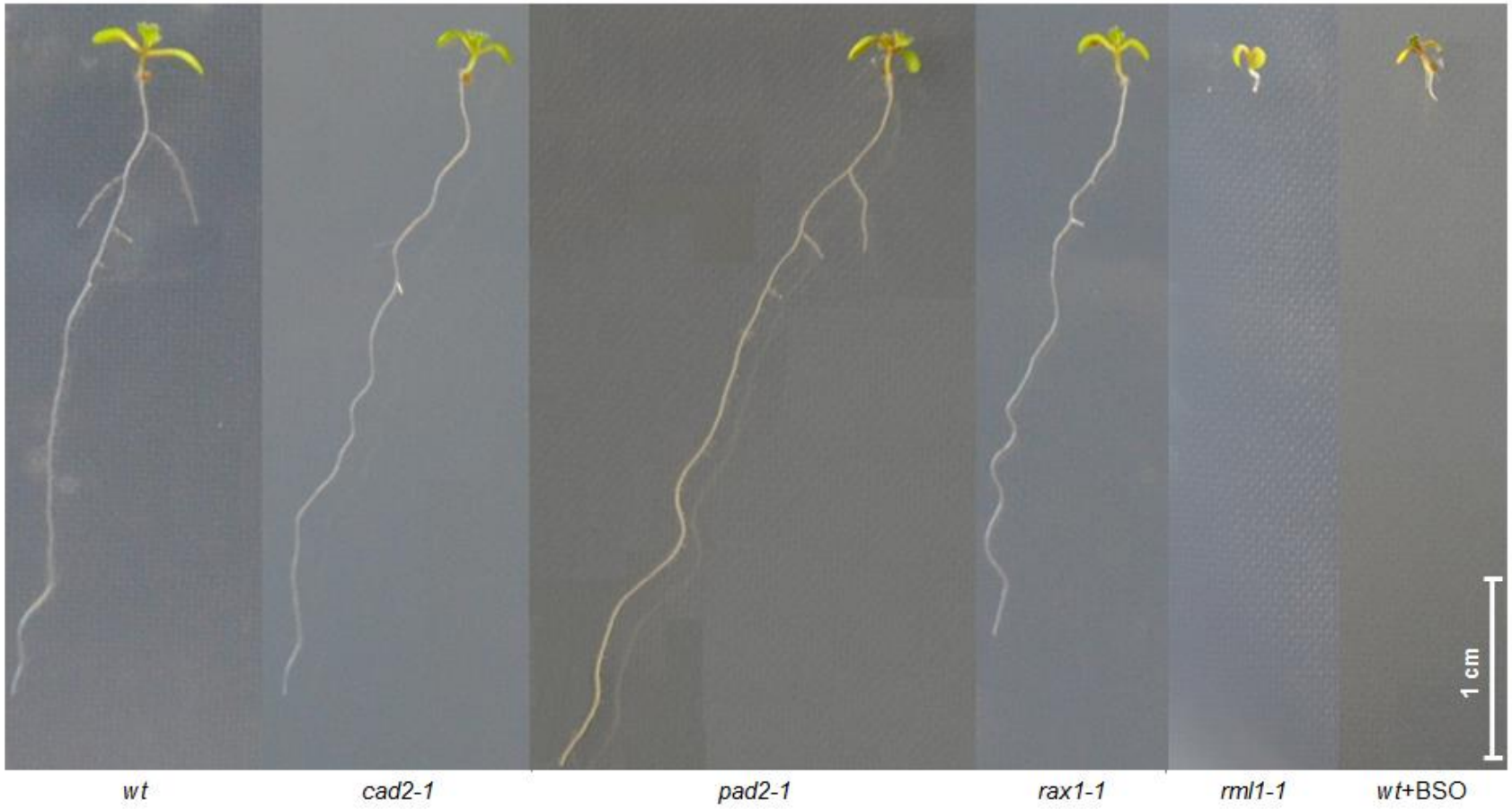

Figure 4-4: Phenotypic comparison of root architecture in a range of GSH deficient mutant genotypes grown along the surface of the medium. A comparison of root phenotypes was performed in a range of 7-day old mutant genotypes deficient in glutathione synthesis with wild-type (*wt*) Arabidopsis grown in the absence and presence of BSO (1 mM BSO). The white bar represents 1 cm.

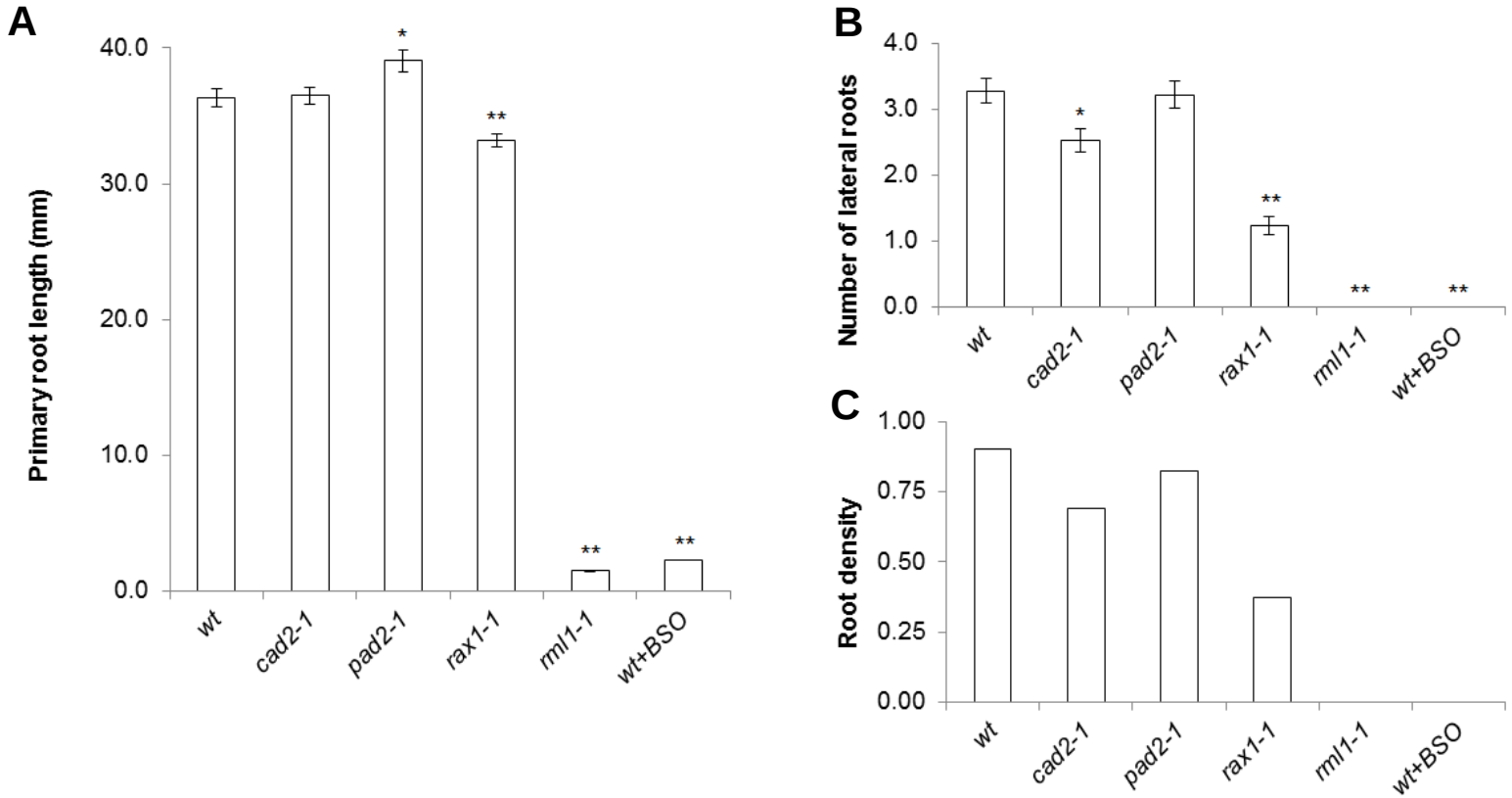

Figure 4-5: Comparison of root architecture in a range of GSH deficient mutant genotypes grown along the surface of the medium. A comparison of root architecture was performed in 7-day old wild-type (*wt*) and wild-type grown in the presence of BSO (1 mM BSO) with a range of mutant plantlets deficient in glutathione synthesis (*cad2-1*, *pad2-1*, *rax1-1* and *rml1-1*). A) Comparison of the average length of the primary root; B) the average number of lateral roots and D) the root density as number of lateral roots per cm primary root length. Data are shown as mean ± standard error. *, significant differences at $p<0.05$ and **, significant differences at <0.01.

4.2.3 Induced stress

The effects of glutathione deficiency on plant responses to induced exposures to various abiotic stresses were determined by comparing the leaf areas of 17-day old plants that had been exposed to stress for 7 days. The stress treatments used in these studies were high light (400 µmol. m^{-2} sec^{-1}), oxidative stress (H_2O_2), salt stress (sodium chloride), disruption of photosynthetic electron transport by paraquat (PQ), which accepts electrons from the photosystem I and transfers them to molecular oxygen to generate reactive oxygen species, and osmotic stress (sorbitol). In parallel plants were grown under standard (low light) conditions for comparison. Leaf areas were determined in a total of 2304 plants (384 plants per genotype and per condition) and relative leaf growth rates were calculated based on leaf area increases between days 10-11, 11-12, 12-14 and 14-17, e.g. leaf area day 11 divided by leaf area day 10.

With the exception of the treatment with 4 mM H_2O_2, which had no significant effect on leaf area, the stress treatments that were applied generally reduced leaf areas in all genotypes relative to the areas measured under control conditions (Figure 4-6A, B, C, D, E). For example, the osmotic stress induced by the addition of sorbitol to the growth media and salt stress induced by the inclusion of NaCl, reduced leaf areas significantly when compared to values obtained under standard growth conditions. However, the greatest reduction in leaf area was observed in plants grown exposed to paraquat (Figure 4-6A, B, C, D, E).

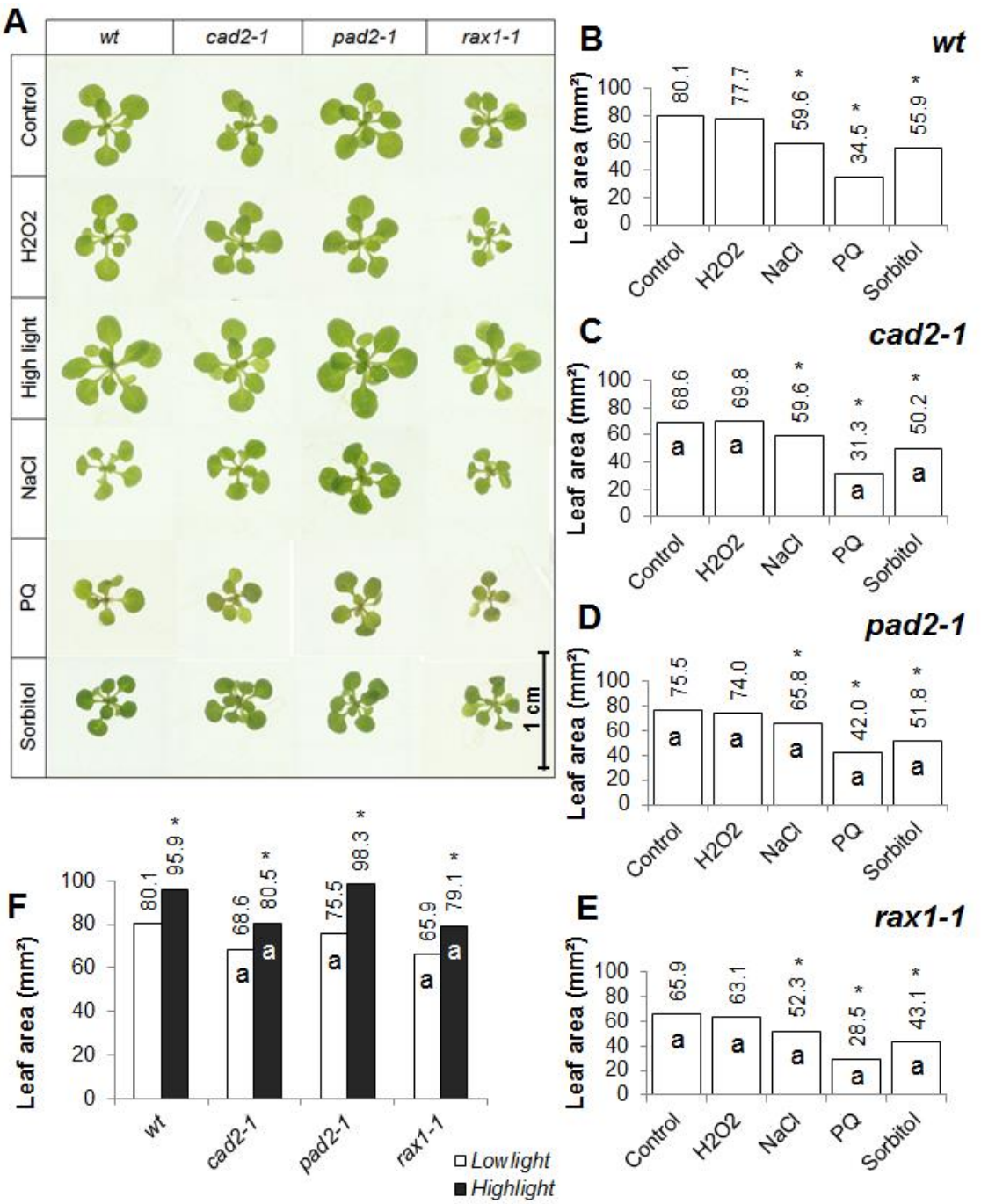

Figure 4-6: Comparison of leaf area in a range of GSH deficient mutant genotypes grown in induced stress conditions. Phenotypic comparison of leaf area phenotypes in 17-day old wild-type and *Arabidopsis* mutant genotypes with general glutathione depletion in the absence of stress (control) and after induced exposure to various stress treatments, A:. The black bar represents 1 cm. Comparisons of leaf areas are displayed for: B: wt, C: *cad2-1*, D: *pad2-1*, E: *rax1-1* and F: all genotypes in low light (control) and high light conditions. Data are shown as mean. Asterisks represent significant differences for control vs treatment comparisons for one genotype and "a" for comparisons of genotype vs wild-type within control or treatment condition ($p<0.01$). Standard error is not displayed, as too small.

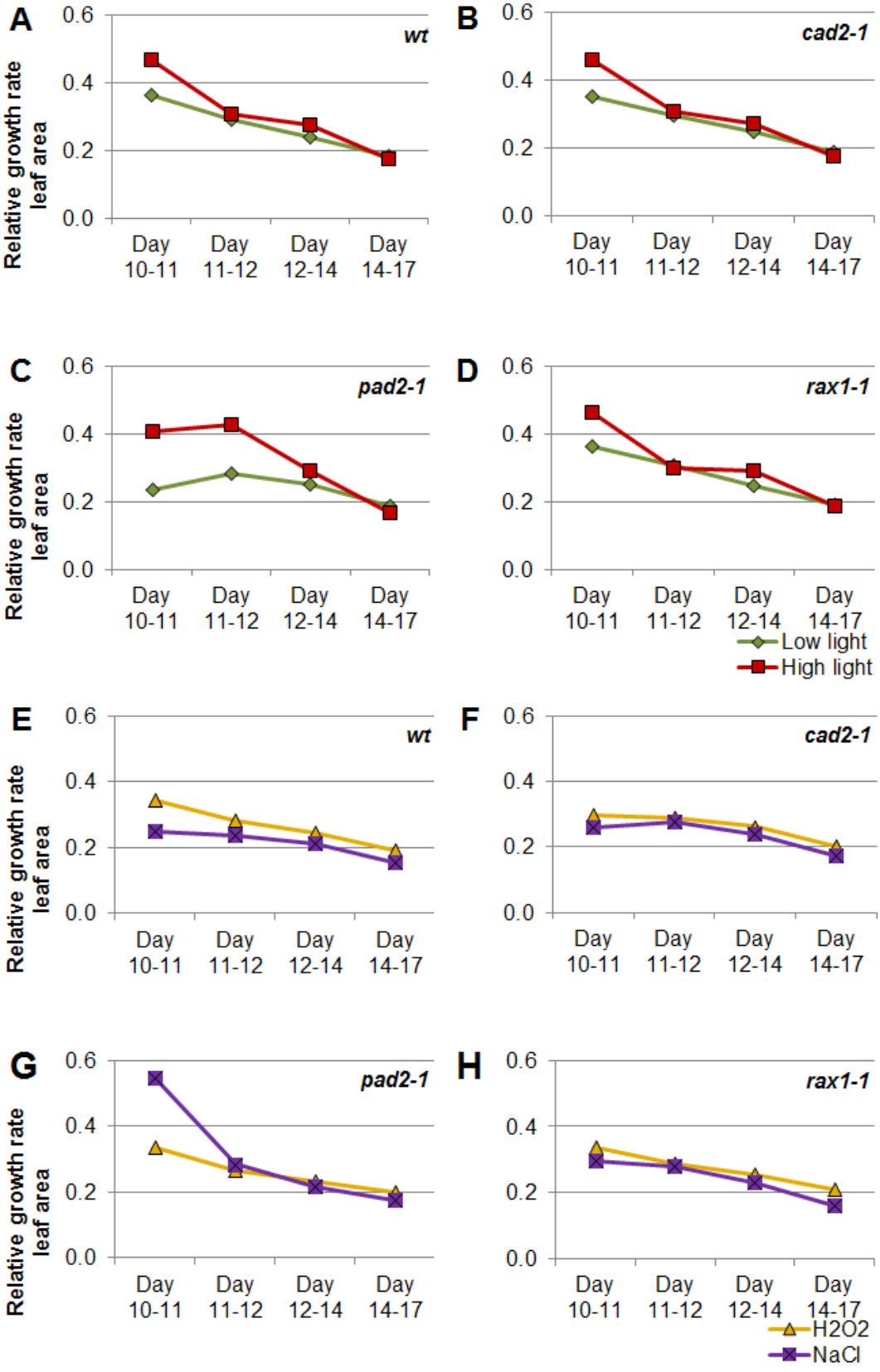
A
wt
B
cad2-1
C
pad2-1
D
rax1-1
E
wt
F
cad2-1
G
pad2-1
H
rax1-1
Relative growth rate leaf area
0.6
0.4
0.2
0.0
Day 10-11
Day 11-12
Day 12-14
Day 14-17
Low light
High light
H2O2
NaCl

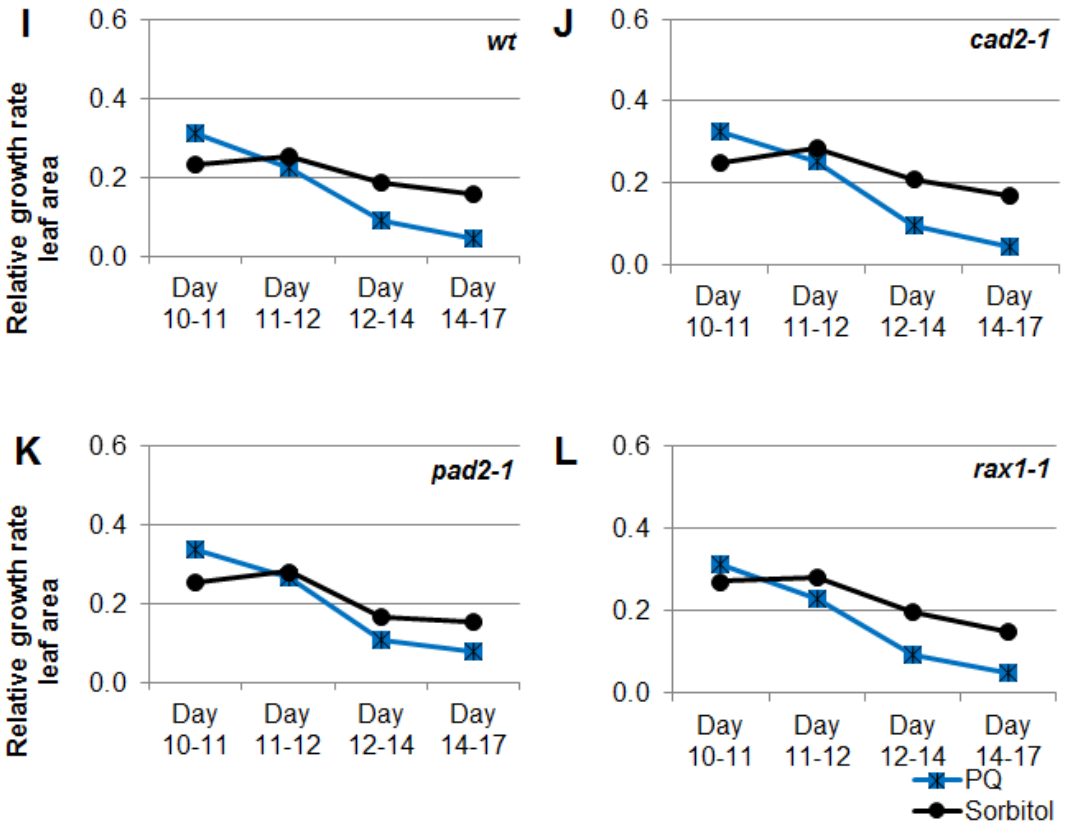

Figure 4-7: Comparison of relative growth rate in a range of GSH deficient mutant genotypes grown in induced stress conditions. A comparison of relative growth rates was performed for leaf areas in wild-type (*wt*, A, E, I) and a range of mutants deficient in glutathione synthesis (*cad2-1*, B, F, J; *pad2-1*, C, G, K and *rax1-1*, D, H, L). Comparisons were made for 17 day-old plants grown for 7 days under the following stress treatments: Low light and high light (A, B, C, D), H_2O_2 and NaCl (E, F, G, H) and PQ and Sorbitol (I, J, K, L). Data are shown as mean growth rates.

In contrast, the wild-type and mutant plants grown under high light conditions had significantly greater leaf areas than controls grown under low light (Figure 4-6F). The stress-induced decreases in relative growth rates in plants exposed to stress were comparable in the wild-type and mutant lines, except for the *pad2-1* mutant, which grew better under high light than the wild-type but which showed greater decreases in relative growth rates, particularly in plants

exposed to osmotic stress (Figure 4-7). Apart from these small differences, the wild-type plants and glutathione-deficient mutants showed similar responses in relative growth rates to the stress treatments (Figure 4-6, Figure 4-7).

4.2.4 Continuous stress

The effects of glutathione deficiency on responses to continuous exposures to various abiotic stresses were determined by comparing the leaf areas of 14-day old plants that had been exposed to various abiotic stresses throughout the growth period. The stress treatments used in these studies were the inhibition of PARP activity by 3-methoxybenzamide (3MB), the disruption of photosynthetic electron transport by paraquat (PQ), PQ-induced disruption of photosynthetic electron transport plus 3MB-induced PARP inhibition (3MB&PQ), salt stress (sodium chloride), and osmotic stress (sorbitol). In these studies, the growth of the leaf rosettes (leaf area) of the wild-type (Figure 4-8B, F) was compared to that of the *cad2-1* (Figure 4-8C, F), *pad2-1* (Figure 4-8D, F) and *rax1-1*mutant (Figure 4-8E, F). Leaf area was significantly reduced in all genotypes when plants were grown under continuous stress conditions compared to the leaf areas measured in the respective genotypes under control conditions (Figure 4-8). As observed previously, the low glutathione mutants had significantly lower leaf areas than the wild-type under standard growth conditions (Figure 4-8B, C, D, E, F). However, under many of the stress conditions applied in these experiments, the mutants exhibited significantly larger leaf areas than the wild-type plantlets grown under the same stress condition (Figure 4-8B, C, D, E, F; where comparisons were made for one treatment at one time point).

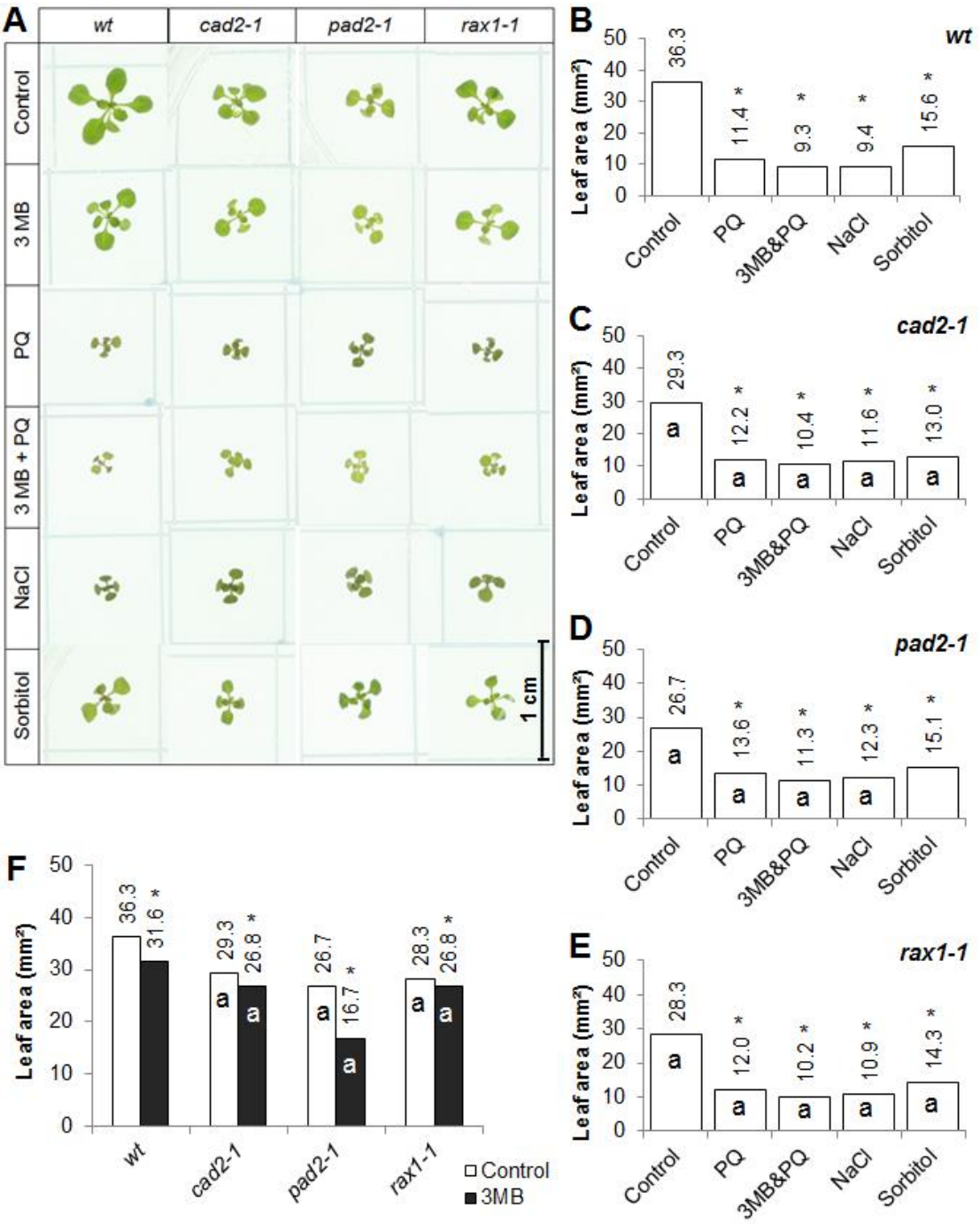

Figure 4-8: Comparison of leaf area in a range of GSH deficient mutant genotypes grown in continuous stress conditions. A: Phenotypic comparison of leaf area phenotypes in 14-day old wild-type and *Arabidopsis* mutant genotypes with general glutathione depletion in the absence of stress (control) and after continuous exposure to various stress treatments. The black bar represents 1 cm. Comparisons of leaf areas are displayed for: B: *wt*, C: *cad2-1*, D: *pad2-1*, E: *rax1-1* and F: all genotypes in control and 3MB treatment. Data are shown as mean. Asterisks represent significant differences for control vs treatment comparisons for one genotype and "a" for comparisons of genotype vs wild-type within control or treatment condition ($p<0.01$). Standard error is not displayed, as too small.

The exception was the osmotic stress conditions induced by the sorbitol treatment, which led to lower leaf areas in the mutants than the wild-type (Figure 4-8B, C, D, E, F). However, leaf area in the *pad2-1* mutant was less changed by the sorbitol treatment than the leaf area in the wild-type plants.

4.3 Results - Cytosolic glutathione deficiency

4.3.1 Shoot phenotype

The effects of cytosolic glutathione deficiency on shoot development were determined in plants grown for 14 days on horizontal plates under standard growth conditions. Rosette leaf area and relative growth rates were determined in plants were grown under low light (control) and high light regimes. A total of 1448 plants were analysed for these studies (Table 4-4). In the following *clt1clt2clt3* triple mutants will be referred to as *clt* mutants.

Table 4-4: Comparison of leaf area in *wt* and a mutant genotype with cytosolic glutathione deficiency grown under standard growth conditions. A comparison of leaf area in a range of 14-day old mutant seedlings exhibiting cytosolic glutathione depletion (*clt*) compared to wild-type (*wt*) *Arabidopsis*. Data are shown as mean ± standard error and number of plants assessed. This data is also shown in graphical form in Figure 4-9 with complementary information.

Genotype	Leaf area (mm^2)	Number of plants
wt	41.91 ± 0.511	743
clt	44.54 ± 0.713	705
Total		**1448**

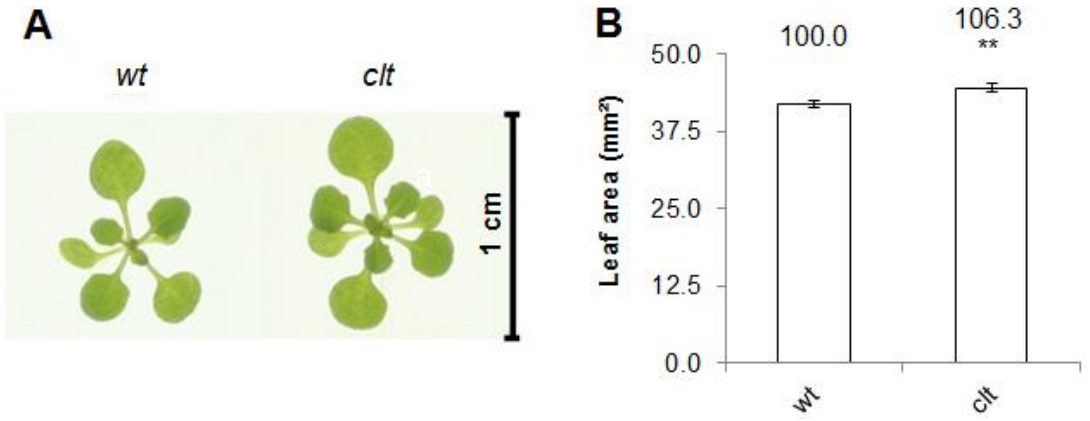

Figure 4-9: Comparison of leaf area in wt and a mutant line with cytosolic glutathione deficiency grown under standard growth conditions. A comparison of leaf area was performed in 14-day old mutant seedlings with glutathione deficiency (*clt*) compared to wild-type (*wt*) *Arabidopsis*. A: Comparison of the leaf area phenotypes. The bar represents 1 cm. B: Histogram comparison of leaf areas. Asterisks indicate the significant differences compared to *wt* a $p<0.01$. Data are shown as mean ± standard error. The percentages relative to the *wt*, which were calculated on average leaf areas, are displayed above each bar.

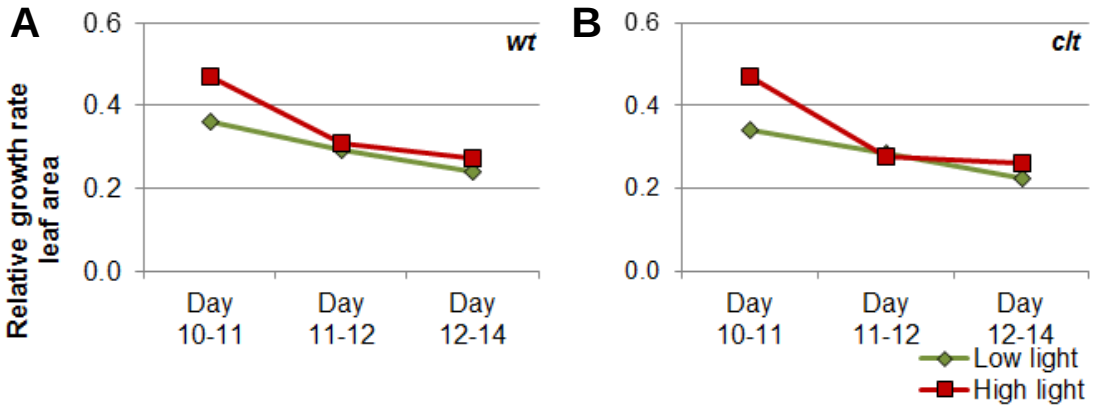

Figure 4-10: Comparison of growth rates in wt and a mutant genotype with cytosolic glutathione deficiency grown under standard conditions. A comparison of relative growth rates was performed for wild-type *Arabidopsis* (*wt*, A) and mutant plants exhibiting cytosolic depletion of glutathione (*clt*, B). Comparisons were made for 14 day-old plants grown for 14 days under low light conditions before they were transferred for another 4 days to low light and high light conditions. Data are shown as mean growth rates.

The *clt1clt2clt3* mutant has altered intracellular glutathione partitioning resulting in cytosolic glutathione deficiency because glutathione and its precursor are restricted to the chloroplast. The *clt* plants developed significantly larger rosettes with greater leaf areas than the wild-type (Figure 4-9, Table 4-4). However, relative leaf growth rates, measured between days 10 to 14, were similar in the *clt* triple mutants and wild-type plants grown under same conditions (Figure 4-10).

4.3.2 Root phenotype

Root architecture was also examined in the *clt* mutants under standard growth conditions on plants grown for either 7 or 10 days on vertical plates. Primary root length, the number of lateral roots and lateral root densities were determined on roots, which were allowed to grow either inside the media for 10 days or along the surface of the media for 7 days.

4.3.2.1 Roots grown inside medium

Seeds of the wild-type and *clt* mutants with cytosolic glutathione deficiency were also sown along a cut edge of the media and grown on vertical plates for 10 days prior to assessment. In total 1162 plants were assessed under these conditions in which the roots grow inside the media (Table 4-5).

The *clt* mutants had similar primary root lengths to the wild-type plants (Figure 4-11B) but they showed a significant reduction in the number of lateral

roots. Therefore lateral root densities were significantly lower in the *clt* mutants than the wild-type (Figure 4-11C; Table 4-5).

Table 4-5: Comparison of root architecture in wt and a mutant genotype with cytosolic glutathione deficiency (*clt*) grown inside the medium. A comparison of root architecture in 10-day old plantlets of wild-type (*wt*) an mutant plantlets with cytosolic deficiency of glutathione (*clt*), which were grown on vertical plates inside the medium. Data are displayed as mean plus standard error and the number of plantlets assessed is shown per genotype and in total. This data is also shown in graphical form in Figure 4-11 with complementary information.

Genotype	Primary root length (mm)	Number of lateral roots	Number of plants
wt	27.74 ± 0.596	1.195 ± 0.065	655
clt	28.38 ± 0.618	0.868 ± 0.063	507
Total			**1162**

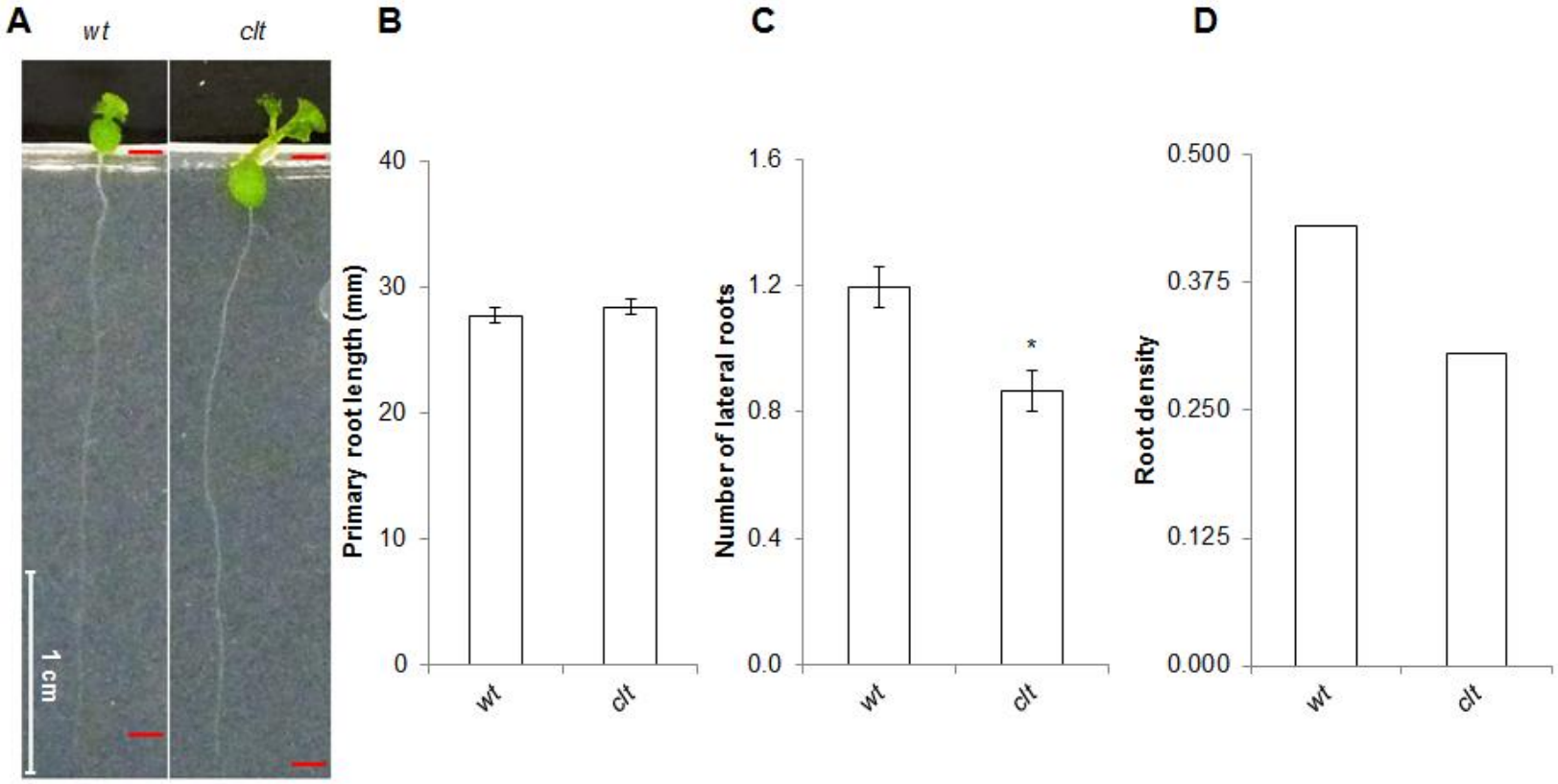

Figure 4-11: Comparison of root architecture in wild-type (*wt*) and a mutant genotype with cytosolic glutathione deficiency (*clt*) grown inside the medium. A comparison of root architecture in 10-day old wild-type (*wt*) and mutant plantlets with altered intracellular partitioning (*clt*). A: Comparison of phenotypes of *wt* and *clt*. The white bar represents 1 cm and the red lines show start and end of the root; B: shows the average length of the primary root; C: the average number of lateral roots and D: the root density as number of lateral roots per cm primary root. Asterisks represent significant differences $p<0.01$.

4.3.2.2 Roots grown on top of medium

Seeds of the wild-type and *clt* mutants were also sown on top of the media and grown on vertical plates for 7 days. Under these conditions, the roots grow along the surface of the medium. For this analysis, primary root lengths, the number of lateral roots and lateral root densities were determined in the roots of 131 plants (Table 4-6).

Table 4-6: Comparison of root architecture in wild-type (*wt*) and a mutant genotype with cytosolic glutathione deficiency grown along the surface of the medium. A comparison of root architecture in 10-day old plantlets of wild-type (*wt*) and mutant plantlets with cytosolic deficiency of glutathione (*clt*), which were grown on vertical plates along the surface of the medium. Data are displayed as mean plus standard error and the number of plantlets assessed is shown per genotype and in total. This data is also shown in graphical form in Figure 4-12 with complementary information.

Genotype	Primary root length (mm)	Number of lateral roots	Plant count
wt	36.34 ± 0.672	3.275 ± 0.186	91
clt	25.54 ± 0.778	0.700 ± 0.135	40
Total			**131**

The *clt* mutants had significantly shorter primary root lengths than the wild-type plants (Figure 4-12B). Moreover, the *clt* mutants had fewer lateral roots. Lateral root densities were significantly lower in the *clt* mutants than the wild-type (Figure 4-12C, D; Table 4-6).

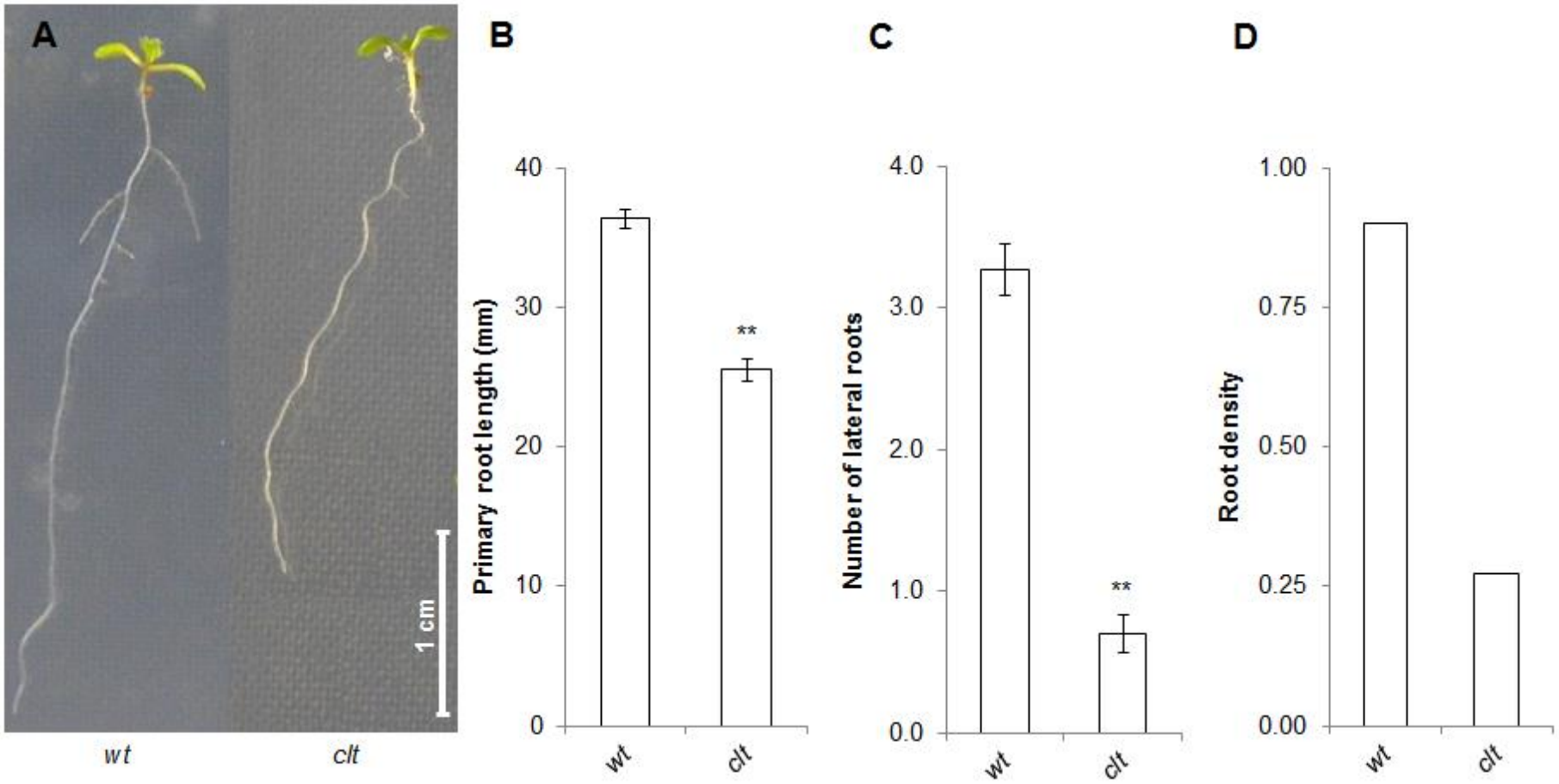

Figure 4-12: A comparison of root architecture in 7-day old wild-type (*wt*) with mutant plantlets deficient in cytosolic glutathione (*clt*). A) Comparison of the phenotypes of the primary root; The white bar represents 1 cm. B) displays a comparison of the average lengths of the primary roots, C) the number of lateral roots and D) the root density as number of lateral roots per cm primary root length. Data are shown as mean ± standard error. ** show significant differences compared to *wt* at $p<0.01$.

4.3.3 Induced stress

The effects of cytosolic glutathione deficiency in the *clt* mutants on the responses to abiotic stress were determined in 17-day old plants.

In these experiments mutant and wild-type plants were grown for 10 days under standard conditions and then grown for a further 7 days in the presence of various abiotic stresses. These were high light stress (400 µmol m^{-2} sec^{-1}), oxidative stress (H_2O_2), salt stress (sodium chloride), inhibition of photosynthetic electron transport by paraquat (PQ) and osmotic stress (sorbitol). The leaf areas of 17-day old rosettes were determined and relative growth rates were calculated based on the leaf area increases between days 10-11, 11-12, 12-14 and 14-17, e.g. leaf area day 11 divided by leaf area day 10. A total of 768 plants were assessed in these experiments, with 384 plants analysed per genotype and per condition.

When the *clt* mutants were grown under control or induced stress treatments, they had significantly larger leaf areas than the wild-type plants (a; Figure 4-13A, B, C, D). With the exception of the treatment with 4 mM H_2O_2, which did not have any significant effect on leaf area (*; Figure 4-13B, C, D) rosette leaf areas were significantly decreased following the stress treatments in both genotypes (Figure 4-13). The wild-type plants had significantly higher leaf areas when grown under high light than under low light (standard) conditions. Likewise, the *clt* rosette leaf areas were significantly larger under high light compared to low light conditions (Figure 4-13D).

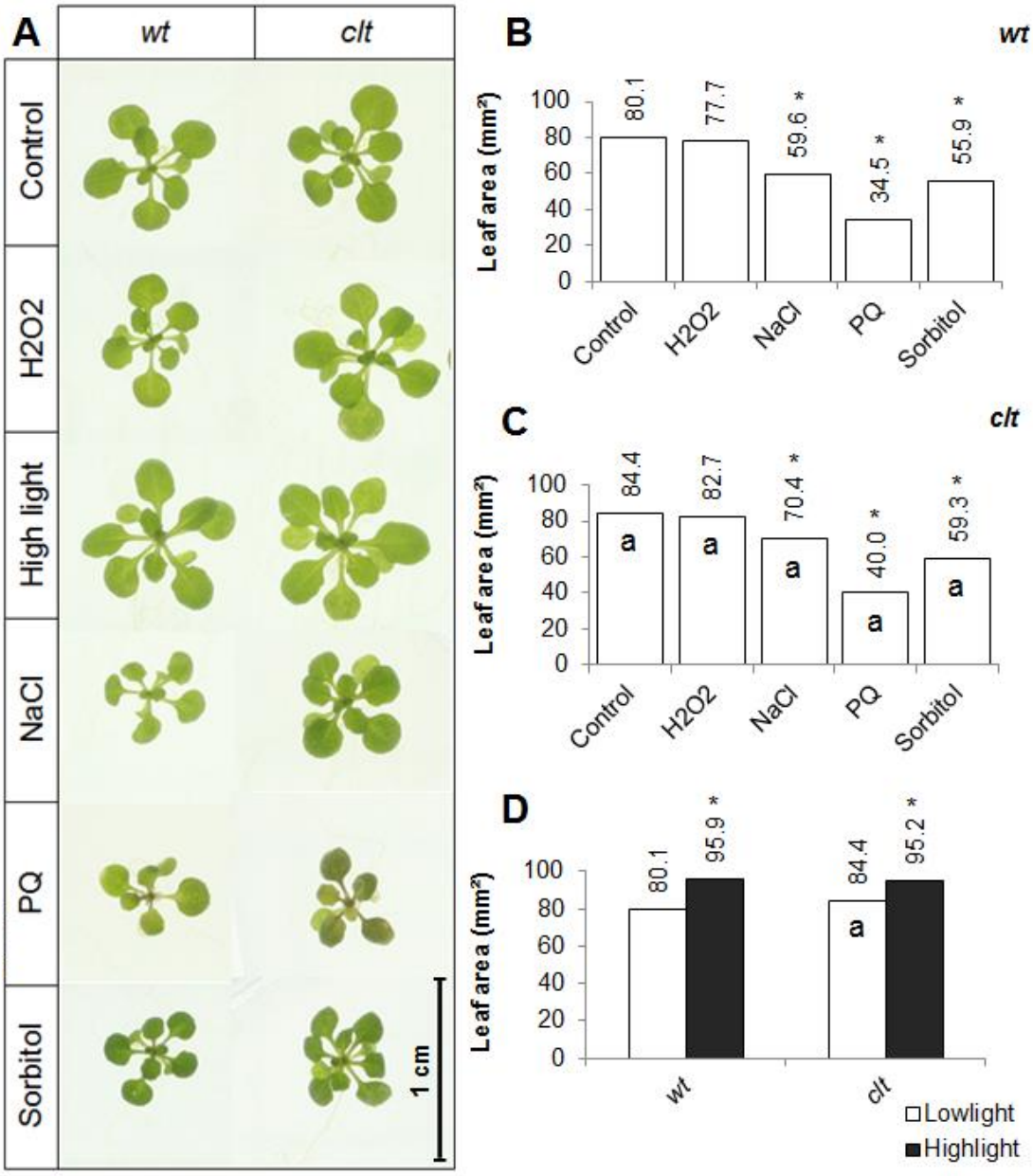

Figure 4-13: Comparison of leaf area in *wt* and a mutant genotype with cytosolic glutathione deficiency (*clt*) grown in induced stress conditions. Phenotypic comparison of leaf area phenotypes in 17-day old wild-type and an *Arabidopsis* mutant genotype with cytosolic glutathione depletion in the absence of stress (control) and after induced exposure to various stress treatments, A). The black bar represents 1 cm. Comparisons of leaf areas are displayed for: B) *wt* and C) *clt* and D) both genotypes in low and high light conditions. Data are shown as mean. Asterisks represent significant differences for control vs treatment comparisons for one genotype and “a” for comparisons of genotype vs wild-type within control or treatment condition ($p<0.01$).

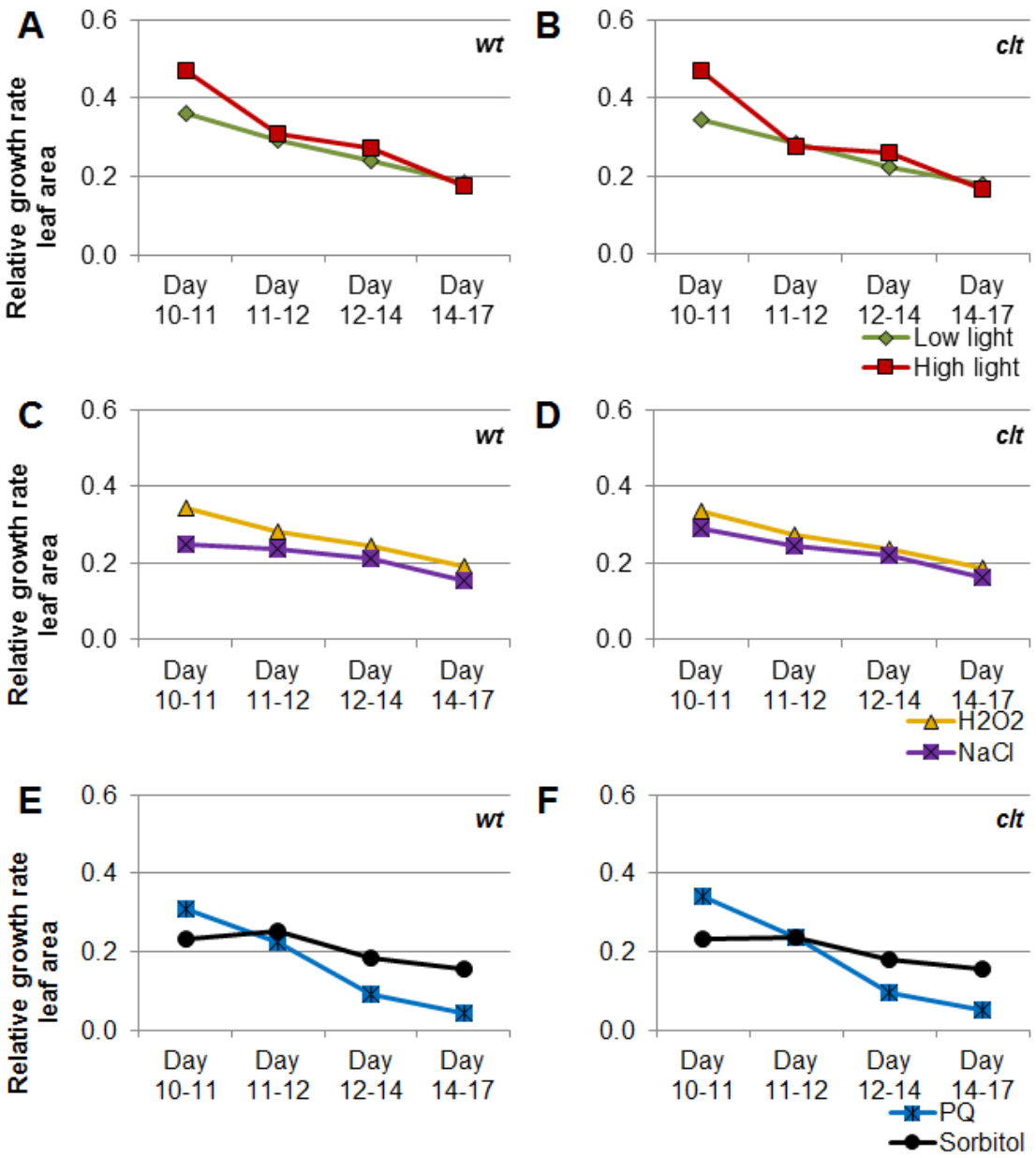

Figure 4-14: A comparison of relative growth rates for wild-type *Arabidopsis* (*wt*, A, C, E) and mutant plants exhibiting cytosolic depletion of glutathione (*clt*, B, D, F) grown in induced stress conditions. Comparisons were made for 17 day-old plants grown for 7 days under the following stress treatments: Low light and high light (A, B), H_2O_2 and NaCl (C, D) and PQ and Sorbitol (E, F). Data are shown as mean growth rates.

However, wild-type and clt plants grown under high light conditions did not exhibit significant differences in leaf area (Figure 4-13D). The PQ treatment resulted in the greatest decrease in leaf areas in the mutant and wild-type

plants (Figure 4-13B, C, D). Relative growth rates and the stress-induced decreases in this parameter were comparable in wild-type and mutant lines (Figure 4-14). The greatest decreases in relative growth rates were observed for the PQ and osmotic stress treatments (Figure 4-14E, F).

4.3.4 Continuous stress

The effects of continuous stress exposure were also compared in the wild-type and *clt* mutants. Leaf areas were determined in 14-day old plants that had been grown throughout in the absence or presence of the abiotic stresses imposed by the inhibition of PARP activity by 3-methoxybenzamide (3MB), the disruption of photosynthetic electron transport by paraquat (PQ), PQ-induced disruption of photosynthesis plus 3MB-induced inhibition of PARP (3MB&PQ), salt stress (sodium chloride), and osmotic stress (sorbitol).

Leaf areas were determined in a total of 768 plants with 384 plants measured per genotype and per condition. The *clt* mutants had significantly smaller leaf areas under stress conditions than the controls grown in the absence of stress, as did the wild-type plants (*; Figure 4-15B, C, D). However, the *clt* mutant had significantly larger leaf areas than the wild-type for plants grown in the presence of 3MB, 3MB&PQ and salt treatments (a; Figure 4-15A, B, C, D).

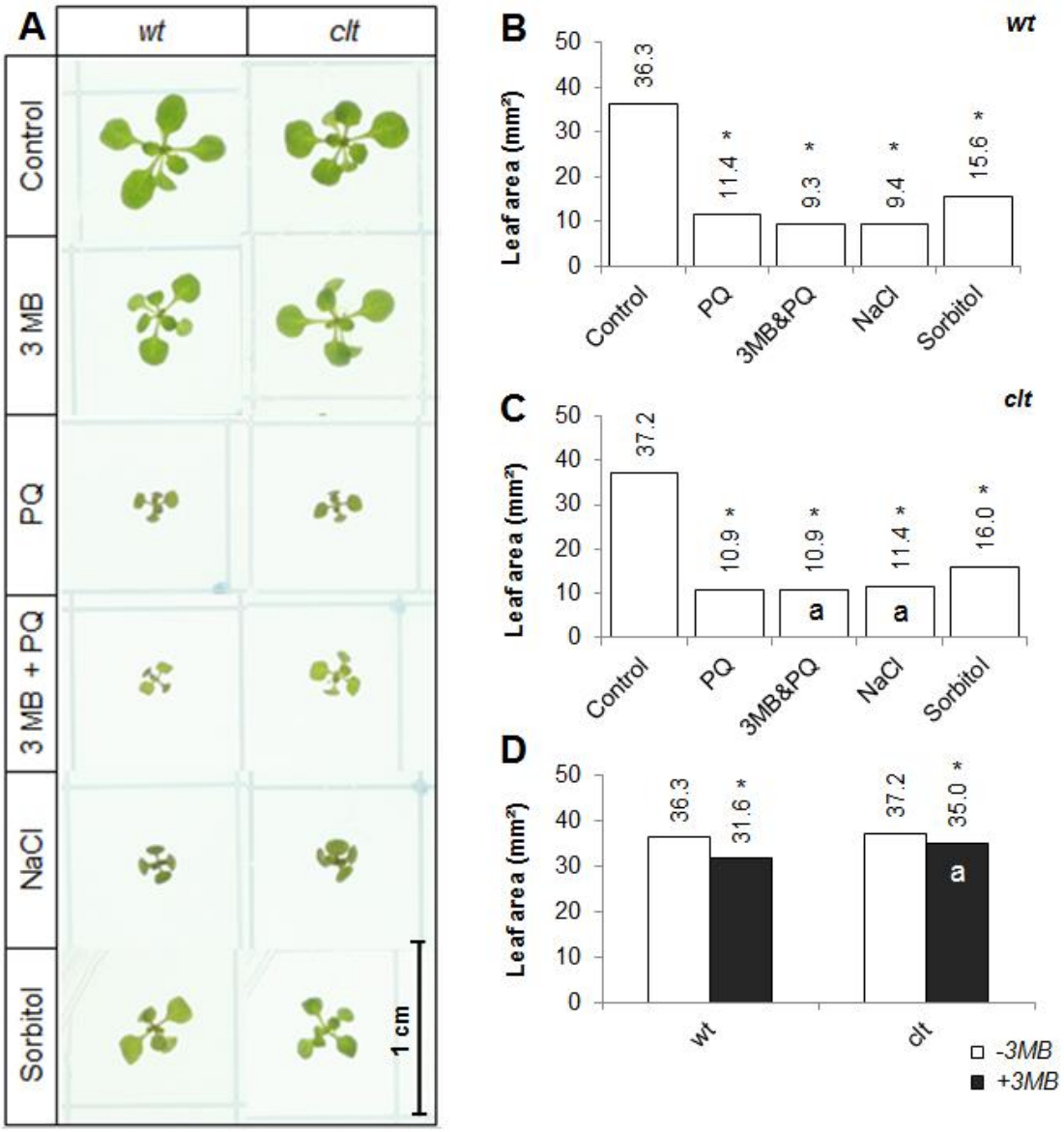

Figure 4-15: Comparison of leaf area in wt and a mutant genotype with cytosolic glutathione deficiency grown in continuous stress conditions. A: Phenotypic comparison of leaf area phenotypes in 14-day old wild-type and an *Arabidopsis* mutant genotype with cytosolic glutathione depletion in the absence of stress (control) and after continuous exposure to various stress treatments. The black bar represents 1 cm. Comparisons of leaf areas are displayed for: B: *wt* and C: *clt* and D: both genotypes in the absence (-3MB) and presence of 3MB (+3MB). Data are shown as mean. Asterisks represent significant differences for control vs treatment comparisons for one genotype and "a" for comparisons of genotype vs wild-type within control or treatment condition ($p<0.01$).

4.4 Conclusions

The data presented here show that a general deficiency in GSH decreases lateral root density. This effect was observed in the *cad2-1*, *pad2-1* and *rax1-1* mutants. Furthermore, altered intracellular partitioning of glutathione, as occurs in the *clt1clt2clt3* triple mutants, also resulted in significantly lower lateral root densities than in the wild-type. These findings demonstrate that a high cytosolic GSH pool is crucial for lateral root development.

The leaf areas of the *cad2-1*, *pad2-1* and *rax1-1* mutants grown under standard (low light) conditions were significantly smaller than the wild-type plants. In contrast, the altered intracellular partitioning of glutathione in the *clt1clt2clt3* triple mutants resulted in significantly larger rosette areas under these growth conditions. However, growth under high light led to a significant increase in overall rosette size in all genotypes and resulted in the restoration of the wild-type shoot phenotype in the *pad2-1* mutants. This observation might be due to the fact that an irradiance of 400 µmol m^{-2} sec^{-1} is hardly sufficient to elicit photoinhibitory effects, but rather stimulates growth. Conversely, the *cad2-1* and *rax1-1* mutants were still smaller than the wild-type under high light. These data suggest that the expression of the low-GSH rosette phenotype, observed in the mutants, is irradiance-dependent.

The effects of glutathione depletion and of altered intracellular GSH partitioning on growth responses to induced and continuous exposure to oxidative stress (paraquat), salt stress and osmotic stress were also analysed in this study.

All of the stress treatments used in these experiments, except H_2O_2, significantly decreased leaf area in all genotypes. However, the GSH-deficient and *clt1clt2clt3* mutants were no more sensitive to the stress treatments than the wild-type. In fact, in several cases the mutants were less sensitive than the wild-type to the stress treatments. These findings would suggest that glutathione depletion does not increase sensitivity to abiotic stress.

5 Chapter 5: Transcriptomic analyses of glutathione depletion

5.1 Introduction

Reduced glutathione plays a crucial role in plant development. Literature evidence demonstrates that knockout mutations in the gene encoding the first enzyme of glutathione biosynthesis (*GSH1*) results in an embryo-lethal phenotype and knockout mutations in the gene encoding the second enzyme of biosynthetic pathway (*GSH2*) results in seedling-lethal phenotypes (Cairns et al., 2006). Moreover, glutathione depletion to tissue amounts of less than 5% of those found in wild-type plants inhibits post-embryonic root development. For example, the *root meristemless 1-1* (*rml1-1*) mutant fails to establish an active post-embryonic root meristem due to an arrest of the cell cycle resulting from low glutathione availability (Vernoux et al., 2000A). The resulting phenotype is characteristic for the *rml1-1* mutant and is defined by an extremely short mature root composed of the same number of cells as the embryonic root (Cheng et al., 1995; Vernoux et al., 2000A).

However, our current knowledge of the mechanisms that explain glutathione functions or how glutathione might regulate gene expression, remains still limited (Cobbett et al., 1998; Vernoux et al., 2000A; Ball et al., 2004; Cairns et al., 2006; Parisy et al., 2006; Schlaeppi et al., 2008). As knockout mutations in the *GSH1* and *GSH2* gene result in embryo- or seedling-lethal phenotypes respectively, the *rml1-1* mutant remains the only non-lethal mutant genotype available to study the effects of severe glutathione depletion on changes in transcriptomic patterns. An analysis of the effects of glutathione on nuclear gene expression and a characterization of the genes affected by glutathione was one particular aim of this PhD study.

Earlier studies demonstrated that glutathione is recruited into the nucleus during early stages of the cell cycle in proliferating cells (Pellny et al., 2009). Furthermore, this increase in the nuclear glutathione pool correlates with an increase in PARP activity and is further known to precede increases in the abundance of *PARP1* and *PARP2* mRNAs (Pellny et al., 2009). Together with studies on glutathione-regulated gene expression in the *regulator of ASCORBATE PEROXIDASE2 1-1* (*rax1-1*) and *cadmium sensitive 2-1* (*cad2-1*) mutants, where transcripts encoding 32 stress-responsive genes changed in response to low glutathione in the mutants, available findings demonstrate an effect of glutathione on nuclear gene expression (Ball et al., 2004).

This PhD study had therefore the aim to investigate the effects of glutathione depletion on nuclear gene expression by using the *rml1-1* mutant, particularly focussing on the effects on stress responses, hormone metabolism and

signalling, expression of transcription factors and genes encoding components of DNA repair mechanisms. Specific objectives were to characterize genes clusters most affected by glutathione depletion in greater detail, allowing for deeper insights into the function of glutathione in plastid-to-nucleus (retrograde) signalling pathways and its impact on plant developmental processes, such as e.g. hormone metabolism and signalling or transcription factors. In general, characterizations of the effects of glutathione depletion on gene expression were performed on the 10 most transcriptionally induced and 10 most repressed genes for each category separately where possible. Analyses were carried out for genes in categories such as: cell cycle components, PARP and DNA repair mechanisms, stress responses, hormonal pathways with particular focus on auxin, abscisic acid and ethylene, as well as transcription factors and redox processes.

While there are various platforms for microarray analysis in *Arabidopsis thaliana*, such as e.g. Affymetrix ATH1 arrays (Redman et al., 2005) or Complete Arabidopsis Transcriptome MicroArray (CATMA) spotted microarrays (Sclep et al., 2007), Agronomics1 tiling arrays (Rehrauer et al., 2010) were chosen for this study. Affymetrix ATH1 arrays are the ones most widely used for transcriptome profiling in Arabidopsis to date and additionally Genvestigator covers more than 4300 hybridization to ATH1 (Rehrauer et al., 2010). However, Agronomics1 tiling arrays offer considerable advantages, such as e.g. coverage of the whole nuclear, chloroplastic and mitochondrial genomes of *Arabidopsis thaliana* (~81% of the known nuclear genome and ~99% of the organelle genomes), inclusion of all ATH1 perfect match probes, ability to measure transcript levels, as well as coverage of both strands of the

genome, which further allows obtaining strand-specific information (Rehrauer et al., 2010). And although Agronomics1 tiling arrays might represent the best possible method available to date for obtaining an initial overall picture of the effects of glutathione depletion on gene expression, the standard limitations inherent to microarrays still apply, such as e.g. variability of results, lack of sufficient reproducibility, insufficient fidelity of gene expression data, possible statistical problems or insufficient sensitivity. Hence, the results presented in the following can only provide initial insights into the effects of glutathione depletion on gene expression.

Agronomics1 tiling arrays and qRT-PCR were applied as methods in this PhD study to analyse GSH-dependent effects on leaf and root transcriptome patterns. In particular, leaf and root trancriptomes of shoots and roots of the *rml1-1* mutant were compared relative to the wild-type to identify any tissue specific effects. For the annotation of genes in the tiling array analysis, the most recent version of the TAIR databases was used (TAIR10, 2012; Lamesch et al., 2011). The full microarray data can be found at NCBI GEO as Series GSE36893 (http://www.ncbi.nlm.nih.gov/geo/query/acc.cgi?acc=GSE36893). Changes in gene expression that were identified in the *rml1-1* might also provide information about the occurrence of the characteristic root phenotype in this mutant. qRT-PCR was finally applied to verify changes in the abundance of a few selected transcripts in the *rml1-1* mutant, in mutant lines with less severe glutathione depletion, as well as in wild-type plants that were grown in the presence of BSO. Each experiment comprised three independent biological replicates per genotype. It was finally hypothesized that less severe

alleles of the *GSH1* gene, with only 20 to 50 % less glutathione compared to the wild-type, would also result in smaller changes in gene expression.

5.2 Results – Microarray analysis of general glutathione deficiency in the *root meristemless 1-1* (*rml1-1*) mutant

Transcriptome analyses of *rml1-1* roots and shoots and of the wild-type were carried out on 7-day old seedlings grown on plates. Preliminary studies had shown that this time point allowed seedling growth without the appearance of any adverse effects in the shoots resulting from the impaired root development in the *rml1-1* mutants. RNA samples were analyzed using Agronomics1 tiling arrays and normalized data were analysed with BINGO cytoscape 2.8.1 (Maere et al., 2005; tool for the determination of gene ontology categories that are statistically overrepresented), MapMan 3.5.1 (Thimm et al., 2004; tool to display large microarray datasets as diagrams of metabolic pathways or other processes) and Multi experiment Viewer 4.6.2 (Saeed et al., 2003; microarray data analysis tool, incorporating sophisticated algorithms for clustering, visualization, classification, statistical analysis).

A total of 1,449 transcripts changed in abundance in the shoots of the *rml1-1* mutants relative to the wild-type (Table 5-1). Of these, 650 decreased in abundance in *rml1-1*, while 799 increased in the *rml1-1* shoots (Table 5-1). As the initial method for tissue disruption did not allow for the extraction of sufficient amounts of highly pure RNA to obtain three separate biological replicates, samples had to be pooled and hence no statistical evaluation of the transcriptome data obtained for roots was possible. However, a preliminary

analysis revealed that 3,771 transcripts were changed in abundance in the *rml1-1* roots relative to the wild-type (Table 5-1) with 2199 decreasing and 1572 increasing in abundance in *the rml1-1* mutant (Table 5-1). Very few transcripts changed in *rml1-1* tissues encoding enzymes involved in primary metabolism (photosynthesis, TCA cycle and glycolysis) (Figure 5-1). In particular relative expression of transcripts encoding γ-ECS and GSH-S was higher in the *rml1-1* roots and shoots than in the wild-type (Figure 5-2).

Table 5-1: Overview of transcripts with altered expression identified from an initial analysis of the microarray data of the *rml1-1* mutant. Shown are the overall number of transcripts that are altered in expression in shoots and roots of the *rml1-1* (Total); the number of transcripts after statistical analysis for the shoot ($p < 0.05$); the number of transcripts after excluding values with a false discovery rate of larger than 0.05 for the shoot (FDR<0.05); the number of transcripts with fold changes in expression larger than 2-fold or smaller than 0.5-fold relative to the wild-type (2<FC<0.5); and the number of transcripts in shoots and roots that show down- (Lower in the *rml1-1*) or up-regulated (Higher in the *rml1-1*) expression in response to glutathione depletion in the *rml1-1*.

	Total	**P < 0.05**	**FDR < 0.05**	**2 < FC < 0.5**	**Lower in *rml1-1***	**Higher in *rml1-1***
Shoot	30608	11046	7251	1449	650	799
Root		Single sample comparison		3771	2199	1572

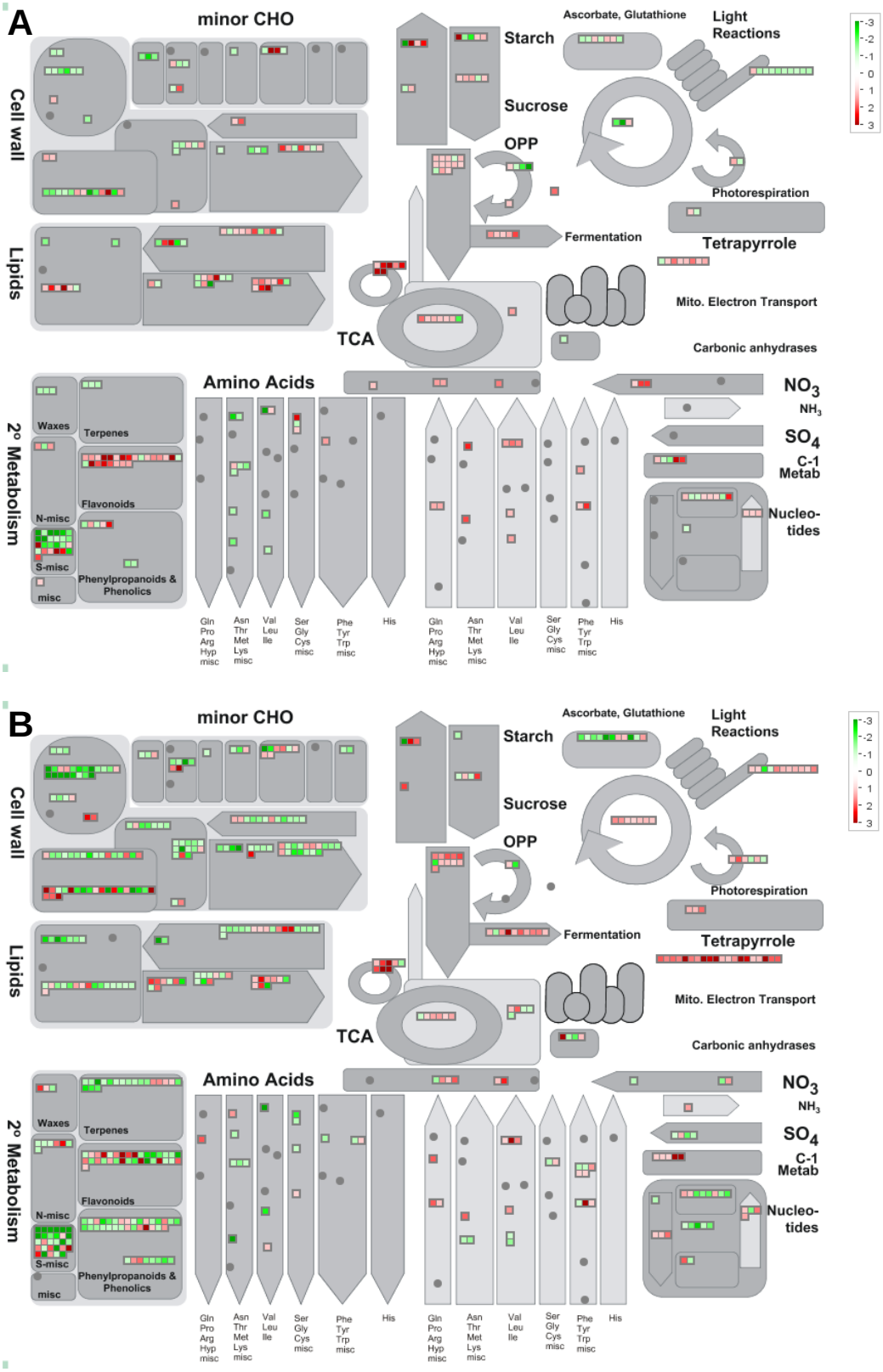

Figure 5-1: MapMan overview for changes in primary metabolism in *rml1-1* mutant. Depicted are changes in primary metabolism in shoots of *rml1-1* plantlets (A), and in roots of *rml1-1* plantlets (B).

Although earlier studies were already able to demonstrate strongly diminished activities of γ-ECS under glutathione depleting conditions (Vernoux et al., 2000A), the results found in this analysis support this finding. Furthermore, it seems that *rml1-1* plants try and compensate for the non-functional γ-ECS and the resulting lower glutathione amounts with higher expression of genes encoding the two enzymes involved in glutathione biosynthesis (Figure 5-2).

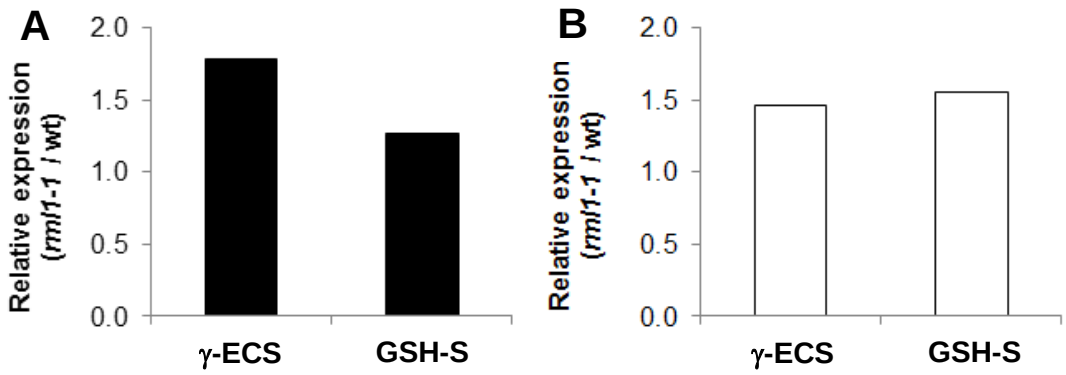

Figure 5-2: Comparison of expression of genes involved in glutathione biosynthesis. Displayed are fold-changes in expression of the genes encoding enzymes of glutathione biosynthesis (γ-ECS and GSH-S) for root (black bars; A) and shoot (white bars; B) of the *rml1-1* mutant relative to the wild-type.

5.2.1 Effects on core cell cycle components

In a next step, the effect of glutathione depletion on cell cycle genes was investigated. A list of genes was retrieved from TAIR for all genes that were annotated as either directly involved in the control of the cell cycle, cell cycle-related or otherwise related to cell division. This list was then compared with transcripts from the *rml1-1* tiling array analysis that exhibited altered expression. For reasons of simplicity AGI codes were avoided from the

graphics in this section, but they can be found in Appendix VI: Overview of selected transcripts that are presented in Chapter 5 “Transcriptomic analyses glutathione depletion”..

This analysis revealed that transcripts encoding core cell cycle components, such as cyclins (CYCs) and cyclin-dependent kinases (CDKs), were changed in *rml1-1* roots relative to the wild-type (Figure 5-3A). CDKs are family of protein kinases that are governing progression through the cell cycle. However, crucial to this control of the cell cycle is the formation of various different CDK-cyclin complexes, which then phosphorylate a large number of substrates at crucial G1 to S and G2 to M transition points (Inze & De Veylder, 2006; Francis, 2007; Gutierrez et al., 2009). Upon phosphorylation of certain substrates further processes are triggered, such as e.g. DNA replication or mitosis (Inze & De Veylder, 2006; Francis, 2007; Gutierrez et al., 2009). Apart from the ability to form CDK-cyclin complexes, little is known about the actual interaction of cyclins with CDKs. However, it is thought that D-type cyclins regulate the G1 to S transition, that A-type cyclins are involved S to M phase control, and that B-type cyclins participate in both G2 to M transition as well as in M phase control (Inze & De Veylder, 2006; Francis, 2007; Gutierrez et al., 2009).

Of such cyclins (CYCs) and cyclin-dependent kinases (CDKs), in particular CYCD3;1, CYCA1;1, CYCB1;2, CYCB1;3, CYCB1;4, CYCB2;1, CYCB2;2, CYCB2;4, CDKB1;2, CDKB2;1, CDKB2;2, CYCP3;2 and CYCP4;1 transcripts were at least two-fold lower in *rml1-1* roots relative to the wild-type (Figure 5-3A).

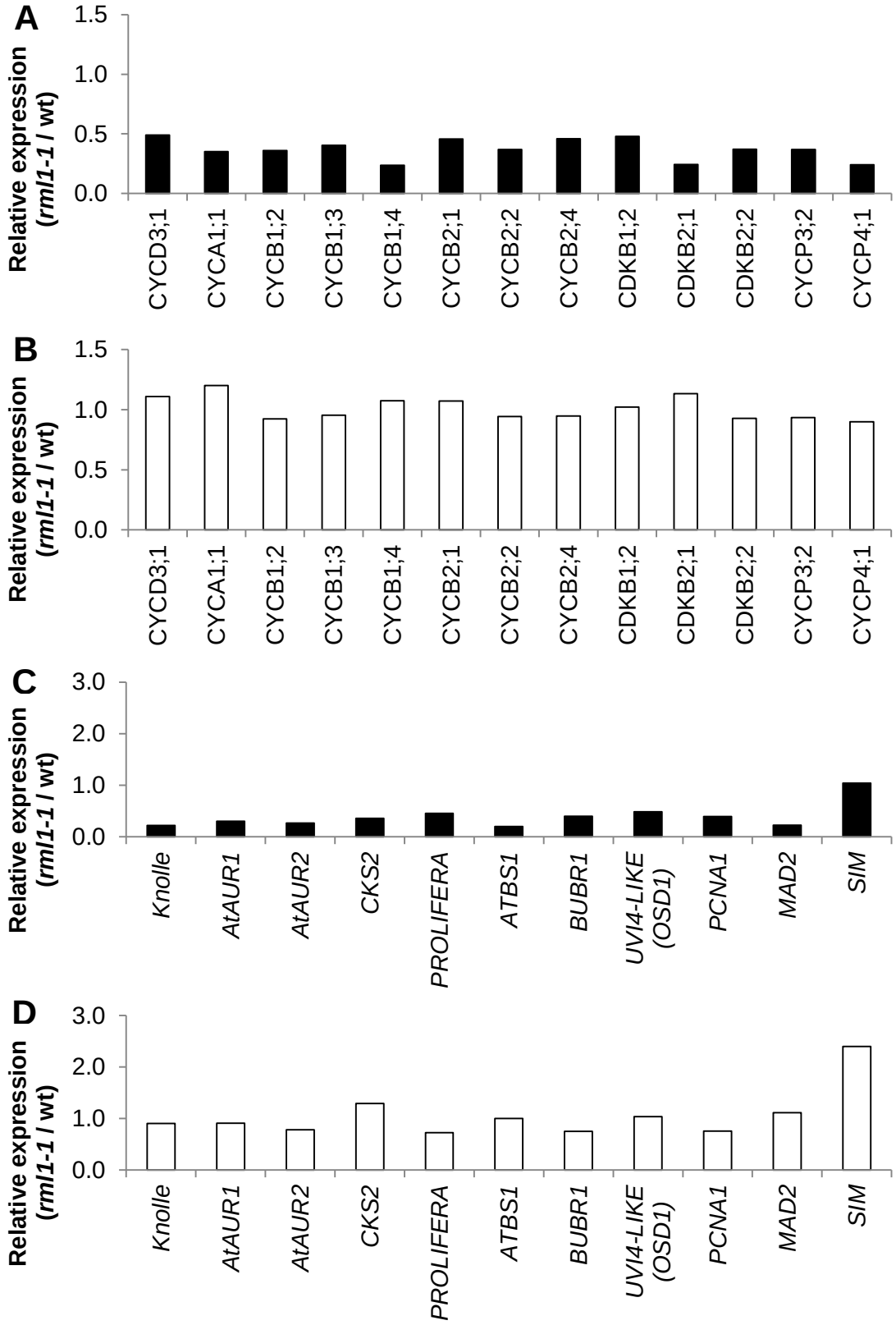

Figure 5-3: Comparisons of expression for transcripts involved in cell cycle regulation. Relative expression is shown as fold-change in the roots (black bars; A and C) and shoots (white bars; B and D) of *rml1-1* mutant relative to wild-type plants. While A and B represent the relative expression of core cell cycle genes, C and D show the genes, whose expression is affected during the cell cycle, in the *rml1-1* seedlings relative to the wild-type.

But none of these transcripts changed in abundance in *rml1-1* shoots, suggesting that the effects of glutathione depletion are stronger in root tissues (Figure 5-3B). Literature evidence described a link between glutathione and thioredoxin. At least within the shoots functional redundancies between glutathione and thioredoxin functions exist, allowing for compensations of a loss of either of these compounds, which might explain why the expression of these transcripts remains unaffected in the shoots of the *rml1-1* (Reichheld et al., 2007).

Transcripts related to the cell cycle and cell division-related processes also changed in *rml1-1* roots relative to the wild-type. Knolle (involved in: acetyl-CoA metabolic process, cell proliferation, cellular membrane fusion, cytokinesis, cytokinesis by cell plate formation, intracellular protein transport, microtubule cytoskeleton organization, spindle assembly; TAIR10), AtAUR1, AtAUR2 (both are necessary for cytokinesis as well as with the microtubule spindle; TAIR10), CKS2 (cyclin-dependent kinase, regulatory subunit; TAIR10), PROLIFERA (involved in DNA replication initiation; TAIR10), ATBS1 (promotes the correct definition of the hypophysis cell division plane; TAIR10), BUR1, UVI4-Like (OSD1), PCNA1 (involved in cell cycle regulation; TAIR10)and MAD2 (spindle assembly checkpoint protein functions; TAIR10) transcripts were at least two-fold lower in *rml1-1* roots than in the wild-type (Figure 5-3C). These are interesting undocumented findings, which suggest that glutathione depletion might result in a full arrest of not only the cell cycle, but also of all cell division-related processes.

In addition, SIAMESE (SIM) transcripts were 2.4-fold higher in *rml1-1* shoots than in the wild-type (Figure 5-3C and D). This finding represents another indicator for a possible very important role for glutathione in the control of the cell cycle, as SIM is required in coordinating cell division and cell differentiation and its expression seems to be controlled by glutathione. Earlier studies had only shown that gibberellic acid-mediated signalling controls cell proliferation and also SIM (Achard et al., 2009). Finally, of the transcripts decreased in *rml1-1* roots that encode either cyclins or cyclin-dependent kinases, which are involved in cell cycle regulation, 11 have functions in the G_2 to M transition, suggesting that cell cycle progression is likely arrested at an earlier stage and therefore expression of proteins required during G_2 to M phase may not be expressed (Figure 5-4). Additionally, the tiling array analysis also revealed that only one repressed transcript in *rml1-1* roots was involved in the G_1 to S transition (CYCD3;1, Figure 5-4). This might indicate that glutathione depletion causes a cell cycle arrest at the G_1 to S transition and genes involved in later stages (CYCA1;1, CYCB1;2, CYCB1;3, CYCB1;4, CYCB2;1, CYCB2;2, CYCB2;4, CDKB1;2; CDKB2;1, CDKB2;2, CYCP3;2, and CYCP4;1) of the cell cycle are consequently not expressed. This indication can be supported by literature evidence provided from studies by Inze and De Veylder (Inze & De Veylder, 2006). They described a model of cell cycle control in which CDKA plays a pivotal role at both G1 to S as well as G2 to M transition points. However, to actually become phosphorylated and facilitate these transitions CDKA is required to form a complex with D-type cyclins (Inze & De Veylder, 2006). CYCD3;1 might be the crucial or one possible interaction partner enabling the activation of CDKA via phosphorylation.

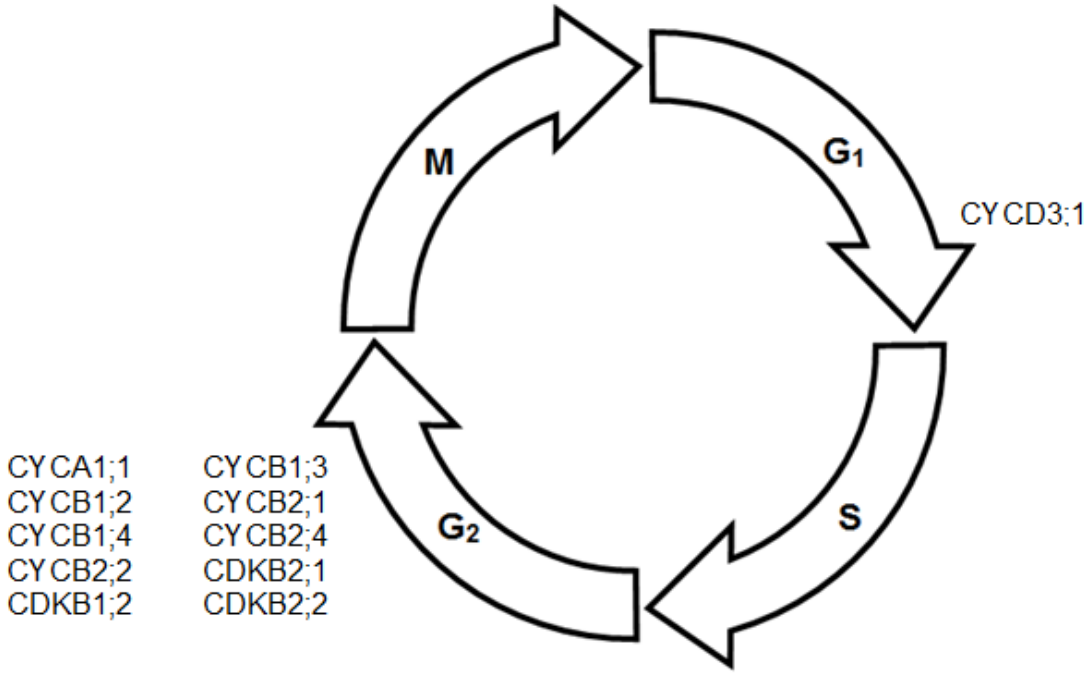

Figure 5-4: Schematic representation of the cell cycle stages with transcripts. Displayed are transcripts that were differentially expressed in the roots of the *rml1-1* mutants relative to the wild-type. Transcripts are shown next to the respective stage of the cell cycle they are associated with.

In addition, an arrest of the cell cycle at G1 to S transition would be in line with other observations made in tobacco cell suspension cultures, where glutathione depletion resulted in an arrest of the cell cycle at G1 to S transition (Vernoux et al., 2000A). Although these considerations require more profound investigation, they can at least serve as stronger indications.

Nevertheless, the findings that CYCD3;1 was the only cell cycle marker that could be identified in the tiling array analysis, as related to the G1 to S transition of the cell cycle, and the finding that this marker was repressed under glutathione depleting conditions has not been documented before. This strongly suggests that glutathione might control cell cycle progression by

having an important impact on the regulation of cell cycle-related transcript expression.

5.2.2 Effects on PARP expression and DNA repair

In a next step, the effect of glutathione depletion was investigated on PARP expression and DNA repair. Oxidative stress, induced by reactive oxygen species (ROS), such as H_2O_2, triggers both a programmed cell death and various stress responses in plants (Houot et al., 2001; Pellinen et al., 2002, Vandenabeele et al., 2003). Reactive oxygen species also modify cellular components and cause genotoxic damage resulting in DNA mutations (Bray and West, 2005; Møller et al., 2007). The plant's ability to trigger programmed cell death and to repair damaged DNA relies crucially on the activity of poly (ADP-ribose) polymerases (PARPs). DNA damage and the subsequent expression of PARPs are associated with cell signalling events with PARP activity correlating with an increase in the nuclear glutathione pool during early stages of the cell cycle (Foyer and Noctor, 2005A, B; Pellny et al., 2009). Therefore, a further interest of this PhD study was to further characterize the association between glutathione, PARPs and DNA repair mechanisms.

The tiling array dataset was mined for expression of PARP genes and genes involved in DNA repair, which revealed that transcript amounts encoding poly-(ADP-ribose) polymerase (PARP) 1 and *SIMILAR TO RCD ONE* (*SRO*) were strongly induced in *rml1-1* roots compared to wild-type roots (Figure 5-5). All five SRO genes indentified in the tiling array analysis to be responsive to glutathione depletion, possess a PARP signature upstream of the C-terminal

protein interaction domain. This PARP signature may bind NAD+ and attach the ADP-ribose-moiety from NAD+ to the target molecule. The presence of particularly PARP signatures in SRO genes suggests a role for the protein in ADP ribosylation (TAIR10, 2012).

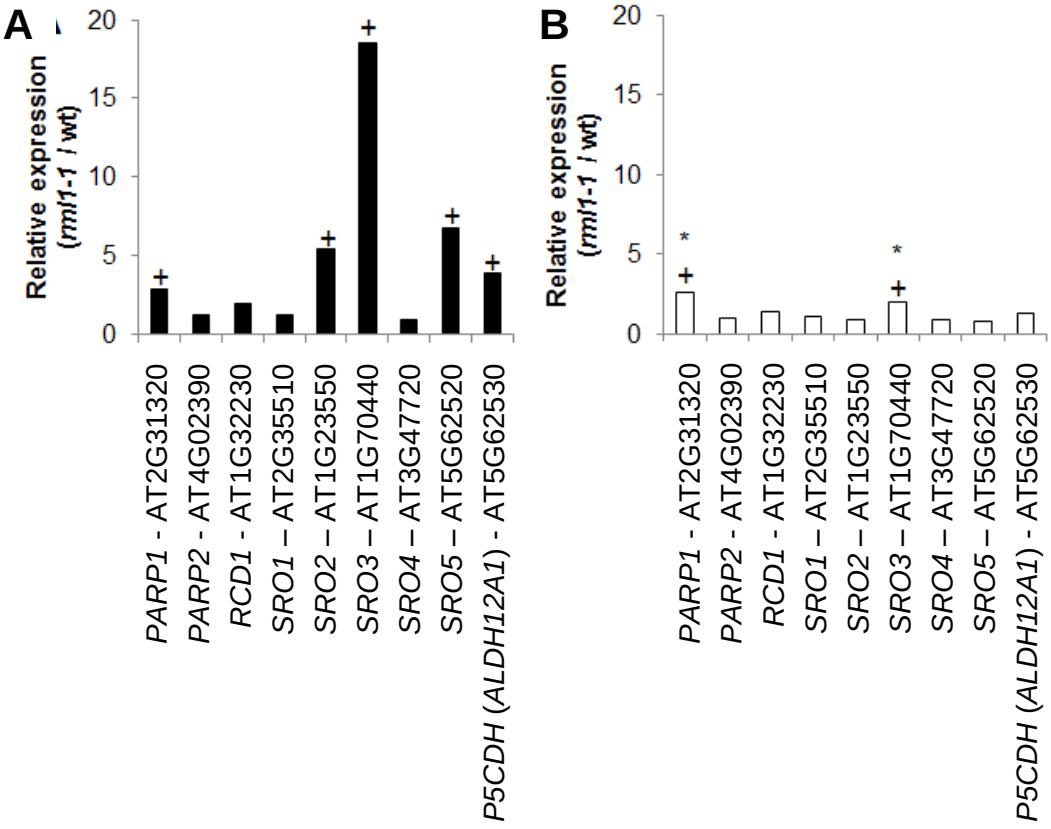

Figure 5-5: Comparisons of expression for transcripts related to PARP and DNA repair. Shown are comparisons of relative expression of suites of genes in the *rml1-1* roots (black bars; A) and shoots (white bars; B) relative to the wild-type. Included are *PARP1* and *PARP2*, *RCD1*, *SRO* genes, and *P5CDH* (*ALDH12A1*). *, p-value<0.05; +, fold-change to wild-type>2.

In addition, the amount of Δ^1-*PYRROLINE-5-CARBOXYLATE DEHYDROGENASE 1* (*P5CDH1*), which is described as involved in catabolism of proline to glutamate and inducible by exogenous proline (Kirch et al., 2004; Verslues & Sharma, 2010; TAIR 10), and *SRO5* mRNAs were higher

in *rml1-1* roots than in the wild-type. The effect of glutathione depletion on DNA repair mechanisms seems to not necessarily affect whole gene families, but has a rather distinct effect on single genes (Figure 5-5A). *P5CDH1* and *SRO5* represent an overlapping gene in the sense orientation, which together can generate 24-nt and 21-nt siRNAs that in turn are components of a regulatory loop controlling reactive oxygen species (ROS) production and stress response (Deuschle et al., 2001; Borsani et al., 2005; Verslues & Sharma, 2010; TAIR10, 2012). Verslues and Sharma suggested that at least SRO5 might be linking proline and reactive oxygen (Verslues & Sharma, 2010).

Furthermore, induction of *SIMILAR TO RCD ONE* (SRO) genes, which are described as homologues to the *RADICAL INDUCED CELL DEATH 1 (RCD1)* gene and belong to the poly (ADP-ribose) superfamily, shows the close interaction between the DNA repair mechanisms (Teotia & Lamb, 2011). *RCD1* and *SRO* genes are described as crucial in maintaining cells in a division-competent state and to regulate division plane placement (Teotia & Lamb, 2011). Based on observations made in *rcd1-3* and *sro1-1* mutants, which both exhibit severe defects in the quiescent centre and show abnormal root apical meristems, it was hypothesized that RCD1 and SRO1 are involved in redox control and that their absence would lead to an altered redox balance causing the observed effects (Teotia & Lamb, 2011).

5.2.3 Effects of glutathione depletion on stress responses and hormones

Earlier studies on the effects of glutathione on expression of stress-responsive genes in *rax1-1* (*regulator of ASCORBATE PEROXIDASE2 1-1*) and *cad2-1* (*cadmium sensitive 2-1*) mutants indicated that transcripts encoding 32 stress-responsive genes changed in response to a low glutathione content (Ball et al., 2004). However, these findings only provided an initial and limited insight into the effects of glutathione depletion on gene expression, but not any in-depth understanding as to why, or how, yield gaps might occur. Yield gaps are described as the difference between a plants maximum attainable yield when grown under standard conditions and the actual yield for plants grown under stress conditions. As plants stop growing early in response to environmental stresses, optimal productivity of crops is hampered. As the link between glutathione and the expression of stress-responsive genes has already been demonstrated, the question remains how it exactly participates in the control of plant growth, particularly under stress. A more detailed investigation was therefore carried out, particularly determining the effects of glutathione on expression of stress- and hormone-related genes, to better understand how glutathione participates in plant development and stress responses.

Hierarchically clustered heat maps were produced using the TIGR-MeV to determine which categories of stress- and hormone-related genes were most affected by glutathione depletion. In this analysis, genes with similar patterns of expression were grouped for shoots and roots of wild-type and *rml1-1* mutant plants, respectively (as shown later in Figure 5-6 and Figure 5-8). The

most recent version of TAIR was applied (Lamesch et al., 2011; TAIR10, 2012) for gene annotation. Genes not precisely annotated in TAIR are displayed in Figure 5-6 (pages 118 and 119) and Figure 5-8 (pages 127 and 128) without a primary name.

5.2.3.1 Effects on stress-related genes

Several genes involved in biotic stress responses were differentially expressed in *rml1-1* plants relative to wild-type plants (Table 5-2). For abiotic stress, genes changed in expression in *rml1-1* relative were particularly involved in the heat stress response (Table 5-2).

Table 5-2: Ranked overview of total number of genes with annotation to stress responses in clusters. Gene annotations were retrieved from TAIR10, clusters created based on the involvement of genes to different types of stress, and ranking was performed according to total number of genes present in each cluster. The two main clusters are represented by genes involved biotic and abiotic stress responses. A more detailed sub-clustering was performed only for the genes involved in abiotic stress responses. Some genes in the cluster with abiotic stress-annotated genes could be found in more than one sub-cluster.

Cluster label	Cluster size
Biotic	136
Abiotic	42
Heat	29
Drought, salt	17
Cold	8
Wounding	2

As heat-shock proteins (hsps)/chaperones are responsible for a variety of processes, such as protein folding, assembly, translocation and degradation, in stabilizing proteins and membranes as well as assisting in the refolding of

proteins under environmental stress conditions, they play a crucial role in the protection of plants from stresses (Wang et al., 2004). The finding that stress-related genes are down-regulated by glutathione depletion and that the majority of these genes are involved in responses to heat stress, suggests a major impact of glutathione on a plants proteins and maintaining their functions.

Among the 10 most increased and decreased transcripts, which responded to glutathione depletion, genes were identified that are involved in responses to drought, cold-acclimation and tolerance to freezing stress, but also encoding pathogenesis-related proteins (Table 5-3, Table 5-4). The wide range of processes these genes relate to demonstrate the central function of glutathione in the control of stress responses in plants. A loss of glutathione therefore results in a mis-regulation of responses to various stresses.

For example, in *rml1-1* shoots the *DROUGHT-INDUCED 21* (*DI21*) gene was 1.8-fold up-regulated (Table 5-3) and this gene has previously been shown to be up-regulated in leaf- and root-tissues under progressive drought and to be responsive to exogenous supply with abscisic acid (Gosti et al., 1995). The *DROUGHT-REPRESSED 4* (*DR4*) gene was down-regulated in both *rml1-1* shoots and roots by 1.6- and 4.4-fold, respectively (Table 5-4). *DR4* encodes a plant-specific protease inhibitor-like protein whose transcripts in roots disappear in response to progressive drought stress (TAIR10, 2012).

Table 5-3: Overview to the 10 most induced and repressed stress-related genes from shoots of the *rml1-1*. Shown are AGI codes, descriptions, p-values from statistical analysis of the shoot as well as fold changes in expression for shoot and root.

		AGI code	Description	p-value (shoot)	fold change shoot	fold change root
Isolated from shoot	Induced	AT4G23680	Polyketide cyclase/dehydrase and lipid transport superfamily protein	0.000	3.14	2.15
		AT1G72900	Toll-Interleukin-Resistance (TIR) domain-containing protein	0.000	2.31	2.55
		AT1G72920	Toll-Interleukin-Resistance (TIR) domain family protein	0.000	2.25	1.88
		AT1G72070	Chaperone DnaJ-domain superfamily protein	0.000	2.18	0.67
		AT1G55210	Disease resistance-responsive (dirigent-like protein) family protein	0.000	1.91	0.65
		AT4G15910	DROUGHT-INDUCED 21 (DI21)	0.000	1.84	1.05
		AT2G36800	DON-GLUCOYLTRANSFERASE 1 (DOGT1)	0.000	1.79	6.38
		AT2G43590	Chitinase family protein	0.004	1.77	2.93
		AT5G09980	ELICITOR PEPTIDE 4 PRECURSOR (PROPEP4)	0.001	1.50	-1.55
		AT5G42050	DCD (Development and Cell Death) domain protein	0.000	1.41	1.24
	Repressed	AT1G73330	DROUGHT-REPRESSED 4 (DR4)	0.000	-1.60	-4.41
		AT4G22212	Encodes a defensin-like (DEFL) family protein	0.001	-1.82	-3.97
		AT4G14630	GERMIN-LIKE PROTEIN 9 (GLP9)	0.001	-1.94	-2.81
		AT4G07820	Cysteine-rich secretory proteins, and Pathogenesis-related 1 superfamily protein	0.001	-2.07	-1.72
		AT1G20440	COLD-REGULATED 47 (COR47)	0.000	-2.11	-2.27
		AT2G01530	MLP-LIKE PROTEIN 329 (MLP329)	0.001	-2.15	-3.81
		AT2G43550	Encodes a defensin-like (DEFL) family protein	0.000	-2.49	-2.30
		AT5G36910	THIONIN 2.2 (THI2.2)	0.000	-2.61	0.48
		AT1G65870	Disease resistance-responsive (dirigent-like protein) family protein	0.000	-3.02	-0.27
		AT1G66100	Predicted to encode a PR (pathogenesis-related) protein	0.000	-5.40	-0.68

Table 5-4: Overview to the 10 most induced and repressed stress-related genes from roots of the *rml1-1*. Shown are AGI codes, descriptions, p-values from statistical analysis of the shoot as well as fold changes in expression for shoot and root.

		AGI code	Description	p-value (shoot)	fold change shoot	fold change root
Isolated from root	Induced	AT2G36800	DON-GLUCOSYLTRANSFERASE 1 (DOGT1)	0.000	1.79	6.38
		AT2G43510	TRYPSIN INHIBITOR PROTEIN 1 (TI1)	0.000	1.03	4.54
		AT5G12030	HEAT SHOCK PROTEIN 17.6A (HSP17.6A)	0.910	-0.07	4.40
		AT1G53540	HSP20-like chaperones superfamily protein	0.667	-0.22	3.80
		AT5G12020	17.6 KDA CLASS II HEAT SHOCK PROTEIN (HSP17.6II)	0.173	-1.39	3.73
		AT1G07400	HSP20-like chaperones superfamily protein	0.881	0.05	3.69
		AT1G75830	LOW-MOLECULAR-WEIGHT CYSTEINE-RICH 67 (LCR67)	0.035	0.40	3.62
		AT5G51440	HSP20-like chaperones superfamily protein	0.073	1.09	3.49
		AT1G64160	DIRIGENT PROTEIN 5 (DIR5)	0.070	-0.28	3.39
		AT2G29500	HSP20-like chaperones superfamily protein	0.027	0.88	3.26
	Repressed	AT2G02130	LOW-MOLECULAR-WEIGHT CYSTEINE-RICH 68 (LCR68)	0.028	-0.25	-2.98
		AT3G50460	HOMOLOG OF RPW8 2 (HR2)	0.132	-0.32	-3.03
		AT4G22214	Encodes a defensin-like (DEFL) family protein.	0.236	-0.21	-3.08
		AT2G01530	MLP-LIKE PROTEIN 329 (MLP329)	0.001	-2.15	-3.81
		AT4G22212	Encodes a defensin-like (DEFL) family protein.	0.001	-1.82	-3.97
		AT5G42500	Disease resistance-responsive (dirigent-like protein) family protein	0.774	0.12	-4.35
		AT1G73330	DROUGHT-REPRESSED 4 (DR4)	0.000	-1.60	-4.41
		AT3G26460	Polyketide cyclase/dehydrase and lipid transport superfamily protein	0.016	0.71	-4.66
		AT4G11210	Disease resistance-responsive (dirigent-like protein) family protein	0.193	-0.37	-4.78
		AT2G01520	MLP-LIKE PROTEIN 328 (MLP328)	0.020	-2.34	-5.95

The finding that drought-related genes are affected under glutathione depletion might be explained by either a regulatory involvement of glutathione in these processes or by the root phenotype of the *rml1-1* mutant. It is more likely, however, that the extremely short primary root might not be able to take up sufficient amounts of water to cover the demands of the plant and thereby drought-related processes are activated. Nevertheless, literature evidence also supports the hypothesis that glutathione might be directly involved in regulatory processes in response to drought stress by demonstrating a link between glutathione and drought stress responses in *glutathione peroxidase 3* (*GPX3*) T-DNA insertion mutants of *Arabidopsis* (Miao et al., 2006). The study conducted by Miao suggested that GPX3 fulfils a double function with roles in H_2O_2 homeostasis and as oxidative signal transducer in ABA and drought stress signalling specifically transmitting H_2O_2 signals (Miao et al., 2006). To determine peroxidase activity of GPX3 against various substrates Miao and colleagues performed further tests and found GPX3 peroxidase activity against thioredoxin as substrate, but in the presence of reduced glutathione (Miao et al., 2006). Complementary experiments further revealed that the oxidized form of the GPX3 peroxidase can be reduced by thioredoxin via the thioredoxin reductase system, even after addition of H_2O_2 (Miao et al., 2006). However, GPX3 could not be reduced through the GSH system, suggesting that GPX3 is in fact a thioredoxin-dependent peroxidase (Miao et al., 2006). Future experiments investigating the role of glutathione in the responses to drought might provide more insights into GPX3 function, but would have to take thioredoxin and abscisic acid into account.

Furthermore, the *COLD-REGULATED47* (*COR47*) gene, a CBF-regulon gene related to cold-acclimation, was down-regulated in both *rml1-1* shoot- and root-tissues by 2-fold (Table 5-3). *COR47*, a C-REPEAT BINDING FACTOR (CBF) regulon gene, is controlled by circadian regulation and is one of at least three CBF regulon genes involved in cold acclimation and freezing tolerance (Dong et al., 2011). CBF genes on the other hand encode transcriptional activators resulting in expression of CBF-targeted genes known as “CBF-regulons” (Dong et al., 2011). COR47 represents one of these CBF-targeted CBF-regulon genes. Plants carrying mutations in *CIRCADIAN CLOCK-ASSOCIATED1* (*CCA1*) and *LATE ELONGATED HYPOCOTYL* (*LHY*) down-regulate CBF genes and *COR47* exhibit impaired cold-acclimation (Dong et al., 2011). The finding that *COR47* is down-regulated in response to glutathione depletion in *rml1-1* suggests that glutathione is at least partially involved in the transcriptional control of cold- and freezing-acclimation in plants.

A gene encoding DON-GLUCOSYLTRANSFERASE 1 (DOGT1) was further up-regulated in both *rml1-1* shoots and roots by 1.8- and 6.4-fold, respectively (Table 5-3). DOGT1 is a UDP-glycosyltransferase involved in the detoxification of deoxynivalenol, a mycotoxin produced by the pathogenic fungi *Fusarium graminearum* and *Fusarium culmorum* (Poppenberger et al., 2003). Expression of DOGT1 is developmentally regulated and induced by deoxynivalenol as well as salicylic acid, ethylene, but also jasmonic acid. Further, overexpression of DOGT1 in *Arabidopsis thaliana* enhances tolerance against deoxynivalenol (Poppenberger et al., 2003). A more recent study in barley has provided evidence that overexpression of *Arabidopsis thaliana* DOGT1 causes a dwarf phenotype (Shin et al., 2012). Since this gene is up-regulated in *rml1-1* and

responds to hormonal stimuli, glutathione very likely interacts with hormonal pathways in the control of fungal infections and any glutathione depletion might actually confer tolerance to *Fusarium* infection.

Overall, this part of the study has indicated that expression of a variety of genes are affected by glutathione depletion, which strongly supports the central function of glutathione in plant developmental and defence processes, additional to the functions that had been reported earlier, such as involvement in responses to heavy metals, resistance to herbivory and in response to oxidative stresses (Cobbett et al., 1998; Parisy et al., 2006; Schlaeppi et al., 2008).

This study has therefore extended the current knowledge by providing new gene expression data indicating that glutathione might have a more important role in regulation of plant developmental on processes such as cold-acclimation, response to heat-stress, resistance to fungal infection and expression of pathogenesis-related (PR) proteins than initially thought.

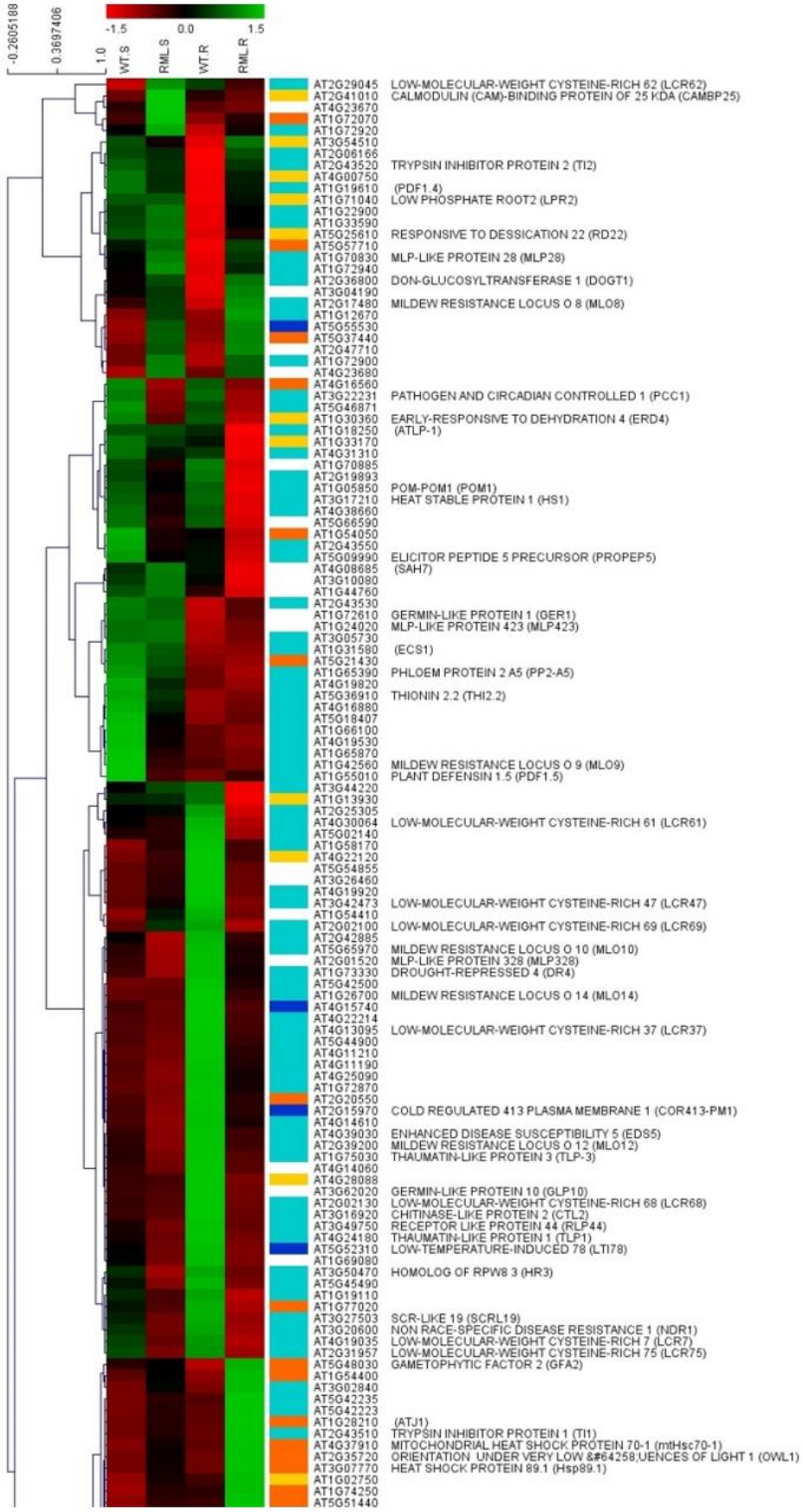
-0.2605188
0.3697406
1.0
-1.5
0.0
1.5
WT.S
RML.S
WT.R
RML.R
AT2G29045 LOW-MOLECULAR-WEIGHT CYSTEINE-RICH 62 (LCR62)
AT2G41010 CALMODULIN (CAM)-BINDING PROTEIN OF 25 KDA (CAMBP25)
AT4G23670
AT1G72070
AT1G72920
AT3G54510
AT2G06166
AT2G43520 TRYPSIN INHIBITOR PROTEIN 2 (TI2)
AT4G00750
AT1G19610 (PDF1.4)
AT1G71040 LOW PHOSPHATE ROOT2 (LPR2)
AT1G22900
AT1G33590
AT5G25610 RESPONSIVE TO DESSICATION 22 (RD22)
AT5G57710
AT1G70830 MLP-LIKE PROTEIN 28 (MLP28)
AT1G72940
AT2G36800 DON-GLUCOSYLTRANSFERASE 1 (DOGT1)
AT3G04190
AT2G17480 MILDEW RESISTANCE LOCUS O 8 (MLO8)
AT1G12670
AT5G55530
AT5G37440
AT2G47710
AT1G72900
AT4G23680
AT4G16560
AT3G22231 PATHOGEN AND CIRCADIAN CONTROLLED 1 (PCC1)
AT5G46871
AT1G30360 EARLY-RESPONSIVE TO DEHYDRATION 4 (ERD4)
AT1G18250 (ATLP-1)
AT1G33170
AT4G31310
AT1G70885
AT2G19893
AT1G05850 POM-POM1 (POM1)
AT3G17210 HEAT STABLE PROTEIN 1 (HS1)
AT4G38660
AT5G66590
AT1G54050
AT2G43550
AT5G09990 ELICITOR PEPTIDE 5 PRECURSOR (PROPEP5)
AT4G08685 (SAH7)
AT3G10080
AT1G44760
AT2G43530
AT1G72610 GERMIN-LIKE PROTEIN 1 (GER1)
AT1G24020 MLP-LIKE PROTEIN 423 (MLP423)
AT3G05730
AT1G31580 (ECS1)
AT5G21430
AT1G65390 PHLOEM PROTEIN 2 A5 (PP2-A5)
AT4G19820
AT5G36910 THIONIN 2.2 (THI2.2)
AT4G16880
AT5G18407
AT1G66100
AT4G19530
AT1G65870
AT1G42560 MILDEW RESISTANCE LOCUS O 9 (MLO9)
AT1G55010 PLANT DEFENSIN 1.5 (PDF1.5)
AT3G44220
AT1G13930
AT2G25305
AT4G30064 LOW-MOLECULAR-WEIGHT CYSTEINE-RICH 61 (LCR61)
AT5G02140
AT1G58170
AT4G22120
AT5G54855
AT3G26460
AT4G19920
AT3G42473 LOW-MOLECULAR-WEIGHT CYSTEINE-RICH 47 (LCR47)
AT1G54410
AT2G02100 LOW-MOLECULAR-WEIGHT CYSTEINE-RICH 69 (LCR69)
AT2G42885
AT5G65970 MILDEW RESISTANCE LOCUS O 10 (MLO10)
AT2G01520 MLP-LIKE PROTEIN 328 (MLP328)
AT1G73330 DROUGHT-REPRESSED 4 (DR4)
AT5G42500
AT1G26700 MILDEW RESISTANCE LOCUS O 14 (MLO14)
AT4G15740
AT4G22214
AT4G13095 LOW-MOLECULAR-WEIGHT CYSTEINE-RICH 37 (LCR37)
AT5G44900
AT4G11210
AT4G11190
AT4G25090
AT1G72870
AT2G20550
AT2G15970 COLD REGULATED 413 PLASMA MEMBRANE 1 (COR413-PM1)
AT4G14610
AT4G39030 ENHANCED DISEASE SUSCEPTIBILITY 5 (EDS5)
AT2G39200 MILDEW RESISTANCE LOCUS O 12 (MLO12)
AT1G75030 THAUMATIN-LIKE PROTEIN 3 (TLP-3)
AT4G14060
AT4G28088
AT3G62020 GERMIN-LIKE PROTEIN 10 (GLP10)
AT2G02130 LOW-MOLECULAR-WEIGHT CYSTEINE-RICH 68 (LCR68)
AT3G16920 CHITINASE-LIKE PROTEIN 2 (CTL2)
AT3G49750 RECEPTOR LIKE PROTEIN 44 (RLP44)
AT4G24180 THAUMATIN-LIKE PROTEIN 1 (TLP1)
AT5G52310 LOW-TEMPERATURE-INDUCED 78 (LTI78)
AT1G69080
AT3G50470 HOMOLOG OF RPW8 3 (HR3)
AT5G45490
AT1G19110
AT1G77020
AT3G27503 SCR-LIKE 19 (SCRL19)
AT3G20600 NON RACE-SPECIFIC DISEASE RESISTANCE 1 (NDR1)
AT4G19035 LOW-MOLECULAR-WEIGHT CYSTEINE-RICH 7 (LCR7)
AT2G31957 LOW-MOLECULAR-WEIGHT CYSTEINE-RICH 75 (LCR75)
AT5G48030 GAMETOPHYTIC FACTOR 2 (GFA2)
AT1G54400
AT3G02840
AT5G42235
AT5G42223
AT1G28210 (ATJ1)
AT2G43510 TRYPSIN INHIBITOR PROTEIN 1 (TI1)
AT4G37910 MITOCHONDRIAL HEAT SHOCK PROTEIN 70-1 (mtHsc70-1)
AT2G35720 ORIENTATION UNDER VERY LOW ﬂUENCES OF LIGHT 1 (OWL1)
AT3G07770 HEAT SHOCK PROTEIN 89.1 (Hsp89.1)
AT1G02750
AT1G74250
AT5G51440

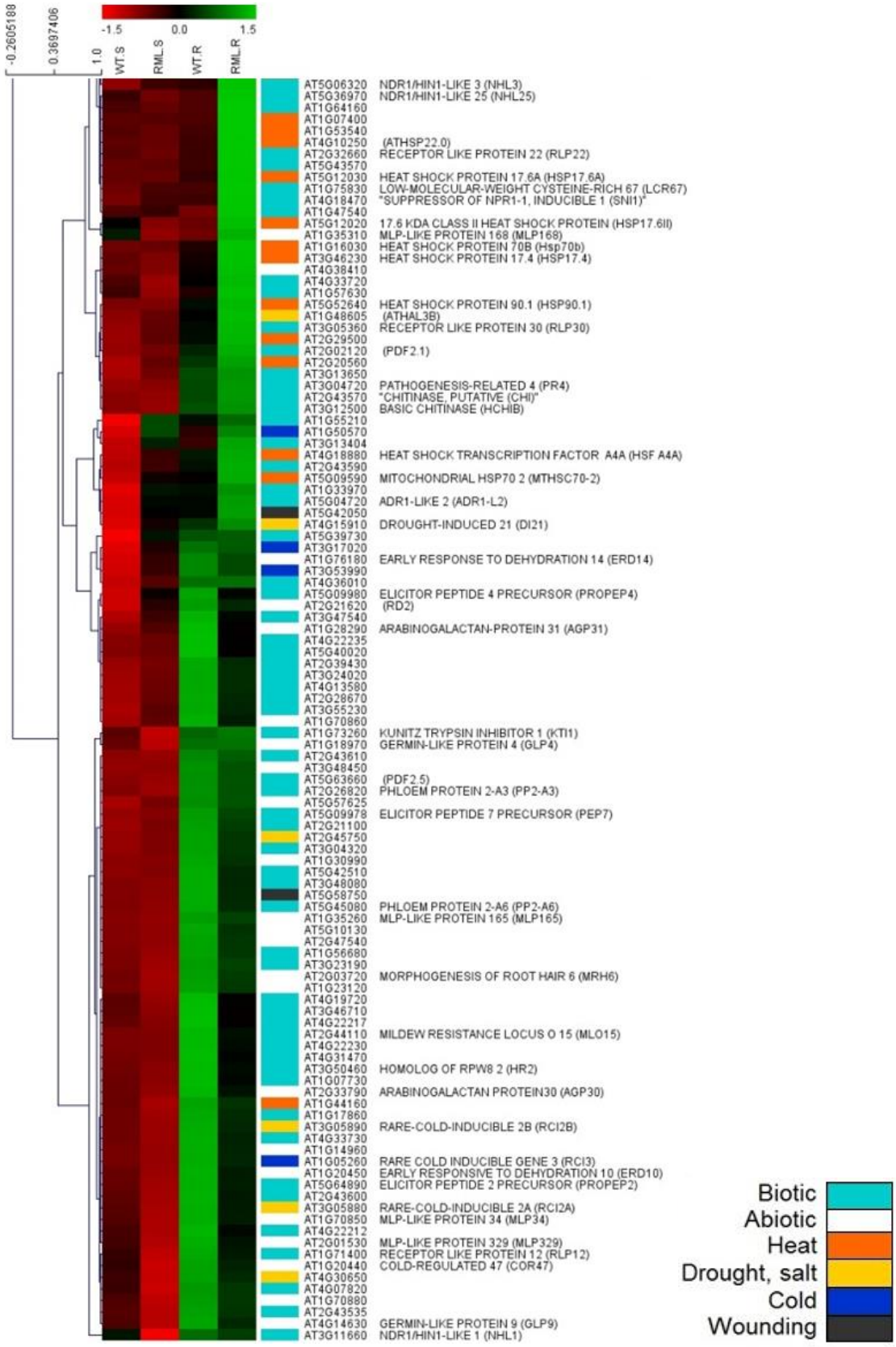

Figure 5-6: Heat map of genes involved in stress responses. The heat map derived from TIGR-MEV analysis showing hierarchical clustering of genes involved in stress responses. The picture was divided into two parts for higher resolution. Colour code is displayed in the legend. Not precisely TAIR annotated genes are left without description.

5.2.3.2 Effects on hormone-related genes

Plant hormones function as crucial regulators of plant growth and development. They also serve as signalling molecules triggering responses to both biotic and abiotic stresses (Santner et al., 2009). In a previous study, glutathione depletion resulted in an arrest of root growth in the *rml1-1* mutant but also in wild-type plants when grown in the presence of BSO (Vernoux et al., 2000A). Arabidopsis root growth crucially depends on glutathione interacting with auxin (Koprivova et al., 2010). Glutathione depletion, due to BSO treatment, affects root growth similar to mis-regulation of auxin homeostasis and results in loss of the polar auxin transporters PIN1, PIN2 and PIN7 (Koprivova et al., 2010). Association studies with double mutants for TRX reductases (*ntra ntrb*) and glutathione biosynthesis (*cad2-1*) also revealed that these two components interact in developmental processes through modulation of auxin signalling.

Furthermore, the *ntra ntrb cad2-1* triple mutant developed normally until flowering and then showed a distinct PIN-formed stem phenotype reminiscent of that of plants affected in auxin transport and biosynthesis (Bashandy et al., 2010).

To obtain a more detailed insight into how glutathione depletion affects hormone pathways and subsequently plant development, this PhD study also aimed in a further step at investigating the expression of genes under glutathione depletion related to hormone metabolic and signalling pathways with a particular focus on auxin. Hierarchical clustering was therefore

performed for genes involved in hormone responses, metabolism and signalling. The majority of genes that were identified to respond to the glutathione depletion in the *rml1-1* were found in the cluster of auxin-related transcripts, followed by genes related to ethylene and abscisic acid (Table 5-5). Figure 5-8 (shown on pages 127 & 128) provides an overview presented as heat map, also shown are AGI codes, expression values and primary gene annotations where available.

Table 5-5: Overview of total number of transcripts annotated as involved in hormone responses and metabolism. Shown is a ranked overview of clusters that were created by total number of transcripts that are annotated as involved in hormone responses and metabolism for each of the major hormones (e.g. auxin, ethylene, abscisic acid, etc.). Gene annotations were retrieved from TAIR10 and ranking was performed according to total number of genes present in each cluster. Some genes could be found in more than cluster.

Cluster label	Cluster size
IAA - (Auxin)	66
Eth - (Ethylene)	28
ABA - (Abscisic acid)	17
GA - (Gibberellic acid)	17
JA - (Jasmonic acid)	14
BR - (Brassino steroid)	12
SA - (Salicylic acid)	8
Cyt - (Cytokinins)	4

An analysis of transcripts involved in hormone response, metabolism and signalling was first performed by comparing transcripts that showed altered expression in the *rml1-1* with all TAIR annotated genes (TAIR10, 2012) reported to be involved in plant hormone metabolism signalling and transport. The majority of transcripts changed in response to glutathione depletion were either linked to abscisic acid, auxin or ethylene (Figure 5-7), and these were then analysed separately.

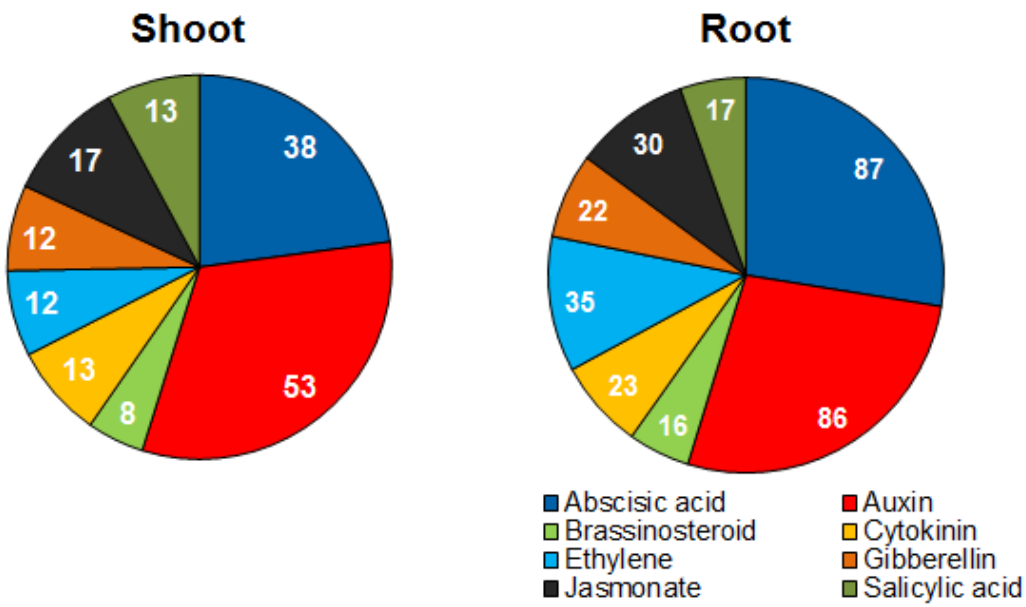

Figure 5-7: Overview of transcripts identified from the *rml1-1* tiling array analysis with annotations to hormone metabolism and signalling. Displayed are percentage enrichments of transcripts as segments of the pie chart relative to the total number of transcripts annotated in TAIR. In each segment of the pie chart the absolute number of transcripts, which are affected by the glutathione depletion in the *rml1-1* mutant, is shown.

Auxin-related genes

The 10 most up and down-regulated auxin-related genes in both *rml1-1* shoot and roots tissues are shown in Table 5-6 and Table 5-7. The majority of genes, altered in response to glutathione depletion, were identified as related to signalling rather than metabolic processes. Among these were MYB15, MYB75, IAA20, IAA24, SAUR-like auxin-responsive genes, and members of the BTB AND TAZ DOMAIN subfamily. MYB75 was up-regulated in *rml1-1* shoot and root tissues in response to glutathione depletion by 4.8- and 2.8-fold, respectively. In contrast, MYB15 was differentially expressed in the *rml1-1* mutant. MYB15 expression remained almost unaltered in the shoot, but decreased 3.3-fold in the root compared to the wild-type.

Table 5-6: Overview of the 10 most induced and repressed auxin-related genes from shoots of the *rml1-1*. Shown are AGI codes, descriptions, p-values from statistical analysis of the shoot as well as fold changes in expression for shoot and root.

		AGI code	Description	p-value	fold change	
				(shoot)	shoot	root
Isolated from shoot	Induced	AT1G56650	MYB DOMAIN PROTEIN 75 (MYB75)	0.000	4.84	2.80
		AT1G05680	UDP-GLYCOSYLTRANSFERASE 74E2 (UGT74E2)	0.000	3.77	3.77
		AT3G44300	NITRILASE 2 (NIT2)	0.000	3.69	3.16
		AT1G48660	Auxin-responsive GH3 family protein	0.000	3.48	3.23
		AT2G46990	INDOLE-3-ACETIC ACID INDUCIBLE 20 (IAA20)	0.000	2.96	0.26
		AT2G47000	ARABIDOPSIS P-GLYCOPROTEIN 4	0.000	2.73	1.81
		AT5G07990	TRANSPARENT TESTA 7 (TT7)	0.000	2.63	-0.58
		AT1G75580	SAUR-like auxin-responsive protein family	0.000	2.14	0.26
		AT5G27520	PEROXISOMAL ADENINE NUCLEOTIDE CARRIER 2 (PNC2)	0.000	2.00	0.93
		AT3G53250	SAUR-like auxin-responsive protein family	0.000	1.79	-0.06
	Repressed	AT1G72430	SAUR-like auxin-responsive protein family	0.000	-1.40	-1.27
		AT1G29420	SAUR-like auxin-responsive protein family	0.000	-1.47	-0.08
		AT1G29490	SAUR-like auxin-responsive protein family	0.000	-1.51	-0.55
		AT4G34760	SAUR-like auxin-responsive protein family	0.000	-1.68	-2.19
		AT5G57560	XYLOGLUCAN ENDOTRANSGLUCOSYLASE/HYDROLASE 22	0.000	-1.69	2.42
		AT3G48360	BTB AND TAZ DOMAIN PROTEIN 2 (BT2)	0.000	-1.84	-0.99
		AT5G17300	REVEILLE 1 (RVE1)	0.000	-1.87	0.05
		AT2G21210	Putative auxin-regulated protein; down-regulated in response to chitin oligomers	0.000	-2.18	-2.40
		AT5G63160	BTB AND TAZ DOMAIN PROTEIN 1 (BT1)	0.000	-3.55	-2.47
		AT4G37610	BTB AND TAZ DOMAIN PROTEIN 5 (BT5)	0.000	-3.82	-2.18

Table 5-7: Overview of the 10 most induced and repressed auxin-related genes from roots of the *rml1-1*. Shown are AGI codes, descriptions, p-values from statistical analysis of the shoot as well as fold changes in expression for shoot and root.

		AGI code	Description	p-value (shoot)	fold change shoot	fold change root
Isolated from root	Induced	AT1G05680	URIDINE DIPHOSPHATE GLYCOSYLTRANSFERASE 74E2 (UGT74E2)	0.000	3.77	3.77
		AT1G47510	INOSITOL POLYPHOSPHATE 5-PHOSPHATASE 11 (5PTASE11)	0.822	-0.02	3.46
		AT3G23250	MYB DOMAIN PROTEIN 15 (MYB15)	0.406	-0.25	3.33
		AT1G48660	Auxin-responsive GH3 family protein	0.000	3.48	3.23
		AT3G44300	NITRILASE 2 (NIT2)	0.000	3.69	3.16
		AT5G13370	Auxin-responsive GH3 family protein	0.000	0.96	3.15
		AT1G56650	MYB DOMAIN PROTEIN 75 (MYB75)	0.000	4.84	2.80
		AT4G32810	CAROTENOID CLEAVAGE DIOXYGENASE 8 (CCD8)	0.271	-0.13	2.58
		AT1G19850	INDOLE-3-ACETIC ACID INDUCIBLE 24 (IAA24)	0.217	0.13	2.47
		AT5G57560	XYLOGLUCAN ENDOTRANSGLUCOSYLASE/HYDROLASE 22 (XTH22)	0.000	-1.69	2.42
	Repressed	AT1G48690	Auxin-responsive GH3 family protein	0.001	-0.53	-2.43
		AT5G63160	BTB AND TAZ DOMAIN PROTEIN 1 (BT1)	0.000	-3.55	-2.47
		AT4G31320	SAUR-like auxin-responsive protein family	0.146	-0.40	-2.50
		AT5G13930	TRANSPARENT TESTA 4 (TT4)	0.000	1.63	-2.62
		AT5G16530	PIN-FORMED 5 (PIN5)	0.000	-1.01	-2.69
		AT4G24670	TRYPTOPHAN AMINOTRANSFERASE RELATED 2 (TAR2)	0.000	-0.61	-2.80
		AT4G19690	IRON-REGULATED TRANSPORTER 1 (IRT1)	0.003	-0.81	-2.86
		AT2G22330	CYTOCHROME P450, FAMILY 79, SUBFAMILY B, POLYPEPTIDE 3 (CYP79B3)	0.566	-0.07	-3.04
		AT5G08640	FLAVONOL SYNTHASE 1 (FLS1)	0.006	0.99	-3.36
		AT4G12550	AUXIN-INDUCED IN ROOT CULTURES 1 (AIR1)	0.419	0.23	-4.29

MYB75 has been implicated in anthocyanin biosynthesis and regulation of formation of the secondary cell wall in inflorescence stems (Bhargava et al., 2010; Shin, et al., 2012), According to the Arabidopsis Information Resource, MYB15 is involved in abscisic acid-, jasmonic acid- and ethylene-mediated signalling pathways as well as in defence responses by callose deposition (TAIR10, 2012).

BT1, BT2 and BT5 expression was uniformly down-regulated in *rml1-1* shoot and root tissues in response to glutathione depletion (Table 5-6 and Table 5-7). In the shoot, BT1 and BT5 had the greatest down-regulation due to glutathione depletion with 3.6- and 3.8-fold decrease, respectively, when compared to the wild-type (Table 5-6) whereas BT2 was down-regulated 1.8-fold (Table 5-6). These genes are members of the BTB and TAZ DOMAIN (BT1-BT5) protein family involved in various signalling pathways (Robert et al., 2009).While BT1 and BT2 are targeted to the nucleus and cytosol, the other members of this subfamily are only targeted to the cytosol. BT1 to BT5 have been previously found to be required in gametophyte development (Robert et al., 2009).

Two IAA genes were differentially expressed in the *rml1-1* mutant, namely *IAA20* and *IAA24*. *IAA 20* expression was 3-fold higher when compared to the wild-type, but was almost unaltered in the root (Table 5-6). In contrast, *IAA24* transcription was 2.5-fold higher in *rml1-1* root tissue than in the wild-type tissue and remained unaltered in shoot tissues (Table 5-7). While currently no studies are available investigating the functions of IAA20 specifically, information available from TAIR indicates that the gene encodes a member of

the AUX/IAA protein family involved in auxin signalling. Furthermore, defects in this gene result in changes in gravitropism, root development, root meristem maintenance, etiolation, as well as cotyledon vascular development (TAIR10, 2012). In comparison, *IAA24* encodes a transcription factor similar to the AUXIN RESPONSIVE FACTOR 1 (ARF1) and is involved in mediating the formation of the embryo axis as well as involved in vascular development (TAIR10, 2012).

CCD8 was 2.8-fold higher in *rml1-1* roots and encodes a protein with similarity to carotenoid cleaving deoxygenases (CCD). *CCD8 is* involved in signalling and suppresses axillary root branching. Mutations in this gene cause increased shoot branching and, together with CCD7, CCD8 is involved in the strigolactone biosynthetic pathway (Bennett et al., 2006; Alder et al., 2012).

Further, UDP-GLYCOSYLTRANSFERASE 74E2 (UGT74E2) transcription increased in *rml1-1* shoot and root tissue by 3.8-fold in response to glutathione depletion. Previous studies identified UGT74E2 as UDP-glycosyltransferase acting on indole-3-butyric acid (IBA) and affects auxin homeostasis. Transcription and translation of the UGT74E2 are strongly induced by H_2O_2 and the protein may act in ROS- and auxin-signalling pathways controlling plant architecture and water stress responses (Tognetti et al., 2010).

Summarizing, findings suggest a complex interplay of glutathione and auxin-related genes in the control of plant development, plant architecture, stress responses and hormonal pathways that are interconnected with auxin or act downstream of auxin.

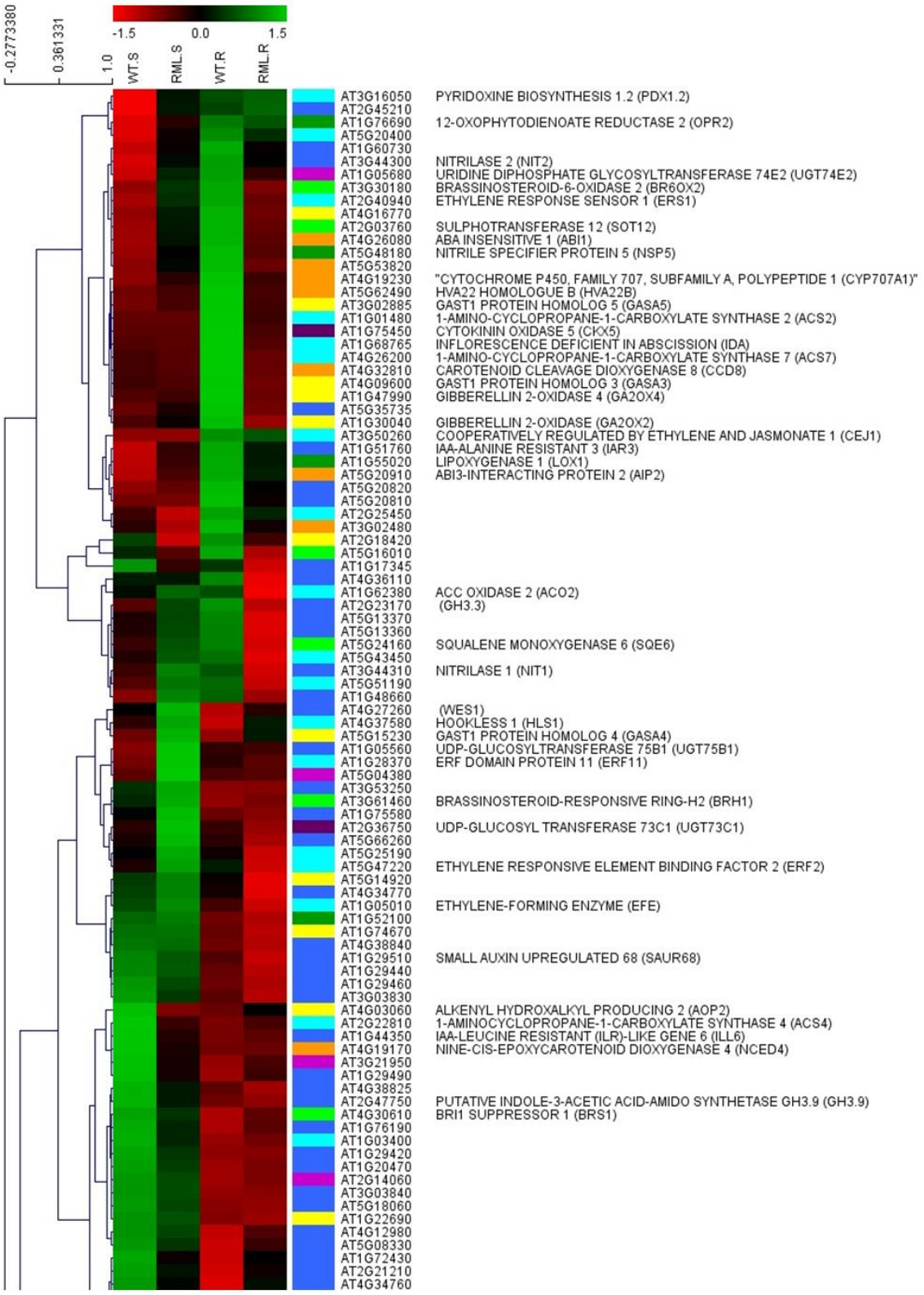
-0.2773380
0.361331
1.0
-1.5
0.0
1.5
WT.S
RML.S
WT.R
RML.R
AT3G16050 PYRIDOXINE BIOSYNTHESIS 1.2 (PDX1.2)
AT2G45210
AT1G76690 12-OXOPHYTODIENOATE REDUCTASE 2 (OPR2)
AT5G20400
AT1G60730
AT3G44300 NITRILASE 2 (NIT2)
AT1G05680 URIDINE DIPHOSPHATE GLYCOSYLTRANSFERASE 74E2 (UGT74E2)
AT3G30180 BRASSINOSTEROID-6-OXIDASE 2 (BR6OX2)
AT2G40940 ETHYLENE RESPONSE SENSOR 1 (ERS1)
AT4G16770
AT2G03760 SULPHOTRANSFERASE 12 (SOT12)
AT4G26080 ABA INSENSITIVE 1 (ABI1)
AT5G48180 NITRILE SPECIFIER PROTEIN 5 (NSP5)
AT5G53820
AT4G19230 "CYTOCHROME P450, FAMILY 707, SUBFAMILY A, POLYPEPTIDE 1 (CYP707A1)"
AT5G62490 HVA22 HOMOLOGUE B (HVA22B)
AT3G02885 GAST1 PROTEIN HOMOLOG 5 (GASA5)
AT1G01480 1-AMINO-CYCLOPROPANE-1-CARBOXYLATE SYNTHASE 2 (ACS2)
AT1G75450 CYTOKININ OXIDASE 5 (CKX5)
AT1G68765 INFLORESCENCE DEFICIENT IN ABSCISSION (IDA)
AT4G26200 1-AMINO-CYCLOPROPANE-1-CARBOXYLATE SYNTHASE 7 (ACS7)
AT4G32810 CAROTENOID CLEAVAGE DIOXYGENASE 8 (CCD8)
AT4G09600 GAST1 PROTEIN HOMOLOG 3 (GASA3)
AT1G47990 GIBBERELLIN 2-OXIDASE 4 (GA2OX4)
AT5G35735
AT1G30040 GIBBERELLIN 2-OXIDASE (GA2OX2)
AT3G50260 COOPERATIVELY REGULATED BY ETHYLENE AND JASMONATE 1 (CEJ1)
AT1G51760 IAA-ALANINE RESISTANT 3 (IAR3)
AT1G55020 LIPOXYGENASE 1 (LOX1)
AT5G20910 ABI3-INTERACTING PROTEIN 2 (AIP2)
AT5G20820
AT5G20810
AT2G25450
AT3G02480
AT2G18420
AT5G16010
AT1G17345
AT4G36110
AT1G62380 ACC OXIDASE 2 (ACO2)
AT2G23170 (GH3.3)
AT5G13370
AT5G13360
AT5G24160 SQUALENE MONOXYGENASE 6 (SQE6)
AT5G43450
AT3G44310 NITRILASE 1 (NIT1)
AT5G51190
AT1G48660
AT4G27260 (WES1)
AT4G37580 HOOKLESS 1 (HLS1)
AT5G15230 GAST1 PROTEIN HOMOLOG 4 (GASA4)
AT1G05560 UDP-GLUCOSYLTRANSFERASE 75B1 (UGT75B1)
AT1G28370 ERF DOMAIN PROTEIN 11 (ERF11)
AT5G04380
AT3G53250
AT3G61460 BRASSINOSTEROID-RESPONSIVE RING-H2 (BRH1)
AT1G75580
AT2G36750 UDP-GLUCOSYL TRANSFERASE 73C1 (UGT73C1)
AT5G66260
AT5G25190
AT5G47220 ETHYLENE RESPONSIVE ELEMENT BINDING FACTOR 2 (ERF2)
AT5G14920
AT4G34770
AT1G05010 ETHYLENE-FORMING ENZYME (EFE)
AT1G52100
AT1G74670
AT4G38840
AT1G29510 SMALL AUXIN UPREGULATED 68 (SAUR68)
AT1G29440
AT1G29460
AT3G03830
AT4G03060 ALKENYL HYDROXALKYL PRODUCING 2 (AOP2)
AT2G22810 1-AMINOCYCLOPROPANE-1-CARBOXYLATE SYNTHASE 4 (ACS4)
AT1G44350 IAA-LEUCINE RESISTANT (ILR)-LIKE GENE 6 (ILL6)
AT4G19170 NINE-CIS-EPOXYCAROTENOID DIOXYGENASE 4 (NCED4)
AT3G21950
AT1G29490
AT4G38825
AT2G47750 PUTATIVE INDOLE-3-ACETIC ACID-AMIDO SYNTHETASE GH3.9 (GH3.9)
AT4G30610 BRI1 SUPPRESSOR 1 (BRS1)
AT1G76190
AT1G03400
AT1G29420
AT1G20470
AT2G14060
AT3G03840
AT5G18060
AT1G22690
AT4G12980
AT5G08330
AT1G72430
AT2G21210
AT4G34760

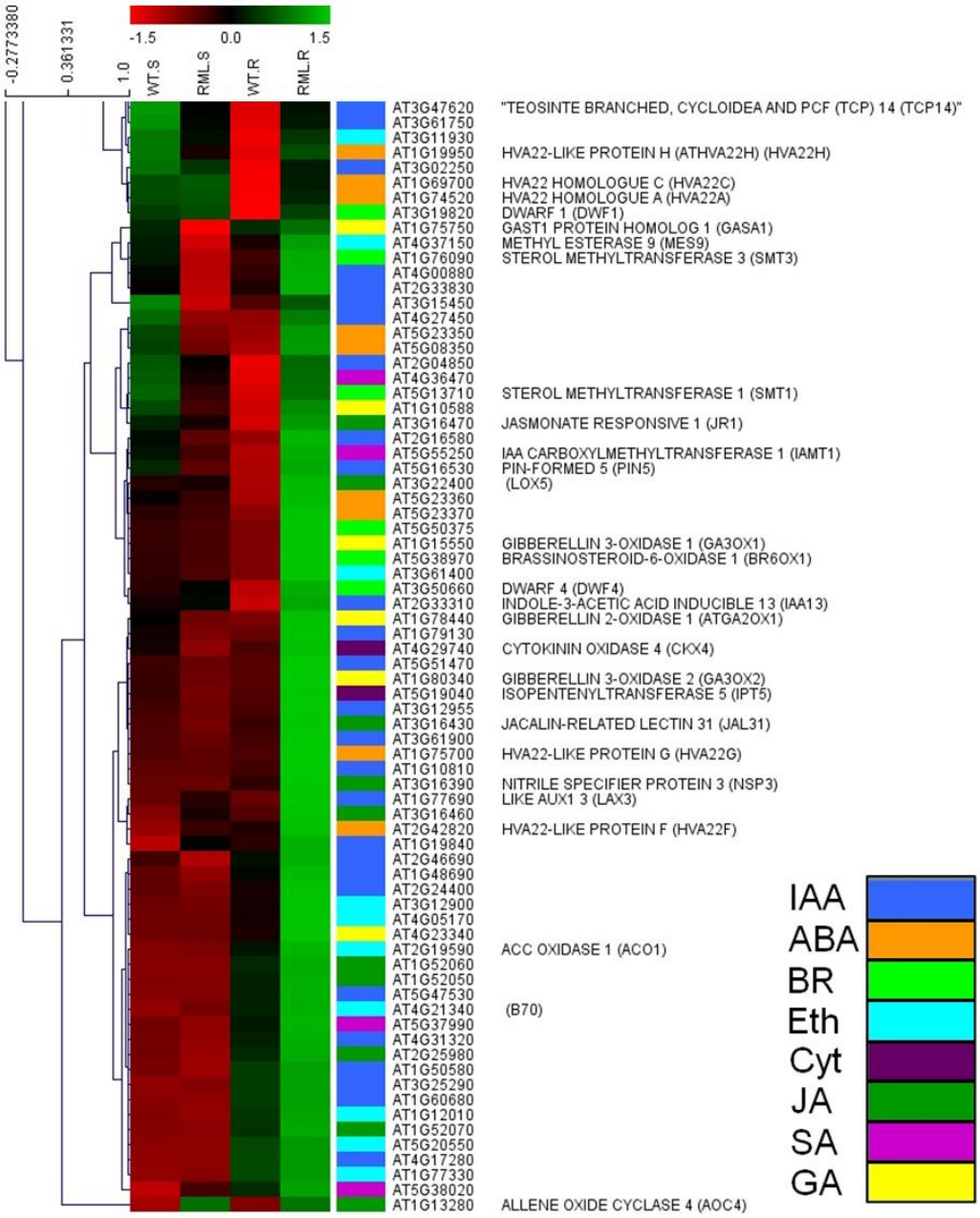

Figure 5-8: Heat map of genes involved in hormone responses and metabolism. The heat map derived from TIGR-MEV analysis showing hierarchical clustering of genes involved in hormone responses and hormone metabolism. The picture was divided into two parts for higher resolution. Colour code is displayed in the legend. Not precisely annotated genes (according to TAIR website) are left without description. Abbreviations in the legend are as follows: auxin (IAA), abscisic acid (ABA), brassinosteroids (BR), ethylene (Eth), cytokinins (Cyt), jasmonic acid (JA), salicylic acid (SA) and gibberellic acid (GA).

Abscisic acid-related genes

When abscisic acid-related genes from *rml1-1* shoot and roots tissues were investigated, the 10 most up- or down-regulated genes were either transcription factors, plasma membrane intrinsic proteins or were related to responses to drought and desiccation stress (Table 5-8 and Table 5-9). Among these were DR4, PAD3, PIP2;4, PIP2B, PIP3B, and RAP2.6L. DR4 was down-regulated 1.6-fold in *rml1-1* shoots and 4.4-fold in *rml1-1* roots in response to glutathione depletion (Table 5-9). Little information is available about DR4 function in plant development. So far, DR4 is known to be a specific protease inhibitor whose transcript levels vanish in response to progressive drought stress (Gosti, et al., 1995).

PHYTOALEXIN DEFICIENT 3 (*PAD3*) transcription increased in *rml1-1* roots 3-fold compared to the wild-type (Table 5-9). Earlier studies have shown that *pad3* mutants are defective in biosynthesis of the indole-derived phytoalexin camalexin and that the *PAD3* gene encodes a cytochrome P450 enzyme that catalyzes the conversion of dihydrocamalexic acid to camalexin (Kettles et al., 2012). Other studies have demonstrated that *pad2* mutants, which are affected in γ-ECS, have increased susceptibilities to the virulent strains of *Pseudomonas syringae* and *P. brassicae* (Parisy et al., 2006). These findings suggest importance of glutathione in plant responses to stress through acting on camalexin synthesis. Further, transcription of PIP2;4, PIP2;2, and PIP2;8, plasma membrane intrinsic proteins (PIP), decreased 2-fold in *rml1-1* (Table 5-9).

Table 5-8: Overview of the 10 most induced and repressed abscisic acid-related genes from shoots of the *rml1-1*. Shown are AGI codes, descriptions, p-values from statistical analysis of the shoot as well as fold changes in expression for shoot and root.

		AGI code	Description	p-value (shoot)	fold change shoot	fold change root
Isolated from shoot	Induced	AT1G43910	P-loop containing nucleoside triphosphate hydrolases superfamily protein	0.000	3.94	3.03
		AT5G13330	Member of the ERF subfamily B-4 of ERF/AP2 transcription factor family	0.000	3.16	2.63
		AT1G05560	UDP-GLUCOSYLTRANSFERASE 75B1 (UGT75B1)	0.000	2.14	0.09
		AT1G54100	Aldehyde dehydrogenase	0.000	2.08	1.38
		AT1G01720	Member of large family of putative transcriptional activators with NAC domain	0.000	1.87	0.85
		AT2G05710	Encodes an aconitase	0.000	1.84	1.42
		AT4G15910	Encodes a gene whose transcript level in root and leaves increases during drought stress	0.000	1.84	1.05
		AT2G33150	Encodes organellar 3-ketoacyl-CoA thiolase, involved in germination and seedling growth	0.000	1.82	1.66
		AT1G27730	Related to Cys2/His2-type zinc-finger proteins found in higher plants	0.002	1.72	1.99
		AT2G32020	Acyl-CoA N-acyltransferases (NAT) superfamily protein	0.000	1.64	2.88
	Repressed	AT3G47620	Encodes a transcription factor AtTCP14 that regulates seed germination	0.000	-1.02	-1.33
		AT5G44610	Encodes a protein with seven repeated VEEKK motifs	0.003	-1.08	-1.03
		AT4G22200	Encodes AKT2, a photosynthate- and light-dependent potassium channel	0.003	-1.19	-0.05
		AT1G73330	Encodes a plant-specific protease inhibitor-like protein; disappears in response to drought	0.000	-1.60	-4.41
		AT1G71030	Encodes a putative MYB family transcription factor	0.000	-1.64	-0.50
		AT3G22060	Contains pfam profile: PF01657 Domain of unknown function	0.000	-2.10	-0.68
		AT1G20440	Belongs to the dehydrin protein family	0.000	-2.11	-2.27
		AT5G28770	bZIP protein BZO2H3 mRNA	0.000	-2.63	-1.89
		AT5G45820	Encodes a CBL-interacting serine/threonine protein kinase	0.000	-2.82	-0.51
		AT1G75750	GA-responsive GAST1 protein homolog regulated by BR and GA antagonistically	0.000	-3.02	-0.87

Table 5-9: Overview of the 10 most induced and repressed abscisic acid-related genes from roots of the *rml1-1*. Shown are AGI codes, descriptions, p-values from statistical analysis of the shoot as well as fold changes in expression for shoot and root.

		AGI code	Description	p-value (shoot)	fold change shoot	fold change root
Isolated from root	Induced	AT3G28580	P-loop containing nucleoside triphosphate hydrolases superfamily protein	0.000	1.42	4.10
		AT1G18100	Encodes a member of the FT and TFL1 family of PE-binding proteins	0.004	1.05	3.76
		AT1G43910	P-loop containing nucleoside triphosphate hydrolases superfamily protein	0.000	3.94	3.03
		AT3G26830	PHYTOALEXIN DEFICIENT 3 (PAD3)	0.000	0.99	3.02
		AT2G05520	GLYCINE-RICH PROTEIN 3 (GRP-3)	0.004	0.34	2.93
		AT2G32020	Acyl-CoA N-acyltransferases (NAT) superfamily protein	0.000	1.63	2.88
		AT4G12480	EARLY ARABIDOPSIS ALUMINUM INDUCED 1 (EARLI1)	0.015	0.71	2.78
		AT5G64750	ABA REPRESSOR1 (ABR1)	0.138	-0.27	2.75
		AT5G25610	RESPONSIVE TO DESSICATION 22 (RD22)	0.001	0.80	2.72
		AT5G13330	RELATED TO AP2 6L (Rap2.6L)	0.000	3.16	2.63
	Repressed	AT2G16850	PLASMA MEMBRANE INTRINSIC PROTEIN 3B (PIP2;8)	0.355	-0.13	-1.91
		AT2G37170	PLASMA MEMBRANE INTRINSIC PROTEIN 2 (PIP2;2)	0.067	-0.35	-1.98
		AT1G20450	LOW TEMPERATURE INDUCED 29 (LTI29)	0.016	-0.54	-1.99
		AT2G38750	ANNEXIN 4 (ANNAT4)	0.397	0.09	-2.01
		AT4G35100	PLASMA MEMBRANE INTRINSIC PROTEIN 3A (PIP3A)	0.081	-0.21	-2.05
		AT2G15970	COLD REGULATED 413 PLASMA MEMBRANE 1 (COR413-PM1)	0.019	-0.48	-2.06
		AT3G02850	STELAR K+ OUTWARD RECTIFIER (SKOR)	0.261	0.10	-2.09
		AT1G20440	COLD-REGULATED 47 (COR47)	0.000	-2.11	-2.27
		AT5G60660	PLASMA MEMBRANE INTRINSIC PROTEIN 2;4 (PIP2;4)	0.004	-0.45	-3.68
		AT1G73330	DROUGHT-REPRESSED 4 (DR4)	0.000	-1.60	-4.41

Table 5-10: Overview of all induced and repressed ethylene-related genes from shoots of the *rml1-1*. Shown are AGI codes, descriptions, p-values from statistical analysis of the shoot as well as fold changes in expression for shoot and root.

		AGI code	Description	p-value (shoot)	fold change shoot	fold change root
Isolated from shoot	Induced	AT5G25190	Encodes a member of the B-6 subfamily of ERF/AP2 transcription factor family (ESE3)	0.000	2.59	2.25
		AT1G28370	Encodes a member of the B-1 subfamily of ERF/AP2 transcription factor family (ERF11)	0.000	1.84	0.25
		AT5G43450	Encodes a protein whose sequence is similar to ACC oxidase	0.000	1.75	4.33
		AT5G47220	Encodes a member of the B-3 subfamily of ERF/AP2 transcription factor family (ERF2)	0.000	1.67	1.74
		AT1G73500	Member of MAP-Kinase Kinase family.	0.000	1.33	0.00
		AT1G25560	Encodes a member of the RAV transcription factor family	0.000	1.24	0.82
		AT5G25350	Arabidopsis thaliana EIN3-binding F-box protein 2 (EBF2) mRNA	0.000	1.23	1.38
		AT1G49820	Encodes 5-methylthioribose kinase, involved in methionine cycle	0.000	1.09	-0.05
		AT5G54190	Light-dependent NADPH:protochlorophyllide oxidoreductase A	0.000	1.07	-0.45
		---	---	---	---	---
	Repressed	AT3G25190	Encodes nodulin-like21; repressed under conditions of Fe-deficient growth.	0.000	-1.65	-4.53
		AT1G03400	Encodes a protein with sequence similarity to tomato E8 (ACC oxidase)	0.000	-1.66	-0.33
		AT5G04950	Encodes a nicotianamide synthase	0.000	-1.82	-1.55
		---	---	---	---	---
		---	---	---	---	---
		---	---	---	---	---
		---	---	---	---	---
		---	---	---	---	---
		---	---	---	---	---
		---	---	---	---	---

132

Table 5-11: Overview of the 10 most induced and repressed ethylene-related genes from roots of the *rml1-1*. Shown are AGI codes, descriptions, p-values from statistical analysis of the shoot as well as fold changes in expression for shoot and root.

		AGI code	Description	p-value (shoot)	fold change shoot	fold change root
Isolated from root	Induced	AT5G43450	Encodes a protein whose sequence is similar to ACC oxidase	0.000	1.75	4.33
		AT4G26200	1-AMINO-CYCLOPROPANE-1-CARBOXYLATE SYNTHASE 7 (ACS7)	0.050	-0.20	4.03
		AT5G55620	Unknown protein	0.161	0.22	3.79
		AT1G01480	1-AMINO-CYCLOPROPANE-1-CARBOXYLATE SYNTHASE 2 (ACS2)	0.917	0.01	2.82
		AT1G62380	ACC OXIDASE 2 (ACO2)	0.000	0.86	2.62
		AT5G25190	Encodes a member of the B-6 subfamily of ERF/AP2 transcription factor family (ESE3)	0.000	2.59	2.25
		AT1G68765	INFLORESCENCE DEFICIENT IN ABSCISSION (IDA)	0.713	-0.03	2.01
		AT5G47220	Encodes a member of the B-3 subfamily of ERF/AP2 transcription factor family (ERF2)	0.000	1.67	1.74
		AT3G59060	PHYTOCHROME INTERACTING FACTOR 3-LIKE 6 (PIL6)	0.121	-0.15	1.60
		AT5G19880	Peroxidase superfamily protein	0.407	-0.14	1.41
	Repressed	AT5G44030	CELLULOSE SYNTHASE A4 (CESA4)	0.028	-0.30	-1.60
		AT5G38820	Encodes a putative amino acid transporter	0.166	-0.15	-1.61
		AT1G18330	EARLY-PHYTOCHROME-RESPONSIVE1 (EPR1)	0.003	-0.78	-1.66
		AT3G61400	1-aminocyclopropane-1-carboxylate oxidase-like protein	0.365	-0.14	-1.76
		AT4G24180	THAUMATIN-LIKE PROTEIN 1 (TLP1)	0.007	-0.43	-1.80
		AT1G26100	Cytochrome b561/ferric reductase transmembrane protein family	0.370	-0.11	-2.00
		AT3G12900	2-oxoglutarate (2OG) and Fe(II)-dependent oxygenase superfamily protein	0.613	-0.08	-2.40
		AT1G76800	Encodes nodulin-like2; repressed under conditions of Fe-deficient growth	0.677	0.08	-2.57
		AT5G56080	NICOTIANAMINE SYNTHASE 2 (NAS2)	0.007	-0.96	-3.02
		AT3G25190	Encodes nodulin-like21; repressed under conditions of Fe-deficient growth	0.000	-1.65	-4.53

PIP2;4 is involved in both the response to iron starvation and in the trans-membrane transport of hydrogen peroxide (TAIR10, 2012) whereas PIP2B and PIP3B are involved in the response to abscisic acid, trans-membrane transport and water transport (TAIR10, 2012).

Finally, UDP-GLUCOSYLTRANSFERASE 75B1 (UGT75B1) transcription was 2.2-fold higher in *rml1-1* shoots relative to the wild-type. UGT75B1 encodes a protein with glucosyltransferase activity and has a high sequence homology with UGT2 (AT1G05530). The protein is possibly involved in callose synthesis during cell wall biogenesis (TAIR10, 2012).

The findings in this section indicate a crucial requirement of glutathione in plant development and stress responses. Glutathione seems to act at the centre of these processes and hence low levels of glutathione will severely affect crucial regulatory processes in plants leaving them vulnerable to abiotic and biotic stress or even disrupting normal plant development.

Ethylene-related genes

When changes in expression of ethylene-related genes from *rml1-1* shoot and root tissues were investigated, the majority of genes changed in transcription were involved in ethylene signalling (Table 5-10 and Table 5-11).

Some of these genes encoded ethylene response factors (ERF) with an AP2 domain of the subfamilies B1 (ERF11), B3 (ERF2) or B6 (ESE3). ESE3 transcription was 2.5-fold higher in both *rml1-1* shoots and roots (Table 5-10

and Table 5-11). In contrast, ERF2 transcription was only 1.8-fold higher in *rml1-1* shoots (Table 5-11).

All three genes are involved in ethylene-mediated signalling and cell communication with ERF11 also involved in the response to salinity and being a crucial repressor of ethylene biosynthesis. ERF2 is very likely a DNA-dependent positive regulator of transcription (Zhang et al., 2011; TAIR10, 2012). Besides being ethylene inducible, ESE3 is also salt-inducible and has functions in seed dormancy (Zhang et al., 2011; TAIR10, 2012).

When finally ACS2 and ACS7 transcription was determined, both changed 2.8- and 4-fold, respectively, but only in *rml1-1* roots (Table 5-11). Both genes are involved in ethylene biosynthesis (Yoon and Kieber, 2013; TAIR10, 2012) with ACS2 being a downstream target of ERF11 (Zhang et al., 2011).

Glutathione depletion affects primarily ethylene-related transcripts of genes encoding proteins involved in signalling and cell-to-cell communication processes. Differential expression of the identified transcripts in shoot and root tissues suggests a complex interplay between glutathione and ethylene in the control of signalling processes. It seems that glutathione has important functions at the centre of these ethylene-mediated signalling processes, but glutathione-dependent changes in transcription are not as severe as identified for abscisic acid-related genes, auxin-related gene or genes related to stress responses.

5.2.4 Effects on transcription factors

The effects of glutathione depletion on the expression of transcription factors were also investigated with a particular focus on genes either related to auxin or redox processes. The 10 most up- and down-regulated transcription factors are shown in Table 5-12 and Table 5-13. Some of these will be described separately in the two subsections below.

Transcription factors related to growth

The transcription factors presented in the following are involved in processes controlling plant growth. Transcription factors involved in both auxin expression and signalling were analysed together with all members of their gene family (Figure 5-9). While INDOLE-3-ACETIC ACID INDUCIBLE GENE 20 (IAA20) was over-expressed in *rml1-1* shoot tissue relative to the wild-type, both IAA30 and IAA 31 were not differentially expressed. IAA20 is induced by auxin treatment, and over-expression leads to defects in gravitropism, root development, root meristem maintenance, etiolation, and also cotyledon vascular development (Sato et al., 2008). Furthermore, members of radialis-like SANT/MYB (RSM) gene family were down-regulated in *rml1-1* shoots, with much smaller transcription differences in *rml1-1* roots (Figure 5-9B). Also, transcription of the hookless1 (HLS1) gene was up-regulated in *rml1-1* shoots but down-regulated in *rml1-1* roots (Figure 5-9B). Mutations in the hookless1 (HLS1) gene causes a phenotype similar to RSM1 overexpressing plants resulting in loss of apical hooks and defects in gravitropism (Hamaguchi et al., 2008).

Table 5-12: Overview to the 10 most induced and repressed transcription factors from shoots of the *rml1-1*. Shown are AGI codes, descriptions, p-values from statistical analysis of the shoot as well as fold changes in expression for shoot and root.

		AGI code	Description	p-value (shoot)	fold change shoot	fold change root
Isolated from shoots	Induced	AT1G56650	PRODUCTION OF ANTHOCYANIN PIGMENT 1 (MYB75; PAP1)	0.000	28.73	6.94
		AT1G66390	PRODUCTION OF ANTHOCYANIN PIGMENT 2 (MYB90; PAP2)	0.000	12.88	8.99
		AT5G67060	HECATE 1 (HEC1)	0.000	10.99	3.92
		AT5G13330	RELATED TO AP2 6L (RAP2.6L)	0.000	8.93	6.19
		AT2G46990	INDOLE-3-ACETIC ACID INDUCIBLE 20 (IAA20)	0.000	7.78	1.20
		AT3G50330	HECATE 2 (HEC2)	0.000	6.47	1.08
		AT4G36930	SPATULA (SPT)	0.000	5.66	2.86
		AT4G09820	TRANSPARENT TESTA 8 (TT8)	0.000	5.44	1.39
		AT5G28300	TRIHELIX DNA-BINDING PROTEIN, PUTATIVE	0.000	3.80	3.59
		AT3G48920	MYB DOMAIN PROTEIN 45 (MYB45)	0.001	3.71	5.27
	Repressed	AT2G32550	RCD1-LIKE CELL DIFFERENTIATION FAMILY PROTEIN	0.000	0.25	0.47
		AT1G73870	ZINC FINGER (B-BOX TYPE) FAMILY PROTEIN	0.000	0.24	0.84
		AT2G21650	MATERNAL EFFECT EMBRYO ARREST 3 (RSM1; MEE3)	0.000	0.22	0.25
		AT4G37540	LOB DOMAIN-CONTAINING PROTEIN 39 (LBD39)	0.000	0.20	0.22
		AT4G36570	ARABIDOPSIS RAD-LIKE 3 (ATRL3)	0.000	0.19	0.39
		AT3G46130	MYB DOMAIN PROTEIN 111 (MYB111)	0.000	0.19	0.15
		AT1G66230	MYB DOMAIN PROTEIN 20 (MYB20)	0.000	0.18	0.52
		AT1G75250	ARABIDOPSIS RAD-LIKE 6 (RSM3; ATRL6)	0.000	0.18	0.96
		AT5G07690	MYB DOMAIN PROTEIN 29 (MYB29)	0.000	0.16	0.92
		AT5G28770	BZO2H3	0.000	0.16	0.27

Table 5-13: Overview of the 10 most induced and repressed transcription factors from roots of *rml1-1.* Shown are AGI codes, descriptions, p-values from statistical analysis of the shoot as well as fold changes in expression for shoot and root.

		AGI code	Description	p-value (shoot)	fold change shoot	fold change Root
Isolated from roots	Induced	AT2G38340	AP2 domain-containing transcription factor, putative (DRE2B)	0.000	1.74	32.31
		AT4G06746	related to AP2 9 (RAP2.9)	0.007	0.77	14.66
		AT2G47520	AP2 domain-containing transcription factor, putative; HRE2	0.002	1.84	14.29
		AT3G23250	MYB DOMAIN PROTEIN 15 (MYB15)	0.406	0.84	10.07
		AT4G18170	WRKY28; transcription factor	0.479	0.92	9.87
		AT3G01600	Arabidopsis NAC domain containing protein 44 (anac044)	0.000	2.85	9.61
		AT1G66390	PRODUCTION OF ANTHOCYANIN PIGMENT 2 (MYB90; PAP2)	0.000	12.88	8.99
		AT5G59820	RESPONSIVE TO HIGH LIGHT 41 (RHL41; ZAT12)	0.005	2.59	7.93
		AT3G01970	WRKY45	0.003	1.53	7.90
		AT2G28700	AGAMOUS-LIKE 46 (AGL46)	0.773	0.98	7.46
	Repressed	AT1G13300	HRS1; myb family transcription factor	0.000	0.58	0.12
		AT2G44940	AP2 domain-containing transcription factor TINY, putative	0.797	0.97	0.12
		AT3G56970	BHLH038	0.364	1.24	0.12
		AT5G07030	aspartic-type endopeptidase	0.006	0.75	0.11
		AT2G40750	WRKY54	0.672	1.03	0.10
		AT3G48940	remorin family protein	0.021	0.80	0.10
		AT3G49760	Arabidopsis thaliana basic leucine-zipper 5 (AtbZIP5)	0.577	0.92	0.10
		AT1G62975	basic helix-loop-helix (bHLH) family protein (bHLH125)	0.123	1.27	0.10
		AT4G00670	DNA binding	0.791	1.04	0.09
		AT4G04840	methionine sulfoxide reductase domain-containing protein	0.000	0.49	0.06

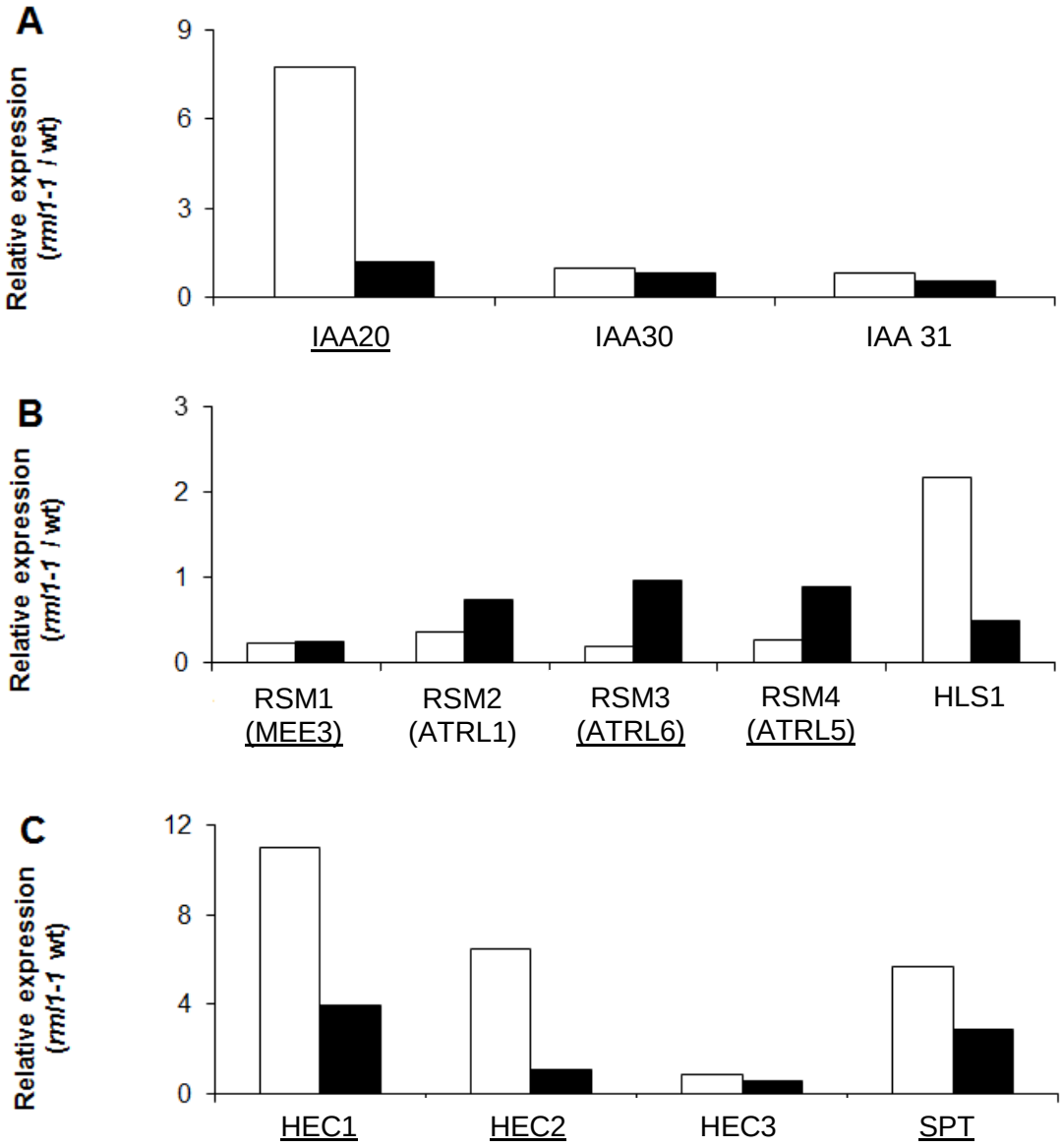

Figure 5-9: Comparison of the relative expression in the *rml1-1* for suites of transcription factor families. Comparisons were made between roots (black bars) and shoots (white bar) relative to expression in wild-type seedlings. The transcription factor families analysed are related to IAA20 (A), RMS1 (B) and HEC1 (C). Underlined genes are represented in the top 10 most induced / repressed transcription factors (Table 5-12 and Table 5-13).

Two HECATE (HEC) genes and the SPATULA (SPT) gene were also found among the most-induced transcription factors linked to growth. *HEC* encodes putative basic helix-loop-helix (bHLH) transcription factors with overlapping functionality. Depending on which HEC function is missing, plants have a

varying degree of infertility, defects in septum, transmitting tract and stigma development and impaired pollen tube growth (Gremski et al., 2007). In addition, these phenotypes are similar to those with mutations in the SPATULA gene. SPT encodes a bHLH transcription factor required for development of plant tissues regulating the development of the female reproductive tract together with the HEC genes (Gremski et al., 2007). While HECATE1 (HEC1) transcription was strongly induced in *rml1-1*shoots (7.7-fold) and roots (3.9-fold) relative to the wild-type, HEC2 transcription was only 6.4-fold induced in *rml1-1* shoots (Figure 5-9C). In contrast, HEC3 transcription decreased in *rml1-1* shoots and roots relative to the wild-type (Figure 5-9C), while SPT transcription increased 5.6-fold in *rml1-1* shoots and 2.8-fold in roots relative to the wild-type. This result indicates a particular involvement of glutathione in the control of transcriptional regulation of hormones and subsequently plant development. Novel is the strong effect of glutathione depletion on transcription induction and in particular on certain hormone-related genes and hormone-related transcription factors suggesting a regulatory effect of glutathione in transcription control. However, the effects of glutathione depletion on transcription of these genes vary with differential expression in shoots and roots.

Transcription factors linked to redox processes

To obtain insight into how glutathione depletion affects transcription of redox process associated transcription factors, shoot transcripts encoding glutathione-s-transferases (GSTs), dehydroascorbatereductases (DHAR), h-type thioredoxins (TH), glutaredoxins (GRX) and glutathione peroxidases (GPX) were analysed (Figure 5-10). Glutathione depletion affected

transcription of a large number of genes encoding GSTs, TRXs and GRXs, with a major effect on the transcription of various GSTs and TRXs (Figure 5-10).

In particular mRNAs encoding two h-type TRXs, *TH7* and *TH8,* were greatly increased in abundance in shoots in response to GSH depletion (Figure 5-10). *TH7* and *TH8* were induced by 2.5- and 5.5-fold, respectively (Figure 5-10). These two TRXs are involved in cellular redox homeostasis, in the organization of the nucleolus and N-terminal myristoylation of proteins (TAIR10, 2012). The induction of TRX expression in shoots is an expected response to glutathione depletion, as the antioxidants glutathione and thioredoxin share functional redundancies and thioredoxins can at least partially compensate for a loss of glutathione and its antioxidant functions.

Furthermore, transcription of the gene encoding dehydroascorbate reductase 1 (DHAR1) was found to be increased by 1.5-fold in response to glutathione depletion. DHAR1 is implicated in protein glutathionylation, thereby suggesting an involvement in signalling pathways in plants (TAIR10, 2012). Glutathione depletion does seem to affect the expression of DHAR 1, but not DHAR2 and thereby might at least partially affects down-stream signalling components. However, it seems likely that the induction of DHAR expression under GSH depletion occurs in response to the loss of glutathione's ROS scavenging function.

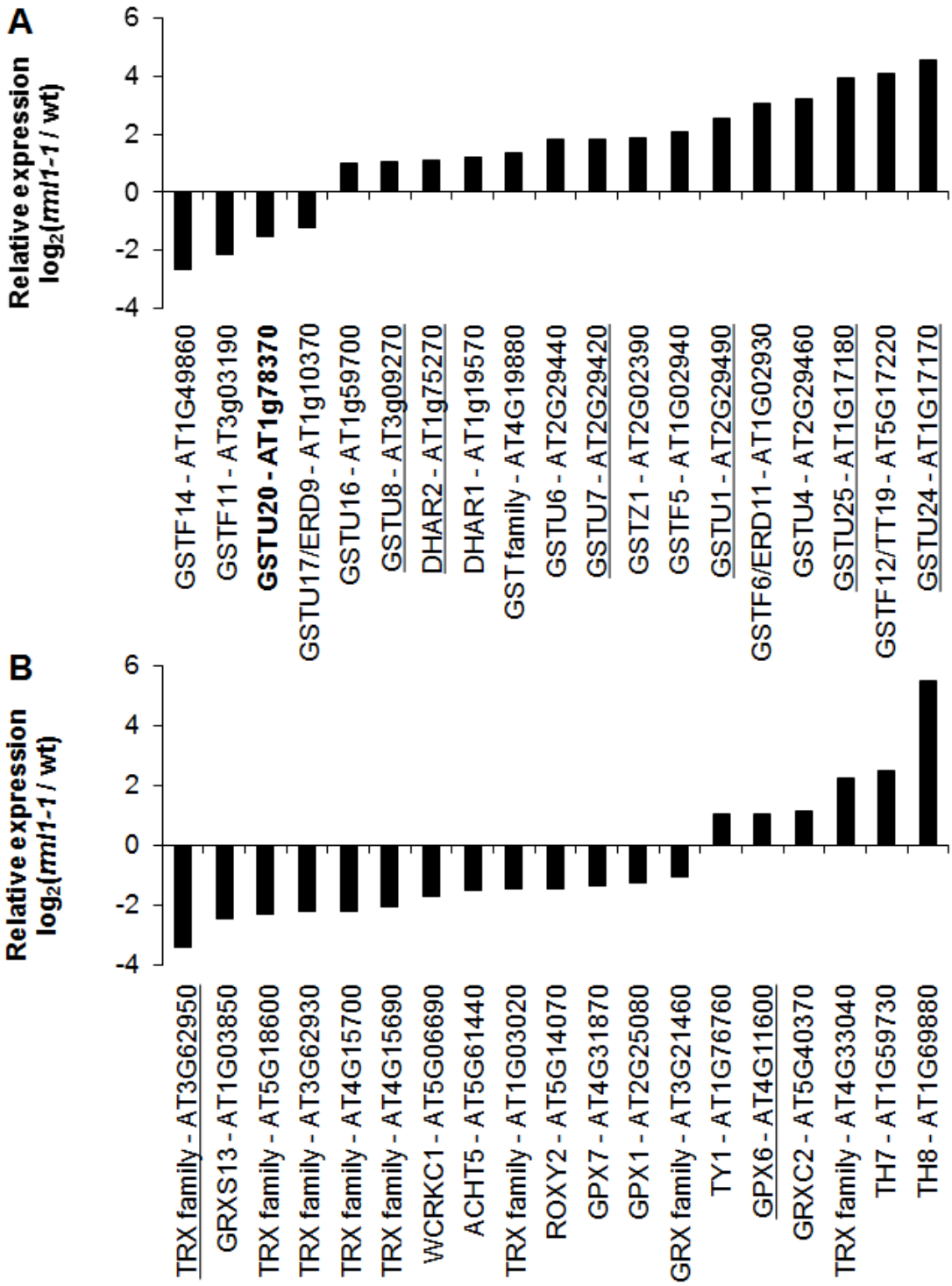

Figure 5-10: The effect of GSH depletion on the expression of redox-related genes. Differential expression of transcripts encoding GST and dehydroascorbatereductases (DHAR) (A) and h-type thioredoxins (TH), glutaredoxins (GRX) and glutathione peroxidases (GPX) (B) in *rml1-1* shoots relative to the wild-type tissues. Genes, identified from the tiling array analysis, that are in bold script indicate involvement in auxin-related processes. Underlining indicates genes that are induced by H_2O_2 in the *catalase2* mutants (Queval et al., 2012).

5.3 Results of the qRT-PCR analysis of the effects of glutathione depletion on selected transcripts

The effects of glutathione depletion on transcript abundance were also studied using qRT-PCR. These analyses were performed firstly to confirm selected findings of the *Agronomics1* tiling array, with a particular focus on core cell cycle components in the *rml1-1* mutant. The analysis of core cell cycle components was used to validate the findings from the tiling array analysis.

The primary aim was to compensate for the lack of three independent biological replications for the *rml1-1* root in the tiling array experiments. Thanks to using the improved tissue disruption method higher extractable RNA yields were possible. Secondly, these analyses should reveal whether glutathione depletion affects abundance of auxin-related transcripts only in the *rml1-1* mutant or also in other glutathione-related mutants. Both analyses were performed to find possible explanations for the occurrence of the very characteristic *rml1-1* root phenotype. Therefore, qRT-PCR analyses were also performed on a set of selected auxin-related genes on mutant genotypes (*cad2-1*, *pad2-1*, *rax1-1*) that had less severe alleles of the *GSH1* gene and therefore higher GSH amounts compared to the *rml1-1* mutant. All experiments were performed relative to wild-type plants and also relative to wild-type plants treated with BSO. Per each genotype at least three independent biological replicates were used.

5.3.1 qRT-PCR analysis of the effects of glutathione depletion on core cell-cycle components

Transcripts encoding core cell cycle marker proteins from the CYC and CDK families decreased in abundance in *rml1-1* roots but not in *rml1-1* shoots (Figure 5-11). The qRT-PCR analysis (Figure 5-11B) therefore confirmed the findings of the transcriptome analysis shown in Figure 5-11A. Interestingly, the only exception was the abundance of CYCD3;1 mRNAs, which was similar in the mutant and wild-type when analyzed by qRT-PCR (Figure 5-11B).

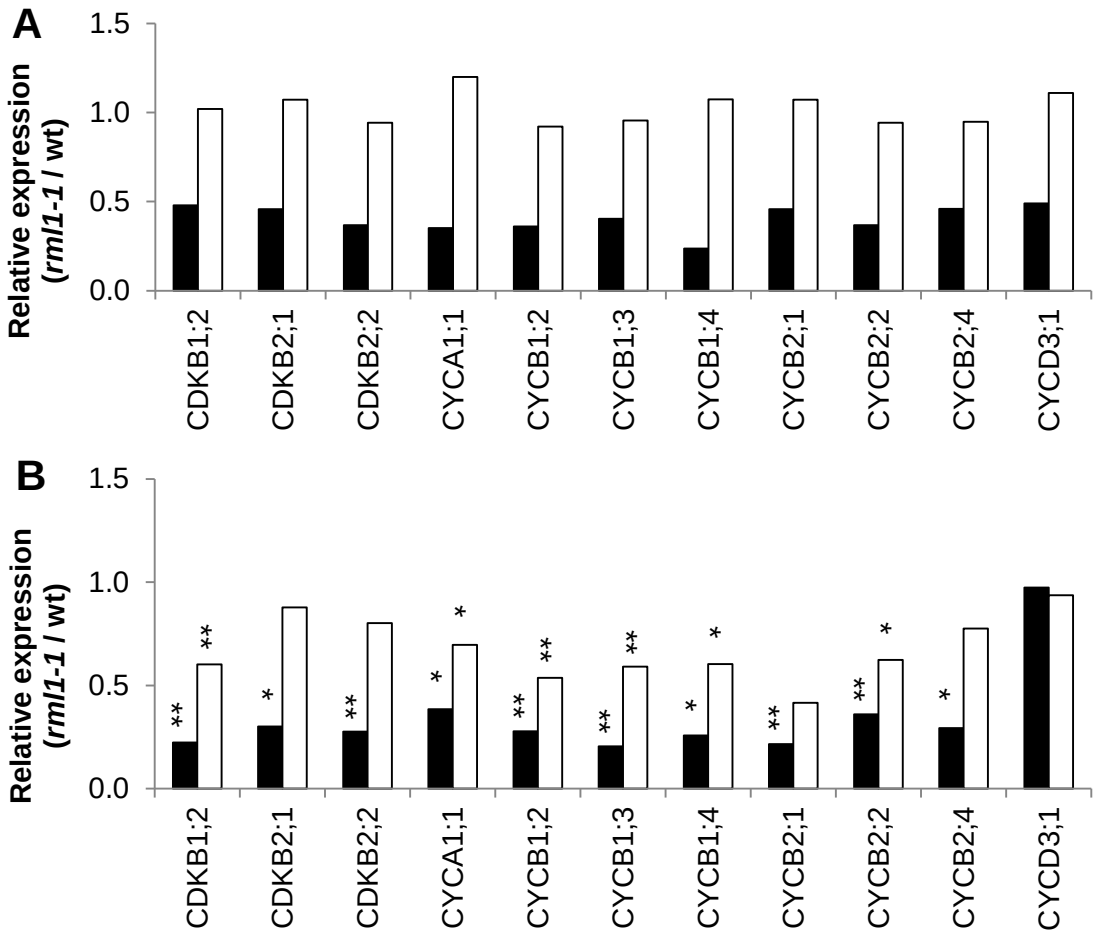

Figure 5-11: Relative expression of core cell-cycle marker transcripts. Relative expression was determined by A: transcriptomic analysis and by B: quantitative real-time PCR. Black columns represent roots; white columns shoots. Asterisks indicate significant differences $p<0.05$ (*) and $p<0.01$ (**) compared to the wild-type.

The result that CYCD3;1 transcript down-regulation could not be validated by qRT-PCR, as found in the tiling array analysis, might point towards a different reason for the cell cycle arrest at the G1 to S transition stage. As transcripts related to G2 stage of the cell cycle were found to be uniformly repressed, the cell cycle might actually arrest between S and G2 stage of the cell cycle. However, an arrest of the cell cycle has to happen before entering G2 stage. While earlier studies demonstrated that cell cycle arrest at G1 to S phase in response to glutathione depletion leads to a down-regulation of two mitotic cyclins (CYCA1;1 & CYCA3;2; Vernoux et al., 2000A), the findings in this study can only partially support the previous findings, in that the cell cycle cannot progress past the S phase.

5.3.2 qRT-PCR analysis of the effects of general glutathione depletion on auxin-linked transcription factors

Abundance of selected transcripts, identified from the tiling array experiment, was further compared in the roots of 7-day old wild-type (Col0) seedlings in the absence or presence of 1 mM BSO and in *rml1-1*, *cad2-1*, *pad2-1* and *rax1-1* mutants (Figure 5-12). Transcripts encoding ATYPICAL CYS HIS RICH THIOREDOXIN 5 (ACHT5) decreased in presence of low GSH amounts in wild-type seedlings when treated with BSO and in the *rml1-1* mutants (Figure 5-12). This observation was also made for ACHT5 in the tiling array analysis of the *rml1-1* mutant. However, this decrease was not observed in the other mutant lines with less severe glutathione depletion (Figure 5-12). Furthermore, the abundance of other mRNAs, such as *GRXS17*, *TH8*, *HEC1*, *SPT* and the *MYB15* and *MYB75,* were strongly induced under low GSH amounts in BSO-treated wild-type seedlings and in *rml1-1* mutants (Figure 5-12). The strong

induction of gene expression in these genes under glutathione-depleting conditions was also observed in the tiling array analysis.

However, the amount of *GRXS17*, *TH8*, *HEC1* and *SPT* transcripts and those of the *MYB* transcription factors *15* and *75* were similar in *cad2-1*, *pad2-1* and *rax1-1* mutants (Figure 5-12). The abundance of *TH7* transcripts was only higher in the *rml1-1* mutants, but not in BSO-treated wild-type seedlings (Figure 5-12). As shown in the next chapter (Figure 6-4A) BSO-induced glutathione depletion results in significantly lower levels of glutathione comparable to those found in the *rml1-1* mutant. These findings suggest that the *rml1-1* mutation itself might lead to additional effects on gene expression than sole BSO-induced glutathione depletion. Overall, these results indicate that gene expression and transcript abundance do not correlate with glutathione amounts in those mutants. However, results also suggest that a certain low amount of glutathione is required before effects on gene expression are detectable since only low glutathione *rml1-1* mutant plants and wild-type plants treated with 1 mM BSO were similarly affected in gene expression.

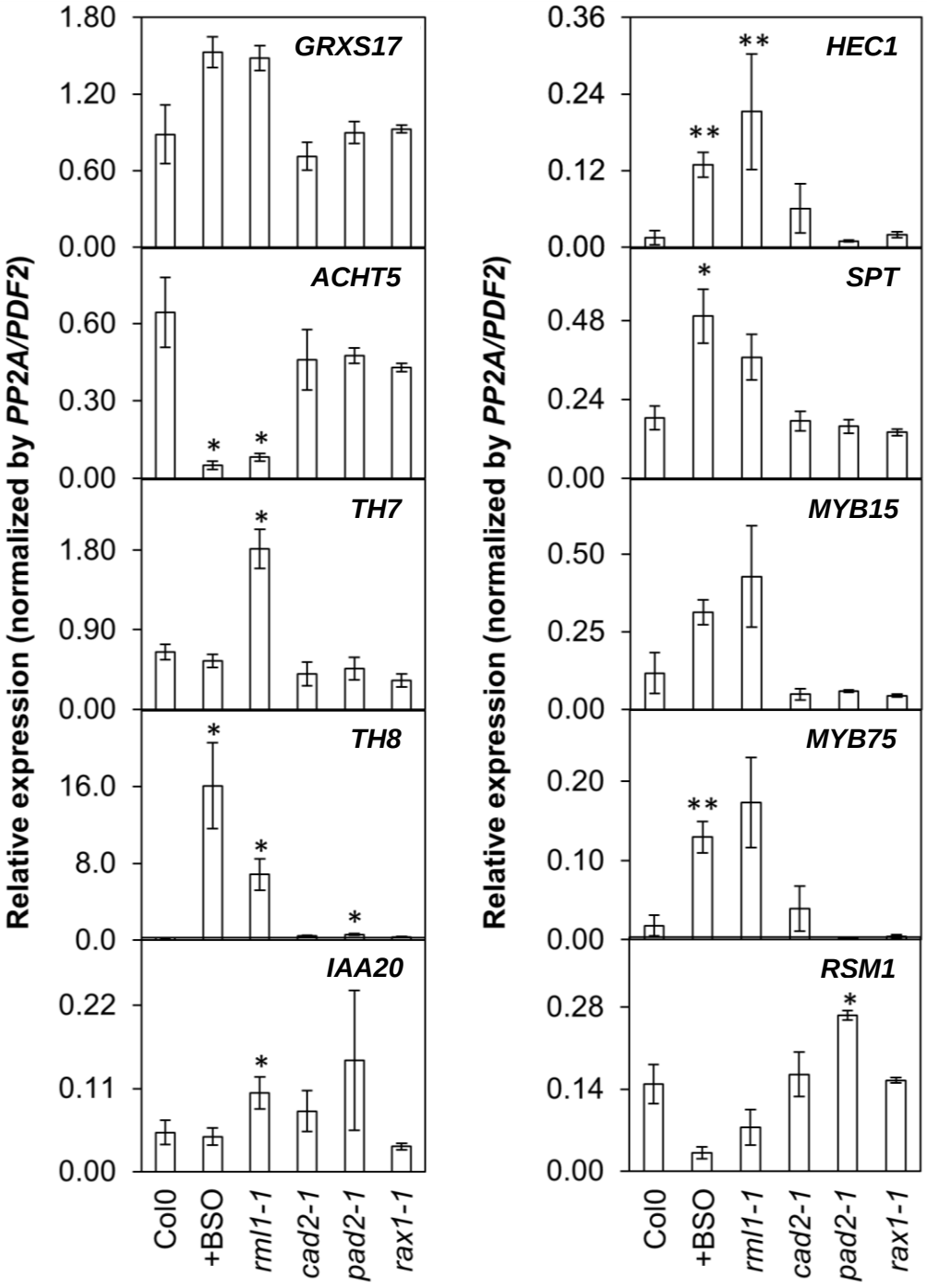

Figure 5-12: The effect of general GSH depletion on gene expression in roots. The relative expression of selected transcripts was measured by qRT-PCR in the roots of 7-day old wild-type (Col0) seedlings in the absence or presence of 1 mM BSO and in the *rml1-1*, *cad2-1*, *pad2-1* and *rax1-1* mutants that are deficient in GSH synthesis and accumulation: *GRXS17*, *ATYPICAL CYS HIS RICH THIOREDOXIN* (*ACHT*) *5*, *TH7*, *TH8*, *IAA20*, *HECATE* (*HEC*) *1*, *SPATULA* (*SPT*), *MYB15*, *MYB75*, and *RADIALIS-LIKE SANT/MYB* (*RSM*) *1*. Asterisks indicate significant differences $p<0.05$ (*) and $p<0.01$ (**) compared to the wild-type.

5.4 Conclusions

An analysis of the effects of glutathione depletion in the *rml1-1* mutant using *AGRONOMICS1* tiling arrays revealed that transcription factors represent the largest proportion among the genes that are the most affected by low cellular amounts of glutathione. Particularly the transcription of transcription factors involved in the control of plant development and associated with auxin were strongly induced. These transcription factors exhibited the highest fold-change inductions of all analysed genes. Cluster analysis of genes involved in hormone metabolism and signalling pathways further demonstrated that the largest numbers of genes, which are changed in response to glutathione depletion, are related to either abscisic acid- or auxin-related genes. And despite various source of possible variability inherent to microarray experiments (, such as e.g. differences arising from dye labelling, efficiency in reverse transcription and hybridization, as well as biological variation within samples), the findings presented in this study indicate a more profound involvement of glutathione in particularly plant developmental, cell cycle-related and hormone-related processes than reported previously.

The results from this study support earlier studies reporting an involvement of glutathione in plant development by regulation of hormonal pathways (Koprivova et al., 2010). Earlier studies further suggested altered PIN-protein expression (PIN1, PIN2 and PIN7) due to glutathione depletion (Koprivova et al., 2010) with altered polar auxin transport in response to glutathione depletion. However, the results identified in this study indicate that only the endoplasmatic reticulum-located PIN5 might be changed in response to

glutathione depletion, pointing more towards an intracellular disruption of auxin transport. Moreover, among genes related to stress responses, the majority were involved in the heat stress responses. Heat-shock proteins/chaperones are involved in protein folding, assembly, translocation and degradation, in stabilizing proteins and membranes as well as assisting in the refolding of proteins under environmental stresses. Glutathione depletion, which leads to more oxidized conditions (unsuitable for proper protein folding) might possibly negatively affect protein folding impairing the maintenance of protein function, rather than altering expression of particularly PIN-proteins. To better understand whether the effects of glutathione depletion are manifested on the protein- or on transcriptional-level, further experiments might also include a focus on PIN-protein expression and folding.

In this study glutathione depletion also resulted in a down-regulation of expression of core cell cycle genes associated with the G2 stage of the cell cycle. It has previously been shown that adequate amounts of glutathione are required for the G1 to S transition (Vernoux et al., 2000A). However, transcription of G1 to S transition marker genes were not affected in the qRT-PCR experiments. Instead a large number of G2 stage marker genes were strongly down-regulated, particularly in the root. To further understand, whether glutathione directly acts on the expression of those cell cycle markers or whether the redox state of the cell determines progression of the cell cycle, further experiments are required. In addition, experiments are also required to investigate if glutathione depletion might impair protein folding of core cell cycle proteins and thereby causing a loss of protein function.

6 Chapter 6: Localisation of glutathione in the nucleus

6.1 Introduction

GSH is found in every compartment of the cell, including the nucleus (Zechmann et al., 2008). Moreover, GSH is recruited into the nucleus during the early phases of the cell cycle (Markovic et al., 2007; Diaz-Vivancos et al., 2010A & B). In mammals, many functions of nuclei, such as transcription, chromatin stability, nuclear protein import and export, as well as DNA replication and repair depend on the function of proteins with oxidizable thiols (Go & Jones, 2010). Glutathione is essential in preventing oxidation and loss of function of such proteins, as well as in re-reducing and restoring functions of these proteins (Go & Jones, 2010).

Although glutathione is as yet considered to diffuse freely from the cytosol into the nucleus through the nuclear pore complex (Zechmann et al., 2008; García-Giménez et al., 2013), little is known about the processes by which it is imported and accumulated in the nucleus during the cell cycle. In animals, GSH transport into mitochondria and the nucleus appears to be actively controlled by the Bcl-2 protein (Voehringer et al., 1998). Bcl-2 is considered to be a pore-forming protein in the particularly the nuclear envelope and considered a major glutathione transporter (Voehringer et al., 1998; Zimmermann et al., 2007). For example, studies on proliferating 3T3 fibroblasts have demonstrated that higher levels of the Bcl-2 protein coincide with higher nuclear glutathione concentrations (Voehringer et al., 1998; Zimmermann et al., 2007; García-Giménez et al., 2013). No genes that encode Bcl-2 proteins have been identified in plants and therefore other proteins must

be present that facilitate an active glutathione import into the nucleus that could possible explain the pronounced accumulation of GSH in the nucleus at the G1 stage of the cell cycle (Markovic et al., 2007;Pellny et al., 2009; Diaz Vivancos et al., 2010A & B). Possible candidates of glutathione transporters that might facilitate the import into the nucleus include the BAG (Bcl-2-associated athanogene) family of proteins (Doukhanina et al., 2006). However, very little information is available on GSH transport into the nucleus and its functions in the nucleus of plant cells.

Earlier studies using roGFP probes have been used to determine the glutathione redox potential of the cytosol (Meyer et al., 2007; Schwarzlaender et al., 2008). However, this approach has never been used to measure the GSH pool of the nuclei even though the roGFP2 probe can diffuse freely into the nuclei. In addition, staining methods have been used to investigate the partitioning of glutathione between the cytosol and nucleus during cell cycle progression (Diaz-Vivancos et al., 2010A & B). The import of glutathione into the nucleus is likely to lead to increases in the cytosolic redox potential, and may also affect glutathione-associated signalling functions in the cytosol. For example, previous studies have shown that responses to pathogens are impaired when GSH is sequestered in the chloroplasts (Maughan et al., 2010). While roGFP probes have long been recognised as specific sensors of the glutathione redox potential (Meyer et al., 2007; Schwarzlaender et al., 2008), they have not been used to investigate the partitioning of GSH between the nuclear and cytosolic GSH pool of plant cells. The following studies were therefore undertaken to investigate the GSH pool in the nucleus. Several different approaches were used to measure GSH in the nucleus. These

included the use of several techniques to isolate intact nuclei, as well as confocal laser scanning microscopy (CLSM) to measure the nuclear GSH pool *in planta*.

For the isolation of intact nuclei, a specific focus was placed on methods that allow the extraction of nuclei with intact outer envelopes. Moreover, for further studies on glutathione functions, the isolated nuclei should ideally retain glutathione during the extraction procedures. A range of different extraction procedures was therefore tested including the INTACT method (Deal and Henikoff, 2010A & B). The INTACT method involves the use of transgenic *Arabidopsis thaliana* plants that expresses a biotin-tagged GFP on the outer membrane of the nucleus envelope. Extracted nuclei can then be purified using streptavidin-coated magnetic beads and GFP used for visualization of the intact nuclei. It is important to note that all methods for nuclear isolation in the literature incorporate extraction from tissue that has been frozen in liquid nitrogen. Moreover, all literature methods include the use of detergents, particularly Trition X-100. Freezing and detergent treatments will favour disruption and loss of function of the nuclear envelope (McKeown et al., 2008; Carrier et al., 2011). Hence, such methods will tend to impair the essential functions of the nuclei with regard to glutathione transport and accumulation, as well as having possible effects on the oxidation state of the glutathione pool. In the following studies, therefore the use of liquid nitrogen and Triton X-100 was avoided as far as possible.

In the following studies, confocal microscopy was used to analyse the redox potential of the nuclei and cytosol of transgenic roGFP2 *Arabidopsis thaliana*

lines grown in the absence and presence of BSO. Previous studies have often used an averaging method for images taken for multiple layers of root material (Meyer et al., 2007; Schwarzlaender et al., 2008). In the present study, laser intensities were modified to allow the analysis of glutathione redox potentials in 1 µm sections of intact root tissue. The glutathione content was also measured in intact roots using standard plate reader methods (Queval & Noctor, 2007).

6.2 Results – Nuclear glutathione redox potential

6.2.1 The nuclear redox potential

The redox potential of the nucleus was determined in the roots of transgenic Arabidopsis plants that constitutively express roGFP2. All measurements were performed on cells in the elongation zone of the primary roots of 7-day old roGFP2-expressing seedlings that had been grown on vertical plates, as illustrated in Figure 6-1. A comparison of the images obtained in this way, with those obtained using the staining procedures for chromatin with Hoechst 33342 and for GSH with CMFDA (García-Giménez et al., 2013) illustrates that the roGFP2 method allows the identification of GSH in both the nuclei and cytosol.

Seedlings were then grown for 7 days either in the absence (0.00 mM BSO; Control) or presence of BSO (0.25, 0.50, 0.75 and 1.00 mM BSO; Treatment). Confocal images of the roGFP2 root cells grown in the absence of BSO show that the fluorescence intensity measured at 405 nm is lower than that measured at 488 nm (Figure 6-1 and Figure 6-2A, F).

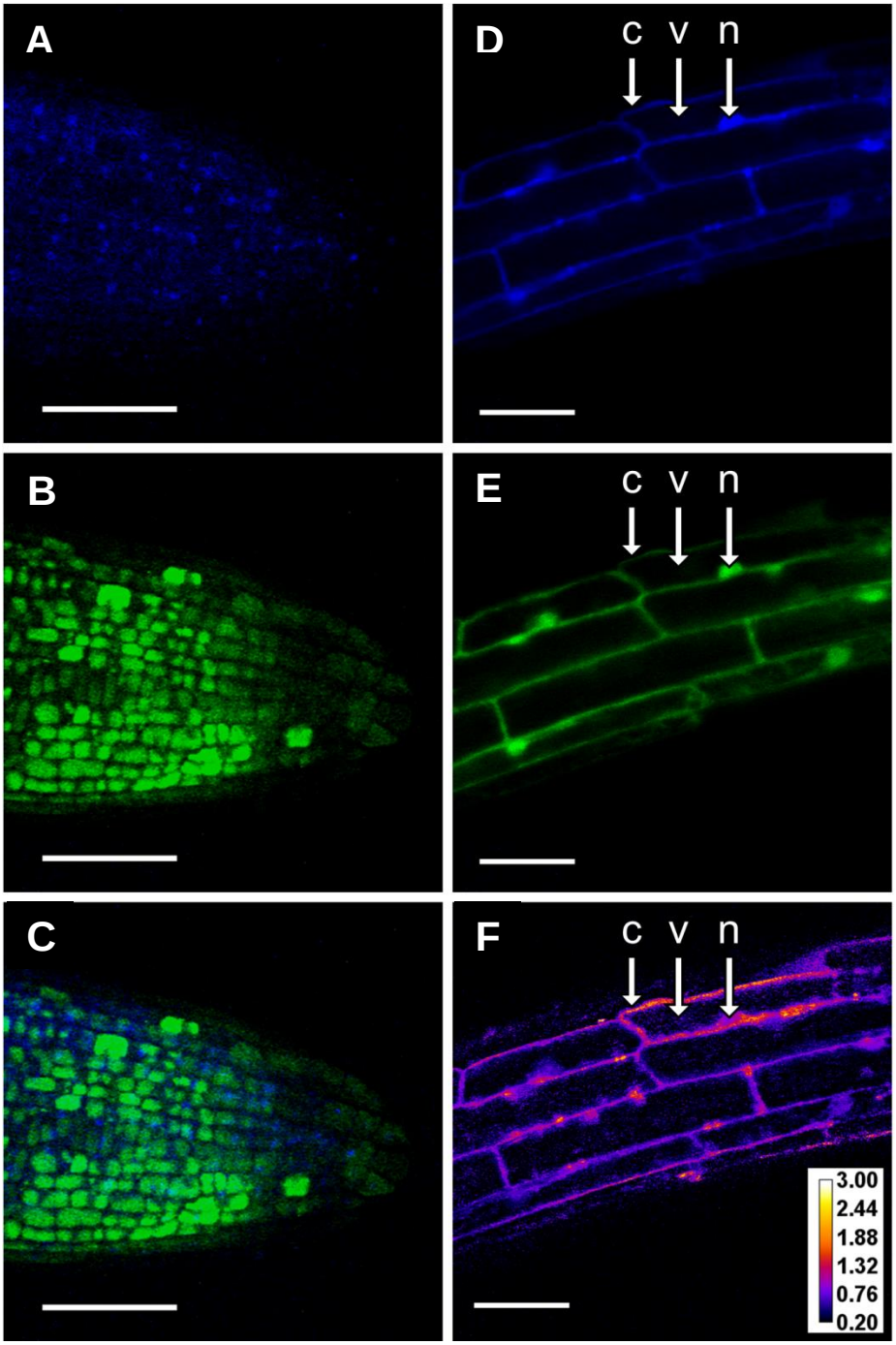

Figure 6-1: Confocal microscopy of *A. thaliana* roots with in situ detection of glutathione in the nuclei and cytosol. Images A, B and C show the primary root tip, while, D, E and F show the elongation zone in the primary root. A: chromatin (nuclei) stained with Hoechst 33342 (blue); B: reduced glutathione (GSH) stained with CMFDA (green); C: overlay image of A and B. D: redox sensitive green fluorescence protein 2 (roGFP2) with fluorescence excitation at 405 nm; E: roGFP2 fluorescence excitation at 488 nm; F: D/E (405/488) ratio. The scale bar in F indicates the variations from reduced (purple) to oxidised (yellow) states. White bars represent 50 µm. c, cytosol; n, nucleus; v, vacuole.

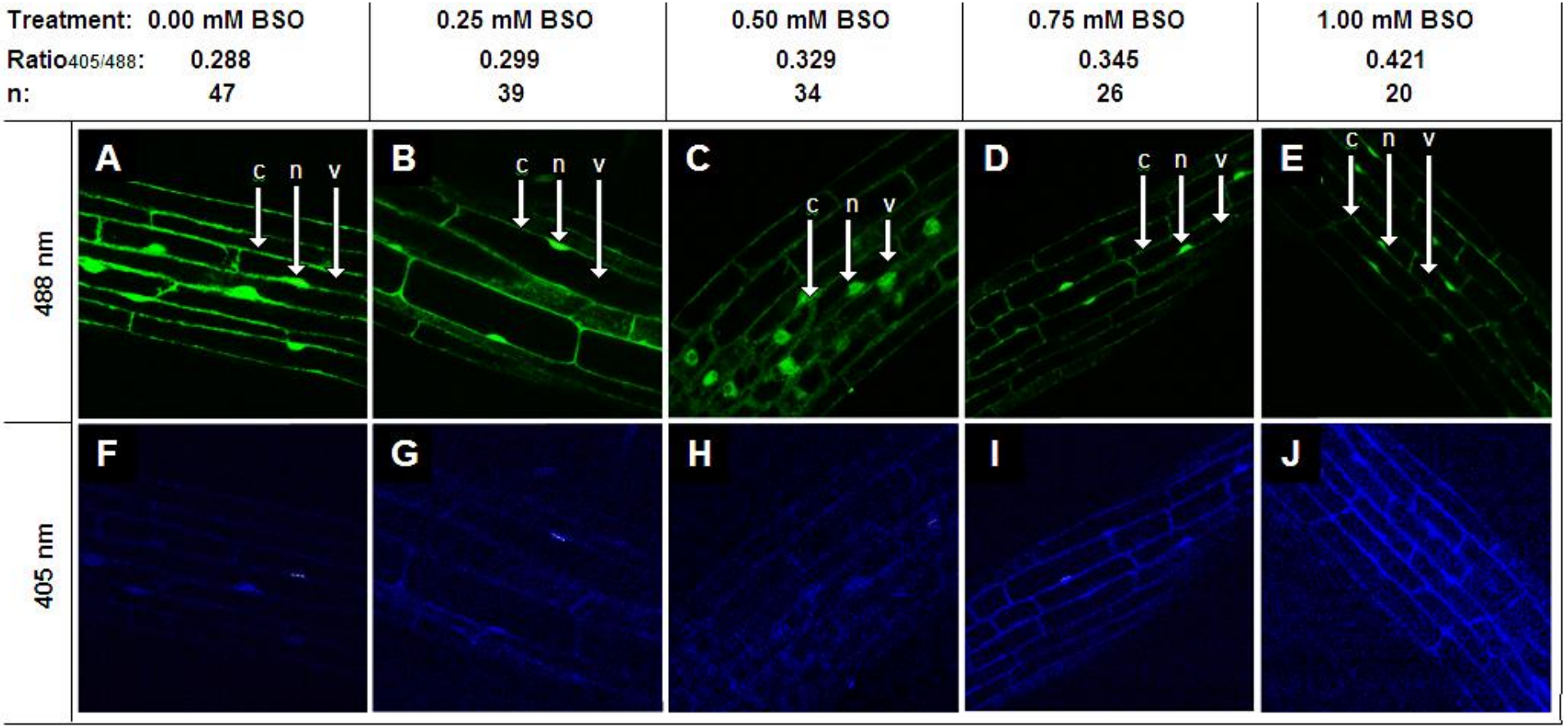

Figure 6-2: A comparison of confocal images obtained of 7-day old roGFP2 seedlings. Displayed are confocal images obtained with a LSM 510 Meta confocal laser scanning microscope at wavelengths 488 nm (A-E) and 405 nm (F-J) for seedlings grown for 7 days in the absence (0.00 mM BSO; Control; A and F) or presence of BSO (0.25, 0.50, 0.75 and 1.00 mM BSO; Treatment; B-E and G-J). Ratios were calculated from fluorescence intensities of nuclei in images obtained at wavelengths 405 nm and 488 nm and averaged across 3 independent biological replications. Average ratios ($Ratio_{405/488}$) and total number of nuclei assessed (n) are shown for each treatment independently.

However, in roots grown in the presence of BSO, the fluorescence intensity measured at 405 nm is increased relative to that measured at 488 nm (Figure 6-2B-E, G-J).

Growth in the presence of BSO significantly decreased the abundance of GSH and GSSG in the roots but it had no effect on the GSH/GSSG ratio (Figure 6-3A). The treatment with 1 mM BSO decreased the total glutathione pool in the roots by over 90% (Figure 6-3A). Moreover, seedlings grown in the presence of the highest concentration of BSO exhibited the highest 405/488 nm ratios (Figure 6-2E, J; Figure 6-3A, B). Quantification of the data derived from these images (Figure 6-3B, C) shows that growth with increasing levels of BSO led to a significant increase in the 405 nm/488 nm ratios of the nuclei in the root cells compared to those grown under control conditions (0.00 mM BSO). The ratio obtained in roots under the 1 mM BSO treatment was over 30% greater than values observed in the absence of BSO (Figure 6-2E, J; Figure 6-3B).

The redox potential of the nuclear glutathione pool calculated from these ratios (Figure 6-3B) reveals that the redox potential of the nuclei in the root cells is highly reduced (-316 mV; Figure 6-3C). However, in the presence of 1 mM BSO, the redox potential of the nuclear glutathione pool was increased by approximately 49 mV (-266.65 mV; Figure 6-3C).

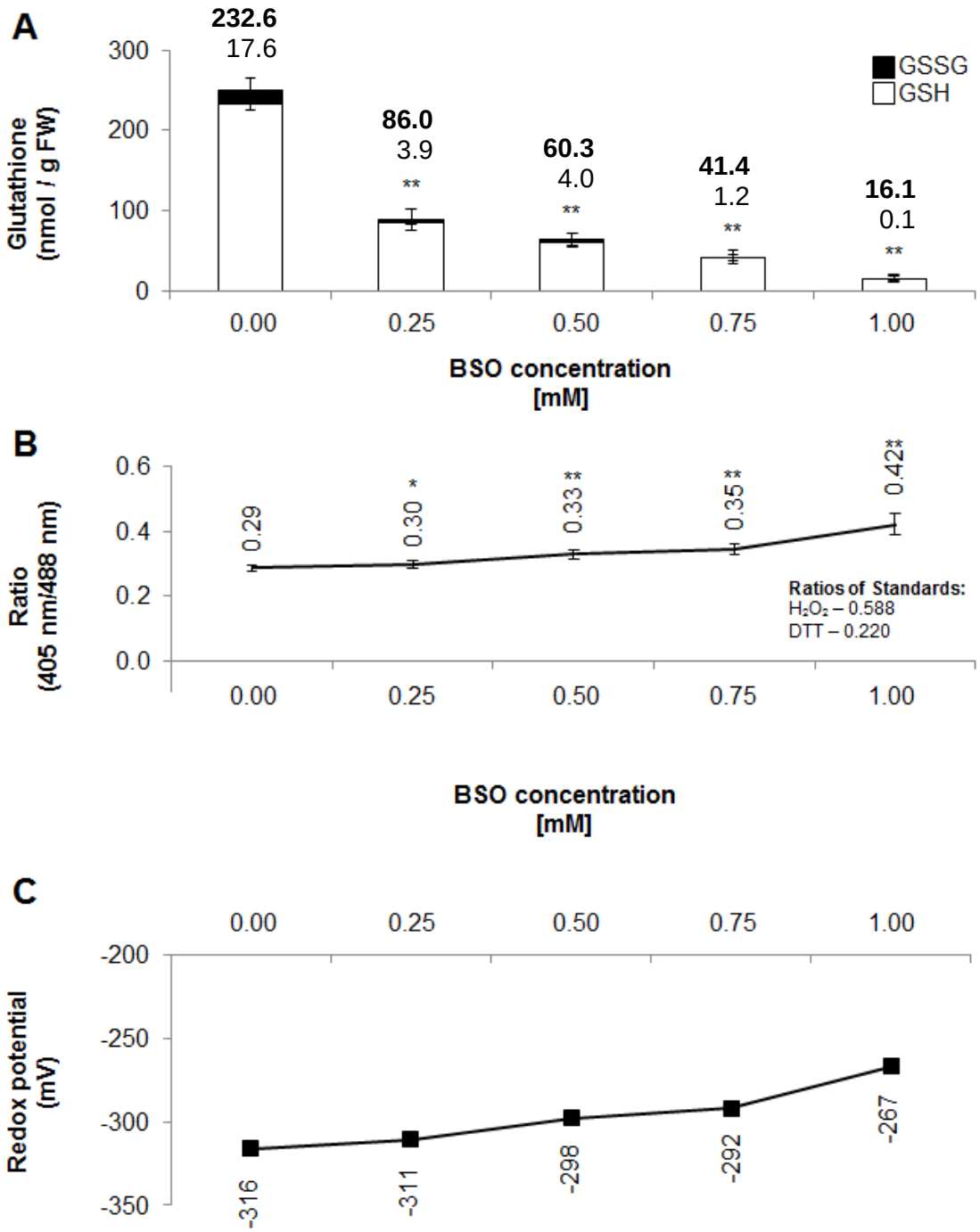

Figure 6-3: Effect of BSO treatment on glutathione concentration in roots and nuclear redox potential. Comparisons were made for plants grown in the absence (0.00 mM BSO, Control) or presence of BSO (0.25, 0.50, 0.75 and 1.00 mM BSO). A comparison of root glutathione contents, with GSH (bold script) and GSSG (normal script) displayed above each bar, is shown in A), ratios (405 nm/488 nm) obtained for nuclear roGFP for each condition as well as the H_2O_2 and DTT standards are displayed in B), and the redox potentials calculated from the ratios are shown in mV in C). * significant differences compared to control conditions $p<0.05$; ** significant differences compared to control conditions $p<0.01$.

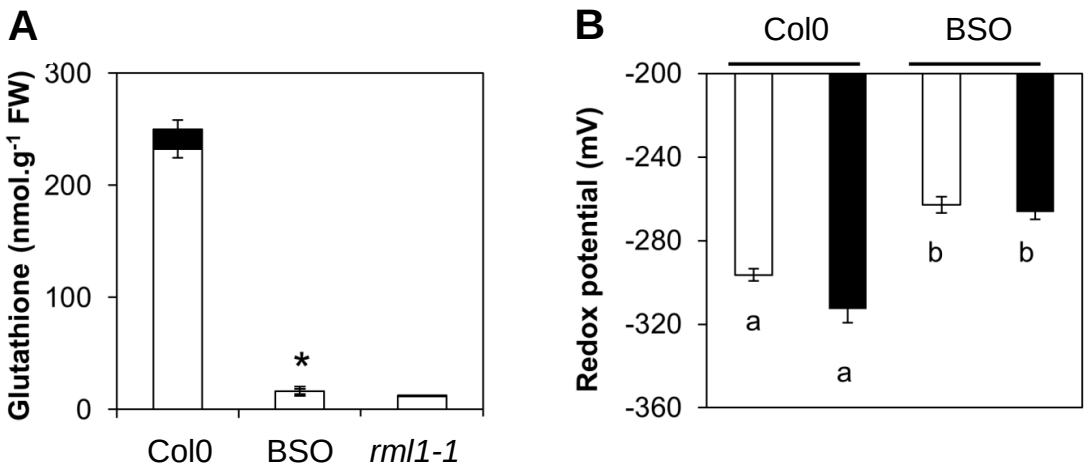

Figure 6-4: Root glutathione contents and redox potentials of the nuclei and cytosol in *Arabidopsis thaliana* in the absence or presence of BSO, and in the *rml1-1* mutants. A: GSH (white bars) and GSSG (black bars) in wild-type roots in the absence or presence of BSO (1 mM) and in the *rml1-1* mutant. B: The glutathione redox potentials of the nuclei and cytosol measured using roGFP2. In B, black columns: nuclei; white columns: cytosol. Letters and asterisks indicate significant differences $p<0.01$.

Growth in the presence of 1 mM BSO decreased the total glutathione pool in the roots by over 90% (Figure 6-3A; Figure 6-4A), resulting in low levels of root glutathione that were comparable to those determined of the *rml1-1* mutants (Figure 6-4A). The redox potentials of the nuclei were similar to those of the cytosol (-316 and -320 mV) in the cells at the root tips in the absence of BSO (Figure 6-4B). Moreover, the values of these parameters increased to the same extent as a result of BSO treatment. In both cases, the redox potentials increased to approximately -260 mV (Figure 6-4B). Although the redox potentials of the nuclei tended to be more negative than those of the cytosol, the values were not significantly different.

6.2.2 The nuclear and cytosolic redox potentials during cell cycle progression

While an analysis of the distribution of GSH between the cytosol and nucleus during cell proliferation using the roGFP2 techniques described above was beyond the scope of the present study, it was possible to gain some insights into how the redox potentials of each compartment might change during the cell cycle from an analysis of unpublished results obtained by Ying Ping Dong, a colleague in the lab, using the staining procedures illustrated in Figure 6-1. In these experiments, Hoechst 33342 (for chromatin) and CMFDA (for GSH) were used to analyse the distribution of GSH between the cytosol and nucleus of *Arabidopsis* cells growing in culture, in which the cell cycle was synchronized using aphidicolin. In this experiment a double-staining method was used employing CMFDA as a specific stain for glutathione and Hoechst 33342 to counterstain nuclei. The re-distribution of glutathione between nucleus and cytosol was then determined from confocal images of cells at various stages in the cell cycle, which derived from the synchronized cell suspension cultures.

Due to the availability of only overall GSH concentrations (from Pellny et al., 2009), the glutathione pool was assumed to be 95 % reduced in order to allow calculations of the redox potential. The overall glutathione concentrations from Pellny which used for calculating nuclear and cytosolic concentrations shown in the following as nmol GSH/mg protein: G0=150, G1=150; S=300, G2=450, P/M=450, A=450, e-T=450 and l-T=450 (Pellny et al., 2009). Based on these values the concentration for nucleus and cytosol were calculated using the

nuclear GSH % values shown in Figure 6-5A, which were obtained from double staining experiments performed by Ying Ping Dong (described above).

This particular analysis of the redox potentials during different stages of the cell cycle is to be regarded as a very initial idea of how the redox potential of nucleus and cytosol might change in response to glutathione redistribution and neglects any possible shifts in GSH/GSSG ratio. Further experiments are required to actually measure the hypothetical values found here and to fully evaluate changes in the redox potential during the cell cycle, which might not only be based on the overall glutathione concentration, but also need to take shifts in GSH to GSSG ratio into consideration, as well as magnitude of the re-synthesis of glutathione when GSH is sequestered into the nucleus at G1. Synchronized root tissue analysis, employing roGFP2 transgenic plants, might provide a useful tool in the analysis of evaluating the redox potentials of glutathione during progression through the cell cycle.

However, based on the present analysis, which allowed a rough approximation of the nuclear and cytosolic glutathione pools at the different stages of the cell cycle, calculations of the redox potentials were performed using the Nernst equation.

The distribution of GSH between the nucleus and cytosol varied at the different stages of the cell cycle. For example, compared to the cells that were not dividing, where only about 19% of the total GSH pool was localized in the nucleus, the percentage of GSH found in the nucleus increased at G1 (Figure 6-5A). Moreover, at some stages of the cell cycle, such as G1 and

telophase stages, over 70 % of the GSH pool was localized in the nucleus (Figure 6-5A).

In contrast, at S, only about 48 % of the GSH pool was localized in the nucleus (Figure 6-5A). It is important to note that the redox potentials calculated from these data are much higher (more positive) than the values obtained with roGFP techniques. Nevertheless, the calculated redox potentials of both the nucleus and cytosol varied at different stages of the cell cycle (Figure 6-5B). In particular, the glutathione redox potential of the nucleus increased by about 19 mV (G0: -171.3 mV to G1:-189.4 mV; Figure 6-5B; lower panel).

The nuclear glutathione redox potential remained steady during S phase and then decreased again by about 10 mV (S: -191.1 mV to G2: -201.0 mV; Figure 6-5B; lower panel). A constant redox potential of glutathione of around -200 mV was maintained throughout the later stages of the cell cycle (Figure 6-5B; lower panel). In contrast to the nuclear glutathione redox potential, the redox potential of the cytosol was decreased by about 15 mV at G1 compared to G0 (Figure 6-5B; upper panel).

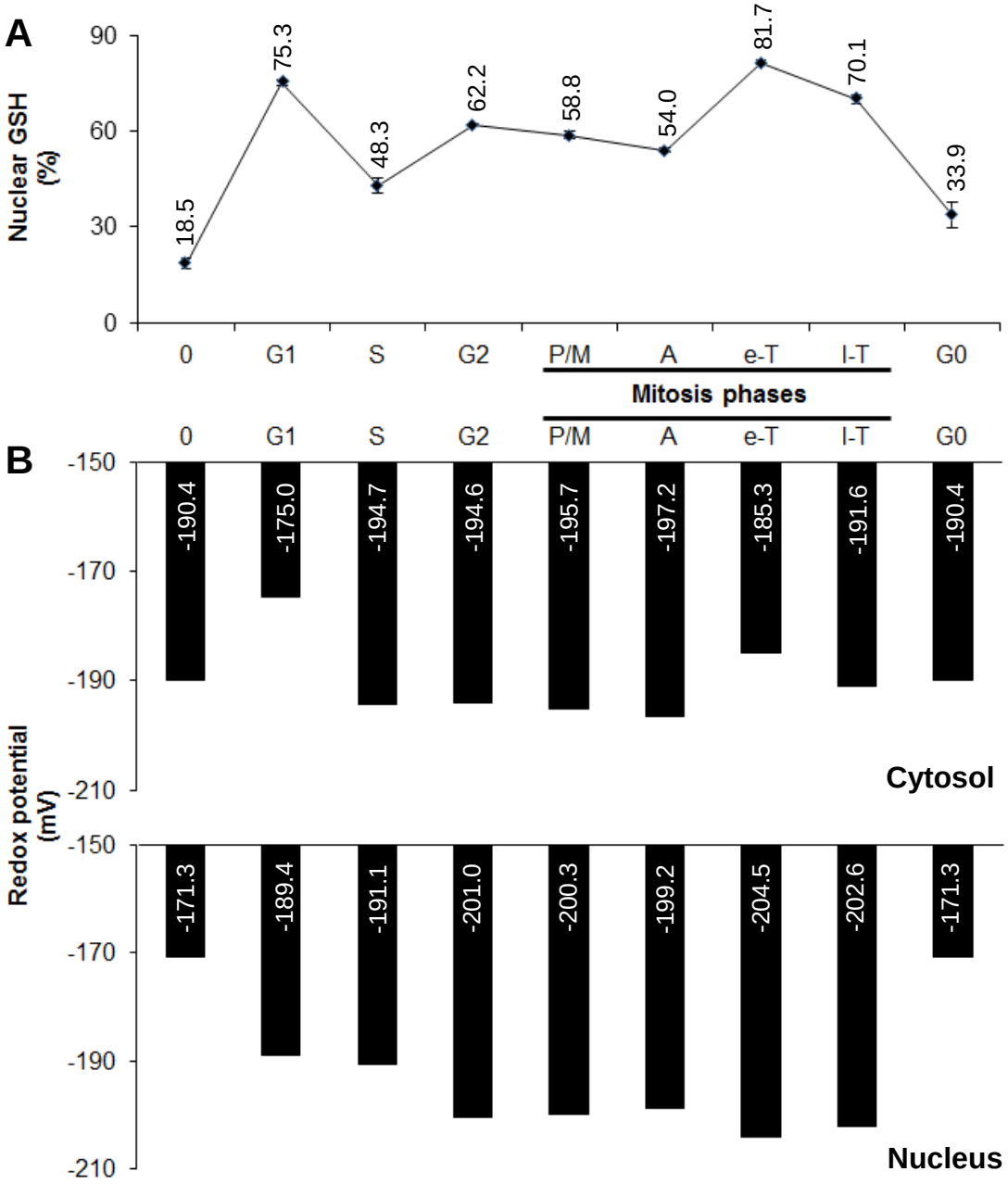

Figure 6-5: Nuclear and cytosolic portions of the cellular glutathione pool and corresponding glutathione redox potentials during cell cycle progression. A: The proportion of GSH present in the nucleus, as % of the overall cellular glutathione pool, during cell cycle progression: O, Prior to proliferation; Mitosis: P/M, pro/metaphase; A, anaphase; e-T, early telophase; l-T, late telophase. The proportion of GSH in the nucleus was established by dividing the mean values for CMFDA fluorescence of the nucleus area by the mean values for CMFDA fluorescence of the whole cell. B: Calculated glutathione redox potentials of the nucleus (lower panel) and cytosol (upper panel) at the different stages of the cell cycle. The redox potentials are shown as white numbers inside the corresponding bar in mV.

Values remained low and constant from G1 phase and late telophase being approximately –200 mV, with exception of early telophase, which exhibited a redox potential of around -185 mV (Figure 6-5B; upper panel).

6.3 Results – Isolation and visualization of nuclei with intact outer envelopes

6.3.1 Isolation of nuclei with intact outer nuclear envelopes

The following studies were performed to isolate nuclei with intact outer envelopes. Techniques that are generally used to isolate nuclei include steps using liquid nitrogen and detergent, such as e.g. Trition X-100, agents that would favour loss of nuclear envelope integrity and alter permeability, such that nuclear proteins might be lost during extraction. A number of attempts were made to isolate nuclei in the absence of these steps and to optimize protocols for purification of nuclei.

Various methods for tissue disruption were tested in relation to the extraction of nuclei using the extraction buffers in the CelLytic PN Kit from Sigma in the first instance (as outlined in Figure 6-6, left panel). Each experiment involved 5 g of roots from 7-day old plantlets, applying appropriate buffer volumes. However, the grinding techniques illustrated in Figure 6-6 (left panel) in combination with the buffers of Sigma's CelLytic PN Kit failed to yield nuclei, as measured by absence of the nuclear envelope GFP signal, as well as the absence of chromatin fluorescence from the chromatin staining using Hoechst 33342. An alternative approach using a modified version of the INTACT method (Deal and Henikoff, 2010B) was therefore tested.

The INTACT method depends on the generation of “biotinylated nuclei” in transgenic *Arabidopsis thaliana* plants that express a fusion protein consisting of a nuclear envelope-targeting sequence, green fluorescent protein (GFP), and the biotin ligase recognition peptide, in the presence of *Escherichia coli* biotin ligase. A transgenic line expressing a GL2p:NTF/ACT2p:BirA his construct (GL2 line), and hence containing biotinylated nuclei in the non-hair root cells, was used in the following studies. The fluorescence of the tagged nuclei is readily observed in the intact roots (Figure 6-7).

In the original method described by Deal and Henikoff (2010B) nuclei are obtained from homogenised frozen root material that is ground to a fine powder. Moreover, one of the purification buffers that are subsequently used contains detergent, and no osmolytes were used. The protocol of Deal and Henikoff (2010B) was therefore modified to avoid liquid nitrogen and detergents, as illustrated in Figure 6-6 (right panel) and 0.3 M Mannitol was included in all buffers in order to avoid swelling of the nuclei due to changed osmolality. In all cases, the extraction and purification steps, illustrated in Figure 6-6 (right panel), were performed twice, but in combination all procedures took no longer than 60 minutes from intact tissue to pure intact nuclei. Various tissue disruption and homogenisation procedures were tested, including grinding and cutting the roots. The most successful method, as shown in Figure 6-8, in terms of the yield of pure nuclei, involved cutting the roots in modified nuclear isolation buffer (mNIB), followed by filtering the homogenate through a 70 µm mesh, followed by centrifugation and purification (Figure 6-8).

Steps of the procedure (all steps performed at 4°C)	Procedures for extraction and purification of nuclei (without using liquid nitrogen or detergent)					
	modified Sigma CelLytic PN Kit				**modified INTACT method**			
	circular grinding		linear grinding		circular grinding		linear grinding	cutting
1 Disruption of tissue								
2 Filtration to remove debris	100 µm filter mesh (Cell strainer) / centrifugation at 500 x g for 10 min.				70 µm filter mesh (Cell strainer) / centrifugation at 500 x g for 10 min.			
3 Decant supernatant	decant supernatant gently and adjust volume to approximately 2 mL using fresh extraction buffer				decant supernatant gently and adjust volume to approximately 2 mL using fresh extraction buffer			
4 Incubation of nuclei with streptavidin-coated beads	---	---	---	---	incubation of nuclei and streptavidin-coated beads for 15 min. under gentle and slow inverting			
5 Purification of nuclei	semi-pure preparation highly-pure preparation				affinity purification			
6 Washing	---	---	---	---	wash nuclei bound to beads and immobilized at the magnet with modified NIB buffer			
7 Resuspending	aspirate nuclei from respective phase and place in fresh Eppendorf tube				resuspend in maximum volume of 1 mL modified NIB buffer and place in fresh Eppendorf tube			

Figure 6-6: Comparison of procedures for extraction of intact nuclei and amounts of recoverable nuclei for each method. Shown are workflows and the different methods of tissue disruption performed. Single red line shows steps that were performed only once, double red line shows procedure steps performed twice.

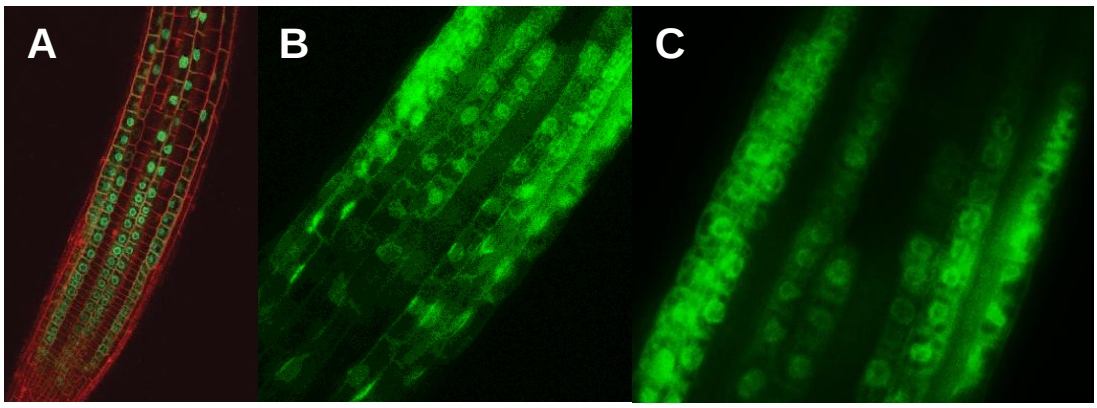

Figure 6-7: Images of GFP-tagged nuclei in root tissue of the GL2 line. A: Confocal image of a root of the transgenic *Arabidopsis thaliana* GL2 line expressing NTF in the epidermal non-hair cells. GFP is shown in green and cell walls are shown in red (Deal and Henikoff, 2010B). B and C: Fluorescence microscopic image of the nuclei inside the root of the GL2 line, which were obtained during this study.

The nuclei prepared as described in Figure 6-8 were intact as determined by bright field images (Figure 6-9A-F), GFP-fluorescence (green, Figure 6-9G-L; white arrows) and chromatin staining with Hoechst 33342 (blue, Figure 6-9M-R; white arrows). While the nuclei prepared in this way were intact, the yield was too low to perform other studies. Therefore, numerous attempts were made to improve this method so as to achieve higher yield. Despite all these efforts, the highest yields obtained were between 17 and 20 nuclei per 20 µL purified preparation (Figure 6-9). Therefore, only about 865 nuclei were obtained from each 5 g of starting root material. In comparison, Deal and Henikoff (2010A) reported a routine recovery of $1\text{-}3*10^5$ nuclei per 3 g of starting root material. The difference in the yields between the present study and that reported by Deal and Henikoff (2010A) implies that other methods of tissue disruption need to be used, such as for example protoplast extraction from cells grown in suspension and lysis of these protoplasts.

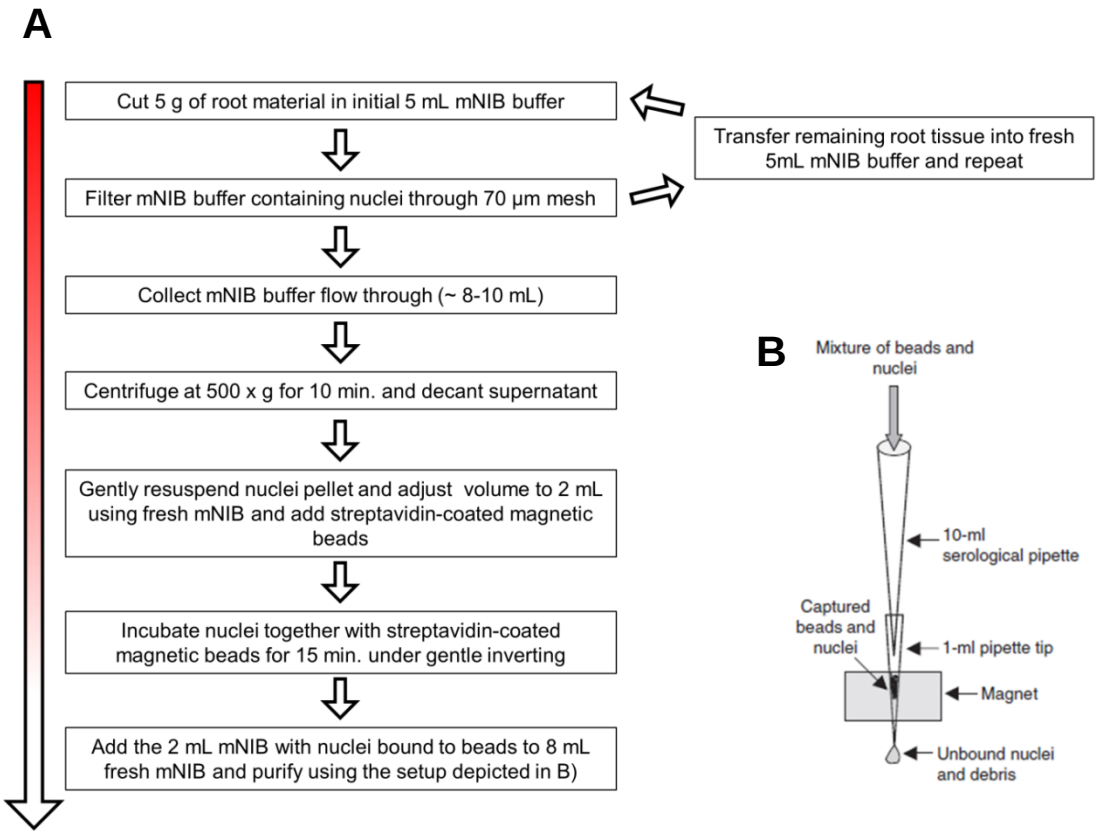

Figure 6-8: Best working method for the extraction of nuclei. The workflow required for the extraction of nuclei is shown in A, and the setup for the purification as described by Deal and Henikoff (2010B) in B. The arrow in A is colour-coded to display the care required during each step (red, extremely careful handling; white, careful handling). All steps of the purification were performed at 4°C in a cold-room and on ice. mNIB (modified Nuclear Isolation Buffer), is the buffer used for the extraction of nuclei as described by Deal and Henikoff (2010B) plus added 0.3 M mannitol.

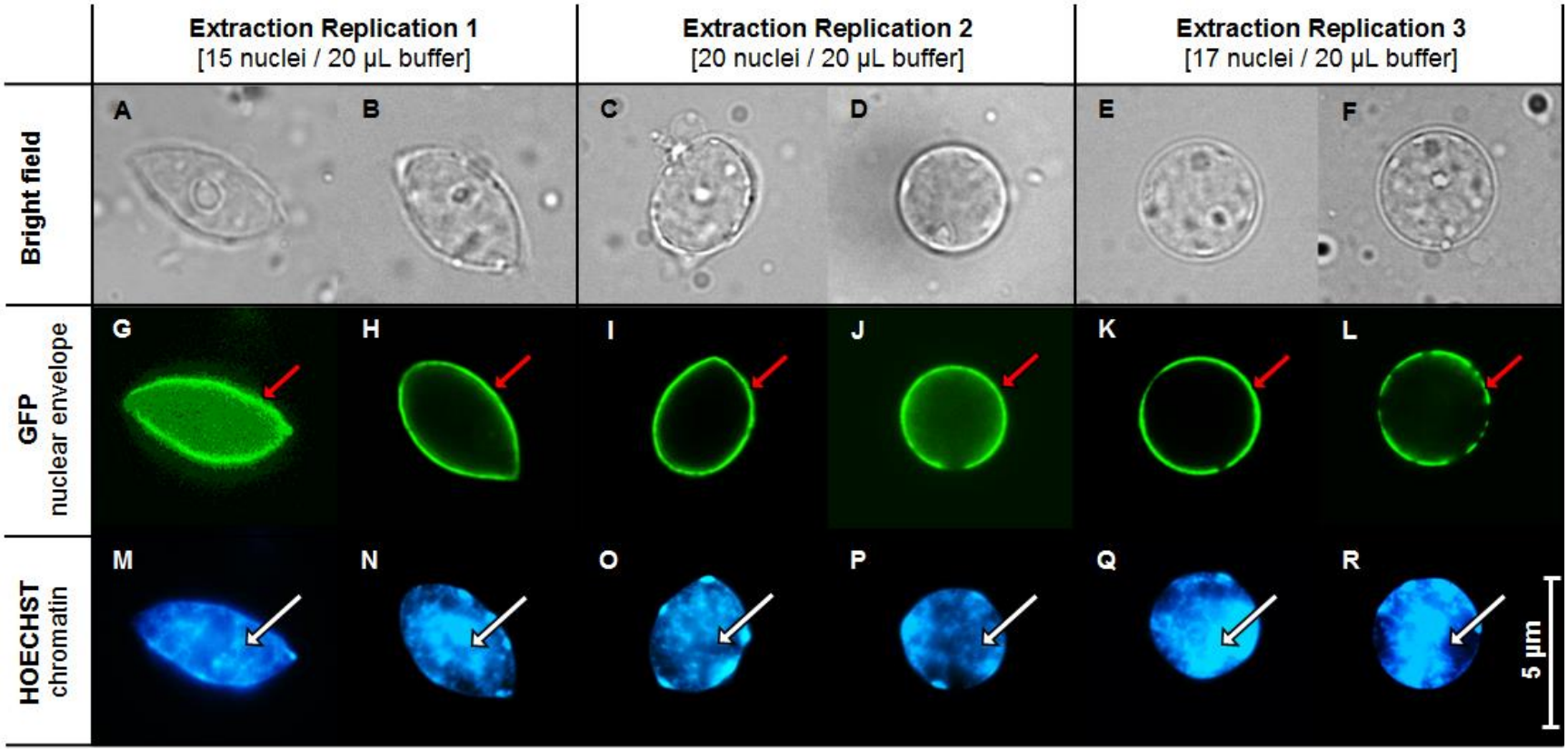

Figure 6-9: Visualization of extracted nuclei. Visualization of nuclei, extracted by cutting 2 g of root tissue of 7-day old GL2 seedlings and a two-step filtering approach, was performed at wavelengths 488 nm for the nuclear envelope GFP and 461 nm for HOECHST 33342. Shown are bright field (nuclei, A-F), GFP (nuclear envelope, red arrows, G-L) and HOECHST (chromatin, white arrows, M-R) images under 100x magnification for 3 independent extraction replications of the best extraction method. The yields of nuclei are displayed for each replication separately. The white bar represents 5 µm.

6.3.2 Visualization of extracted nuclei

Scanning electron microscopy (SEM) using a FEI Quanta 200 F environmental scanning electron microscope, was also used to visualise the structure of the isolated nuclei. For this analysis, the nuclei were fixed onto slides using a protocol that has been used in yeast (Kiseleva et al., 2007). Nuclei prepared as in Figure 6-8 were fixed onto 5 mm² polysine glass slides. In total, 4 slides were prepared for each nuclear isolation.

This analysis revealed that while the M280 streptavidin-coated beads were clearly visible, very few intact nuclei were present following the fixation procedures (Figure 6-10). In many cases, the M280 beads were associated with cell debris, presumably nuclear envelopes (blue arrows, Figure 6-10A, B and C). Nevertheless, the single nucleus, which is indicated by the green arrows on Figure 6-10C and D) is very similar in appearance to images of isolated nuclei in published work (Fiserova et al., 2009).

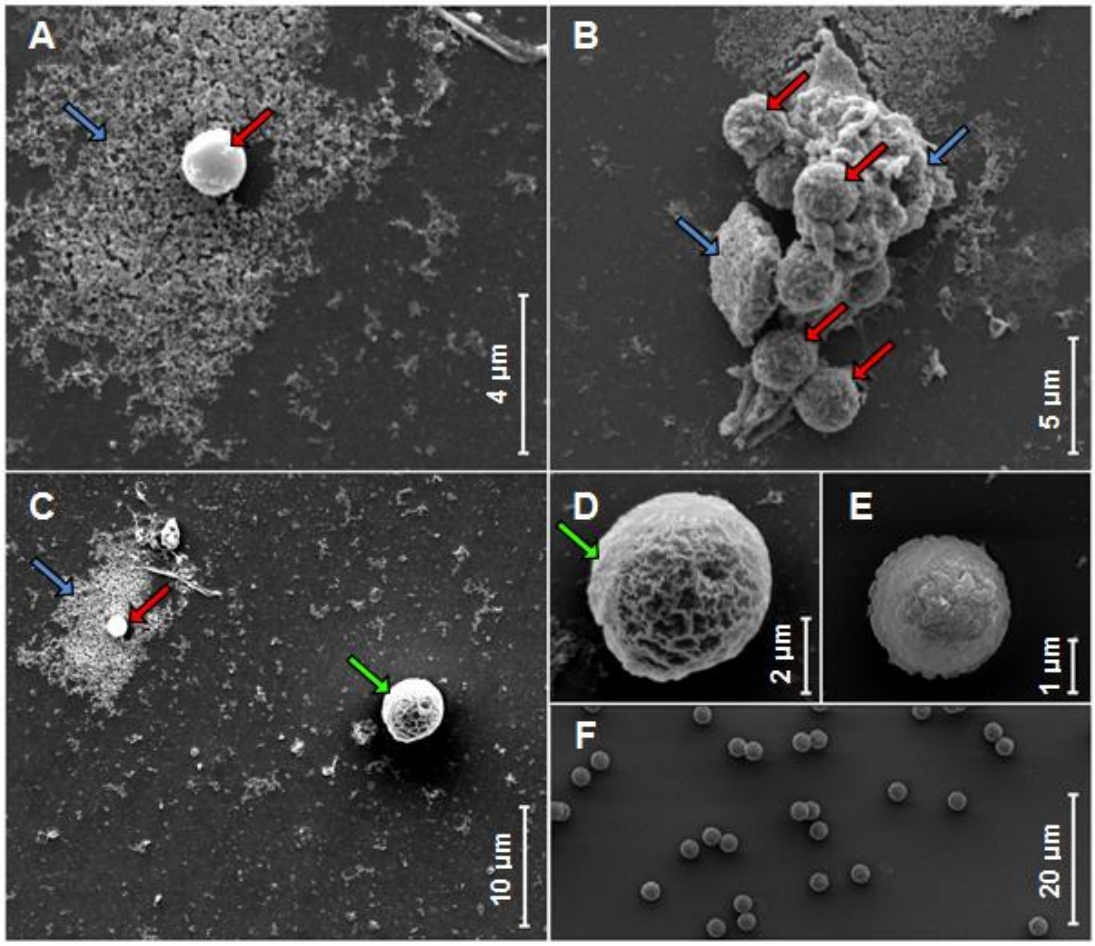

Figure 6-10: Scanning electron microscopy images of nuclear debris and extracted nuclei. Images were acquired using a FEI Quanta 200 FEG scanning electron microscope. Displayed are selected images of M280 streptavidin-coated magnetic beads used during the extraction of nuclei (A, E and F), debris of nuclei (blue arrows A, B and C) bound to beads (blue arrow, B), and a nucleus at different magnifications (green arrow; C, right half and D). For comparison M280 beads were visualized separately at different magnifications (E and F). All images were acquired at 5.00 kV using an ETD detector. Magnifications factors were either 22000x (A), 12500x (B), 6600x (C), 40000 (D), 60000x (E), or 3600x (F). The white bars provide a size scale for each image individually. Red arrows point to M280 streptavidin-coated beads used in the purification process of nuclei from plant extracts.

6.4 Conclusion

The roGFP probe used in this analysis has been widely used previously to determine the glutathione redox potential of the cytosol. The data presented

here demonstrate that the roGFP probe that is targeted to the cytosol can also be used to determine the glutathione redox potential of the nucleus. Presumably this is possible because the probe can diffuse across the nuclear envelope.

GSH is abundant in the cytosol of plant cells (Zechmann et al., 2008). It is considered to diffuse freely from the cytosol into the nucleus through the nuclear pores (García-Giménez et al., 2013). However, there are no published values for the redox potential of the nucleus in plant cells. In this study the glutathione redox potential of the nucleus and cytosol were measured in *A. thaliana* roots in the absence or presence of BSO using the roGFP system (Meyer et al., 2007). The data presented in this chapter not only confirm previous estimates of the cytosolic glutathione redox potential in the absence of BSO (Meyer et al., 2007), but provide the first measurements of the redox potential of the nucleus in plant cells. Moreover, the redox potential of the cytosol and nucleus were also measured in root cells in which the glutathione pool had been severely depleted by BSO treatment. The addition of BSO significantly decreased the cellular glutathione concentration ($p<0.01$; Figure 6-3A), without markedly affecting the GSH to GSSG ratio. In the presence of BSO the 405 nm/488 nm ratios for the nucleus and cytosol were greatly increased compared to control conditions (0.00 mM BSO). However, the redox potentials of the nucleus and the cytosol were decreased to a similar extent as a result of GSH depletion. Therefore, the pools of GSH in the nucleus and the cytosol fluctuate in a similar manner. A recent study on yeast indicated that the redox states of the nucleus and cytosol were independent, at least to some extent (Dardalhon et al., 2012). It will be interesting to determine the the redox

potential of the cytosol and nucleus during the cell cycle in synchronized *A. thaliana* roots using the roGFP system. The movement of GSH into the nucleus at G1 should lead to changes in the redox potentials of both the nucleus and cytosol. However, this would be technically challenging because the cell cycle has first to be synchronised in the root cells. The data presented in Figure 6-5, which are derived from measurements made in synchronised *A. thaliana* cells proliferating in culture, provide a first approximation of how GSH sequestration in the nucleus might alter the redox potentials of both the nucleus and cytosol. It is important to note that the redox potentials calculated from these data are much higher than the values obtained with roGFP techniques. Such differences might be explained by the different methods used in each case. Whereas the measurements made by roGFP probe directly reflect the GSH pool in either the cytosol or the nucleus, the data presented in Figure 6-5 were obtained from values for GSH and GSSG in tissue extracts, which include all cellular compartments.

While the purification procedures for intact nuclei used in this study failed to yield the quantities required for further analysis, the data nevertheless illustrate that nuclei with intact envelopes can be prepared by these procedures. The data presented here demonstrate that it is difficult to obtain nuclei when avoiding liquid nitrogen and detergent steps during the extraction without comprising on yield. Therefore, an alternative method of tissue disruption, circumventing the use of liquid nitrogen or detergents, might be the extraction of nuclei from protoplasts through lysis and subsequent affinity purification (using transgenic line that would ubiquitously and constitutively generate biotin-labeled nuclei through expression of 35S:NTF/ACT2p:BirA instead of

non root-hair specific GL2p:NTF/ACT2p:BirA). This technique might therefore be considered as an alternative that would enhance not only tissue disruption, but also increase recoverable nuclei yields. Furthermore, this approach would allow production of high densities of single cells, which could also be subjected to further treatments, such as glutathione depletion by BSO, prior to protoplastation and isolation of nuclei.

7 Discussion

Although the functions of glutathione in plants have been intensively studied for many years, and genetic evidence has demonstrated links between glutathione levels and shoot and root meristem activity (Bashandy et al., 2010; Koprivova et al., 2010; Reichheld et al., 2007; Vernoux et al., 2000A), the precise roles of GSH in plant growth, development and signalling remain poorly characterised. A multidisciplinary approach was therefore employed incorporating phenomic, transcriptomic, pharmacological and cell biology techniques in order to obtain new mechanistic information on the GSH functions in *Arabidopsis thaliana*, with a particular focus on growth, abiotic stress tolerance and signalling. Mutants that were defective in GSH synthesis capacity, particularly the *rml1-1* mutant, have proved to be useful tools in this analysis.

Earlier studies, using BSO had demonstrated that inhibition of GSH synthesis also leads to an arrest of root growth and provided evidence of effects of GSH depletion on auxin signalling (Koprivova et al., 2010). Although the inhibition of GSH synthesis by BSO appeared to have little effect on gene expression in experiment (Koprivova et al., 2010), *rml1-1* mutant plants were used in the present studies for comparative purposes. The data presented here demonstrate that low GSH, in the *rml1-1* mutant, regulates the expression of a wide range of genes, particularly those that encode transcription factors and proteins involved in hormone-dependent regulation of plant growth and development. Taken together, the findings presented in this thesis provide new information concerning the effects of a low abundance of GSH on growth,

abiotic stress tolerance and gene expression patterns, and also the effects of altered intracellular partitioning of GSH on these parameters. These studies enable several conclusions to be drawn:

7.1 Low GSH availability, particularly in the cytosol, decreases lateral root density

While the very low levels of GSH found in the *rml1-1* mutants and in the wild-type treated with BSO led to an inhibition of the growth of the primary roots at an early stage, which is linked to an arrest of the cell cycle, less severe depletion of the GSH pool led to a specific decrease in lateral root density. The effect of low GSH on lateral root density was observed in the *cad2-1*, *pad2-1* and *rax1-1* mutants, as described previously (Marquez-Garcia et al., 2013).

Moreover, like the GSH synthesis mutants, the *clt1clt2clt3* triple mutants, which show specific decreases in the cytosolic GSH pool (Maughan et al., 2010), have significantly lower lateral root densities than the wild-type. These data demonstrate that a high cytosolic GSH pool is required in the control of lateral root development. This suggests that a cytoplasmic factor controlling root architecture is sensitive to the availability of this thiol.

7.2 GSH availability exerts an influence on leaf area

The data in the literature concerning the properties of the *cad2-1*, *rax1-1* and the *pad2-1* mutants do not describe effects of low GSH availability on leaf growth development. The phenomics approach used in these studies, which allowed the analysis of between 300 to 2000 plants per experiment, revealed

that the *cad2-1*, *rax1-1* and the *pad2-1* rosettes were significantly smaller than the wild-type at similar time points of measurement. In contrast, the rosettes of the *clt1clt2clt3* triple mutants were significantly larger than the wild-type under low light growth conditions. These data implicate GSH in the control of leaf area. However, growth under high light led to a significant increase in leaf area in all genotypes. The overall size of the rosettes was significantly enhanced by high light. This effect was pronounced in the *pad2-1* mutants, which outperformed the *cad2-1* and *rax1-1* mutants, achieving leaf areas that were similar to or even slightly higher than the wild-type. This finding suggests that the effect of light can overcome the adverse influence of low GSH in signalling that controls leaf area. This observation may also explain why previous studies have not reported a change in rosette parameters in the low GSH mutants.

7.3 Low GSH does not increase sensitivity to a range of abiotic stresses

Abiotic stress tolerance is an important factor determining plant growth and productivity. Antioxidants, such as glutathione, are considered to be important in abiotic stress tolerance because they protect against stress-induced oxidation (Noctor et al., 2013). The data presented in chapter 4 shows that induced exposures to oxidative stress (paraquat), salt stress and osmotic stress resulted in a decrease in leaf area in all genotypes. However, the stress effects were similar in the GSH synthesis mutants and in the *clt1clt2clt3* triple mutants to the wild-type, the only exception was the *rax1-1* mutant, which was slightly more sensitive to the paraquat treatment. Continuous abiotic stress treatments caused larger decreases in leaf area in all genotypes. However, in

contrast to the *clt1clt2clt3* triple mutants, which showed a similar response to the abiotic stresses to the wild-type plants, the GSH synthesis mutants, with the exception of *pad2-1*, had a significantly greater leaf area than the wild-type under oxidative stress and high salt treatments. These results suggest that, rather than increasing sensitivity to abiotic stress, low GSH synthesis capacity mitigates the adverse effects of some abiotic stresses, such as salt and osmotic stress on leaf growth. This finding emphasises the specificity of GSH in protection against some forms of abiotic stress, such as those caused by exposure to heavy metals, where GSH is required for defence pathways such as phytochelatin biosynthesis. The observation that GSH deficiency decreases the adverse effect of salt stress and dehydration on leaf growth may be related to the central role of glutathione in the regulation of gene expression linked to oxidative stress signaling (Noctor et al., 2013). In addition, the altered intracellular compartmentalization of glutathione in the *clt1clt2clt3* triple mutants led to either no change (relative to the wild-type) or a small, but significant, increase in abiotic stress tolerance. These findings contrast with the effects of low cytosolic GSH on biotic stress tolerance, which is impaired in the *clt1clt2clt3* triple mutants (Maughan et al., 2010).

7.4 The redox potential of the nucleus is similar to that of the cytosol

The redox potential of the nucleus and cytosol were determined in the roots of wild-type plants and the wild-type treated with BSO to deplete the GSH pool. The glutathione redox potential, which is a key factor governing interactions between oxidative signals and protein targets, is related to $[GSH]^2$:[GSSG] and is hence influenced by the absolute concentration of GSH as well as by

changes in GSSG relative to GSH (Meyer et al., 2007). Thus, changes in GSH levels alone are sufficient to increase the redox potential in a given cellular compartment, even if the GSH: GSSG ratio is unchanged (Meyer at al., 2007). The roGFP measurements reported here demonstrate that the redox potentials of the nuclei and cytosol are similar. Moreover, the redox potentials of the nuclei and cytosol were changed to similar extent by BSO (Figure 6-1). These data suggest that the nuclear GSH pool of non-dividing cells is no more resistant to GSH depletion than that of the cytosol. This finding is perhaps not surprising given that the redox state of the nucleus and cytosol are often considered to inter-dependent (García-Giménez et al., 2013). However, there are very few reports in the literature in which the redox states of the nucleus and cytosol have been measured. A recent study in yeast suggested that the redox states of the nucleus and cytosol were independent, at least to some extent (Dardalhon et al., 2012). Moreover, the finding that GSH is accumulated and sequestered in the nucleus during cell proliferation (Pallardó et al., 2009; Diaz-Vivancos et al., 2010A & B; Go & Jones, 2010; García-Giménez et al., 2013) suggests that the redox states of the nucleus and cytosol would also be independent under some circumstances in plants. A first analysis of how GSH sequestration in the nucleus during might affect the relative redox states of the nucleus and cytosol is shown in Figure 6-5. Oxidative activation of the CDK/CYC D complex at the G1-to-S transition initiates the cell cycle in animal cells (Menon et al., 2003; Menon & Goswami, 2007), but this type of regulation has not been reported in plants.

The estimates of redox potentials of the nuclei and cytosol were calculated from measurements of the glutathione pool in extracts (Pellny et al., 2009),

together with data obtained from dual staining technique for GSH and chromatin, illustrated in Figure 6-1. These calculations suggest that a transient oxidation of the cytosolic GSH pool occurs at G1, but the redox potential of the cytosol is restored to values similar to G0 at S and thereafter. Conversely, the redox potential of the nucleus is decreased at G1 and the nuclei remain at a higher reduction level throughout mitosis. Low GSH synthesis capacity causes cell cycle arrest at G1, as occurs in the *rml1-1* mutants. Hence, the capacity to overcome the transient oxidation of the cytosolic GSH pool in the G1/S transition is crucial to the progression of the cell cycle.

7.5 Low glutathione alters cell cycle transcripts in roots but not shoots

The data presented in Chapter 5 allow the identification of transcripts involved in cell cycle regulation, whose abundance is changed by low GSH availability (Figure 5-3). In these studies on the *rml1-1* mutants, it is in parts possible to distinguish changes in transcripts that are a result of growth inhibition (*rml1-1* mutant) from those that occur because of the lack of GSH per se (wild-type+BSO; Figure 5-12). However, low GSH decreased the abundance of transcripts encoding core cell cycle components only in the *rml1-1* root, and not in the shoot (Figure 5-3). This finding suggests a localised organ-specific response of the thiol-sensing component that regulates these genes either directly or indirectly. The majority of the mRNAs that were changed in abundance in response to low GSH encode CYCs and CDKs that are required for the G2 to M transition (Inze and De Veylder, 2006; Gutierrez, 2009). Other low GSH-responsive transcripts that were decreased in abundance in *rml1-1*

roots include *Knolle*, *AtAUR1*, *AtAUR2*, *CKS2*, *PROLIFERA*, *ATBS1*, *BUBR1*, *OSD1* (*UVI4-Like*), *PCNA1*, *MITOTIC ARREST-DEFICIENT* (*MAD*)*2*. These genes encode proteins that are involved in processes related to cell cycle regulation. The data presented here therefore demonstrate that redox regulation involving GSH is important for a component that controls a step prior to the G2 to M transition. The changes in the levels of cell cycle transcripts reported here not only provide new insights into how GSH deficiency influences cell cycle progression but also help to explain the molecular mechanisms that lead to the failure of the root meristem in the *rml1-1* mutants (Vernoux et al., 2000A) and the defects in root development observed in wild-type plants treated with BSO.

7.6 Low GSH alters transcripts involved in auxin-dependent processes

Of the large number of transcripts encoding transcription factors and enzymes involved metabolism, protein turnover, stress responses, transport and signalling were differentially changed in abundance in the *rml1-1* mutants relative to the wild-type, many, such as *IAA17/AXR3, IAA20*, *SPT*, *HEC1* and *RSM1,* are linked to the regulation of growth and development. In particular, the transcriptome signature of the *rml1-1* revealed a large proportion of transcripts that are involved in auxin-dependent processes. For example, the levels of *HEC1* transcripts were increased in *rml1-1* relative to the wild-type and they were also increased in the roots of the wild-type following treatment with BSO (Figure 5-12). This finding is interesting, because the *ntra ntrb cad2-1* triple mutants that are deficient in both reduced TRX and GSH

have a similar pin-like phenotype compared to *HEC1* overexpressing lines (Gremski et al., 2007; Bashandy et al., 2010). Both the *HEC1* overexpressing lines and the *ntra ntrb cad2-1* triple mutants suffer from impaired polar auxin transport (Gremski et al., 2007; Bashandy et al., 2010).

Furthermore, the levels of *SPT* mRNAs, which restrain growth (Josse et al., 2011) were also increased in *rml1-1* relative to the wild-type. Moreover, *SPT* transcripts were also significantly increased in the roots of the wild-type following treatment with BSO. Other transcripts involved in pathways that regulate growth were also increased in *rml1-1* relative to the wild-type. For example, *IAA20* transcripts were increased in *rml1-1* relative to the wild-type. The overexpression of *IAA20* was found to cause root meristem collapse (Sato and Yamamoto, 2008).

GSH depletion decreased the abundance of *RSM1* and *HLS1* mRNAs, which are involved in the control early morphogenesis (Hamaguchi et al., 2008). These findings are consistent with the observations from previous studies showing that glutathione homeostasis exerts a strong influence on the auxin signalling pathways that control growth (Bashandy et al., 2010, Koprivova et al., 2010; Gao et al., 2013). An earlier study had reported decreased fluorescence from a $PIN1_{Pro}$::PIN1:GFP construct expressed in *A. thaliana* roots following BSO treatment (Koprivova et al., 2010). In the present study however, the abundance of transcripts encoding all the PIN transporters were similar in the *rml1-1* and wild-type seedlings. The exception was the *PIN5* mRNAs that encodes an ER-localized PIN auxin transporter (Mravec et al., 2009), which were decreased as a result of low GSH. The apparent

discrepancy between these findings might be explained by GSH availability influencing post-translational mechanisms that regulate the abundance of PIN proteins.

The abundance of transcripts encoding several UDP-glycosyltransferases (UGT), such as *IAGLU*, *UGT74E2, UGT75B1* and *UGT75B2,* which are involved in auxin glucosylation was changed in *rml1-1* relative to the wild-type. *UGT75B1* and *UGT75B2* encode enzymes that use IAA as a substrate (Jackson et al., 2001). *UGT74E2* regulates the balance between indole-3-butyric acid (IBA) and indole-3-acetic acid (IAA) to control plant architecture under stress conditions (Tognetti et al., 2010).

7.7 GSH availability alters the abundance of redox-related transcripts

The data presented here allows the identification of TRX transcripts, whose abundance is responsive to GSH depletion. In particular, mRNAs encoding two cytosolic h-type TRXs (*TH7* and *TH8*) and an *ACHT5*, were changed in *rml1-1* relative to the wild-type. The levels of *TH7* and *TH8* mRNAs were greatly increased by GSH depletion. The abundance of these transcripts was not changed by increased H_2O_2 in the *cat2* mutants (Queval and Foyer, 2012). Little is known about the functions of h-type TRXs, or their target proteins, but they are localized to the nucleus, mitochondria, plasma membrane and the apoplast (Gelhaye et al., 2004; Serrato et al., 2008). For example, one of the 10 members of the h-type TRX family in rice (*OsTRXh1*) is important in the regulation of the redox state of the apoplast (Zhang et al., 2011). A plasmamembrane-associated TRX (H9) in *Arabidopsis* was found to move

between cells suggesting a role in intercellular communication (Meng et al., 2009). GSTs and GRXs, such as GRXS17, can also link GSH to auxin transport and the regulation of the cell cycle, through altering auxin sensitivity and perturbing polar auxin transport (Edwards & Dixon, 2010; Cheng et al., 2011). The expression of *GSTU* genes, such as *GSTU5,* is regulated by auxin, (van der Kop et al., 1996; Cheng et al., 2005) as is the expression of *GSTF2*, which binds IAA, NAA and NPA (Smith et al., 2003). The GSH-dependent changes in the levels of *MYB29, GSTU20* and *GSTU11 mRNAs* are consistent with a possible influence on auxin-dependent regulation of glucosinolate synthesis (Sonderby et al., 2010). However, the abundance of transcripts encoding GRXS17, which has been implicated in the regulation of the cell cycle and to auxin transport (Cheng et al., 2011), was not significantly changed by GSH depletion. The levels of *GRXS13* and *GRX480/ROXY19* mRNAs were decreased by GSH depletion in *rml1-1* tissues. Like other GSH-related proteins GRX480/ROXY19 and GRXS13 interact with TGA transcription factors to regulate growth and defence responses (Ndamukong et al., 2007; La Camera et al., 2011; Laporte et al., 2012) and they also exert an influence over other phytohormone signalling pathways (Cheng et al., 2011; La Camera et al., 2011).

7.8 Low GSH availability appears to have an altered gene expression in a different manner to enhanced oxidative stress

Accumulating evidence supports the concept that glutathione status is involved in the cross talk between oxidative signalling and hormones signalling pathways (Mhamdi et al., 2010; Han et al., 2013A, B). In particular, enhanced

oxidative signalling in the *cat2* mutants led to changes in salicylic acid and jasmonic acid signalling that were to a large extent dependent on glutathione (Mhamdi et al., 2010; Han et al., 2013A, B). However, a comparison of transcriptome profiles of the *rml1-1* mutants reported here and that of the *cat2* mutants revealed little overlap in the patterns of transcript changes (Queval & Foyer, 2012). In particular, relatively few salicylic acid and jasmonic acid responsive transcripts were differentially changed in the *rml1-1* mutants relative to the wild-type (Figure 5-7). This finding indicates that thiol deficiency (i.e. low GSH) alone results in a different response to that observed in GSH-dependent oxidative signalling in the *cat2* mutants (Han et al., 2013A). Other aspects of the transcriptome profiles are also different in the *cat2* and *rml1-1* mutants. *For example,* while the expression of *GST* type U genes, which are considered to be markers for oxidative (H_2O_2) signalling (Vanderauwera et al., 2005; Queval et al., 2012) were increased by GSH depletion, the abundance of TRX-related AT3G62950 transcripts, which encode a CC-type GRX, was greatly decreased in the *rml1-1* leaves, but increased in the leaves of *cat2* mutants (Queval et al., 2012). While little is known about AT3G62950 in particular, CC-type GRX are described as specific to land plants and are implicated in functions, such as general plant development, petal development, response to pathogens and are further considered to interact with TGA transcription factors in the regulation of pathogenesis-related genes (Kesarwani et al., 2007; Li et al., 2009; Ziemann et al., 2009). One example is *ROXY1* that encodes a GRX with CC-type motif and is suggested to interact with TGA factors during flower development, by probably modulating TGA factors (Li et al., 2009). Moreover, transcripts encoding proteins involved in the heat shock response were decreased, rather than increased, in the *rml1-1*

mutants, suggesting that low GSH is accompanied by a decrease in ROS-specific signalling. These differences between observations in the *cat2* and *rml1-1* mutants might be explained by the absence of a change in the GSH:GSSG ratio in the *rml1-1* tissues. Hence, the oxidative signalling pathways that trigger altered salicylic acid and jasmonic acid responsive genes may be more dependent on a shift in the GSH:GSSG ratio than on changes in the abundance of GSH alone. Finally, the absence of an oxidative stress transcript signature in plants with low GSH is important, because it demonstrates that thiol deficiency, leading to significant increases in the redox states of the nucleus and cytosol, may result in a different response to that observed in GSH-dependent oxidative signalling.

8 Perspectives

While there are many possible experiments that would extend existing knowledge on glutathione functions in plant growth, development and signalling that might beautifully complement this thesis, the ones that I consider the most interesting would be e.g.:

I) Further experiments to evaluate if the effects, in induced and continuous stress treatments, observed the mutant genotypes in this study are directly related to the GSH level or not.

The use of only use wild-type plants across all induced and continuous stress treatments, which include growth in the absence or presence of various concentrations of BSO (and all combinations of stress and BSO treatments) would allow a more detailed insight into how the GSH level affects stress responses in general. These experiments would be designed to allow for in parallel testing of e.g. wild-type grown in the absence and presence of BSO without stress compared to wild-type grown in the absence and presence of stress with BSO. Using only wild-type plants would also bypass possible mutant genotype-specific effects that might not have been detected in this study.

II) Experiments that allow a determination of how directly GSH level is related to gene expression.

To allow for a determination of how directly GSH level is related to gene expression, qRT-PCR on selected genes, which were identified in the transcriptomic analysis in this study, seem to be the best possible route.

Comparisons of gene expression in wild-type plants grown in the absence and presence of BSO (various concentrations) with gene expression in the *rml1-1* mutant, might allow establishing a link between GSH level and gene expression, as well as allowing identification of possible *rml1-1*-specific effects. In parts this study performed such experiments (Figure 5-12; Figure 6-4A), however, 1mM BSO treatment did not seem sufficient to obtain fully block GSH synthesis in a way comparable to that found in the *rml1-1* mutant, and hence gene expression might not have shown uniform patterns among *rml1-1* mutant and wild-type plants grown in the presence of 1mM BSO. Therefore using a wider range of BSO treatment (e.g. 0.1 mM, 0.2 mM, 0.3 mM, 0.4 mM up to 3.0 mM BSO), as well as a higher maximum BSO treatment (e.g. 3mM BSO), might allow to identify possible linear correlations of GSH level with gene expression levels and might also provide more insights, as to whether the maximum possible BSO inhibition leads to similar effects to that observed in the *rml1-1* mutant.

III) Experiments determining the specific effects of GSH depletion compared to those found in the *rml1-1* mutant plants.

Proteomics of wild-type plants grown in the absence and presence of BSO (only maximum BSO concentration, e.g. 3 mM) in comparison to proteomics of the *rml1-1* mutant might be a useful tool. These experiments would follow up on the ones described in II) and might provide more in-depth knowledge as to the specific effects of glutathione depletion compared to possible *rml1-1* mutant-specific effects relative to the wild-type. Taken together the experiments proposed in II) and III) would also allow to differentiate between

possible transcriptional and post-transcriptional effects of glutathione depletion.

IV) A full analysis of glutathione redox potentials throughout all stages of the cell cycle with in parallel determinations of overall glutathione, GSH and GSSG concentrations.

A detailed analysis of the redox potential of glutathione throughout the cell cycle stage would allow better insights into the possible redox control of the cell cycle. This analysis would particularly benefit from a combination with experiments aimed on an evaluation of the effects of glutathione on nuclear proteins. One possibility to investigate the redox potential of glutathione during the various stages of the cell cycle could be the use of roGFP2 plants. Earlier studies showed that it possible to achieve a stress-induced synchronization of Arabidopsis root meristems using hydroxyurea (Toon et al., 2010). Synchronization of the cells in roots of roGFP2 plants using hydoxyurea treatment and alleviation of this stress might allow to directly follow changes in the redox potential of glutathione using confocal imaging, as well as distribution of glutathione within cellular compartments as the cell cycle resumes. In combination with a determination overall glutathione, GSH and GSSG this kind of experiments might provide actual insights into the redox potential of glutathione for each stage of the cell cycle, the GSH to GSSG ratio at a certain stage in the cell cycle and might also allow to identify stages at which glutathione synthesis could be induced to compensate for more oxidized conditions in the cytosol.

V) Establishing a functional method that allows for the isolation of nuclei with intact outer envelopes and subsequent visualization of the nuclear pore complex, as well as proteomics.

As the procedure to isolate nuclei with intact outer envelopes, which is described in this study, did not allow for the extraction of sufficient amounts of nuclei that would allow follow-up experiments, a completely different approach might yield better results. This study identified amount of plant material and in particular tissue disruption method as the crucial steps to a successful isolation of nuclei. Hence, isolating nuclei from protoplasts generated from high-density cell suspension cultures might be one possibility that would allow for the generation large quantities of single cells, while at the same time reducing excess plant material. A further improvement to this method might be the use of transgenic plants that constitutively generate biotinylated nuclei in all plant tissues, rather than the lines used in the present study, which used a non-root hair specific promotor to achieve tagging in specific cell types. However, this would rather be a longer term project, as the generation of transgenic plants and the validation of stable expression of the transgene is very time-consuming. Nevertheless, the advantage of obtaining large quantities of nuclei in highly-pure preparations would pay off in follow-up experiments, such as e.g. proteomics on nuclear genes, or visualization of nuclear pore complexes via SEM. A further advantage might be the ability to subject the cell cultures to various treatments like e.g. BSO-induced glutathione depletion prior to the isolation of nuclei. This might in turn allow direct identification of possible effects of glutathione depletion on nuclear proteins and distinguish between transcriptional and posttranslational effects of glutathione depletion on these proteins. Furthermore, this would also allow for a determination of possible

posttranslational effects on e.g. proteins involved in the formation of the nuclear pore complex.

9 References

ABRAMOFF, M. D., MAGALHAES, P. J. & RAM, S. J. 2004. Image processing with ImageJ. *Biophotonics Int.*, 11(7), 36-42.

ACHARD, P., GUSTI, A., CHEMINANT, S., ALIOUA, M., DHONDT, S., COPPENS, F., BEEMSTER, G. T. & GENSCHIK, P. 2009. Gibberellin signaling controls cell proliferation rate in *Arabidopsis*. *Curr Biol,* 19**,** 1188-1193.

ALDER, A., JAMIL, M., MARZORATI, M., BRUNO, M., VERMATHEN, M., BIGLER, P., GHISLA, S., BOUWMEESTER, H., BEYER, P. & AL-BABILI, S. 2012. The path from beta-carotene to carlactone, a strigolactone-like plant hormone. *Science,* 335**,** 1348-1351.

AU, K. K., PEREZ-GOMEZ, J., NETO, H., MULLER, C., MEYER, A. J., FRICKER, M. D. & MOORE, I. 2012. A perturbation in glutathione biosynthesis disrupts endoplasmic reticulum morphology and secretory membrane traffic in *Arabidopsis thaliana*. *Plant J,* 71**,** 881-894.

BALL, L., ACCOTTO, G. P., BECHTOLD, U., CREISSEN, G., FUNCK, D., JIMENEZ, A., KULAR, B., LEYLAND, N., MEJIA-CARRANZA, J., REYNOLDS, H., KARPINSKI, S. & MULLINEAUX, P. M. 2004. Evidence for a direct link between glutathione biosynthesis and stress defense gene expression in *Arabidopsis*. *Plant Cell,* 16**,** 2448-2462.

BASHANDY, T., GUILLEMINOT, J., VERNOUX, T., CAPARROS-RUIZ, D., LJUNG, K., MEYER, Y. & REICHHELD, J. P. 2010. Interplay between the NADP-linked thioredoxin and glutathione systems in *Arabidopsis* auxin signaling. *Plant Cell,* 22**,** 376-391.

BASHANDY, T., MEYER, Y. & REICHHELD, J. P. 2011. Redox regulation of auxin signaling and plant development in *Arabidopsis*. *Plant Signaling & Behavior*, 6(1), 117-119.

BENNETT, T., SIEBERER, T., WILLETT, B., BOOKER, J., LUSCHNIG, C. & LEYSER, O. 2006. The *Arabidopsis* MAX pathway controls shoot branching by regulating auxin transport. *Curr Biol,* 16**,** 553-563.

BHARGAVA, A., MANSFIELD, S. D., HALL, H. C., DOUGLAS, C. J. & ELLIS, B. E. 2010. MYB75 functions in regulation of secondary cell wall formation in the Arabidopsis inflorescence stem. *Plant Physiol,* 154**,** 1428-1438.

BLUM, R., BECK, A., KORFTE, A., STENGEL, A., LETZEL, T., LENDZIAN, K. & GRILL, E. 2007. Function of phytochelatin synthase in catabolism of glutathione-conjugates. *The Plant Journal*, 49, 740-749.

BLUM, R., MEYER, K. C., WUENSCHMANN, J., LENDZIAN, K. J. & GRILL, E. 2010. Cytosolic action of phytochelatin synthase. *Plant Physiol*, 153, 159-169.

BORSANI, O., ZHU, J., VERSLUES, P. E., SUNKAR, R. & ZHU, J. K. 2005. Endogenous siRNAs derived from a pair of natural cis-antisense transcripts regulate salt tolerance in *Arabidopsis*. *Cell*, 123, 1279-1291.

BRAY, C. M. & WEST, C. E. 2005. DNA repair mechanisms in plants: crucial sensors and effectors for the maintenance of genome integrity. *New Phytol,* 168**,** 511-528.

BRAZIER-HICKS, M., EVANS, K. M., CUNNINGHAM, O. D., HODGSON, D. R. W., STEEL, P. G. & EDWARDS, R. 2008. Catabolsim of glutathione-conjugates in Arabdisopsis thaliana: role in metabolic reactivation of the herbicide safener fenchlorim. *J Bio Chem*, 283, 21102-21112.

CAIRNS, N. G., PASTERNAK, M., WACHTER, A., COBBETT, C. S. & MEYER, A. J. 2006. Maturation of arabidopsis seeds is dependent on glutathione biosynthesis within the embryo. *Plant Physiol,* 141**,** 446-455.

CARRIER, G., SANTONI, S., RODIER-GOUD, M., CANAGUIER, A., KOCHKO, A., DUBREUIL-TRANCHANT, C., THIS, P., BOURSIQUOT, J. M. & LE CUNFF, L. 2011. An efficient and rapid protocol for plant nuclear DNA preparation suitable for next generation sequencing methods. *Am J Bot,* 98**,** e13-5.

CHENG, J.-C., SEELEY, K. A. & SUNG, Z. R. 1995. *RML1* and *RML2*, *Arabidopsis* genes required for cell proliferation at the root tip. *Plant Physiol*, 107, 365-376.

CHENG, N. H., LIU, J. Z., LIU, X., WU, Q., THOMPSON, S. M., LIN, J., CHANG, J., WHITHAM, S. A., PARK, S., COHEN, J. D. & HIRSCHI, K. D. 2011. *Arabidopsis* monothiol glutaredoxin, AtGRXS17, is critical for temperature-dependent postembryonic growth and development via modulating auxin response. *J Biol Chem,* 286**,** 20398-20406.

CHEW, O., WHELAN, J & MILLAR, A. H. 2003. Molecular definition of the ascorbate-glutathione cycle in Arabidopsis mitochondria reveals dual targeting of antioxidant defense in plants. *J Bio Chem*, 278, 46869-46877.

COBBETT, C. S., MAY, M. J., HOWDEN, R. & ROLLS, B. 1998. The glutathione-deficient, cadmium sensitive mutant, *cad2-1*, of *Arabidopsis thaliana* is deficient in γ-glutamylcysteine synthetase. *Plant J*, 16(1), 73-78.

COOLS, T., IANTCHEVA, A., MAES, S., VAN DEN DAELE, H. & DE VEYLDER, L. 2010. A replication stress-induced synchronization method for Arabidopsis thaliana root meristems. *Plant J*, 64(4), 705-714.

CREISSEN, G., REYNOLDS, H., XUE, Y. B. & MULLINEAUS, P. 1995. Simultaneous targeting of pea glutathione reductase and of a bacterial fusion protein to chloroplasts and mitochondria. *Plant J*, 8, 167-175.

CREISSEN, G., FIRMIN, J., FRYER, M., KULAR, B., LEYLAND, N., REYNOLDS, H., PASTORI, G., WELLBURN, F., BAKER, N., WELLBURN, A. & MULLINEAUX, P. 1999. Elevated glutathione biosynthetic capacity in the chloroplasts of transgenic tobacco plants paradoxically causes increased oxidative stress. *Plant Cell*, 11, 1277-1291.

CZECHOWSKI, T., STITT, M., ALTMANN, T., UDVARDI, M. K. & SCHEIBLE, W. R. 2005. Genome-wide identification and testing of superior reference genes for transcript normalization in *Arabidopsis*. *Plant Physiol,* 139**,** 5-17.

DARDALHON, M., KUMAR, C., IRAQUI, I., VERNIS, L., KIENDA, G., BANACH-LATAPY, A., HE, T., CHANET, R., FAYE, G., OUTTEN, C. E. & HUANG, M. E. 2012. Redox-sensitive YFP sensors monitor dynamic nuclear and cytosolic glutathione redox changes. *Free Radic Biol Med,* 52, 2254-2265.

DEAL, R. B. & HENIKOFF, S. 2010 A. A simple method for gene expression and chromatin profiling of individual cell types within a tissue. *Dev Cell,* 18**,** 1030-1040.

DEAL, R. B. & HENIKOFF, S. 2011 B. The INTACT method for cell type-specific gene expression and chromatin profiling in *Arabidopsis thaliana*. *Nature Protoc,* 6**,** 56-68.

DE SMET, I., LAU, S., VOSS, U., VANNESTE, S., BENJAMINS, R., RADEMACHER, E. H., SCHLERETH, A., DE RYBEL, B., VASSILEVA, V., GRUNEWALD, W., NAUDTS, M., LEVESQUE, M. P., EHRISMANN, J. S., INZE, D., LUSCHNIG, C., BENFEY, P. N., WEIJERS, D., VAN MONTAGU, M. C., BENNETT, M. J., JURGENS, G. & BEECKMAN, T. 2010. Bimodular auxin response controls organogenesis in Arabidopsis. *Proc Natl Acad Sci U S A,* 107**,** 2705-2710.

DESTRO, T., PRASAD, D., MARTIGNAGO, D., BERNET, I. L., TRENTIN, A. R., RENU, I. K., FERRETTI, M. & MASI, A. 2011. Compensatory expression and substrate inducibility of γ-glutamyl transferase GGT2 isoform in *Arabidopsis thaliana*. *J Exp Bot*, 62, 805-814.

DEUSCHLE, K., FUNCK, D., HELLMANN, H., DASCHNER, K., BINDER, S. & FROMMER, W. B. 2001. A nuclear gene encoding mitochondrial Δ^1-pyroline-5-carboxylate dehydrogenase and its potential role in protection from proline toxicity. *Plant J*, 27, 345-355.

DEWITTE, W. & MURRAY, J. A. H. 2003. The plant cell cycle. *Annu Rev Plant Biol.*, 54, 235-264.

DIAZ VIVANCOS, P., WOLFF, T., MARKOVIC, J., PALLARDO, F. V. & FOYER, C. H. 2010A. A nuclear glutathione cycle within the cell cycle. *Biochem J,* 431**,** 169-178.

DIAZ VIVANCOS, P.; DONG, Y. P.; ZIEGLER, K.; MARKOVIC, J.; PALLARDO, F. V.; PELLNY, T. K.; VERIER, P. J. & FOYER, C. H. 2010B. Recruitment of glutathione into the nucleus during cell proliferation adjusts whole-cell redox homeostasis in *Arabidopsis thaliana* and lowers the oxidative defence shield. *Plant J*, 64, 825-838.

DIXON, D. P., SKIPSEY, M., GRUNDY, N. M. & EDWARDS, R. 2005. Stress-induced protein S-glutathionylation in *Arabidopsis*. *Plant Physiol*, 138, 2233-2244.

DIXON, D. P., HAWKINS, T., HUSSEY, P. J. & EDWARDS, R. 2009. Enzyme activities and subcellular localization of members of the *Arabidopsis* glutathione transferase superfamily. *J Exp Bot*, 60, 1207-1218.

DIXON, D. P., SKIPSEY, M. & EDWARDS, R. 2010. Roles for glutathione transferases in plant secondary metabolism. *Phytochemistry*, 71(4), 338-350.

DONG, M. A., FARRE, E. M. & THOMASHOW, M. F. 2011. Circadian clock-associated 1 and late elongated hypocotyl regulate expression of the C-repeat binding factor (CBF) pathway in *Arabidopsis*. *Proc Natl Acad Sci U S A,* 108**,** 7241-7246.

DOUKHANINA, E. V., CHEN, S., VAN DER ZALM, E., GODZIK, A., REED, J. & DICKMAN, M. B. 2006. Identification and functional characterization

of the BAG protein family in *Arabidopsis thaliana*. *J Biol Chem,* 281**,** 18793-18801.

EDWARDS, R., DIXON, D. P. & WALBOT, V. 2000. Plant glutathione S-transferases: enzymes with multiple functions in sickness and in health.*Trends in Plant Sci,* 5(5), 193-198.

FERRETTI, M., DESTRO, T., TOSATTO, S. C. E., LA ROCCA, N., RASCIO, N & MASI, A. 2009. Gamma-glutamyl transferase in the cell wall participates in extracellular glutathione salvage from the root apoplast. *New Physiologist*, 181, 115-126.

FISEROVA, J., KISELEVA, E. & GOLDBERG, M. W. 2009. Nuclear envelope and nuclear pore complex structure and organization in tobacco BY-2 cells. *Plant J,* 59, 243-255.

FOYER, C. H. & NOCTOR, G. 2005 A. Oxidant and antioxidant signalling in plants: a re-evaluation of the concept of oxidative stress in a physiological context. *Plant Cell and Environm,* 28, 1056-1071.

FOYER, C. H. & NOCTOR, G. 2005 B. - Redox homeostasis and antioxidant signaling: A metabolic interface between stress perception and physiological responses. *Plant Cell,* 17, 1866-1875.

FOYER, C. H. & NOCTOR, G. 2011. Ascorbate and glutathione: the heart of the redox hub. *Plant Physiol,* 155**,** 2-18.

FRANCIS, D. 2007. The plant cell cycle. *New Phytologist*, 174, 261-278.

GARCIA-GIMENEZ, J. L., MARKOVIC, J., DASI, F., QUEVAL, G., SCHNAUBELT, D., FOYER, C. H. & PALLARDO, F. V. 2013. Nuclear glutathione. *Biochim Biophys Acta,* 1830**,** 3304-3316.

GELHAYE, E., ROUHIER, N. & JACQUOT, J. P. 2004. The thioredoxin h system of higher plants. *Plant Physiol Biochem,* 42**,** 265-271.

GO, Y.-M. & JONES, D. P. 2010. Redox control systems in the nucleus: mechanisms and functions. *Antioxidants & Redox Signaling,* 13(4), 489-509.

GOSTI, F., BERTAUCHE, N. VARTANIAN, N. & GIRAUDAT, J. 1995. Abscisic acid-dependent and -independent regulation of gene expression by progressive drought in *Arabidopsis thaliana*. *Mol Gen Genet*, 246(1), 10-18.

GREMSKI, K., DITTA, G. & YANOFSKY, M. F. 2007. The HECATE genes regulate female reproductive tract development in *Arabidopsis thaliana*. *Development,* 134**,** 3593-3601.

GRIFFITH. O. W. & MEISTER, A. 1979. Potent and specific inhibition of glutathione synthesis by buthionine sulfoximine (S-n-butyl homocysteine sulfoximine). *J.Bio Chem*, 254, 7558-7560.

GROMES, R., HOTHORN, M., LENHERR, E. D., RYBIN, V., SHEFFZEK, K. & RAUSCH, T. 2008. The redox switch of γ-glutamylcysteine ligase via a reversible monomer-dimer transition is a mechanism unique to plants. *The Plant Journal*, 54, 1063-1075.

GRZAM, A., TENNSTEDT, P., CLEMENS, S., HELL, R. & MEYER, A. J. 2006. Vacuolar sequestration of glutathione S-conjugates outcompetes a possible degradation of the glutathione moiety by phytochelatin synthase. *FEBS Letters*, 580, 6384-6390.

GUTIERREZ, C. 2009. The *Arabidopsis* cell division cycle. *The Arabidopsis Book*, e0120.10.1199/tab.0120.

HAMAGUCHI, A., YAMASHINO, T., KOIZUMI, N., KIBA, T., KOJIMA, M., SAKAKIBARA, H. & MIZUNO, T. 2008. A Small Subfamily of Arabidopsis RADIALIS-LIKE SANT/MYB Genes: A Link to HOOKLESS1-Mediated Signal Transduction during Early Morphogenesis. *Bioscience, Biotechnology, and Biochemistry,* 72**,** 2687-2696.

HAN, Y., CHAOUCH, S., MHAMDI, A., QUEVAL, G., ZECHMANN, B. & NOCTOR, G. 2013A. Functional analysis of *Arabidopsis* mutants points to novel roles for glutathione in coupling H_2O_2 to activation of salicylic acid accumulation and signaling. *Antioxidants & Redox Signaling*, 18, 2106-2121.

HAN, Y., MHAMDI, A., CHAOUCH, S. & NOCTOR, G. 2013B. Regulation of basal and oxidative stress-triggered jasmonic acid-related gene expression by glutathione. *Plant Cell and Environment*, 36, 1135-1146.

HANSON, G. T., AGGELER, R., OGLESBEE, D., CANNON, M. CAPALDI, R. A., TSIEN, R. Y. & REMINGTON, S. J. 2004. Investigating mitochondrial redox potential with redox-sensitive green fluorescence protein indicators. Journal of Biological Chemistry, 279, 13044-13053.

HARMS, K., VAN BALLMOSS, P., BRUNOLD, C., HÖFGEN, R. & HESSE, H. 2000. Expression of a bacterial serine acetyltransferase in transgenic potato plants leads to increased levels of cysteine and glutathione. *The Plant Journal*, 22, 335-343.

HELL, R. & BERGMANN, L. 1990. γ-glutamycysteine synthetase in higher plants: catalytic properties and subcellular localization. *Planta*, 180, 603-612.

HICKS, L. M., CAHOON, R. E., BONNER, E. R., RIVARD, R. S., SHEFFIELD, J. & JEZ, J. M. 2007. Thiol-based regulation of redox-active glutamate-cysteine ligase from Arabdisopsis thaliana. *The Plant Cell*, 19, 2653-2661.

HORNIK, K. 2013. The R FAQ. http://CRAN.R-project.org/doc/FAQ/R-FAQ.html

HOTHORN, M., WACHTER, A., GROMES, R., STUWE, T., RAUSCH, T. & SCHEFFZEK, K. 2006. Structural basis for the redox control of plant glutamate cysteine ligase. *J Biol Chem*, 281, 557-565.

HOUOT, V., ETIENNE, P., PETITOT, A.-S., BARBIER, S., BLEIN, J.-P. & SUTY, L. 2001. Hydrogen peroxide induces programmed cell death features in cultured tobacco BY-2 cells in a dose dependent manner. *J Exp Bot,* 52(361), 1721-1730.

HOWDEN, R., ANDERSEN, C. R., GOLDSBROUGH, P. B. & COBBETT, C. S. 1995. A cadmium-sensitive, glutathione-deficient mutant of *Arabidopsis thaliana*. *Plant Physiol*, 107, 1067-1073.

INZE, D. & DE VEYLDER, L. 2006. Cell cycle regulation in plant development. *Annu Rev Genet,* 40**,** 77-105.

IQBAL, A., YABUTA, Y., TAKEDA, T., NAKANO, Y. & SHIGEOKA, S. 2006. Hydroperoxide reduction by thioredoxin-specific glutathione peroxidase isoenzymes of *Arabidopsis thaliana*. *FEBS J*, 273, 5589-5597.

JACKSON, R. G., LIM, E. K., LI, Y., KOWALCZYK, M., SANDBERG, G., HOGGETT, J., ASHFORD, D. A. & BOWLES, D. J. 2001. Identification and biochemical characterization of an *Arabidopsis* indole-3-acetic acid glucosyltransferase. *J Biol Chem,* 276**,** 4350-4356.

JEZ, J. M., CAHOON, R. E. & CHEN, S. 2004. *Arabidopsis thaliana* glutamate-cysteine ligase: Funcational properties, kinetic mechanisms, and regulation of activity. *Journal of Biol Chem*, 279, 33463-33470.

JOSSE, E. M., GAN, Y., BOU-TORRENT, J., STEWART, K. L., GILDAY, A. D., JEFFREE, C. E., VAISTIJ, F. E., MARTINEZ-GARCIA, J. F., NAGY, F., GRAHAM, I. A. & HALLIDAY, K. J. 2011. A DELLA in disguise: SPATULA restrains the growth of the developing *Arabidopsis* seedling. *Plant Cell,* 23**,** 1337-1351.

KATAYA, A. M. R. & REUMANN, S. 2010. *Arabidopsis* glutathione reductase 1 is dually targeted to peroxisomes and the cytosol. *Plant Signalling & Behavior*, 5, 171-175.

KESARWANI, M., YOO, J & DONG, X. 2007. Genetic interactions of TGA transcription factors in the regulation of pathogenesis-related genes and disease resistance in *Arabidopsis*. *Plant Physiol*, 144, 336-346.

KETTLES, G. J., DRUREY, C., SCHOONBEEK, H. J., MAULE, A. J. & HOGENHOUT, S. A. 2013. Resistance of *Arabidopsis thaliana* to the green peach aphid, *Myzus persicae*, involves camalexin and is regulated by microRNAs. *New Phytol,* 198**,** 1178-1190.

KIRCH, H. H., BARTELS, D., WEI, Y., SCHNABLE, P. S. & WOOD, A. J. 2004. The ALDH gene superfamily of Arabidopsis. *TRENDS in Plant Science*, 9(8), 1360-1385.

KISELEVA, E., ALLEN, T. D., RUTHERFORD, S. A., MURRAY, S., MOROZOVA, K., GARDINER, F., GOLDBERG, M. W. & DRUMMOND, S. P. 2007. A protocol for isolation and visualization of yeast nuclei by scanning electron microscopy (SEM). *Nature Protoc,* 2**,** 1943-1953.

KOMAKI, S. & SUGIMOTO, K. 2012. Control of the plant cell cycle by developmental and environmental cues. *Plant Cell Physiol*, 53(6), 953-964.

KOPRIVOVA, A., MUGFORD, S. T. & KOPRIVA, S. 2010. *Arabidopsis* root growth dependence on glutathione is linked to auxin transport. *Plant Cell Reports,* 29**,** 1157-1167.

LA CAMERA, S., L'HARIDON, F., ASTIER, J., ZANDER, M., ABOU-MANSOUR, E., PAGE, G., THUROW, C., WENDEHENNE, D., GATZ, C., METRAUX, J. P. & LAMOTTE, O. 2011. The glutaredoxin ATGRXS13 is required to facilitate *Botrytis cinerea* infection of *Arabidopsis thaliana* plants. *Plant J,* 68(3), 507-519

LAMESCH, P., BERARDINI, T. Z., LI, D., SWARBRECK, D., WILKS, C., SASIDHARAN, R., MULLER, R., DREHER, K., ALEXANDER, D. L., GARCIA-HERNANDEZ, M., KARTHIKEYAN, A. S., LEE, C. H., NELSON, W. D., PLOETZ, L., SINGH, S., WENSEL, A. & HUALA, E. 2012. The Arabidopsis Information Resource (TAIR): improved gene annotation and new tools. *Nucleic Acids Res,* 40, 1202-1210.

LAPORTE, D., OLATE, E., SALINAS, P., SALAZAR, M., JORDANA, X. & HOLUIGUE, L. 2012. Glutaredoxin GRXS13 plays a key role in protection against photooxidative stress in Arabidopsis. *J Exp Bot,* 63, 503-515.

LEE, S., MOON, J. S., KO, T. S., PETROS, D., GOLDSBROUGH, P. B. & KORBAN, S. S. 2003. Overexpression of *Arabidopsis* phytochelatin synthase paradoxically leads to hypersensitivity to cadmium stress. *Plant Physiol,* 131**,** 656-663.

LEVINE, A., TENHAKEN, R., DIXON, R. & LAMB, C. 1994. H_2O_2 from the oxidative burt orchestrates the plant hypersensitive disease resistance response. *Cell*, 79, 583-593.

LI, S., LAURI, A., ZIEMANN, M., BUSCH, A., BHAVE, M. & ZACHGO, S. 2009. Nuclear activity of ROXY1, a glutaredoxin interacting with TGA factors, is required for petal development in *Arabidopsis thaliana*. *Plant Cell*, 21, 429-441.

LI, Z., ZHANG, L., YU, Y., QUAN, R., ZHANG, Z., ZHANG, H. & HUANG, R. 2011. The ethylene response factor AtERF11 that is transcriptionally modulated by the bZIP transcription factor HY5 is a crucial repressor for ethylene biosynthesis in *Arabidopsis*. *Plant J,* 68**,** 88-99.

LIVAK, K. J. & SCHMITTGEN, T. D. 2001. Analysis of relative gene expression data using real-time quantitative PCR and the 2(-Delta Delta C(T)) Method. *Methods,* 25**,** 402-408.

MAERE, S., HEYMANS, K. & KUIPER, M. 2005. BiNGO: a Cytoscape plugin to assess overrepresentation of gene ontology categories in biological networks. *Bioinformatics,* 21**,** 3448-3449.

MARCHENT, A., KARGUL, J., MAY, S. T., MULLER, P., DELBARRE, A., PERROT-RECHENMANN, C. & BENNETT, M. J. 1999. AUX1 regulates root gravitropism in *Arabidopsis* by facilitating auxin uptake within root apical tissues. *The EMBO Journal*, 18(8), 2066-2073.

MARKOVIC, J., BORRAS, C., ORTEGA, A., SASTRE, J., VINA, J. & PALLARDO, F. V. 2007. Glutathione is recruited into the nucleus in arly phases of cell proliferation. *J Biol Chem,* 282**,** 20416-24.

MARQUEZ-GARCIA, B., NJO, M., BEECKMAN, T., GOORMACHTIG, S. & FOYER, C. H. 2013. A new role for glutathione in the regulation of root architecture linked to strigolactones. *Plant Cell and Environment*, doi:10.1111/pce.12172

MARTIN, M. N. & SLOVIN, J. P. 2000. Purified γ-glutamyl transpeptidases from tomato exhibit high affinity for glutathione and glutathione S-conjugates. *Plant Physiol*, 122, 1417-1426.

MATTSSON, J., CKURSHUMOVA, W. & BERLETH, T. 2003. Auxin signaling in Arabidopsis leaf vascular development. *Plant Physiol,* 131**,** 1327-1339.

MAUGHAN, S. C., PASTERNAK, M., CAIRNS, N., KIDDLE, G., BRACH, T., JARVIS, R., HAAS, F., NIEUWLAND, J., LIM, B., MULLER, C., SALCEDO-SORA, E., KRUSE, C., ORSEL, M., HELL, R., MILLER, A. J., BRAY, P., FOYER, C. H., MURRAY, J. A., MEYER, A. J. & COBBETT, C. S. 2010. Plant homologs of the Plasmodium falciparum chloroquine-resistance transporter, PfCRT, are required for glutathione homeostasis and stress responses. *PNAS,* 107**,** 2331-2336.

MAY, M. J. & LEAVER, C. J. 1993. Oxidative stimulation of glutathione synthesis in *Arabidopsis thaliana* suspension cultures. *Plant Phsiol*, 103, 621-627.

MAY, M. J., VERNOUX, T., LEAVER, C. VAN MONTAGU, M. & INZE, D. 1998. Glutathione homeostasis in plants: implications for environmental sensing and plant development. *J Exp Bot,* 49(321), 649-667.

MCKEOWN, P., PENDLE, A. F. & SHAW, P. J. 2008. Preparation of *Arabidopsis* nuclei and nucleoli. *Methods Mol Biol*, 463, 67-75.

MEISTER, A. 1988. Glutathione metabolism and its selective modification. *Journal of Biol Chem*, 263, 17205-17208.

MENG, L., WONG, J. H., FELDMAN, L. J., LEMAUX, P. G. & BUCHANAN, B. B. 2009. A membrane-associated thioredoxin required for plant growth moves from cell to cell, suggestive of a role in intracellular communication. *PNAS*, 107, 3900-3905

MENON, S. G., SARSOUR, E. H., SPITZ, D., R., HIGASHIKUBO, R., STURM, M., ZHANG, H. & GOSWAMI, P. C. 2003. Redox regulation of the G1 to S phase transition in the mouse embryo fibroblast cell cycle. *Cancer Res,* 63, 2109-2117.

MENON, S. G. & GOSWAMI, P. C. 2007. A redox cycle within the cell cycle: ring in the old with the new. *Oncogene,* 26**,** 1101-1109.

MEYER, A. J., BRACH, T., MARTY, L., KREYE, S., ROUHIER, N., JACQUOT, J. P. & HELL, R. 2007. Redox-sensitive GFP in *Arabidopsis thaliana* is a quantitative biosensor for the redox potential of the cellular glutathione redox buffer. *Plant J,* 52**,** 973-986.

MHAMDI, A., HAGER, J., CHAOUCH, S., QUEVAL, G., HAN, Y., TACONNAT, L., SAINDRENAN, P., GOUIA, H., ISSAKIDIS-BOURGUET, E., RENOU, J. P. & NOCTOR, G. 2010. *Arabidopsis* GLUTATHIONE REDUCTASE1 plays a crucial role in leaf responses to intracellular hydrogen peroxide and in ensuring appropriate gene expression through both salicylic acid and jasmonic acid signaling pathways. *Plant Physiol,* 153**,** 1144-1160.

MIAO, Y., LV, D., WANG, P., WANG, X. C., CHEN, J., MIAO, C. & SONG, C. P. 2006. An *Arabidopsis* glutathione peroxidase functions as both a redox transducer and a scavenger in abscisic acid and drought stress responses. *Plant Cell,* 18**,** 2749-2766.

MOLLER, I. M., JENSEN, P. E. & HANSSON, A. 2007. Oxidative modifications to cellular components in plants. *Annu Rev Plant Biol,* 58**,** 459-481.

MRAVEC, J:, SKUPA, P., BAILLY, A., HOYEROVA, K., KRECEK, P., BIELACH, A., PETRASEK, J., ZHANG, J:, GAYKOVA, V., STIERHOF, Y. D., DOBREV, P. I., SCHWARZEROVA, K., ROLCIK, J., SEIFEROVA, D., LUSCHNIG, C., BENKOVA, E., ZAZIMALOVA, E., GEISLER, M. & FRIML, J. 2009. Subcellular homeostasis of phytohormone auxin is mediated by the ER-localized PIN5 transporter. *Nature*, 459(7250), 1136-1140.

NDAMUKONG, I., ABDALLAT, A. A., THUROW, C., FODE, B., ZANDER, M., WEIGEL, R. & GATZ, C. 2007. SA-inducible *Arabidopsis* glutaredoxin interacts with TGA factors and suppresses JA-responsive PDF1.2 transcription. *Plant J,* 50**,** 128-139.

NOCTOR, G., MHAMDI, A., CHAOUCH, S., HAN, Y., NEUKERMANS, J., MARQUEZ-GARCIA, B., QUEVAL, G. & FOYER, C. H. 2012. Glutathione in plants: an integrated overview. *Plant Cell and Environment,* 35, 454-484.

NOCTOR, G., MHAMDI, A., QUEVAL, G. & FOYER, C. H. 2013. Regulating the redox gatekeeper: vacuolar sequestration puts glutathione disulfide in its place. *Plant Physiol,* 163**,** 665-671.

NOCTOR, G., QUEVAL, G., MHAMDI, A., CHAOUCH, S. & FOYER, C. H. 2011. Glutathione. *Arabidopsis Book,* 9, doi: 10.1199/tab.0142.

OHKAMA-OHTSU, N., RADWAN, S., PETERSON, A., ZHAO, P., BADR, A. F., XIANG, C. & OLIVER, D. J. 2007. Characterization of the extracellular γ-glutamyl transpeptidases, GGT1 and GGT2, in *Arabidopsis*. *Plant J*, 49, 865-877.

OHKAMA-OHTSU, N., OIKAWA, A., ZHAO, P., XIANG, C., SAITO, K. & OLIVER, D. J. 2008. A γ-glutamyl transpeptidase-idependent pathway of glutathione catabolism to glutamate via 5-oxoproline in *Arabidopsis*. *Plant Physiol*, 148, 1603-1613.

OHKAMA-OHTSU, N., SASAKI-SEKIMOTO, Y., OIKAWA, A., JIKUMARU, Y., SHINODA, S., INOUE, E., KAMIDE, Y., YOKOYAMA, T., HIRAI, M. Y., SHIRASU, K., KAMIYA, Y., OLIVER, D. J. & SAITO, K. 2011. 12-oxo-phytodienoic acid-glutathione conjugate is transported into the vacuole in *Arabidopsis*. *Plant Cell Physiol*, 52(1), 205-209.

ORLOWSKI, M. & MEISTER, A. 1973. γ-glutamyl cyclotransferase: distribution, isozymic forms, and specificity. *Journal of Biol Chem*, 248, 2836-2844.

PALLARDO, F. V., MARKOVIC, J., GARCIA, J. L. & VINA, J. 2009. Role of nuclear glutathione as a key regulator of cell proliferation. *Mol Aspects Med,* 30**,** 77-85.

PARISY, V., POINSSOT, B., OWSIANOWSKI, L., BUCHALA, A., GLAZEBROOK, J. & MAUCH, F. 2007. Identification of PAD2 as a gamma-glutamylcysteine synthetase highlights the importance of glutathione in disease resistance of *Arabidopsis*. *Plant J,* 49**,** 159-172.

PASTERNAK, M., LIM, B., WIRTZ, M., HELL, R., COBBETT, C. S. & MEYER, A. J. 2008. Restricting glutathione biosynthesis to the cytosol is sufficient for normal plant development. *Plant J,* 53**,** 999-1012.

PELLINEN, R. I., KORHONEN, M. S., TAURIAINEN, A. A., PALVA, E. T. & KANGASJARVI, J. 2002. Hydrogen peroxide activates cell death and defense gene expression in birch. *Plant Physiol,* 130**,** 549-560.

PELLNY, T. K., LOCATO, V., VIVANCOS, P. D., MARKOVIC, J., DE GARA, L., PALLARDO, F. V. & FOYER, C. H. 2009. Pyridine nucleotide cycling and control of intracellular redox state in relation to poly (ADP-ribose) polymerase activity and nuclear localization of glutathione during exponential growth of *Arabidopsis* cells in culture. *Mol Plant,* 2**,** 442-456.

POPPENBERGER, B., BERTHILLER, F., LUCYSHYN, D., SIEBERER, T., SCHUHMACHER, R., KRSKA, R., KUCHLER, K., GLOSSL, J.,

LUSCHNIG, C. & ADAM, G. 2003. Detoxification of the Fusarium mycotoxin deoxynivalenol by a UDP-glucosyltransferase from *Arabidopsis thaliana*. *J Biol Chem,* 278**,** 47905-47914.

QUEVAL, G. & FOYER, C. H. 2012. Redox regulation of photosynthetic gene-expression. *Philos Trans R Soc Lond B Biol Sci*, 367(1608), 3475-3485.

QUEVAL, G. & NOCTOR, G. 2007. A plate reader method for the measurement of NAD, NADP, glutathione, and ascorbate in tissue extracts: Application to redox profiling during Arabidopsis rosette development. *Anal Biochem,* 363**,** 58-69.

QUEVAL, G., NEUKERMANS, J., VANDERAUWERA, S., VAN BREUSEGEM, F. & NOCTOR, G. 2012. Day length is a key regulator of transcriptomic responses to both CO_2 and H_2O_2 in *Arabidopsis*. *Plant Cell and Environment*, 35, 374-387.

RAMAKERS, C., RUIJTER, J. M., DEPREZ, R. H. L. & MOORMAN, A. F. M. 2003. Assumption-free analysis of quantitative real-time polymerase chain reaction (PCR) data. *Neuroscience Letters,* 339**,** 62-66.

RASBAND, W. S. 1997-2012. ImageJ. *U.S. National Institutes of Health*, Bethesda, Maryland, USA, http://imagej.nih.gov/ij/

REDMAN, J. C., HAAS, B. J., TANIMOTO, G. & TOWN, C. D. 2004). Development and evaluation of an *Arabidopsis* whole genome Affymetrix probe array. *Plant J*, 38, 545-561.

REHRAUER, H., AQUINO, C., GRUISSEM, W., HENZ, S. R., HILSON, P., LAUBINGER, S., NAOUAR, N., PATRIGNANI, A., ROMBAUTS, S., SHU, H., VAN DE PEER, Y., VUYLSTEKE, M., WEIGEL, D., ZELLER, G. & HENNIG, L. 2010. AGRONOMICS1: a new resource for *Arabidopsis* transcriptome profiling. *Plant Physiol,* 152**,** 487-99.

REICHHELD, J. P., KHAFIF, M., RIONDET, C., DROUX, M., BONNARD, G. & MEYER, Y. 2007. Inactivation of thioredoxin reductases reveals a complex interplay between thioredoxin and glutathione pathways in *Arabidopsis* development. *Plant Cell,* 19**,** 1851-1865.

ROBERT, H. S., QUINT, A., BRAND, D., VIVIAN-SMITH, A. & OFFRINGA, R. 2009. BTB and TAZ domain scaffold proteins perform a crucial function in *Arabidopsis* development. *Plant J,* 58**,** 109-121.

ROUHIER, N., GELHAYE, E. & JACQUOT, J. P. 2002. Glutaredoxin-dependent peroxiredoxin from poplar: protein-protein interaction and catalytic mechanisms. *J Bio Cem*, 277, 13609-13614.

ROZEN, S. & SKALETSKY, H. 2000. Primer3 on the WWW for general users and for biologist programmers. *Whitehead Institute for Biomedical Research*, Cambridge, MA, USA.

SAEED, A. I., SHAROV, V., WHITE, J., LI, J., LIANG, W., BHAGABATI, N., BRAISTED, J., KLAPA, M., CURRIER, T., THIAGARAJAN, M., STURN, A., SNUFFIN, M., REZANTSEV, A., POPOV, D., RYLTSOV, A., KOSTUKOVICH, E., BORISOVSKY, I., LIU, Z., VINSAVICH, A., TRUSH, V. & QUACKENBUSH, J. 2003. TM4: a free, open-source system for microarray data management and analysis. *Biotechniques*, 34(2), 374-378

SANTNER, A., CALDERON-VILLALOBOS, L. I. & ESTELLE, M. 2009. Plant hormones are versatile chemical regulators of plant growth. *Nat Chem Biol,* 5**,** 301-307.

SATO, A. & YAMAMOTO, K. T. 2008. Overexpression of the non-canonical Aux/IAA genes causes auxin-related aberrant phenotypes in *Arabidopsis*. *Physiol Plant,* 133**,** 397-405.

SCHINDELIN, J., ARGANDA-CARRERAS, I., FRISE, E., KAYNIG, V., LONGAIR, M., PIETZSCH, T., PREIBISCH, S., RUEDEN, C., SAALFELD, S., SCHMID, B., TINEVEZ, J. Y., WHITE, D. J., HARTENSTEIN, V., ELICEIRI, K., TOMANCAK, P. & CARDONA, A. 2012. Fiji: an open-source platform for biological-image analysis. *Nature Methods,* 9**,** 676-682.

SCHLAEPPI, K., BODENHAUSEN, N., BUCHALA, A., MAUCH, F. & REYMOND, P. 2008. The glutathione-deficient mutant *pad2-1*

accumulates lower amounts of glucosinolates and is more susceptible to the insect herbivore *Spodoptera littoralis*. *Plant J,* 55**,** 774-786.

SCLEP, G., ALLEMEERSCH, J., LIECHTI, R., DE MEYER, B., BEYNON, J., BHALERO, R., MOREAU, Y., NIETFELD, W., RENOU, J. P., REYMOND, P., KUIPER, M. T. & HILSON, P. 2007. CATMA, a comprehensive genome-scale resource for silencing and transcript profiling of *Arabidopsis thaliana* genes. *BMC Bioinformatics*, 8:400.

SCHWARZLÄNDER, M., FRICKER, M. D., MÜLLER, C., MARTY, L., BRACH, T., NOVAK, J., SWEETLOVE, L. J., HELL, R. & MEYER, A. J. 2008. Confocal imaging of glutathione redox potential in living plant cells. *Journal of Microscopy*, 231(2), 299-316

SERRATO, A. J., GUILLEMINOT, J., MEYER, Y. & VIGNOLS, F. 2008. AtCXXS: atypical members of the *Arabidopsis thaliana* thioredoxin h family with a remarkably high disulfide isomerase activity. *Physiol Plant*, 133(3), 611-622.

SHIN, S., TORRES-ACOSTA, J. A., HEINEN, S. J., MCCORMICK, S., LEMMENS, M., PARIS, M. P., BERTHILLER, F., ADAM, G. & MUEHLBAUER, G. J. 2012. Transgenic *Arabidopsis thaliana* expressing a barley UDP-glycosyltransferase exhibit resistance to the mycotoxin deoxynivalenol. *J Exp Bot,* 63(13), 4731-4740

SMITH, A. P., NOURIZADEH, S. D., PEER, W. A., XU, J., BANDYOPADHYAY, A., MURPHY, A. S.& GOLDSBROUGH, P. B. 2003. Arabidopsis *AtGSTF2* is regulated by ethylene and auxin, and encodes a glutathione S-transferase that interacts with flavonoids. *Plant J*, 36, 433-442

SMITH, I. K., KENDALL, A. C., KEYS, A. J., TURNER, J. C. & LEA, P. J. 1984. Increased levels of glutathione in a catalase-deficient mutant of barley (*Hordeum vulgare* L.). *Plant Science Letters*, 36, 29-33.

SONDERBY, I. E., BUROW, M., ROWE, H. C., KLIEBENSTEIN, D. J. & HALKIER, B. A. 2010. A complex interplay of three R2R3 MYB transcription factors determines the profile of aliphatic glucosinolates in *Arabidopsis*. *Plant Physiol,* 153**,** 348-363.

SPSS Inc. Released 2007. SPSS for Windows, Version 16.0, Chicago, SPSS Inc.

STEINKAMP, R. & RENNENBERG, H. 1984. γ-glutamyltranspeptidase in tobacco suspension cultures: catalytic properties and subcellular localization. *Physiologia Plantarum*, 61, 251-256.

STEINKAMP, R. & RENNENBERG, H. 1985. Degradation of glutathione in plant cells: evidence against the participation of a γ-glutamyltranspeptidase. *Zeitschrift für Naturforschung Section C*, 40, 29-33.

STEINKAMP, R., SCHWEIHOFEN, B. & RENNENBERG, H. 1987. γ-glutamylcyclotransferase in tobacco suspension cultures: catalytic properties and subcellular localization. *Physiologia Plantarum*, 69, 499-503.

STOROZHENKO, S., BELLES-BOIX, E., BABIYCHUK, E., HEROUART, D., DAVEY, M. R., SLOOTEN, L., VAN MONTAGU, M., INZE, D. & KUSHNIR, S. 2002. γ-glutamyl transpeptidase in transgenic tobacco plants: cellular localization, processing, and biochemical properties. *Plant Physiol*, 128, 1109-1119.

STROHM, M., JOUANIN, L., KUNERT, K. J., PRUVOST, C., POLLE, A., FOYER, C. H. & RENNENBERG, H. 1995. Regulation of glutathione synthesis in leaves of transgenic poplar (Populus tremula x P. alba) overexpressing glutathione synthetase. *The Plant Journal*, 7(1), 141-145.

TARRAGO, L., LAUGIER, E., ZAFFAGNINI, M., MARCHAND, C., LE MARECHAL, P., ROUHIER, N., LEMAIRE, S. D. & REY, P. 2009. Regeneration mechanisms of *Arabidopsis thaliana* methionine sulfoxide reductases B by glutaredoxins and thioredoxins. *J Bio Chem*, 284, 18963-18971.

TEOTIA, S. & LAMB, R. S. 2011. RCD1 and SRO1 are necessary to maintain meristematic fate in *Arabidopsis thaliana*. *J Exp Bot,* 62**,** 1271-1284.

THIM, O., BLÄSING, O., GIBON, Y., NAGEL, A., MEYER, S., KRÜGER, P., SELBIG, J., MÜLLER, L. A., RHEE, S. Y. & STITT, M. 2004. MAPMAN: a user-driven tool to display genomics data sets onto diagrams of metabolic pathways and other biological processes. *Plant J,* 37, 914-939

TOGNETTI, V. B., VAN AKEN, O., MORREEL, K., VANDENBROUCKE, K., VAN DE COTTE, B., DE CLERCQ, I., CHIWOCHA, S., FENSKE, R., PRINSEN, E., BOERJAN, W., GENTY, B., STUBBS, K. A., INZE, D. & VAN BREUSEGEM, F. 2010. Perturbation of indole-3-butyric acid homeostasis by the UDP-glucosyltransferase UGT74E2 modulates *Arabidopsis* architecture and water stress tolerance. *Plant Cell,* 22**,** 2660-2679.

UNTERGASSER, A., CUTCUTACHE, I., KORESSAAR, T., YE, J., FAIRCLOTH, B. C., REMM, M. & ROZEN, S. G. 2012. Primer3--new capabilities and interfaces. *Nucleic Acids Res,* 40**,** e115.

VANDENABEELE, S., VAN DER KELEN, K., DAT, J., GADJEV, I., BOONEFAES, T., MORSA, S., ROTTIERS, P., SLOOTEN, L., VAN MONTAGU, M., ZABEAU, M., INZE, D. & VAN BREUSEGEM, F. 2003. A comprehensive analysis of hydrogen peroxide-induced gene expression in tobacco. *PNAS,* 100**,** 16113-16118.

VANDERAUWERA, S., ZIMMERMANN, P., ROMBAUTS, S., VANDENABEELE, S., LANGEBARTELS, C., GRUISSEM, W., INZE, D. & VAN BREUSEGEM, F. 2005. Genome-wide analysis of hydrogen peroxide-regulated gene expression in *Arabidopsis* reveals a high light-induced transcriptional cluster involved in anthocyanin biosynthesis. *Plant Physiol*, 139, 806-821.

VAN DER KOP, D. A., SCHUYER, M., SCHERES, B., VAN DER ZAAL, B. J. & HOOYKAAS, P. J. 1996. Isolation and characterization of an auxin-inducible glutathione S-transferase gene of *Arabidopsis thaliana. Plant Mol Biol*, 30(4), 839-844

VERNOUX, T., WILSON, R. C., SEELEY, K. A., REICHHELD, J. P., MUROY, S., BROWN, S., MAUGHAN, S. C., COBBETT, C. S., VAN MONTAGU, M., INZE, D., MAY, M. J. & SUNG, Z. R. 2000A. The *ROOT MERISTEMLESS1*/*CADMIUM SENSITIVE2* gene defines a glutathione-dependent pathway involved in initiation and maintenance of cell division during postembryonic root development. *The Plant Cell,* 12, 97-109

VERNOUX, T., KRONENBERGER, J., GRADJEAN, G., LAUFS, P. & TRAAS, J. 2000B. PIN-FORMED 1 regulates cell fate at the periphery of the shoot apical meristem. *Development*, 127, 5157-5165.

VERSLUES, P. E. & SHARMA, S. 2010. Proline metabolism and its implications for plant-environment interaction. *Arabidopsis Book*, 8, doi: 10.1199/tab.0140.

VIVANCOS, P. D., DONG, Y., ZIEGLER, K., MARKOVIC, J., PALLARDO, F. V., PELLNY, T. K., VERRIER, P. J. & FOYER, C. H. 2010. Recruitment of glutathione into the nucleus during cell proliferation adjusts whole-cell redox homeostasis in *Arabidopsis thaliana* and lowers the oxidative defence shield. *Plant J,* 64**,** 825-838.

VOEHRINGER, D. W., MCCONKEY, D. J., MCDONNELL, T. J., BRISBAY, S. & MEYN, R. E. 1998. Bcl-2 expression causes redistribution of glutathione to the nucleus. *PNAS*, 95, 2956-2960

WANG, W., VINOCUR, B., SHOSEYOV, O. & ALTMAN, A. 2004. Role of plant heat-shock proteins and molecular chaperones in the abiotic stress response. *Trends Plant Sci,* 9**,** 244-252.

WILLEKENS, H., CHAMNONGPOL, S., DAVEY, M., SCHRAUDNER, M., LANGE-BARTELS, C., VAN MONTAGU, M., INZE, D. & VAN CAMP, W. 1997. Catalase is a sink for H_2O_2 and is indispensable for stress defense in C_3 plants. *EMBO J*, 16, 4806-4816.

WOLF, A. E., DIETZ, K. J. & SCHROEDER, P. 1996. Degradation of glutathione S-conjugates by carboxypeptidase in the plant vacuole. *FEBS Letters*, 384, 31-34.

XIANG, C. & OLIVER, D. J. 1998. Glutathione metabolic genes coordinately respond to heavy metals and jasmonic acid in *Arabidopsis*. *Plant Cell*, 10, 1539-1550.

YOON, G. M. & KIEBER, J. J. 2013. ACC synthase and its cognate E3 ligase are inversely regulated by light. *Plant Signal Behav*, 8(12).

YU, X., PASTERNAK, T., EIBLMEIER, M., DITENGOU, F., KOCHERSPERGER, P., SUN, J., WANG, H., RENNEBERG, H., TAELE, W., PAPONOV, I., ZHOU, W., LI, C., LI, X. & PALME, K. 2013. Plastid-localized glutathione reductase2-regulated glutathione redox status is essential for Arabidopsis root apical meristem maintenance. *The Plant Cell*, 25, 4451-4468.

ZECHMANN, B., MAUCH, F., STICHER, L. & MULLER, M. 2008. Subcellular immunocytochemical analysis detects the highest concentrations of glutathione in mitochondria and not in plastids. *J Exp Bot,* 59**,** 4017-4027.

ZIEMANN, M., BHAVE, M. & ZACHGO, S. 2009. Origin and diversification of land plant CC-type glutaredoxins. *Genome Biol Evol*, 2009, 265-277.

ZIMMERMANN, A. K., LOUCKS, F. A., SCHROEDER, E. K., BOUCHARD, R. J., TYLER, K. L & LINSEMAN, D. A. 2007. Glutathione binding to the

Bcl-2 Homology-3 domain grove: A molecular basis for Bcl-2 antioxidant function at mitochondria. *J Bio Chem*, 282(40), 29269-29304

ZHANG, C. J., ZHAO, B. C., GE, W. N., ZHANG, Y. F., SONG, Y., SUN, D. Y. & GUO, Y. 2011. An apoplastic h-type thioredoxin is involved in the stress response through regulation of the apoplastic reactive oxygen species in rice. *Plant Physiol,* 157**,** 1884-1899.

ZHAO, Y. 2010. Auxin biosynthesis and its role in plant development. *Annu Rev Plant Biol,* 61**,** 49-64.

Appendices

Appendix I: Composition of growth medium I:

1x Murashige & Skoog (MS) medium

Component	Amount per Litre
MS basal salts	4.40 g
Sucrose	30 g
Agar-Agar (A/1080/53, Fisher Scientific)	10 g
pH not adjusted	

Appendix II: Composition of growth medium II:

0.5x Murashige & Skoog (MS) medium

Component	Amount per Litre
MS basal salts without vitamins	2.15 g
Glucose	12 g
B5 vitamins	0.112 g
Agar-Agar	7 g
pH adjusted with 1 M KOH to pH=5.80	

Appendix III: Composition of growth medium III
(modified PANG2 medium)

Component	**Amount per Litre**
$CaCl_2$	150 µM
NaH_2PO_4	100 µM
$MgSO_4$	20 µM
KNO_3	1000 µM
KI	1.80 µM
H_3BO_3	20 µM
$ZnSO_4$	3 µM
$CuSO_4$	0.06 µM
$NaMoO_4$	0.40 µM
$CoCl_2$	4 µM
Ferrous sulphate chelate solution (Sigma Aldrich)	0.04 % (v/v)
MES	0.05 % (w/v)
Sucrose	0.50 % (w/v)
Agar-Agar	1.00 % (w/v)
pH adjusted with 1 M KOH to pH=5.80	

Appendix IV: Composition of growth medium IV:

0.5x Murashige & Skoog (MS) medium

Component	Amount per Litre
MS basal salts	2.15 g
Sucrose	10 g
MES	0.50 g
Myo-Inositol	0.10 g
Agar-Agar	10 g
pH adjusted with 1 M KOH to pH=5.70	

Appendix V: Composition of the mNPB buffer for isolation of nuclei

Component	Concentration
MOPS (pH=7)	20 mM
NaCl	40 mM
KCl	90 mM
EDTA	2 mM
EGTA	0.5 mM
Spermidine	0.5 mM
Spermine	0.2 mM
Complete protease inhibitors	1 x
Mannitol	0.3 mM
Prepare freshly on the day of use, filter sterilized and cooled down to 4°C prior to use.	

Appendix VI: Overview of selected transcripts that are presented in Chapter 5 "Transcriptomic analyses glutathione depletion".
Transcripts are displayed sorted by AGI code together with their primary gene name (where available inside the description), a general description, annotation, as well as fold-changes in expression level in shoots and roots, relative to the wild-type. The full microarray data can be found at NCBI GEO as Series GSE36893 (http://www.ncbi.nlm.nih.gov/geo/query/acc.cgi?acc=GSE36893).

AGI	Description	Annotated as:	fold-change	
			Shoot	Root
AT1G01480	1-AMINO-CYCLOPROPANE-1-CARBOXYLATE SYNTHASE 2 (ACS2)	Ethylene-related	0.01	2.82
AT1G01720	MEMBER OF LARGE FAMILY OF PUTATIVE TRANSCRIPTIONAL ACTIVATORS WITH NAC DOMAIN	ABA-related	1.87	0.85
AT1G02930	GSTF6/ERD11	Redox-related	3.07	5.11
AT1G02940	GSTF5	Redox-related	2.06	0.60
AT1G03020	TRX FAMILY	Redox-related	-1.47	0.07
AT1G03400	ENCODES A PROTEIN WITH SEQUENCE SIMILARITY TO TOMATO E8 (ACC OXIDASE)	Ethylene-related	-1.66	-0.33
AT1G03850	GRXS13	Redox-related	-2.43	-1.27
AT1G05560	UDP-GLUCOSYLTRANSFERASE 75B1 (UGT75B1)	ABA-related	2.14	0.09
AT1G05680	UDP-GLYCOSYLTRANSFERASE 74E2 (UGT74E2)	Auxin-related	3.77	3.77
AT1G05680	URIDINE DIPHOSPHATE GLYCOSYLTRANSFERASE 74E2 (UGT74E2)	Auxin-related	3.77	3.77
AT1G07370	PCNA1 (PROLIFERATING CELLULAR NUCLEAR ANTIGEN)	Cell cycle-related	-0.41	-1.35
AT1G07400	HSP20-LIKE CHAPERONES SUPERFAMILY PROTEIN	Stress-related	0.05	3.69
AT1G08560	SYP111 (SYNTAXIN OF PLANTS 111); SNAP RECEPTOR	Cell cycle-related	-0.15	-2.17
AT1G10370	GSTU17/ERD9	Redox-related	-1.22	0.84
AT1G13300	HRS1; MYB FAMILY TRANSCRIPTION FACTOR	Transcription factor	-0.79	-3.12
AT1G17170	GSTU24	Redox-related	4.55	1.88
AT1G17180	GSTU25	Redox-related	3.94	1.79
AT1G18100	ENCODES A MEMBER OF THE FT AND TFL1 FAMILY OF PE-BINDING PROTEINS	ABA-related	1.05	3.76
AT1G18330	EARLY-PHYTOCHROME-RESPONSIVE1 (EPR1)	Ethylene-related	-0.78	-1.66
AT1G19570	DHAR1	Redox-related	1.22	-0.73
AT1G19850	INDOLE-3-ACETIC ACID INDUCIBLE 24 (IAA24)	Auxin-related	0.13	2.47
AT1G20440	COLD-REGULATED 47 (COR47)	Stress-related	-2.11	-2.27
AT1G20440	BELONGS TO THE DEHYDRIN PROTEIN FAMILY	ABA-related	-2.11	-2.27
AT1G20440	COLD-REGULATED 47 (COR47)	ABA-related	-2.11	-2.27
AT1G20450	LOW TEMPERATURE INDUCED 29 (LTI29)	ABA-related	-0.54	-1.99
AT1G20930	CDKB2;2 (CYCLIN-DEPENDENT KINASE B2;2)	Cell cycle	-0.11	-1.43

AGI	Description	Annotated as:	fold-change	
			Shoot	Root
AT1G23550	SRO2 (SIMILAR TO RCD ONE 2)	DNA repair	-0.28	2.42
AT1G25560	ENCODES A MEMBER OF THE RAV TRANSCRIPTION FACTOR FAMILY	Ethylene-related	1.24	0.82
AT1G26100	CYTOCHROME B561/FERRIC REDUCTASE TRANSMEMBRANE PROTEIN FAMILY	Ethylene-related	-0.11	-2.00
AT1G27730	RELATED TO CYS2/HIS2-TYPE ZINC-FINGER PROTEINS FOUND IN HIGHER PLANTS	ABA-related	1.72	1.99
AT1G28370	ENCODES A MEMBER OF THE B-1 SUBFAMILY OF ERF/AP2 TRANSCRIPTION FACTOR FAMILY (ERF11)	Ethylene-related	1.84	0.25
AT1G29420	SAUR-LIKE AUXIN-RESPONSIVE PROTEIN FAMILY	Auxin-related	-1.47	-0.08
AT1G29490	SAUR-LIKE AUXIN-RESPONSIVE PROTEIN FAMILY	Auxin-related	-1.51	-0.55
AT1G32230	RCD1 (RADICAL-INDUCED CELL DEATH1); PROTEIN BINDING	DNA repair	0.44	0.93
AT1G43910	P-LOOP CONTAINING NUCLEOSIDE TRIPHOSPHATE HYDROLASES SUPERFAMILY PROTEIN	ABA-related	3.94	3.03
AT1G43910	P-LOOP CONTAINING NUCLEOSIDE TRIPHOSPHATE HYDROLASES SUPERFAMILY PROTEIN	ABA-related	3.94	3.03
AT1G44110	CYCA1;1 (CYCLIN A1;1); CYCLIN-DEPENDENT PROTEIN KINASE REGULATOR	Cell cycle	0.27	-1.51
AT1G47510	INOSITOL POLYPHOSPHATE 5-PHOSPHATASE 11 (5PTASE11)	Auxin-related	-0.02	3.46
AT1G48660	AUXIN-RESPONSIVE GH3 FAMILY PROTEIN	Auxin-related	3.48	3.23
AT1G48660	AUXIN-RESPONSIVE GH3 FAMILY PROTEIN	Auxin-related	3.48	3.23
AT1G48690	AUXIN-RESPONSIVE GH3 FAMILY PROTEIN	Auxin-related	-0.53	-2.43
AT1G49820	ENCODES 5-METHYLTHIORIBOSE KINASE, INVOLVED IN METHIONINE CYCLE	Ethylene-related	1.09	-0.05
AT1G49860	GSTF14	Redox-related	-2.64	-1.71
AT1G53540	HSP20-LIKE CHAPERONES SUPERFAMILY PROTEIN	Stress-related	-0.22	3.80
AT1G54100	ALDEHYDE DEHYDROGENASE	ABA-related	2.08	1.38
AT1G55210	DISEASE RESISTANCE-RESPONSIVE (DIRIGENT-LIKE PROTEIN) FAMILY PROTEIN	Stress-related	1.91	0.65
AT1G56650	MYB DOMAIN PROTEIN 75 (MYB75)	Auxin-related	4.84	2.80
AT1G56650	MYB DOMAIN PROTEIN 75 (MYB75)	Auxin-related	4.84	2.80
AT1G56650	PRODUCTION OF ANTHOCYANIN PIGMENT 1 (MYB75; PAP1)	Transcription factor	4.84	2.80
AT1G59700	GSTU16	Redox-related	1.02	1.27
AT1G59730	TH7	Redox-related	2.52	-0.71
AT1G62380	ACC OXIDASE 2 (ACO2)	Ethylene-related	0.86	2.62
AT1G62975	BASIC HELIX-LOOP-HELIX (BHLH) FAMILY PROTEIN (BHLH125)	Transcription factor	0.34	-3.33
AT1G64160	DIRIGENT PROTEIN 5 (DIR5)	Stress-related	-0.28	3.39
AT1G65870	DISEASE RESISTANCE-RESPONSIVE (DIRIGENT-LIKE PROTEIN) FAMILY PROTEIN	Stress-related	-3.02	-0.27
AT1G66100	PREDICTED TO ENCODE A PR (PATHOGENESIS-RELATED) PROTEIN	Stress-related	-5.40	-0.68
AT1G66230	MYB DOMAIN PROTEIN 20 (MYB20)	Transcription factor	-2.50	-0.95
AT1G66390	PRODUCTION OF ANTHOCYANIN PIGMENT 2 (MYB90; PAP2)	Transcription factor	3.69	3.17
AT1G66390	PRODUCTION OF ANTHOCYANIN PIGMENT 2 (MYB90; PAP2)	Transcription factor	3.69	3.17
AT1G68765	INFLORESCENCE DEFICIENT IN ABSCISSION (IDA)	Ethylene-related	-0.03	2.01

AGI	Description	Annotated as:	fold-change	
			Shoot	Root
AT1G69880	TH8	Redox-related	5.49	5.25
AT1G70440	SRO3 (SIMILAR TO RCD ONE 3); NAD+ ADP-RIBOSYLTRANSFERASE	DNA repair	1.00	4.21
AT1G71030	ENCODES A PUTATIVE MYB FAMILY TRANSCRIPTION FACTOR	ABA-related	-1.64	-0.50
AT1G72070	CHAPERONE DNAJ-DOMAIN SUPERFAMILY PROTEIN	Stress-related	2.18	0.67
AT1G72430	SAUR-LIKE AUXIN-RESPONSIVE PROTEIN FAMILY	Auxin-related	-1.40	-1.27
AT1G72900	TOLL-INTERLEUKIN-RESISTANCE (TIR) DOMAIN-CONTAINING PROTEIN	Stress-related	2.31	2.55
AT1G72920	TOLL-INTERLEUKIN-RESISTANCE (TIR) DOMAIN FAMILY PROTEIN	Stress-related	2.25	1.88
AT1G73330	DROUGHT-REPRESSED 4 (DR4)	Stress-related	-1.60	-4.41
AT1G73330	DROUGHT-REPRESSED 4 (DR4)	Stress-related	-1.60	-4.41
AT1G73330	ENCODES A PLANT-SPECIFIC PROTEASE INHIBITOR-LIKE PROTEIN; DISAPPEARS IN RESPONSE TO DROUGHT	ABA-related	-1.60	-4.41
AT1G73330	DROUGHT-REPRESSED 4 (DR4)	ABA-related	-1.60	-4.41
AT1G73500	MEMBER OF MAP-KINASE KINASE FAMILY	Ethylene-related	1.33	0.00
AT1G73870	ZINC FINGER (B-BOX TYPE) FAMILY PROTEIN	Transcription factor	-2.06	-0.25
AT1G74500	BHLH FAMILY PROTEIN	Cell cycle-related	0.00	-2.31
AT1G75250	ARABIDOPSIS RAD-LIKE 6 (RSM3; ATRL6)	Transcription factor	-2.45	-0.06
AT1G75270	DHAR2	Redox-related	1.10	0.33
AT1G75580	SAUR-LIKE AUXIN-RESPONSIVE PROTEIN FAMILY	Auxin-related	2.14	0.26
AT1G75750	GA-RESPONSIVE GAST1 PROTEIN HOMOLOG	ABA-related	-3.02	-0.87
AT1G75830	LOW-MOLECULAR-WEIGHT CYSTEINE-RICH 67 (LCR67)	Stress-related	0.40	3.62
AT1G76310	CYCB2;4 (CYCLIN B2;4); CYCLIN-DEPENDENT PROTEIN KINASE REGULATOR	Cell cycle	-0.08	-1.12
AT1G76540	CDKB2;1 (CYCLIN-DEPENDENT KINASE B2;1); CYCLIN-DEPENDENT PROTEIN KINASE	Cell cycle	0.18	-2.04
AT1G76760	TY1	Redox-related	1.03	-0.42
AT1G76800	ENCODES NODULIN-LIKE2; REPRESSED UNDER CONDITIONS OF FE-DEFICIENT GROWTH	Ethylene-related	0.08	-2.57
AT1G78370	GSTU20	Redox-related	-1.54	-2.61
AT2G01520	MLP-LIKE PROTEIN 328 (MLP328)	Stress-related	-2.34	-5.95
AT2G01530	MLP-LIKE PROTEIN 329 (MLP329)	Stress-related	-2.15	-3.81
AT2G01530	MLP-LIKE PROTEIN 329 (MLP329)	Stress-related	-2.15	-3.81
AT2G02130	LOW-MOLECULAR-WEIGHT CYSTEINE-RICH 68 (LCR68)	Stress-related	-0.25	-2.98
AT2G02390	GSTZ1	Redox-related	1.90	0.79
AT2G05520	GLYCINE-RICH PROTEIN 3 (GRP-3)	ABA-related	0.34	2.93
AT2G05710	ENCODES AN ACONITASE	ABA-related	1.84	1.42
AT2G15970	COLD REGULATED 413 PLASMA MEMBRANE 1 (COR413-PM1)	ABA-related	-0.48	-2.06
AT2G16850	PLASMA MEMBRANE INTRINSIC PROTEIN 3B (PIP2;8)	ABA-related	-0.13	-1.91
AT2G17620	CYCB2;1 (CYCLIN B2;1); CYCLIN-DEPENDENT PROTEIN KINASE REGULATOR	Cell cycle	0.10	-1.14

AGI	Description	Annotated as:	fold-change	
			Shoot	Root
AT2G21210	PUTATIVE AUXIN-REGULATED PROTEIN; DOWN-REGULATED IN RESPONSE TO CHITIN OLIGOMERS	Auxin-related	-2.18	-2.40
AT2G21650	MATERNAL EFFECT EMBRYO ARREST 3 (RSM1; MEE3)	Transcription factor	-2.18	-1.99
AT2G22330	CYTOCHROME P450, FAMILY 79, SUBFAMILY B, POLYPEPTIDE 3 (CYP79B3)	Auxin-related	-0.07	-3.04
AT2G25080	GPX1	Redox-related	-1.27	0.59
AT2G25880	ATAUR2 (ATAURORA2); HISTONE KINASE(H3-S10 SPECIFIC) / KINASE	Cell cycle-related	-0.36	-1.90
AT2G26760	CYCB1;4 (CYCLIN B1;4); CYCLIN-DEPENDENT PROTEIN KINASE REGULATOR	Cell cycle	0.10	-2.08
AT2G27970	CKS2 (CDK-SUBUNIT 2); CYCLIN-DEPENDENT PROTEIN KINASE / REGULATOR	Cell cycle-related	0.36	-1.48
AT2G28700	AGAMOUS-LIKE 46 (AGL46)	Transcription factor	-0.03	2.90
AT2G29420	GSTU7	Redox-related	1.85	0.08
AT2G29440	GSTU6	Redox-related	1.83	-0.39
AT2G29460	GSTU4	Redox-related	3.20	3.95
AT2G29490	GSTU1	Redox-related	2.53	0.69
AT2G29500	HSP20-LIKE CHAPERONES SUPERFAMILY PROTEIN	Stress-related	0.88	3.26
AT2G31320	PARP1 (POLY(ADP-RIBOSE) POLYMERASE 1)	DNA repair	-0.09	0.28
AT2G32020	ACYL-COA N-ACYLTRANSFERASES (NAT) SUPERFAMILY PROTEIN	ABA-related	1.64	2.88
AT2G32020	ACYL-COA N-ACYLTRANSFERASES (NAT) SUPERFAMILY PROTEIN	ABA-related	1.64	2.88
AT2G32550	RCD1-LIKE CELL DIFFERENTIATION FAMILY PROTEIN	Transcription factor	-1.99	-1.09
AT2G33150	ENCODES ORGANELLAR 3-KETOACYL-COA THIOLASE, INVOLVED IN GERMINATION AND SEEDLING GROWTH	ABA-related	1.82	1.66
AT2G33560	BUB1-RELATED (BUDDING UNINHIBITED BY BEZYMIDAZOL1); SPINDLE CHECKPOINT PROTEIN-RELATED	Cell cycle	-0.41	-1.32
AT2G35510	SRO1 (SIMILAR TO RCD ONE 1); NAD+ ADP-RIBOSYLTRANSFERASE	DNA repair	0.10	0.27
AT2G36800	DON-GLUCOYLTRANSFERASE 1 (DOGT1)	Stress-related	1.79	6.38
AT2G36800	DON-GLUCOSYLTRANSFERASE 1 (DOGT1)	Stress-related	1.79	6.38
AT2G37170	PLASMA MEMBRANE INTRINSIC PROTEIN 2 (PIP2;2)	ABA-related	-0.35	-1.98
AT2G38340	AP2 DOMAIN-CONTAINING TRANSCRIPTION FACTOR, PUTATIVE (DRE2B)	Transcription factor	0.80	5.01
AT2G38620	CDKB1;2 (CYCLIN-DEPENDENT KINASE B1;2); CYCLIN BINDING	Cell cycle	0.03	-1.06
AT2G38750	ANNEXIN 4 (ANNAT4)	ABA-related	0.09	-2.01
AT2G40750	WRKY54	Transcription factor	0.04	-3.38
AT2G43510	TRYPSIN INHIBITOR PROTEIN 1 (TI1)	Stress-related	1.03	4.54
AT2G43550	ENCODES A DEFENSIN-LIKE (DEFL) FAMILY PROTEIN	Stress-related	-2.49	-2.30
AT2G43590	CHITINASE FAMILY PROTEIN	Stress-related	1.77	2.93
AT2G44740	CYCP4;1 (CYCLIN P4;1); CYCLIN-DEPENDENT PROTEIN KINASE	Cell cycle	-0.15	-2.06
AT2G44940	AP2 DOMAIN-CONTAINING TRANSCRIPTION FACTOR TINY, PUTATIVE	Transcription factor	-0.04	-3.06
AT2G46990	INDOLE-3-ACETIC ACID INDUCIBLE 20 (IAA20)	Auxin-related	2.96	0.26
AT2G46990	INDOLE-3-ACETIC ACID INDUCIBLE 20 (IAA20)	Transcription factor	2.96	0.26

AGI	Description	Annotated as:	fold-change	
			Shoot	Root
AT2G47000	ARABIDOPSIS P-GLYCOPROTEIN 4	Auxin-related	2.73	1.81
AT2G47520	AP2 DOMAIN-CONTAINING TRANSCRIPTION FACTOR, PUTATIVE; HRE2	Transcription factor	0.88	3.84
AT3G01600	ARABIDOPSIS NAC DOMAIN CONTAINING PROTEIN 44 (ANAC044)	Transcription factor	1.51	3.26
AT3G01970	WRKY45	Transcription factor	0.61	2.98
AT3G02850	STELAR K+ OUTWARD RECTIFIER (SKOR)	ABA-related	0.10	-2.09
AT3G03190	GSTF11	Redox-related	-2.12	-2.69
AT3G09270	GSTU8	Redox-related	1.03	-0.60
AT3G11520	CYCB1;3 (CYCLIN B1;3); CYCLIN-DEPENDENT PROTEIN KINASE REGULATOR	Cell cycle	-0.07	-1.31
AT3G12900	2-OXOGLUTARATE (2OG) AND FE(II)-DEPENDENT OXYGENASE SUPERFAMILY PROTEIN	Ethylene-related	-0.08	-2.40
AT3G21460	GRX FAMILY	Redox-related	-1.03	-0.06
AT3G22060	CONTAINS PFAM PROFILE: PF01657 DOMAIN OF UNKNOWN FUNCTION	ABA-related	-2.10	-0.68
AT3G23250	MYB DOMAIN PROTEIN 15 (MYB15)	Auxin-related	-0.25	3.33
AT3G23250	MYB DOMAIN PROTEIN 15 (MYB15)	Transcription factor	-0.25	3.33
AT3G25190	ENCODES NODULIN-LIKE21; REPRESSED UNDER CONDITIONS OF FE-DEFICIENT GROWTH.	Ethylene-related	-1.65	-4.53
AT3G25190	ENCODES NODULIN-LIKE21; REPRESSED UNDER CONDITIONS OF FE-DEFICIENT GROWTH	Ethylene-related	-1.65	-4.53
AT3G25980	MITOTIC ARREST DEFICIENT 2 (MAD2); MITOTIC SPINDLE CHECKPOINT PROTEIN, PUTATIVE	Cell cycle-related	0.15	-2.16
AT3G26460	POLYKETIDE CYCLASE/DEHYDRASE AND LIPID TRANSPORT SUPERFAMILY PROTEIN	Stress-related	0.71	-4.66
AT3G26830	PHYTOALEXIN DEFICIENT 3 (PAD3)	ABA-related	0.99	3.02
AT3G28580	P-LOOP CONTAINING NUCLEOSIDE TRIPHOSPHATE HYDROLASES SUPERFAMILY PROTEIN	ABA-related	1.42	4.10
AT3G44300	NITRILASE 2 (NIT2)	Auxin-related	3.69	3.16
AT3G44300	NITRILASE 2 (NIT2)	Auxin-related	3.69	3.16
AT3G46130	MYB DOMAIN PROTEIN 111 (MYB111)	Transcription factor	-2.38	-2.76
AT3G47620	ENCODES A TRANSCRIPTION FACTOR ATTCP14 THAT REGULATES SEED GERMINATION	ABA-related	-1.02	-1.33
AT3G47720	SRO4 (SIMILAR TO RCD ONE 4); NAD+ ADP-RIBOSYLTRANSFERASE	DNA repair	-0.17	-0.14
AT3G48360	BTB AND TAZ DOMAIN PROTEIN 2 (BT2)	Auxin-related	-1.84	-0.99
AT3G48920	MYB DOMAIN PROTEIN 45 (MYB45)	Transcription factor	1.89	2.40
AT3G48940	REMORIN FAMILY PROTEIN	Transcription factor	-0.33	-3.36
AT3G49760	ARABIDOPSIS THALIANA BASIC LEUCINE-ZIPPER 5 (ATBZIP5)	Transcription factor	-0.12	-3.35
AT3G50330	HECATE 2 (HEC2)	Transcription factor	2.69	0.11
AT3G50460	HOMOLOG OF RPW8 2 (HR2)	Stress-related	-0.32	-3.03
AT3G53250	SAUR-LIKE AUXIN-RESPONSIVE PROTEIN FAMILY	Auxin-related	1.79	-0.06
AT3G56970	BHLH038	Transcription factor	0.31	-3.03
AT3G57860	UVI4-LIKE (UV-B-INSENSITIVE 4-LIKE)	Cell cycle	0.06	-1.04
AT3G59060	PHYTOCHROME INTERACTING FACTOR 3-LIKE 6 (PIL6)	Ethylene-related	-0.15	1.60

AGI	Description	Annotated as:	fold-change	
			Shoot	Root
AT3G60550	CYCP3;2 (CYCLIN P3;2); CYCLIN-DEPENDENT PROTEIN KINASE	Cell cycle	-0.10	-1.44
AT3G61400	1-AMINOCYCLOPROPANE-1-CARBOXYLATE OXIDASE-LIKE PROTEIN	Ethylene-related	-0.14	-1.76
AT3G62930	TRX FAMILY	Redox-related	-2.21	-0.91
AT3G62950	TRX FAMILY	Redox-related	-3.40	-0.04
AT4G00670	DNA BINDING	Transcription factor	0.06	-3.52
AT4G02060	PRL (PROLIFERA); DNA REPLICATION INITIATION	Cell cycle-related	-0.46	-1.13
AT4G02390	PARP2 (POLY(ADP-RIBOSE) POLYMERASE 2)	DNA repair	1.36	1.49
AT4G04840	METHIONINE SULFOXIDE REDUCTASE DOMAIN-CONTAINING PROTEIN	Transcription factor	-1.02	-4.13
AT4G06746	RELATED TO AP2.9 (RAP2.9)	Transcription factor	-0.38	3.87
AT4G07820	CYSTEINE-RICH SECRETORY PROTEINS, AND PATHOGENESIS-RELATED 1 SUPERFAMILY PROTEIN	Stress-related	-2.07	-1.72
AT4G09820	TRANSPARENT TESTA 8 (TT8)	Transcription factor	2.44	0.48
AT4G11210	DISEASE RESISTANCE-RESPONSIVE (DIRIGENT-LIKE PROTEIN) FAMILY PROTEIN	Stress-related	-0.37	-4.78
AT4G11600	GPX6	Redox-related	1.07	0.49
AT4G12480	EARLY ARABIDOPSIS ALUMINUM INDUCED 1 (EARLI1)	ABA-related	0.71	2.78
AT4G12550	AUXIN-INDUCED IN ROOT CULTURES 1 (AIR1)	Auxin-related	0.23	-4.29
AT4G14630	GERMIN-LIKE PROTEIN 9 (GLP9)	Stress-related	-1.94	-2.81
AT4G15690	TRX FAMILY	Redox-related	-2.05	-0.74
AT4G15700	TRX FAMILY	Redox-related	-2.18	0.50
AT4G15910	DROUGHT-INDUCED 21 (DI21)	Stress-related	1.84	1.05
AT4G15910	ENCODES A GENE WHOSE TRANSCRIPT LEVEL IN ROOT AND LEAVES INCREASES DURING DROUGHT STRESS	ABA-related	1.84	1.05
AT4G18170	WRKY28; TRANSCRIPTION FACTOR	Transcription factor	-0.12	3.30
AT4G19690	IRON-REGULATED TRANSPORTER 1 (IRT1)	Auxin-related	-0.81	-2.86
AT4G19880	GST FAMILY	Redox-related	1.34	0.20
AT4G22200	ENCODES AKT2, A PHOTOSYNTHATE- AND LIGHT-DEPENDENT POTASSIUM CHANNEL	ABA-related	-1.19	-0.05
AT4G22212	ENCODES A DEFENSIN-LIKE (DEFL) FAMILY PROTEIN	Stress-related	-1.82	-3.97
AT4G22212	ENCODES A DEFENSIN-LIKE (DEFL) FAMILY PROTEIN	Stress-related	-1.82	-3.97
AT4G22214	ENCODES A DEFENSIN-LIKE (DEFL) FAMILY PROTEIN	Stress-related	-0.21	-3.08
AT4G23100	GSH1 (GLUTAMATE-CYSTEINE LIGASE)	Glutathione synth.	0.54	0.83
AT4G23680	POLYKETIDE CYCLASE/DEHYDRASE AND LIPID TRANSPORT SUPERFAMILY PROTEIN	Stress-related	3.14	2.15
AT4G24180	THAUMATIN-LIKE PROTEIN 1 (TLP1)	Ethylene-related	-0.43	-1.80
AT4G24670	TRYPTOPHAN AMINOTRANSFERASE RELATED 2 (TAR2)	Auxin-related	-0.61	-2.80
AT4G26200	1-AMINO-CYCLOPROPANE-1-CARBOXYLATE SYNTHASE 7 (ACS7)	Ethylene-related	-0.20	4.03
AT4G31320	SAUR-LIKE AUXIN-RESPONSIVE PROTEIN FAMILY	Auxin-related	-0.40	-2.50
AT4G31870	GPX7	Redox-related	-1.32	-0.06

AGI	Description	Annotated as:	fold-change	
			Shoot	Root
AT4G32810	CAROTENOID CLEAVAGE DIOXYGENASE 8 (CCD8)	Auxin-related	-0.13	2.58
AT4G32830	ATAUR1 (ATAURORA1); HISTONE KINASE (H3-S10 SPECIFIC)	Cell cycle-related	-0.13	-1.73
AT4G33040	TRX FAMILY	Redox-related	2.27	2.35
AT4G34160	CYCD3;1 (CYCLIN D3;1); CYCLIN-DEPENDENT PROTEIN KINASE REGULATOR	Cell cycle	0.15	-1.03
AT4G34760	SAUR-LIKE AUXIN-RESPONSIVE PROTEIN FAMILY	Auxin-related	-1.68	-2.19
AT4G35100	PLASMA MEMBRANE INTRINSIC PROTEIN 3A (PIP3A)	ABA-related	-0.21	-2.05
AT4G35620	CYCB2;2 (CYCLIN B2;2); CYCLIN-DEPENDENT PROTEIN KINASE REGULATOR	Cell cycle	-0.09	-1.43
AT4G36570	ARABIDOPSIS RAD-LIKE 3 (ATRL3)	Transcription factor	-2.41	-1.36
AT4G36930	SPATULA (SPT)	Transcription factor	2.50	1.51
AT4G37540	LOB DOMAIN-CONTAINING PROTEIN 39 (LBD39)	Transcription factor	-2.33	-2.18
AT4G37610	BTB AND TAZ DOMAIN PROTEIN 5 (BT5)	Auxin-related	-3.82	-2.18
AT5G04470	SIM (SIAMESE); CYCLIN-DEPENDENT PROTEIN KINASE INHIBITOR	Cell cycle-related	1.26	0.06
AT5G04950	ENCODES A NICOTIANAMIDE SYNTHASE	Ethylene-related	-1.82	-1.55
AT5G06150	CYC1BAT; CYCLIN-DEPENDENT PROTEIN KINASE REGULATOR	Cell cycle	-0.12	-1.47
AT5G06690	WCRKC1	Redox-related	-1.67	-0.82
AT5G07030	ASPARTIC-TYPE ENDOPEPTIDASE	Transcription factor	-0.41	-3.18
AT5G07690	MYB DOMAIN PROTEIN 29 (MYB29)	Transcription factor	-2.66	-0.11
AT5G07990	TRANSPARENT TESTA 7 (TT7)	Auxin-related	2.63	-0.58
AT5G08640	FLAVONOL SYNTHASE 1 (FLS1)	Auxin-related	0.99	-3.36
AT5G09980	ELICITOR PEPTIDE 4 PRECURSOR (PROPEP4)	Stress-related	1.50	-1.55
AT5G12020	17.6 KDA CLASS II HEAT SHOCK PROTEIN (HSP17.6II)	Stress-related	-1.39	3.73
AT5G12030	HEAT SHOCK PROTEIN 17.6A (HSP17.6A)	Stress-related	-0.07	4.40
AT5G13330	MEMBER OF THE ERF SUBFAMILY B-4 OF ERF/AP2 TRANSCRIPTION FACTOR FAMILY	ABA-related	3.16	2.63
AT5G13330	RELATED TO AP2 6L (RAP2.6L)	ABA-related	3.16	2.63
AT5G13330	RELATED TO AP2 6L (RAP2.6L)	Transcription factor	3.16	2.63
AT5G13370	AUXIN-RESPONSIVE GH3 FAMILY PROTEIN	Auxin-related	0.96	3.15
AT5G13930	TRANSPARENT TESTA 4 (TT4)	Auxin-related	1.63	-2.62
AT5G14070	ROXY2	Redox-related	-1.45	-1.91
AT5G16530	PIN-FORMED 5 (PIN5)	Auxin-related	-1.01	-2.69
AT5G17220	GSTF12/TT19	Redox-related	4.10	2.28
AT5G17300	REVEILLE 1 (RVE1)	Auxin-related	-1.87	0.05
AT5G18600	TRX FAMILY	Redox-related	-2.28	0.35
AT5G19880	PEROXIDASE SUPERFAMILY PROTEIN	Ethylene-related	-0.14	1.41
AT5G25190	ENCODES A MEMBER OF THE B-6 SUBFAMILY OF ERF/AP2 TRANSCRIPTION FACTOR FAMILY (ESE3)	Ethylene-related	2.59	2.25

AGI	Description	Annotated as:	fold-change	
			Shoot	Root
AT5G25190	ENCODES A MEMBER OF THE B-6 SUBFAMILY OF ERF/AP2 TRANSCRIPTION FACTOR FAMILY (ESE3)	Ethylene-related	2.59	2.25
AT5G25350	ARABIDOPSIS THALIANA EIN3-BINDING F-BOX PROTEIN 2 (EBF2)	Ethylene-related	1.23	1.38
AT5G25610	RESPONSIVE TO DESSICATION 22 (RD22)	ABA-related	0.80	2.72
AT5G27380	GSH2 (GLUTATHIONE SYNTHETASE 2); GLUTATHIONE SYNTHASE	Glutathione synth.-	0.63	0.34
AT5G27520	PEROXISOMAL ADENINE NUCLEOTIDE CARRIER 2 (PNC2)	Auxin-related	2.00	0.93
AT5G28300	TRIHELIX DNA-BINDING PROTEIN, PUTATIVE	Transcription factor	1.93	1.84
AT5G28770	BZIP PROTEIN BZO2H3 MRNA	Transcription factor	-2.63	-1.89
AT5G36910	THIONIN 2.2 (THI2.2)	Stress-related	-2.61	0.48
AT5G38820	ENCODES A PUTATIVE AMINO ACID TRANSPORTER	Ethylene-related	-0.15	-1.61
AT5G40370	GRXC2	Redox-related	1.16	0.85
AT5G42050	DCD (DEVELOPMENT AND CELL DEATH) DOMAIN PROTEIN	Stress-related	1.41	1.24
AT5G42500	DISEASE RESISTANCE-RESPONSIVE (DIRIGENT-LIKE PROTEIN) FAMILY PROTEIN	Stress-related	0.12	-4.35
AT5G43450	ENCODES A PROTEIN WHOSE SEQUENCE IS SIMILAR TO ACC OXIDASE	Ethylene-related	1.75	4.33
AT5G43450	ENCODES A PROTEIN WHOSE SEQUENCE IS SIMILAR TO ACC OXIDASE	Ethylene-related	1.75	4.33
AT5G44030	CELLULOSE SYNTHASE A4 (CESA4)	Ethylene-related	-0.30	-1.60
AT5G44610	ENCODES A PROTEIN WITH SEVEN REPEATED VEEKK MOTIFS	ABA-related	-1.08	-1.03
AT5G45820	ENCODES A CBL-INTERACTING SERINE/THREONINE PROTEIN KINASE	ABA-related	-2.82	-0.51
AT5G47220	ENCODES A MEMBER OF THE B-3 SUBFAMILY OF ERF/AP2 TRANSCRIPTION FACTOR FAMILY (ERF2)	Ethylene-related	1.67	1.74
AT5G47220	ENCODES A MEMBER OF THE B-3 SUBFAMILY OF ERF/AP2 TRANSCRIPTION FACTOR FAMILY (ERF2)	Ethylene-related	1.67	1.74
AT5G51440	HSP20-LIKE CHAPERONES SUPERFAMILY PROTEIN	Stress-related	1.09	3.49
AT5G54190	LIGHT-DEPENDENT NADPH:PROTOCHLOROPHYLLIDE OXIDOREDUCTASE A	Ethylene-related	1.07	-0.45
AT5G55620	UNKNOWN PROTEIN	Ethylene-related	0.22	3.79
AT5G56080	NICOTIANAMINE SYNTHASE 2 (NAS2)	Ethylene-related	-0.96	-3.02
AT5G57560	XYLOGLUCAN ENDOTRANSGLUCOSYLASE/HYDROLASE 22 (XTH22)	Auxin-related	-1.69	2.42
AT5G59820	RESPONSIVE TO HIGH LIGHT 41 (RHL41; ZAT12)	Transcription factor	1.37	2.99
AT5G60660	PLASMA MEMBRANE INTRINSIC PROTEIN 2;4 (PIP2;4)	ABA-related	-0.45	-3.68
AT5G61440	ACHT5	Redox-related	-1.50	-2.34
AT5G62520	SRO5 (SIMILAR TO RCD ONE 5); NAD+ ADP-RIBOSYLTRANSFERASE	DNA repair	-0.31	2.75
AT5G62530	ALDEHYDE DEHYDROGENASE 12A1 (ALDH12A1)	DNA repair	0.40	1.94
AT5G63160	BTB AND TAZ DOMAIN PROTEIN 1 (BT1)	Auxin-related	-3.55	-2.47
AT5G63160	BTB AND TAZ DOMAIN PROTEIN 1 (BT1)	Auxin-related	-3.55	-2.47
AT5G64750	ABA REPRESSOR1 (ABR1)	ABA-related	-0.27	2.75
AT5G67060	HECATE 1 (HEC1)	Transcription factor	3.46	1.97